Aluminum Coordination Complexes in Polymerization Catalysis

By

© Hart Plommer

A thesis submitted to the School of Graduate Studies

in partial fulfillment of the requirements for the degree of

Doctor of Philosophy

Department of Chemistry

Memorial University of Newfoundland

September 2019

St. John's, Newfoundland and Labrador

ABSTRACT

Polymers based on renewable feedstocks are desirable alternatives to fossil fuel-based conventional plastics. Aliphatic polycarbonates and some polyesters including poly(ε-caprolactone) (PCL) are biodegradable polymers commonly produced by ring-opening copolymerization (ROCOP) and ring-opening polymerization (ROP). Controlled, active, inexpensive, and non-toxic catalysts are needed for these ROP reactions. In this thesis, aluminum amino-phenolate complexes bearing different pendent donors were synthesized and fully characterized by NMR spectroscopy, X-ray crystallography, and elemental analysis. The complexes were investigated as catalysts for ROP of cyclohexene oxide (CHO), ROCOP of CHO/CO_2, and ROP of ε-caprolactone (ε-CL). The produced polymers were analyzed by gel permeation chromatography (GPC), matrix assisted laser desorption/ionization time-of-flight mass spectrometry (MALDI-TOF MS), and differential scanning calorimetry (DSC).

Complexes containing different outer-sphere heteroatoms (NMe in *N*-piperazinyl or O in *N*-morpholinyl) showed markedly different reactivities in ROP of CHO, with the *N*-morpholinyl catalyst being more active. In ROCOP of CHO/CO_2, pendent donors within the aluminum complexes had considerable influence on the selectivity towards copolymer. In addition, removal of the pendent donor generated catalyst systems that were more active. Generally, the copolymers produced were of strictly alternating character when bis(triphenylphosphoranylidene)iminium chloride (PPNCl) was used as a co-catalyst. Cationic aluminum complexes were prepared which contained a weakly coordinating anion (WCA) and the cationic aluminum centre was stabilized by a bidentate *N*-morpholinyl

moiety bound through both the oxygen and nitrogen atoms. When the aluminum complexes containing a WCA stable to alcoholysis were combined with protic co-initiators (EtOH, glycerol carbonate) they formed living catalyst systems for the ROP of ε-CL, producing poly(ε-caprolactone) (PCL) with narrow dispersity ($Đ$ = 1.00–1.05). Kinetic studies allowed the determination of activation parameters, which were consistent with a coordination-insertion mechanism.

ACKNOWLEDGMENTS

First, I would like to thank my supervisor Dr. Francesca Kerton for her steadfast support over the past six years. You have been instrumental in guiding me and giving me just the right amount of push to become a more independent researcher. Your knowledge and assistance made it possible for me to complete this thesis. I would also like to express my gratitude to my supervisory committee members, Dr. Christopher Kozak and Dr. Christopher Rowley, for their advice and encouragement during the course of my studies. Special thanks to Chris K. for his advice and suggestions both in the lab and in group meetings. Also, Dr. Nelaine Mora-Diez for her computational advice, support, and encouragement.

My studies would not have been as fun and surmountable without the amazing past and present members of the Green Chemistry and Catalysis group. Thanks go to Jenna for initially mentoring me. Katalin, for her laugh and positive attitude. Kenson and Kaijie, for always willing to bounce ideas off each other. Jen, for the X-ray structure solutions and assistance. George, Yi, Yi (Charlene), Dalal, Ali, Kori, and Ju, you are not forgotten and the memories we made make me smile still. Special thanks to the undergraduates that helped carry out my research including Immanuel Reim, Laura Stein, and Julia Pennell.

I would also like to extend my thanks to the MUN Chemistry department members including Main office staff Mary Flinn, Ebony Penney, Debbie Hickey, and Melissa Petten. Special thanks to Rosalind Collins for handling my conference funding requests and maximizing my funding potential. Thanks to the Glassblowing Shop (Brian Power and

Sabrina Bélanger) for their great work in repairing broken glassware and creating new pieces. The Machine and Electronics Shop as well for their advice on, and repairs of, any broken or dysfunctional instruments. Many thanks go to the C-CART (Centre for Chemical Analysis, Research and Training) facilitators including Dr. Brent Myron, Linda Winsor, Dave Davidson, Dr. Stefana Egli, Adam Beaton, and in particular, Dr. Celine Schneider, who provided countless help and suggestions for the NMR instruments and experiments. Also, thanks to the Chemistry Stores staff for procurement of chemicals needed for our research.

This research would not have been possible without funding, and for that I thank NSERC (PGS-D and Dr. Kerton's Discovery Grant), Department of Chemistry, School of Graduate Studies (SGS), RDC-NL, Graduate Students' Union (GSU), and Memorial University.

Many thanks to my CHHA community who made me feel welcome and helped me to become a better mentor and leader outside of research. I have enjoyed the fun outings we had. Finally, I would like to express enormous gratitude to my amazing family. Throughout these six years, they have always been available to chat and give me strength to carry on.

Dedicated to the memory of

Esther Plommer, Robert Delorme Plommer, and Sybil Grove Plommer

Table of Contents

List of Tables

List of Figures

List of Schemes

List of Abbreviations and Symbols

atm: atmosphere

bp: boiling point

BPA: Bisphenol A

CHO: cyclohexene oxide

CHC: cyclohexene carbonate

cis: on the same side

ε-CL: ε-caprolactone

d: doublet

Đ: dispersity

Da: dalton

DFT: density functional theory

DMAP: (4-dimethylamino)pyridine

DSC: differential scanning calorimetry

E_a: activation energy

ESI: electrospray ionization

GPC: gel permeation chromatography

h: hour

J: coupling constant

K: kelvin

k_{obs}: observed rate constant

L_n: ligand

m: multiplet (in NMR)

M: molar (mol L^{-1})

MALDI-TOF: matrix assisted laser desorption/ionization time-of-flight

Me: methyl

mg: milligram (10^{-3} g)

MHz: megahertz (10^{6} Hz)

min: minute

mL: milliliter (10^{-3} L)

mmol: millimole (10^{-3} mol)

μmol: micromole (10^{-6} mol)

MAD: methylaluminum bis(2,6-di-*tert*-butyl-4-methylphenoxide)

M_n: number average molecular weight

mp: melting point

MS: mass spectrometry

Mt: megatonne

m/*z*: mass-to-charge ratio

N-MeIm: *N*-methylimidazole

NMR: nuclear magnetic resonance

Nu: nucleophile

o: *ortho*

PC: propylene carbonate

PCHC: poly(cyclohexene carbonate)

PCHO: poly(cyclohexene oxide)

PCL: poly(ε-caprolactone)

PLA: poly(lactic acid) or polylactide

pK_aH: pK_a of the conjugate acid

PPNCl: bis(triphenylphosphoranylidene)iminium chloride

$PPNN_3$: bis(triphenylphosphoranylidene)iminium azide

PO: propylene oxide

ppm: parts per million

PPO: poly(propylene oxide)

q: quartet (NMR)

rac: racemic

ROP: ring-opening polymerization

ROCOP: ring-opening copolymerization

s: singlet (NMR)

t: triplet (NMR)

τ: geometry index

τ_4': geometry index for 4-coordinate compounds

^{t}Bu: tertiary butyl

T_g: glass transition temperature

THF: tetrahydrofuran

TOF: turnover frequency

trans: on the other side

vs.: versus

WCA: weakly coordinating anion

X_c: crystallinity

δ: chemical shift

μL: microlitre (10^{-6} L)

List of Appendices

Appendix A: NMR Spectroscopy

Appendix C: Crystallography

Appendix D:

Appendix E:

Appendix F: Miscellaneous Data

CHAPTER 1

Literature Review

Chapter 1. Literature Review

1.1 Introduction

Polymers have become ubiquitous in everyday life since the mid-20th century. For instance, we rely on them for packaging and clothing, and they are present in virtually every area of our lives. Polymers also play a critical role in the biomedical field including, but not limited to, syringes, tubing, and intravenous/blood bags. Unfortunately, production of conventional plastics requires the derivatization of fossil fuels which are finite in supply and extracted from the earth using increasingly unsustainable methods. Moreover, significant attention has been directed towards avoiding single-use plastic waste by opting for reusable and environmentally-sensitive alternatives. Most focus has been directed towards plastic shopping bags and drinking straws, the former which have even been banned in some municipalities. However, the utility of plastic products remains. Consequently, there are various avenues to produce polymers from renewable resources that are attracting considerable interest.

1.2 Historic Perspective

Life cycle assessment (LCA) is an important consideration for any product that is manufactured with chemicals. A LCA looks at all stages of life for a product, from raw materials production to manufacture to application and finally to end-of-life, which typically involves incineration or disposal in landfill (cradle to grave).[1] Incineration and landfill disposal of polymers is deleterious to the environment in the form of air, water, and land pollution.[2] Microplastics, regardless of whether they are synthesized or broken down

from bulk plastic materials, pose serious environmental risks.[3-4] For instance, the finding of plastic microbeads polluting the Great Lakes led the Canadian government to label microbeads as a toxin under the Canadian Environmental Protection Act (1999) in 2016.[5] One way around this problem is designing monomers and polymers with biodegradable and biocompatible properties, both of which are already produced abundantly in nature such as celluloses from biomass. Though sustainable polymers based on renewable feedstocks only account for 1% of global polymer production, promising work has already been achieved in this area. For instance, cyclic monomer synthesis from sugars and their ring-opening polymerization (ROP) has been reviewed by Buchard *et al.*[6]

From a cradle to cradle LCA perspective, polymers that can be recycled and reused are desirable since the energy requirements for recycling are significantly less than those associated with manufacture. This desirability led Chen's group to synthesize fully recyclable poly(γ-butyrolactone)s from the typically non-polymerizable γ-butyrolactone monomer.[7] By a simple change in temperature they could depolymerize the poly(γ-butyrolactone)s back to the monomer at 220 °C (linear polymer) or 300 °C (cyclic polymer) in only 1 h. Polymerization thermodynamics that are not strongly exergonic will allow energy efficient depolymerization using a catalyst.[8] While fossil fuel-derived plastics may be recycled and reused, as of 2018, the rates of recycling of plastics was less than 10% due to the lack of innovation and economic incentives in this area.[8] This is partially a consequence of the single-use (resource-to-waste) cultural and commercial mindset which has embodied the linear economy.[9] In contrast, a plastics circular economy maximizes reuse and recycling of plastics at the end of their life cycle and therefore minimizes waste.

Businesses, governments, and organizations that are signatories to the New Plastics Economy Global Commitment aim to collectively tackle the problems of plastic pollution by eliminating plastic in products where possible, developing and implementing biodegradable plastics, and creating a circular economy.[10]

1.3 Carbon Dioxide as a Feedstock

The aim of CO_2 utilization is to make use of CO_2 that is emitted into the atmosphere from industrial processes and energy generation. However, CO_2 is highly thermodynamically and kinetically stable with a standard Gibbs energy of formation equal to −396 kJ/mol and this has presented barriers to its chemical utilization.[11] In 2014, CO_2 utilization reached approximately 200 Mt which equates to only 0.62% of CO_2 emissions.[11] The utilization of CO_2 may take place *via* thermal or catalytic processes to produce fuel, chemicals, or materials. Some examples of CO_2 utilization are outlined in Scheme 1.1. A few of these products have been commercially exploited such as sodium salicylate and its *p*-isomer, which find usage in the synthesis of aspirin and as a monomer for specialty polymers, respectively. For a net CO_2 reduction in emissions to the atmosphere, one must consider the CO_2 utilized and emitted in such processes with a LCA. Catalysts which may be metal-based or metal-free are able to activate CO_2 in an efficient manner by overcoming the barrier to its reactivity.[12]

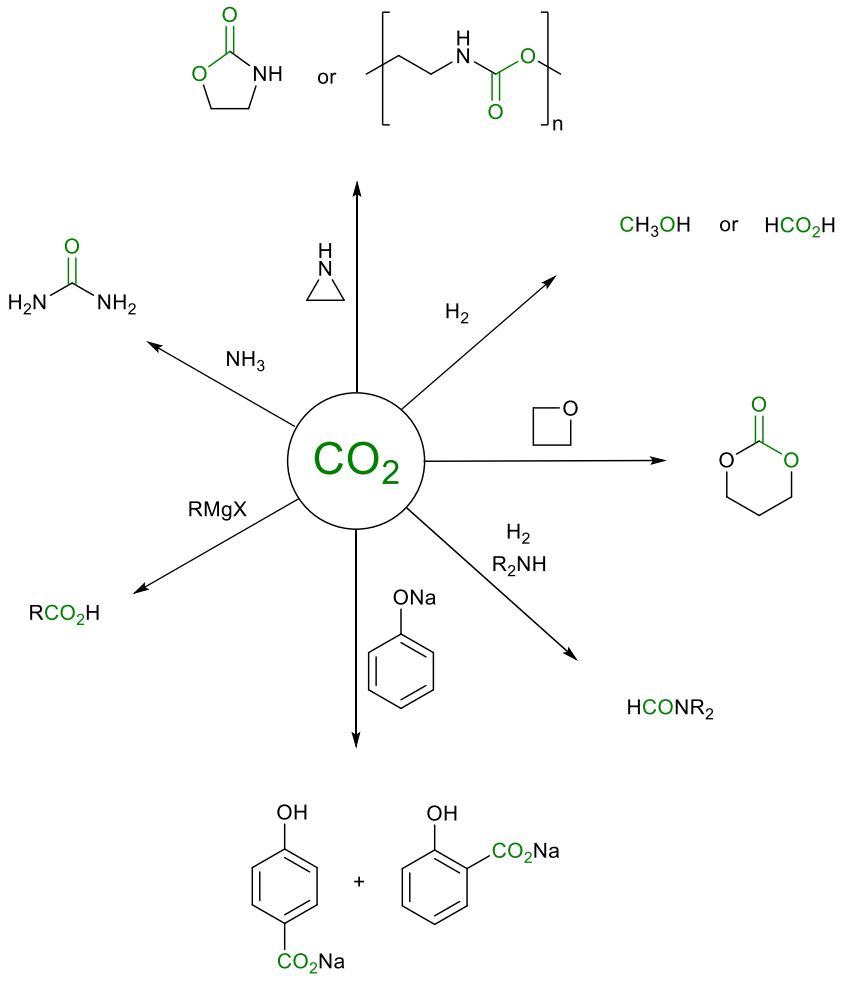

Scheme 1.1. Examples of CO_2 utilization[11, 13]

1.3.1 Polycarbonate

Production of polycarbonate is forecast to reach 9–10 Mt/year by 2030 due to desirable properties including strength, transparency, impact resistance, and durability.[11] These polymers find applications in CDs and DVDs, automobiles, office equipment, and electronics.[14] Aliphatic polycarbonates are typically used as comonomers to produce other polymers whereas aromatic polycarbonates are used as thermoplastics. The most prevalent aromatic polycarbonate is based on Bisphenol A (BPA) and phosgene (Scheme 1.2 – **A**).

This synthetic route is hazardous since phosgene is a highly toxic gas prohibited in several countries and BPA is an endocrine disruptor.[11] Moreover, the process is wasteful as large quantities of contaminated aqueous waste are produced containing sodium chloride that must be treated prior to disposal. Notably, to bypass the use of phosgene, Chimei-Asahi opened a chemical plant in 2002 that produces BPA-based polycarbonate and ethylene glycol from ethylene oxide, CO_2, and BPA (Scheme 1.2 – **B**).[14]

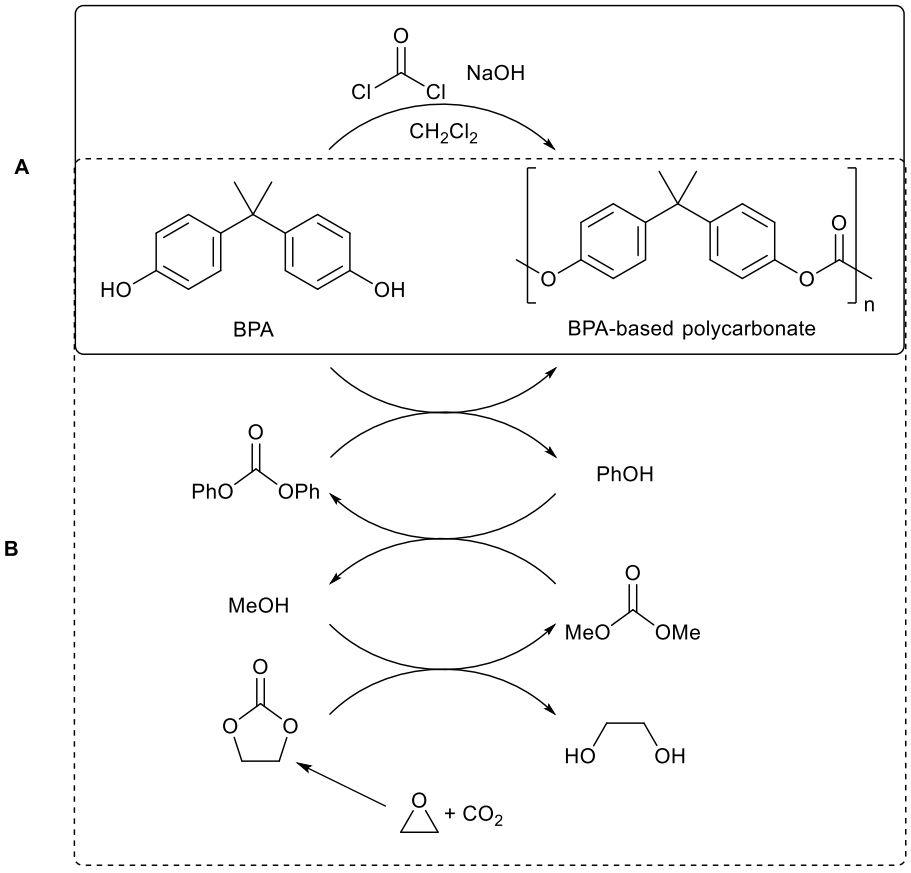

Scheme 1.2. Conventional synthetic routes to polycarbonates[14]

An attractive alternative to conventional polycarbonate synthesis is the ring-opening copolymerization (ROCOP) of epoxide and CO_2 to give aliphatic polycarbonate (Scheme

1.3). This route is not only less hazardous than the predominant BPA/phosgene route, it utilizes CO_2 which is an abundant, non-toxic gas that is the primary driver of anthropogenic climate change. Instead of stoichiometric base reagents, a catalyst is employed. Depending on the selectivity of the catalyst and reaction conditions, substantial quantities of cyclic carbonate by-product may be obtained. Cyclic carbonates are commonly used as organic solvents for electrolytes in lithium-ion batteries.[15] The most commonly used epoxides are propylene oxide (PO) and cyclohexene oxide (CHO) as they are inexpensive and easily synthesized by oxidizing propylene or cyclohexene.

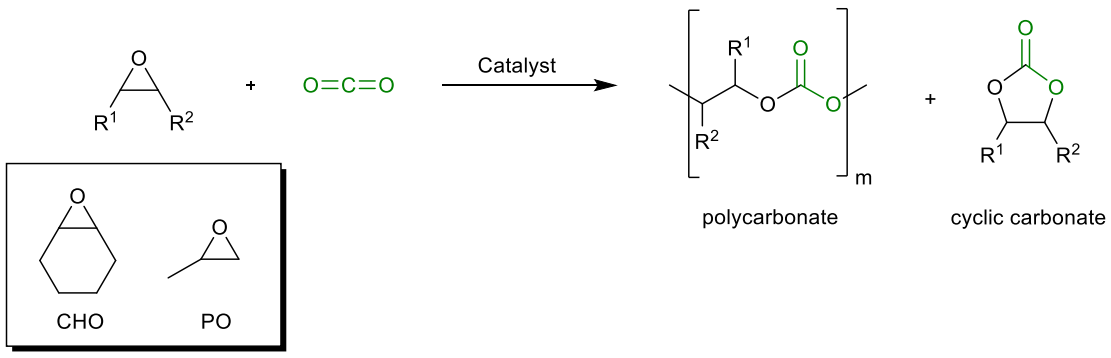

Scheme 1.3. Copolymerization of epoxide and CO_2

It is important to note that the polycarbonates resulting from PO and CHO, poly(propylene carbonate) (PPC) and poly(cyclohexene carbonate) (PCHC), have little utility as engineering plastics as their properties are inferior to that of BPA-based polycarbonate,[16] but they are important as standard test substrates to screen catalyst systems. Even so, both PPC and PCHC have been synthesized commercially and the more favourable properties of PPC relative to PCHC have led to its use in degradable packaging and polyurethane production.[17] The limited scope of these epoxides has encouraged the

design and synthesis of new epoxides that will give desirable copolymer characteristics such as improved thermal, solubility, and self-healing properties. Recycling of polycarbonate is more viable than fossil-fuel based plastics as the thermodynamics for epoxide/CO_2 copolymerization are not as exergonic.[8]

1.4 Biodegradable Polymers

Biodegradable polymers are degraded to H_2O and CO_2 in the presence of microorganisms such as bacteria, fungi, or algae.[18] The bonds in functional groups such as esters and carbonates are amenable to hydrolysis hence biodegradation is generally favoured by high oxygen content in the polymer backbone. For example, aliphatic polycarbonates produced by copolymerization of renewable epoxides and CO_2 have been shown to decompose to nontoxic metabolites in the human body by Darensbourg *et al.*[19] These environmentally benign polymers are particularly applicable to drug delivery systems due to their biocompatible nature. On the other hand, BPA-based polycarbonate is non-biodegradable.[20] Aliphatic polycarbonate and polyesters are currently the most promising polymers in Green Chemistry since their respective monomers may be renewably sourced and their structures are biodegradable.[8] For instance, limonene oxide (LO) can be derived from limonene in citrus peel and its copolymers may be further functionalized due to the presence of a C–C double bond.[21-23] In this vein, the group of Williams has produced polycarbonates from epoxidized 1,4-cyclohexadiene.[24]

1.4.1 Poly(ε-caprolactone)

Poly(ε-caprolactone) (PCL) is a biodegradable and biocompatible polymer synthesized primarily by ring-opening polymerization (ROP) of ε-caprolactone (ε-CL), since ROP

catalysts may offer control over the polymer molecular weights.[25] PCL can also be produced by polycondensation of 6-hydroxyhexanoic acid, in which vacuum is applied to remove water produced, thereby shifting the equilibrium towards polymer.[26] Although ε-CL is produced mainly by Baeyer-Villiger oxidation of cyclohexanone using peracetic acid, it can potentially be synthesized from renewable resources. These routes are illustrated in Scheme 1.4.

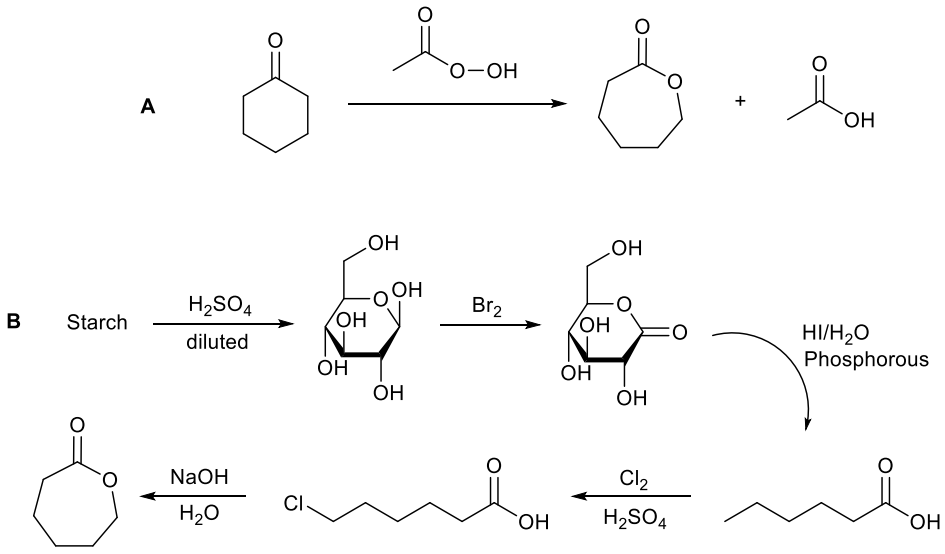

Scheme 1.4. Synthesis of ε-CL from fossil fuels (**A**) or renewable resources (**B**).[25-26]

1.5 Ring-Opening Polymerization

The thermodynamic driving force for ROP is the relief of ring strain in the cyclic monomer. This allows the unfavourable (negative) entropy change to be overcome, as *n* monomer molecules are enchained into a polymer chain.

1.5.1 ROP of Epoxides

Polyethers are valuable polymers produced annually on a Mt scale from epoxides such as ethylene and propylene oxide.[27-29] For example, poly(ethylene glycol) is a biocompatible polymer used in pharmaceuticals and cosmetics. Mechanistically, the ROP may occur *via* coordination-insertion, anionic, or cationic routes as illustrated in Scheme 1.5 with CHO as the epoxide. Common initiators of anionic ROP include alkali metal alkoxides, except for lithium which aggregates after the first epoxide insertion step. Anionic ROP is characterized by attack of a nucleophile (alkoxide) at the electropositive carbon adjacent to the epoxide oxygen followed by consecutive attacks of the generated alkoxide at the electropositive carbon of another epoxide (Scheme 1.5 – **B**). Termination with a proton source such as water furnishes the polyether, in the example illustrated below it is poly(cyclohexene oxide) (PCHO). This route is limited by the molecular weights achievable when substituted epoxides (e.g. PO, CHO) are employed as substrates since the alkoxide can also act as a base, forming a new initiating species (Scheme 1.5 – **D**).

The coordination-insertion route begins with coordination of an epoxide to the Lewis acidic metal, which attracts the nucleophile (Nu) to attack the partially positive methine carbon, forming a metal-bound alkoxide (Scheme 1.5 – **A**). The cationic mechanism generally takes place in the absence of a reactive nucleophile (Scheme 1.5 – **C**). Initiation begins when an epoxide coordinated to a Lewis acidic metal ring-opens to form a metal-bound alkoxide and a carbocation stabilized by epoxide monomer and sometimes, the weakly coordinating anion (WCA). The carbocation continues to propagate the polymerization by continuous ring-opening of epoxide monomer. Most of the reported

cationic complexes for this purpose include aluminum and zinc for PO and CHO polymerization, which have been reviewed by Sarazin and Carpentier.[30] Control of cationic polymerizations are typically poor leading to low molecular weights and high dispersities ($Đ$ = 1.5–4.0).

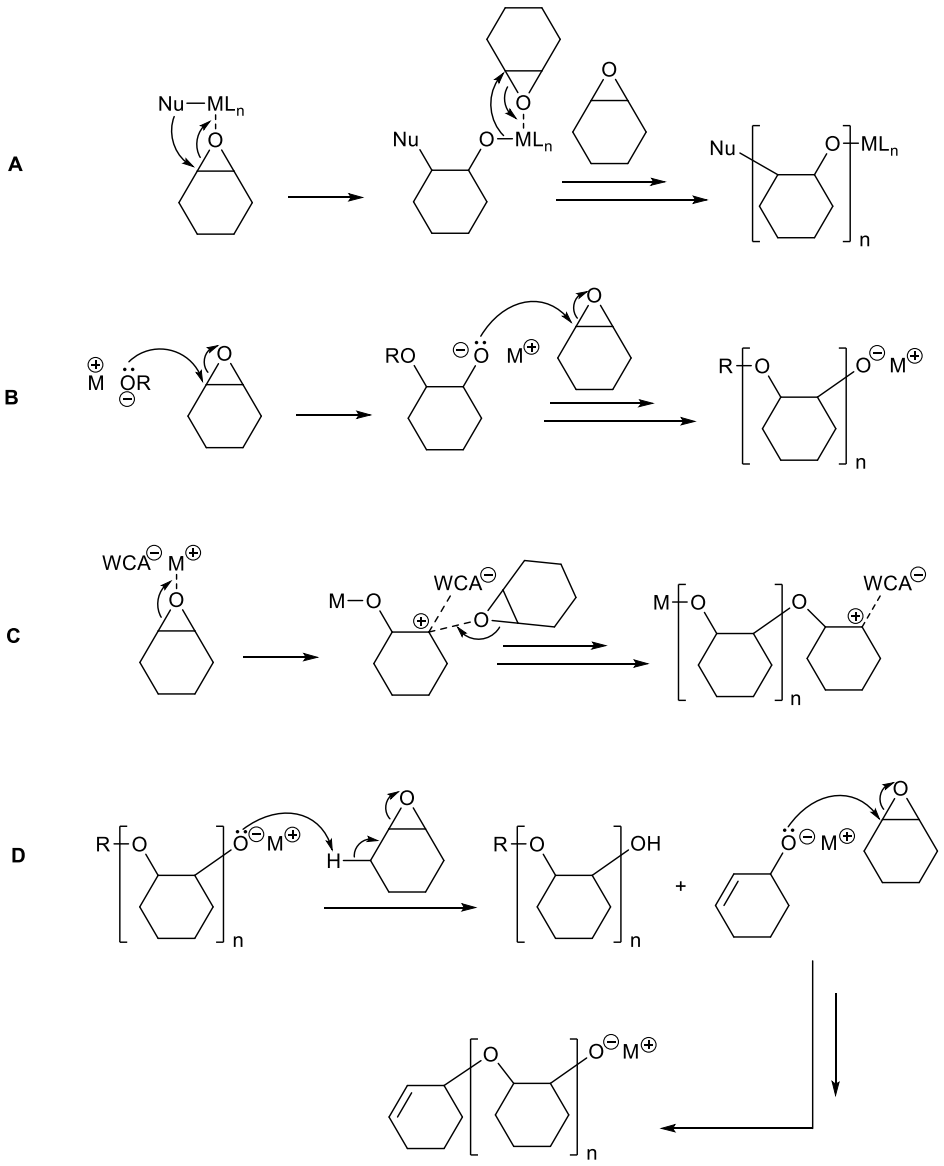

Scheme 1.5. Proposed coordination-insertion (**A**), anionic (**B**), cationic (**C**), and anionic side-reaction (**D**) mechanisms for ROP of epoxides[27, 30]

1.5.2 ROP of ε-Caprolactone

Mechanistically, the ROP of cyclic esters may occur *via* anionic, activated monomer, cationic, and coordination-insertion processes. The two most relevant to metal catalysis, activated monomer and coordination-insertion, are illustrated in Scheme 1.6 and Scheme 1.7, respectively, with ε-CL as the monomer. With an activated monomer route, exogenous alcohol attacks the electrophilic carbonyl carbon of the metal-activated ε-CL, followed by a concerted ring-opening of the heterocycle by oxygen-acyl bond cleavage. Attack of the alcohol (i.e. hydroxyl chain end of polymer or exogenous alcohol) on the metal-activated ε-CL followed by oxygen-acyl bond cleavage continues to give the growing polymer chain.

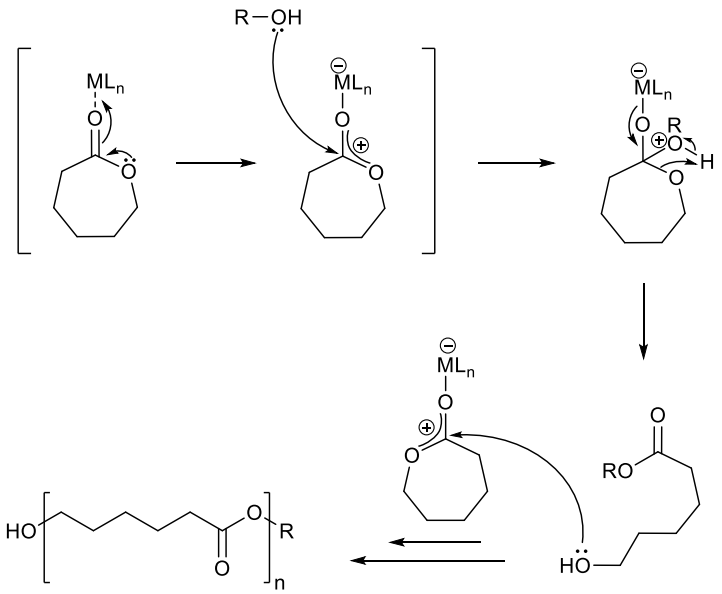

Scheme 1.6. Activated monomer ROP mechanism

The coordination-insertion route is analogous to that seen for ROP of epoxides. A reactive metal-bound nucleophile attacks the electrophilic carbonyl carbon of ε-CL, generating a tetrahedral alkoxide intermediate. This tetrahedral intermediate undergoes

oxygen-acyl bond cleavage to give a metal-bound alkoxide which continues to insert coordinated ε-CL into a growing polymer chain.

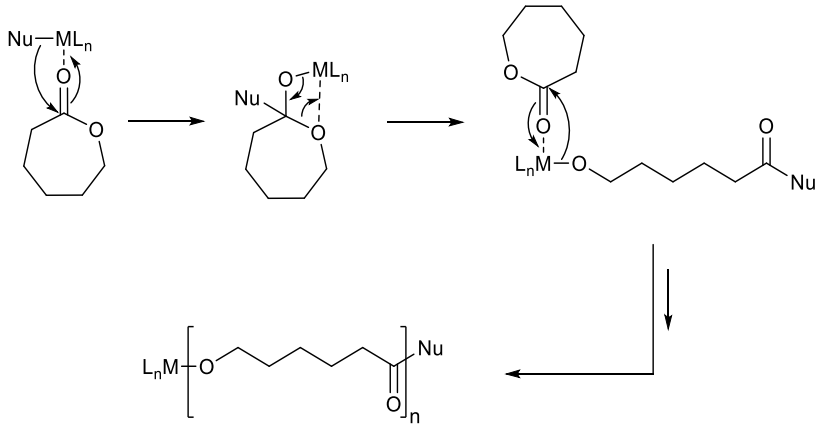

Scheme 1.7. Coordination-insertion ROP mechanism

1.5.3 Control of Polymerization

A few important distinctions of catalyst systems for polymerization can be made with respect to catalyst behaviour. A controlled catalyst is one that generates polymer chains with experimental molecular weights (M_n) in good agreement with those calculated from monomer-to-catalyst ratios ($M_{n,calcd}$).[30] Furthermore, the polymer must have a narrow dispersity, typically less than 1.2. The criteria for a living polymerization are more stringent. For a catalyst to be living, it must initiate polymerization with 100% efficiency, i.e. all catalyst species must contain a single growing polymer chain. Experimentally this is observed as very narrow dispersities, typically less than 1.10. Experimentally determined M_n values must be dictated by monomer-to-catalyst ratios. Immortal polymerization is also living polymerization, but it is characterized by the use of an excess of a protic nucleophile, typically an alcohol. The nucleophile behaves as both the exogenous initiator as well as a

chain transfer agent and there must be fast and reversible exchange between growing and dormant polymer chains for immortal criteria to be met. In this case, M_n values are proportional to monomer-to-alcohol ratios. Notably, immortal polymerizations have enabled the use of very small amounts of metal catalyst meaning less catalyst residue remains in the produced polymer.

1.5.4 Chemistry of Aluminum

Aluminum is a Group 13 element with the electron configuration [Ne] $3s^2 3p^1$. It exists mostly in the +3 oxidation state, Al^{III}, but it has the potential to form species with the +1 oxidation state under unusual conditions.[31] Since Al^{III} is classified as a hard acid by Pearson's Hard Soft Acid Base theory, it will readily accept electrons from hard donors such as oxygen to form complexes. Although aluminum is the most abundant metal within the Earth's crust and large quantities are recycled each year, it is a lengthy multi-step process to isolate pure aluminum metal, which then must be turned into organoaluminum compounds or aluminum trichloride for the synthesis of coordination complexes. It is worth noting that organoaluminum compounds are highly reactive due to the polarity of the aluminum–carbon bond and will react vigorously with oxygen or water present to form decomposition products such as aluminum oxides.[32]

1.6 Amine-Phenol Pro-Ligands

The oxophilic and hard nature of Al^{III} has led to a variety of oxygen-based ligand frameworks for this metal. In particular, phenolate ligands bound to Al^{III} have historically been important in a number of organic reactions due to the Lewis acidity of the Al^{III} centre.[33-34] Amine-phenol pro-ligands are a well-established ligand class that stabilize a

variety of metal ions including Al^{III} (Figure 1.1).[35] Amine-phenols are particularly attractive as the substitution of the aromatic ring can modulate the steric and electronic properties of the ligand and the coordinated metal(s). For instance, substituents with electron-withdrawing or donating character as well as bulky or non-bulky character may be installed. Moreover, the position of these substituents within the aromatic ring is highly influential. For example, alkyl substituents in the *para* position (R^3) have little effect on sterics due to the distance from the metal centre but can improve the solubility of the complex as a whole. On the other hand, substituents in the *ortho* position (R^1) greatly affect sterics and reactivity of the complex. In the case of amine-bis(phenol) ligands, the pendent donor (R^4) containing an O, N, or S atom may modulate the steric and electronic properties of the metal centre directly. This is important as controlled catalyst systems for polymerization must have appropriate Lewis acidity and steric balance to promote desired reactivity and discourage deleterious side reactions.

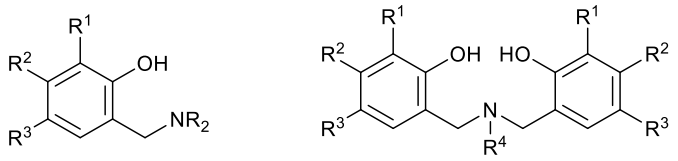

R = Me, Et, methoxyethyl
R_1 = H, Me, ^{t}Bu, ^{t}Am, or Cl
R_2 = H or Me
R_3 = H, Me, ^{t}Bu, ^{t}Am, OMe, NO_2, or Cl
R_4 = dimethylaminoethyl, morpholinylethyl, diethylaminoethyl, pyridylethyl

Figure 1.1. Structural variation within amino-phenol and amino-bis(phenol) pro-ligands

The preparation of these ligands follows a modified Mannich condensation reaction using (para)formaldehyde, a primary or secondary amine, and a substituted phenol. Reactions may take place neat or in a suitable organic solvent.[36] Kerton and co-workers have reported greener Mannich condensations that use water in place of conventional organic solvents.[37-38] Yields for the reactions conducted in water were remarkably higher, with higher yields observed for phenols containing greater alkylation of the aromatic ring. These results were attributed to a hydrophobic effect. Microwave heating could also be applied, giving shorter reaction times. The product is easily isolated by decanting the aqueous phase and washing the crude product with an appropriate solvent such as methanol to remove unreacted phenol. Further recrystallization is typically performed using a $CHCl_3$/MeOH mixture.

1.7 Metal Catalysts for ROP of Epoxides

1.7.1 Aluminum Catalysts for ROP of PO

Dagorne and co-workers have reported cationic aluminum complexes (**1.1a–b**, **1.2a–b**, and **1.3**, Figure 1.2) for polymerization of PO.[39-40] Polymerizations were performed in CH_2Cl_2. Fluorinated complex **1.3** was investigated at various temperatures and in all cases, full conversion of 200 equiv PO was achieved e.g. within 1 h at 20 °C. Although the isolated poly(propylene oxide)s (PPOs) exhibited narrow dispersities ($Đ$ = 1.1–1.3), the molecular weights were below 1 kDa, suggesting that a significant degree of chain transfer took place. The amino-phenolate cations (**1.1a–b** and **1.2a–b**) all exhibited similar activities (80–95% yield), furnishing PPO with significantly higher molecular weights (M_n

= 2530–3960 Da) but broader dispersities (*Đ* = 1.4–1.7). The absence of end group signals in MALDI-TOF MS experiments supported a cationic mechanism for these catalysts.

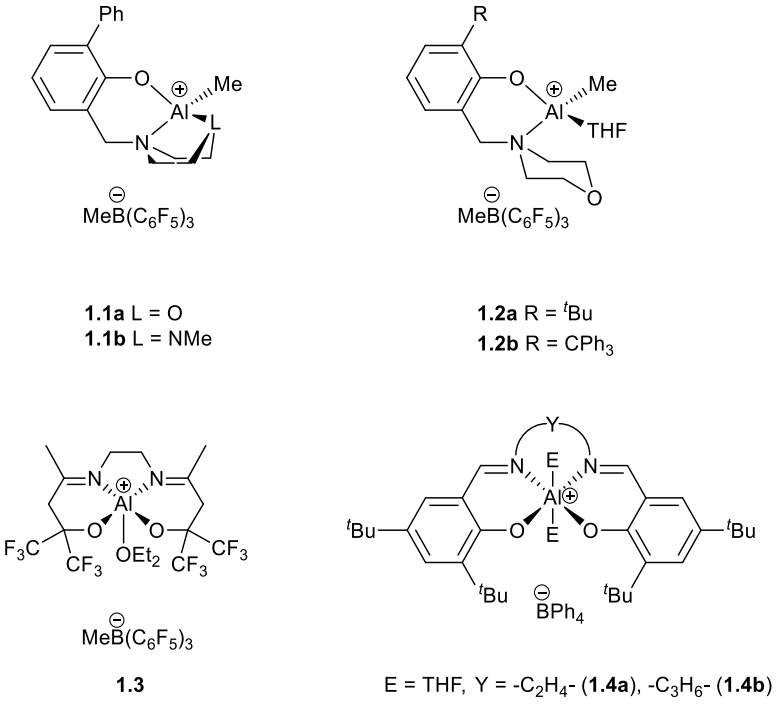

Figure 1.2. Cationic aluminum complexes for ROP of PO

Atwood and co-workers prepared cationic aluminum salen complexes (**1.4a–b**, Figure 1.2) for ROP of PO.[41] Polymerizations were performed in the presence or absence of CH_2Cl_2. High molecular weight PPO was produced. While evidence was consistent with a cationic mechanism operating, remarkably narrow dispersities were obtained (*Đ* = 1.16–1.32). It was proposed that the propagating carbocation was well-stabilized by unreacted PO and the tetraphenylborate anion.

1.7.2 Aluminum Catalysts for ROP of CHO

Liu *et al.* reported aluminum β-ketoamino complexes (**1.5a–d**, Figure 1.3) for ROP of CHO in toluene at 50–70 °C.[42] Increased reaction temperatures had very little effect on the conversion of CHO and degree of polymerization. The electron-withdrawing Cl-substituted ligand afforded the most active complex (**1.5d**), which achieved 68.9% conversion after 1 h but the polymers obtained had relatively broad dispersities (*Đ* = 2.20–2.84).

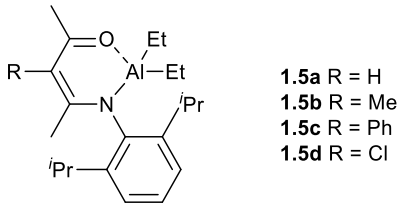

Figure 1.3. Aluminum β-ketoamino complexes for ROP of CHO

Mazzeo and co-workers investigated bimetallic aluminum complexes containing various linker lengths (**1.6a–c**, Figure 1.4) for CHO polymerization.[43] The shortest linker where the aluminum centres are in closest proximity yielded the most active catalyst (**1.6a**), converting 22% of CHO in 48 h at room temperature in CH_2Cl_2. Using **1.6b** or **1.6c**, no activity was observed in CH_2Cl_2. However, in neat CHO moderate conversion to PCHO (40%) could be obtained using **1.6a** and **1.6b**, but **1.6c** remained inactive. The monometallic analogue **1.7** was inactive even at concentrations ten-fold greater than **1.6a**, suggesting that these ROP reactions proceed *via* a bimetallic mechanism. The resulting polymers had high molecular weights (M_n 223.7–398.7 kDa) and relatively broad dispersities (*Đ* = 1.43–1.77) and the long reaction times needed are likely due to the methyl

groups being poor initiators of polymerization. Employing *iso*-PrOH as a co-initiator led to a significant drop in molecular weights and at 70 °C excellent agreement with theoretical M_n values could be obtained. Using **1.6a**, ROP of PO, styrene oxide, and epichlorohydrin were unsuccessful both at room temperature and 70 °C.

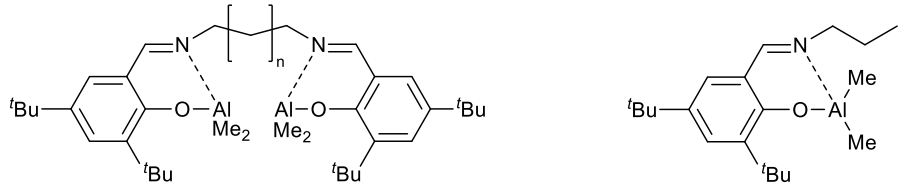

1.6a n = 1
1.6b n = 3
1.6c n = 10

1.7

Figure 1.4. Mono and bimetallic aluminum complexes for ROP of CHO

Yao and co-workers reported mono and bimetallic aluminum complexes (**1.8a–c** and **1.9a–c**, Figure 1.5) for ROP of CHO.[44] Polymerizations were typically carried out in hexane at 30 °C. The most active catalyst was the di-*tert*-butyl substituted bimetallic complex **1.8a** and this was proposed to be due to improved solubility and also greater stabilization of the aluminum centres as the activities increased with more electron-rich phenolate groups, in the order: dimethyl < methyl *tert*-butyl < di-*tert*-butyl. Unfortunately, the polymerizations were poorly controlled, particularly when the bimetallic systems were used ($Đ$ = 2.62–3.37). At identical conditions but in neat CHO, the polymer yield dropped from 86 to 69%. Kinetic studies showed that the order in **1.8a** was one whereas it was second order with respect to the monometallic analogue **1.9a**, supporting a cooperative effect between the two aluminum centres. **1.8a** was also active in ROP of PO (neat), achieving 84% yield after 12 h at 80 °C but no activity was observed at lower temperatures.

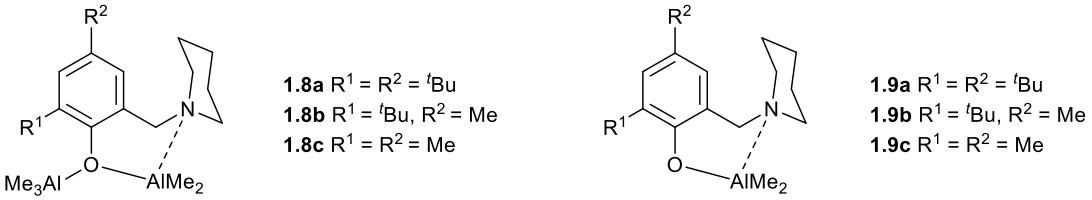

Figure 1.5. Mono and bimetallic aluminum complexes for ROP of CHO

Diaconescu and co-workers reported the use of ferrocene-containing aluminum alkoxide complexes (**1.10** and **1.10**$^+$, Scheme 1.8) for polymerization of a variety of oxygen-containing monomers, including CHO.[45] The polymerization activity was dependent on the Lewis acidity of the aluminum centre, which could be adjusted *via* oxidation (or reduction) of the ferrocene moiety in the ligand backbone. At room temperature, the oxidized (cationic) complex **1.10**$^+$ could convert 90% CHO to PCHO within 20 min, albeit the PCHO had a broad dispersity ($Đ$ = 2.20). In stark contrast, **1.10** converted less than 5% CHO after 24 h at 70 °C. DFT calculations favoured a coordination-insertion mechanism over a cationic mechanism and explained the fast, non-living character of the polymerization as a consequence of low activation barriers for initiation and propagation using **1.10**$^+$.

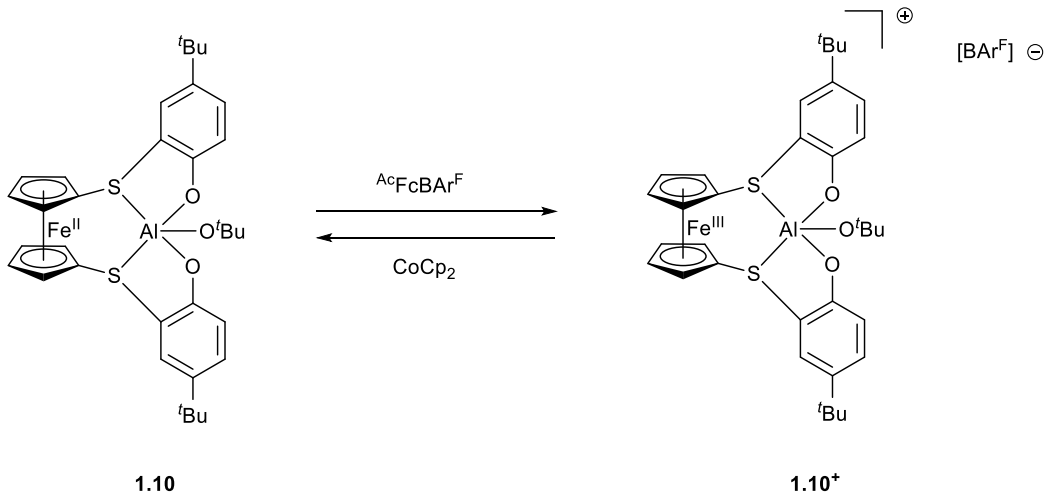

1.10 **1.10⁺**

Scheme 1.8. Redox-switchable aluminum thiophenolate complexes for ROP of CHO

1.8 Metal Catalysts for Copolymerization of Epoxides and CO_2

Metal catalyst systems for copolymerization of epoxides and CO_2 are comprised of Lewis acidic and basic portions. The Lewis acidic (metal) portion functions to withdraw electron density from CO_2 or epoxide, while the Lewis basic (nucleophile) component initiates the ring-opening of the epoxide. Even when the metal contains a bound nucleophile, excess nucleophile is sometimes mandatory in the form of an added co-catalyst. Co-catalysts may be anionic or neutral and are sometimes crucial for reactivity or obtaining high quantities of carbonate linkages in the resulting polymer (Figure 1.6). In this thesis, bis(triphenylphosphoranylidene)iminium chloride (PPNCl), bis(triphenylphosphoranylidene)iminium azide ($PPNN_3$), and 4-dimethylaminopyridine (DMAP) are used as co-catalysts.

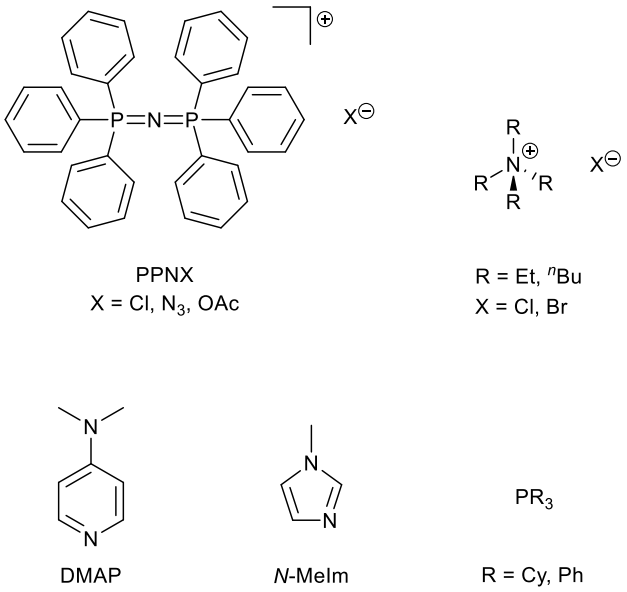

Figure 1.6. Anionic (top) and neutral (bottom) co-catalysts for copolymerization

The mechanistic proposals reported thus far for epoxide/CO_2 ROCOP are summarized in Scheme 1.9, with CHO as the epoxide. The initiation step is similar to that observed in coordination-insertion ROP of epoxides and it may proceed by attack of a nucleophile bound to the same metal or another metal in the vicinity of the activated CHO (monometallic intramolecular and bimetallic intermolecular pathways). Alternatively, a free nucleophile (i.e. not metal-bound) typically in the form of added co-catalyst may attack the electrophilic methine carbon of the CHO (monometallic intermolecular). In the absence of CO_2 and depending on the nature of the catalyst system, the metal-alkoxide intermediate may undergo ROP of CHO to yield polyether (homopolymer).

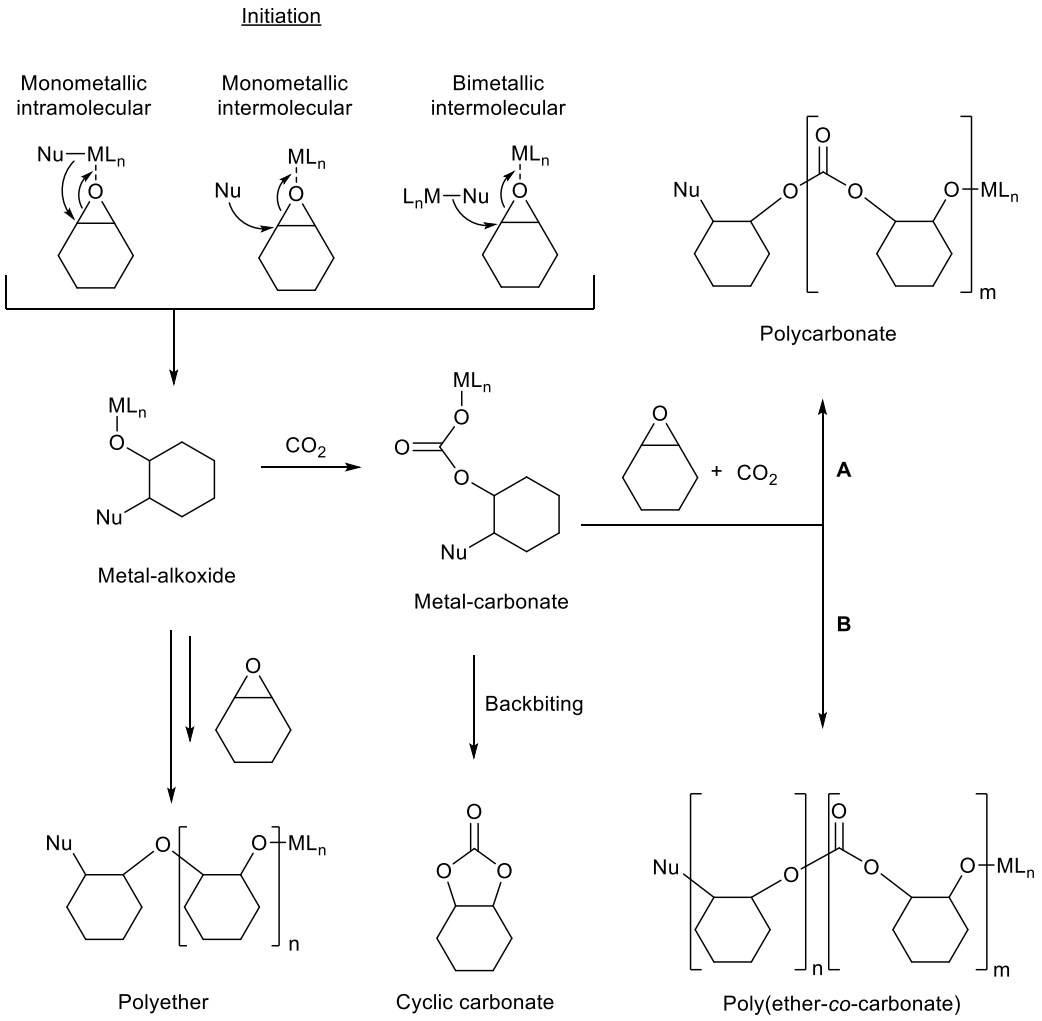

Scheme 1.9. Proposed initiation and propagation steps in copolymerization (Nu = nucleophile, L_n = ligand)

Once CO_2 is added to the system, CO_2 may insert into the metal-alkoxide to form a metal-carbonate. Alternating insertions of CHO and CO_2 into the polymer chain then yield a strictly alternating polycarbonate (Pathway **A**). If consecutive CHO insertions take place, ether linkages form and the polymer is termed a poly(ether-*co*-carbonate) (Pathway **B**). The presence of ether linkages is not detrimental if it can be controlled by tuning the

amount of ether linkages in the copolymer, however, it means that less CO_2 is utilized. One advantage to sequential epoxide reactions is that ether linkages are thermodynamically stable to backbiting depolymerization of the copolymer.[46] Cyclic carbonate may be produced *via* two different mechanisms. The metal-bound carbonate may attack the Nu-bound methine carbon of the cyclohexyl ring. Alternatively, the metal-bound alkoxide may attack the carbonate of the growing polymer chain (Scheme 1.10).

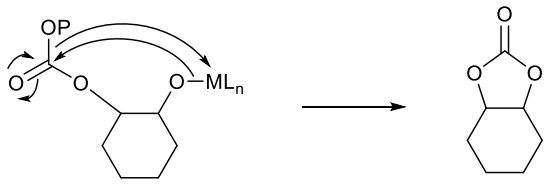

Scheme 1.10. Backbiting of metal-alkoxide (P = polymer chain)

Many excellent catalyst systems producing cyclic carbonates have been reported.[47-48] The selectivity for cyclic carbonate is dependent on the catalyst system, reaction conditions, and epoxide employed. For example, a more Lewis acidic metal centre will bind the carbonate or alkoxide groups more strongly and disfavour backbiting whereas a more electronically saturated metal will favour backbiting. This was demonstrated by Rieger and co-workers who studied bimetallic zinc catalysts experimentally and theoretically.[49] With respect to the choice of epoxide, Darensbourg *et al.* investigated the thermodynamics and kinetics for copolymerization of CHO or PO with CO_2 catalyzed by a model Cr^{III} salen system and they found that cyclic carbonates were the thermodynamically favoured product in both cases.[50] However, the activation barrier for the formation of cyclic cyclohexene carbonate was nearly 80 kJ/mol more than the

corresponding polycarbonate, whereas for cyclic propylene carbonate the barrier difference was much lower (33 kJ/mol). Therefore, the temperature range for producing copolymer from CHO is much more conducive than for PO.

1.8.1 Historical Background to Copolymerization

The first systems reported for ROCOP of epoxides and CO_2 were heterogeneous catalysts based on $ZnEt_2$ and H_2O.[51-52] An equimolar mixture of $ZnEt_2$ and H_2O could copolymerize PO and CO_2 with turnover frequency (TOF) up to 0.12 h^{-1} at 80 °C and 20–50 atm CO_2. Many other heterogeneous zinc systems followed this initial development, but these exhibited low activities and poor control of polymerization (high dispersities). Since the structures of these first catalysts were unclear, it was impossible to build up the structure-activity relationships needed to develop new generations of catalyst. Therefore, studies into well-defined single-site homogeneous catalysts for copolymerization followed. The first well-defined single-site metal catalyst for epoxide/CO_2 copolymerization was an aluminum porphyrinato (**1.11**, Figure 1.7).[53] It was able to produce copolymer from PO/CO_2 under mild conditions (20 °C, 8 bar CO_2) without any added co-catalyst. While the copolymer contained only 40% carbonate linkages and reactions proceeded quite slowly (TOF = 4.4 day^{-1}), the complex had a high degree of control over the copolymerization ($Đ$ = 1.15).

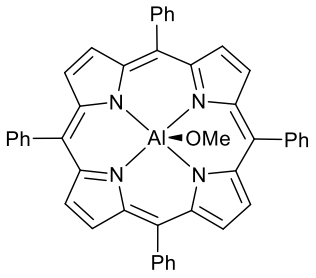

1.11

Figure 1.7. Seminal aluminum porphyrinato complex for PO/CO_2 copolymerization

Nearly twenty years later, Darensbourg and Holtcamp reported the first well-defined single-site zinc complexes that showed improved activities (TOF 1.3–3.6 h^{-1}) for copolymerization of CHO/CO_2 and terpolymerization of $CHO/PO/CO_2$.[54] They were able to produce copolymers with a low quantity of ether linkages (8–16%), but control of the copolymerization was quite poor.

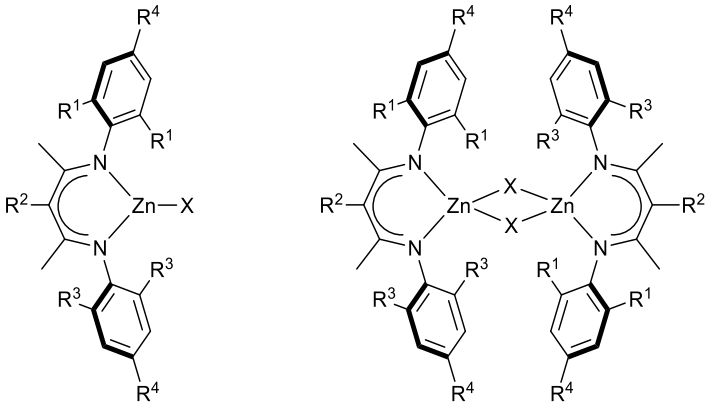

1.12a

X = Et, $N(SiMe_3)_2$

1.12b

X = OAc, Br, Cl, OH, OMe, O^iPr

Figure 1.8. Zinc β-diiminate complexes for copolymerizations

Coates and co-workers pioneered the development of zinc β-diiminate complexes as copolymerization catalysts (**1.12a–b**, Figure 1.8).[55-57] The activity of these complexes depended highly on the electronic and steric properties of the ligand substituents. Sterically hindered complexes favoured a dimeric (bimetallic) structure (**1.12b**) both in the solid state and in solution whereas sterically unencumbered complexes remained monomeric (**1.12a**). The best activities (TOF up to 2290 h^{-1}) in CHO/CO_2 copolymerization were obtained for loosely bound dimers (moderate steric bulk in the R^1 and R^3 *ortho* positions). Notably, monomeric structures showed better activity for PO/CO_2 copolymerization. This finding of a bimetallic mechanism[58] spurred research towards bimetallic catalyst systems, and representative examples will be discussed in Section 1.8.3.

The other most commonly studied complexes over the past two decades are metal salen complexes, primarily with chromium and cobalt. Research into this area was encouraged by Jacobsen's Cr^{III} salen complexes which could ring-open epoxides in an asymmetric fashion.[59] Darensbourg's group was at the forefront of developing Cr^{III} salen complexes including **1.13a–b** shown in Figure 1.9.[60] In a similar fashion to the zinc β-diiminate complexes, the variation of the steric and electronic properties of the salen ligand greatly influenced the activity of the complexes in copolymerization. Generally, electron donating substituents yielded more active catalysts.[61] Lower activities were obtained when sterically encumbering substituents occupied the diimine backbone in such a manner that they oriented perpendicular to the salen ligand plane. Further tuning the added co-catalyst and CO_2 pressure led to very high activities with TOF up to 1153 h^{-1} using **1.13b** with 1 equiv PPNCl.[62] These types of catalyst systems have been named bicomponent as the metal

catalyst and co-catalyst form two separate components of the system. The field of metal catalyzed epoxide/CO_2 ROCOP was recently reviewed by the Kozak group.[63]

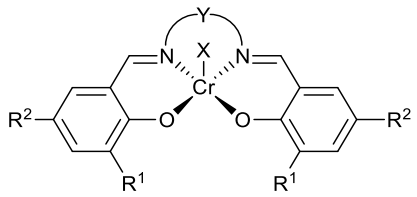

1.13a $R^1 = R^2 = {}^t$Bu, X = N_3, Y = -C_2H_4-
1.13b $R^1 = {}^t$Bu, R^2 = OMe, X = N_3, Y = (1R, 2R)-C_6H_{10}-

Figure 1.9. Chromium salen complexes for copolymerization

1.8.2 Bifunctional Catalyst Systems

The likelihood of backbiting from a metal-free carbonate is lessened if cationic groups are installed near the metal centre. These electrostatically attract free carbonate anions and keep them in the vicinity of the metal centre to react with epoxide once more. This has led to the development of bifunctional (single component) catalysts incorporating quaternary side-arms that function as both backbiting deterrent and anionic co-catalyst. These systems not only provide improved selectivity for copolymer but also obviate the need for added co-catalyst which was a drawback for bicomponent systems. The first such example was a Co^{III} salen containing piperidinyl and piperidinium end-capping arms (**1.14**, Figure 1.10) reported by Nozaki and co-workers.[64] They found **1.14** to be effective at copolymerizing epoxides (PO, butylene oxide, and hexylene oxide) and CO_2 to strictly alternating copolymer in a controlled fashion with excellent selectivity for copolymer. The piperidinium arm was proposed to control this selectivity by protonating the anionic

polymer chain once it detaches from the cobalt centre, making it sufficiently non-nucleophilic to backbite to form cyclic carbonate. Immortal copolymerizations with PO could be carried out with a 20-fold excess of MeOH.

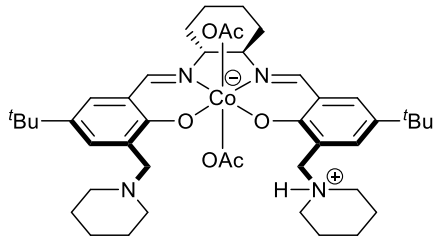

1.14

Figure 1.10. Bifunctional cobalt acetate complex for epoxide/CO_2 copolymerization

1.8.3 Bimetallic Catalyst Systems

Bimetallic complexes have been actively researched since bimetallic mechanisms were first implicated in copolymerization using monometallic complexes, and this has led to the development of highly active systems. The group of Williams has developed a series of bimetallic systems using a macrocyclic amino-phenolate ligand framework (**1.15a–e**, **1.16a–f**, and **1.17**, Figure 1.11) for CHO/CO_2 copolymerization and these show good activities under atmospheric pressures of CO_2.[65-70] Atmospheric pressures are desirable as industrial processes would be safer running at low pressures and the energy requirements would be substantially reduced. At 80–100 °C, the seminal dizinc complex (**1.16a**) was able to achieve TOF ranging from 18–25 h^{-1} with only 1 atm CO_2 and 0.1 mol% catalyst.[65] The copolymers produced were strictly alternating and dispersities were narrow ($Đ$ = 1.19–1.21) showing very good control of the polymerization. Excellent selectivity (94–96%) for

copolymer was obtained regardless of the reaction conditions. Identical activity and dispersity were obtained when the copolymerization was performed in the presence of air, demonstrating the ability of the catalyst to resist decomposition. The presence of two narrow distributions of copolymer with one distribution exhibiting an M_n approximately double of the other distribution, observed for many other catalyst systems as well, warranted further mechanistic investigation. Consequently, it was proposed that rapid chain transfer allows growth of the polymer chain from both sides of cyclohexane diol (adventitious or produced *in situ*, possibly due to trace quantities of H_2O), leading to the higher molecular weight fraction.[71]

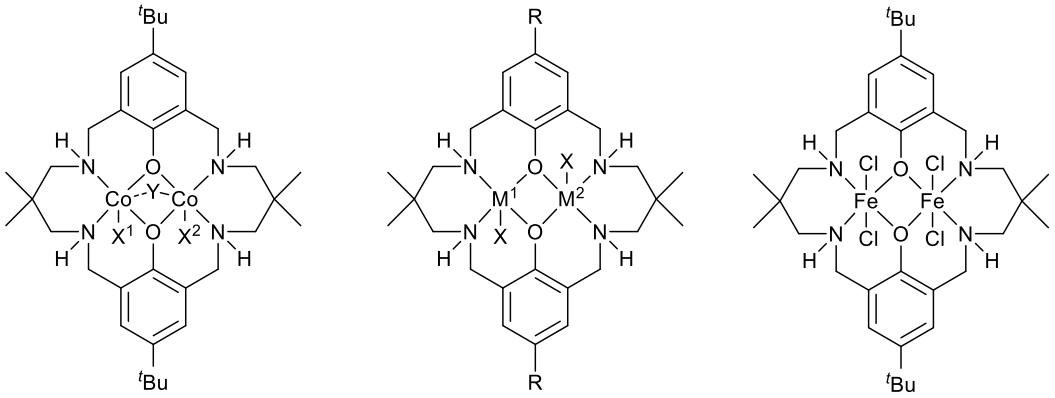

1.15a $X^1 = X^2 = OAc$, Y = OAc
1.15b $X^1 = X^2 = OAc$, Y = none
1.15c $X^1 = Y = Cl$, X^2 = DMAP
1.15d $X^1 = Y = Cl$, X^2 = *N*-MeIm
1.15e $X^1 = Y = Cl$, $X^2 = C_5H_5N$

1.16a $M^1 = M^2 = Zn$, R = ^{t}Bu, X = OAc
1.16b $M^1 = M^2 = Zn$, R = OMe, X = OAc
1.16c $M^1 = M^2 = Mg$, R = ^{t}Bu, X = OAc
1.16d $M^1 = M^2 = Mg$, R = ^{t}Bu, X = Br
1.16e $M^1 = M^2 = Mg$, R = ^{t}Bu, X = O_2CCF_3
1.16f $M^1 = Zn$, $M^2 = Mg$, R = ^{t}Bu, X = OAc

1.17

Figure 1.11. Macrocyclic bimetallic complexes for CHO/CO_2 copolymerization

When the dizinc complex contained better electron-donating methoxy groups (**1.16b**) in place of the *tert*-butyl groups a decrease in TOF from 9.2 to 6 h^{-1} was observed.[67] This

was rationalized on the basis of the decreased Lewis acidity of the zinc centres resulting in a weaker binding and activation of CHO and CO_2. In contrast to **1.16a**, the dimagnesium analogues with various initiating groups (**1.16c–e**) were totally selective for copolymer even at 100 °C.[68] A zinc-magnesium heterobimetallic complex (**1.16f**) was also studied.[72] Although **1.16f** could not be isolated from a mixture containing the analogous homobimetallic complexes **1.16a** and **1.16c**, the mixture showed significant improvement in activities compared to **1.16a** and **1.16c** whether they were employed alone or as an equimolar mixture (TOF 79 vs. 17–52 h^{-1}). This increase in activity was proposed to result from the chain shuttling of the growing polymer chain between two metal centres. Notably, the **1.16f** mixture was active for cycloaddition of PO/CO_2 and produced propylene carbonate with 90% selectivity, in contrast to the homobimetallic system which was totally inactive with PO at identical conditions. Dicobalt systems (**1.15a–e**) were approximately 9 times more active than **1.16a** (TOF 159, 172 vs. 18 h^{-1}) and like the dimagnesium systems showed total selectivity towards copolymer.[70] It is worth noting that one of the advantages of bimetallic systems is that added co-catalyst is typically not needed as the second metal centre provides the nucleophilic initiating group.

1.8.4 Aluminum Catalysts for PO/CO_2 Copolymerization

Chisholm and Chatterjee recently investigated a variety of aluminum porphyrinato complexes (**1.18a–d** and **1.19a–b**, Figure 1.12) in PO/CO_2 copolymerization with particular focus on mechanistic investigations using a variety of analytical methods including ESI-MS and IR spectroscopy.[73] Their interest in these complexes lies in the geometric constraints afforded by the porphyrinato ligand framework, in which the metal

centre can only move slightly in or out of the ligand plane, forcing a *trans* orientation of any axial ligands. Homopolymerization of PO and copolymerization with CO_2 proceeded slowly in the absence of co-catalyst. However, when paired with a co-catalyst, **1.19a** was essentially unreactive in homopolymerization compared with a TOF of 21 h^{-1} when it was used alone for ROP of PO. For other porphyrinato complexes (**1.18a** and **1.18c**), the presence of 0.5 equiv co-catalyst increased conversions of PO markedly, with PPNCl generally outperforming DMAP as a co-catalyst. For PO/CO_2 ROCOP, the **1.18c**/PPNCl system quantitatively converted PO to nearly perfectly alternating PPC with 97% selectivity (nearly identical results were obtained with DMAP). When the CO_2 pressure was lowered from 50 to 10 bar, the **1.18c**/DMAP system was still highly selective for PPC, in contrast to the less Lewis acidic **1.18a** which produced an ether-rich PPC. No evidence for nucleophilic co-catalyst incorporation into the PPC was found, leading them to conclude that only one polymer chain was growing per Al centre. They also found that backbiting of the PPC to propylene carbonate (PC) took place once CO_2 was removed from the reaction vessel. Thus, it was concluded that an Al-alkoxide was responsible for this polymer degradation process rather than an Al-alkylcarbonate.

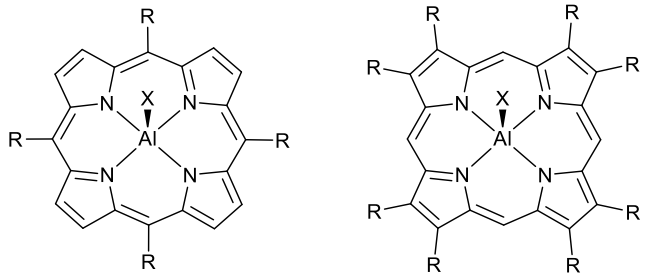

1.18a R = Ph, X = Cl
1.18b R = Ph, X = OEt
1.18c R = C_6F_5, X = Cl
1.18d R = C_6F_5, X = OEt

1.19a R = Et, X = Cl
1.19b R = Et, X = OEt

Figure 1.12. Aluminum porphyrinato complexes for PO/CO_2 copolymerization

Building on these results, several bifunctional aluminum porphyrinato complexes that were very active for PO/CO_2 copolymerization were reported following the general structure in Figure 1.13. [46, 74-75] Catalyst optimization was performed by tuning (i) the electronic properties of the aluminum centre (aromatic substituents, $R^{1–5}$), (ii) the nucleophilicity of the incorporated co-catalytic quaternary ammonium nitrate groups (quaternary ammonium substituents, R), and (iii) the linker length (n) separating the co-catalyst from the aluminum centre. The most active variant, **1.20**, gave a high selectivity for copolymer (around 90% depending on reaction conditions) containing 98% carbonate linkages, even at a remarkably low catalyst loading of 0.005 mol% (TOF = 2824 h^{-1}).

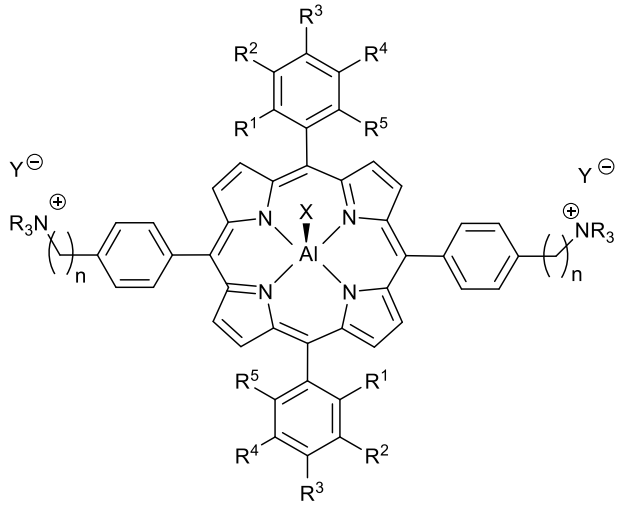

1.20 n = 6, R = hexyl, $R^1 = R^3 = R^5 = OMe$, $R^2 = R^4 = H$, X = Y = NO_3

Figure 1.13. Bifunctional aluminum porphyrinato complexes for PO/CO_2 copolymerization

1.8.5 Aluminum Catalysts for CHO/CO_2 Copolymerization

Sârbu and Beckman investigated aluminum alkoxide and ester complexes (**1.21–1.23**, Figure 1.14) for homopolymerization of CHO and copolymerization with CO_2.[76] Copolymerizations were carried out at 60–62 °C and 83 bar CO_2 for 24 h (i.e. under supercritical conditions). The most active catalyst **1.22** produced 340 g copolymer per g of Al but this copolymer contained only 7.7% carbonate linkages, which implies a high rate of ROP compared with ROCOP. Moreover, the polymer obtained had a broad dispersity ($Đ$ = 2.62). Significantly higher carbonate content (21.7%), although still quite low, was attained using **1.23**. ^{1}H NMR and molecular weight data suggested that both alkoxide and ester groups initiate the polymerization such that two polymer chains grow per Al centre,

which may explain the broad polymer dispersities obtained using such systems compared with the porphyrinato examples discussed above.

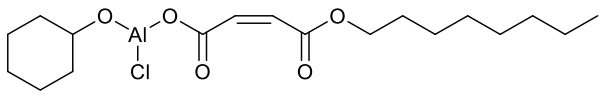

1.21

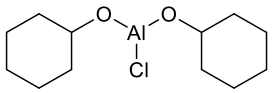

1.22

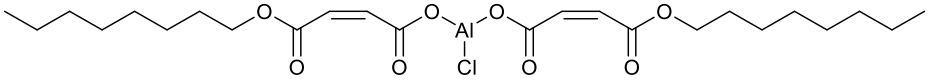

1.23

Figure 1.14. Aluminum alkoxide and ester complexes for homopolymerization of CHO and copolymerization with CO_2

As mentioned in the historical background (Section 1.8.1), salen transition metal complexes have been widely studied as catalysts in ROCOP of CHO/CO_2. Darensbourg and Billodeaux investigated an extensive library of aluminum salen complexes including **1.24a–e** (Figure 1.15) for copolymerization of CHO/CO_2.[77] Their initial catalytic studies focused on the aluminum derivatives containing *tert*-butyl substituents in the 3- and 5-positions of the phenolate ring as chromium analogues are known to be efficient catalysts. Interestingly, **1.24a** or **1.24b** in combination with PPNCl yielded only cyclic carbonate and not the desired polycarbonate. Inspired by successes in the area of lactide ROP, where electron-deficient aluminum centres were more adept at polymerization, they replaced the electron-donating *tert*-butyl groups with hydrogen atoms to yield a catalyst (**1.24c**). This

new complex could produce copolymer selectively when coupled with tetrabutylammonium salts. By introducing electron-withdrawing nitro substituents at the 5-position of the phenolate rings, the most active catalyst system (**1.24e**) in this series was obtained (TOF = 24.2–35.4 h^{-1}) and resulted in excellent selectivity for copolymer formation and % carbonate linkages.

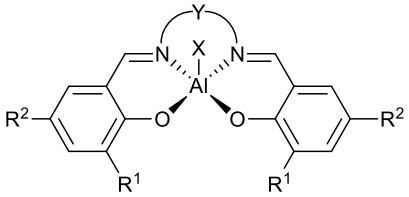

1.24a $R^1 = R^2 = {}^t$Bu, X = Et, Y = $-C_6H_{10}-$
1.24b $R^1 = R^2 = {}^t$Bu, X = Cl, Y = $-C_2H_4-$
1.24c $R^1 = R^2$ = H, X = Cl, Y = $-C_6H_4-$
1.24d $R^1 = {}^t$Bu, $R^2 = NO_2$, X = Et, Y = $-C_2H_4-$
1.24e $R^1 = {}^t$Bu, $R^2 = NO_2$, X = Cl, Y = $-C_2H_4-$

Figure 1.15. Aluminum salen complexes for CHO/CO_2 copolymerization

Another series of aluminum Schiff base complexes (**1.25a–g** and **1.26**, Figure 1.16) were also studied as catalysts for CHO/CO_2 copolymerization at around the same time.[78] The most active complex **1.25a** performed optimally at 50 bar CO_2 and 80 °C with an equimolar amount of tetra-*n*-butylammonium acetate. Under these conditions, greater than 95% selectivity for copolymer containing 94% carbonate linkages was achieved. However, the control of the copolymerization was relatively poor in the presence of the standard co-catalyst tetra-*n*-butylammonium acetate regardless of the reaction conditions employed ($Đ$ = 1.54–3.82). Poorer selectivities were obtained using complexes containing flexible (ethylene diamine and propylene diamine) backbones (**1.25d–e**) as well as the mono Schiff

base complex **1.26** (copolymer selectivity, 35–50%). As a by-product, *cis*-cyclohexene carbonate (*cis*-CHC) was observed and it was proposed that this side-reaction only occurred at the initial stages of the copolymerization, after the first insertion of CO_2 and not *via* a polymer degradation mechanism. It was shown using MALDI-TOF MS, NMR spectroscopy, and gas chromatography studies that CH_2Cl_2 and tetra-*n*-butylammonium acetate reacted to form methylene diacetate and tetra-*n*-butylammonium chloride under reflux conditions. This explained the similar reaction results using these two co-catalysts with **1.25a**.

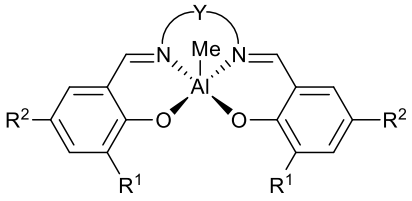

1.25a $R^1 = R^2 = H$, Y = *o*-C_6H_4
1.25b $R^1 = H$, $R^2 = {}^t$Bu, Y = *o*-C_6H_4
1.25c $R^1 = R^2 = {}^t$Bu, Y = *o*-C_6H_4
1.25d $R^1 = R^2 = {}^t$Bu, Y = -C_2H_4-
1.25e $R^1 = R^2 = {}^t$Bu, Y = -C_3H_6-
1.25f $R^1 = R^2 = H$, Y = (1R, 2R)-C_6H_{10}-
1.25g $R^1 = R^2 = H$, Y = (1R, 2S)-C_6H_{10}-

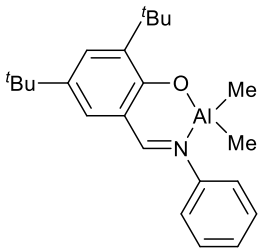

1.26

Figure 1.16. Aluminum Schiff base complexes for CHO/CO_2 copolymerization

A number of research groups have investigated aluminum phenolate (phenoxide) complexes for CHO/CO_2 ROCOP based on the initial successes using salen species. Zevaco *et al.* prepared a series of aluminum 2,2'-methylene-bisphenolate complexes (**1.27a–d** and **1.28a–b**, Figure 1.17) and tested their efficacies in CHO/CO_2 copolymerization.[79] The chlorido complexes (**1.27b** and **1.27d**) were consistently more

active in copolymerizations compared to their ethyl analogues (**1.27a** and **1.27c**). Addition of a co-catalyst to **1.27b** led to a switch in selectivity, with PPNCl giving 50% conversion to cyclic carbonate rather than polymer. These differences in reactivity were attributed to the tetrahedral geometry around the aluminum centre, in contrast to the aluminum salens which exhibit a constrained square pyramidal environment that allows *trans* coordination of the nucleophilic co-catalyst, labilizing the Al–X bond towards epoxide ring-opening. More recent work by the same group explored the effect of electron-withdrawing chloro substituents in the 5-position of the phenolates (**1.28c** and **1.29**, Figure 1.17).[80] Compared to the bisphenolates bearing sterically bulky and electron-donating alkyl groups, these catalysts introduced more ether linkages into the copolymer due to the higher Lewis acidity of the aluminum centres and increased rate of epoxide ROP compared with ROCOP.

More recently, the catalytic activity of an aluminum-N_2O_2 complex (**1.30**, Figure 1.18) in copolymerization of CHO/CO_2 and coupling of PO/CO_2 was reported.[81] Copolymerizations primarily used tetra-*n*-butylammonium bromide (TBAB) as the co-catalyst and fully alternating copolymers were obtained, even at low CO_2 pressure (2 bar) if a high catalyst loading and long reaction times were used. Under the standard conditions employed (80 °C, 50 bar CO_2, 20 h) the halide co-catalysts differed very little in terms of activity (TOF = 22.8–24.4 h^{-1}) but use of the neutral co-catalyst DMAP led to less active systems (TOF = 19.2 h^{-1}). This suggests that DMAP may form a stable adduct with the aluminum centre that blocks a coordination site, which would otherwise be available for CHO coordination and activation. The dispersities of the copolymers obtained ($Đ$ = 1.23–1.65) indicated that the catalyst system offered good control over the copolymerization.

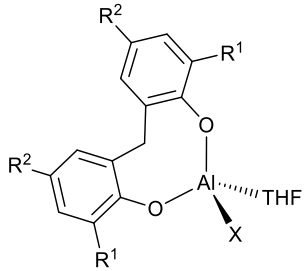

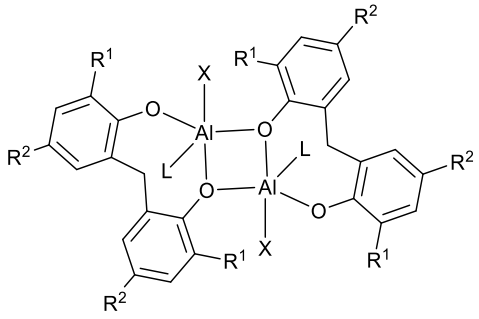

1.27a $R^1 = R^2 = {}^t$Bu, X = Et
1.27b $R^1 = R^2 = {}^t$Bu, X = Cl
1.27c R^1 = 1-methylcyclohexyl, R^2 = Me, X = Et
1.27d R^1 = 1-methylcyclohexyl, R^2 = Me, X = Cl

1.28a $R^1 = R^2 = {}^t$Bu, X = Et
1.28b R^1 = 1-methylcyclohexyl, R^2 = Me, X = Cl
1.28c R^1 = H, R^2 = Cl, X = Et, L = THF

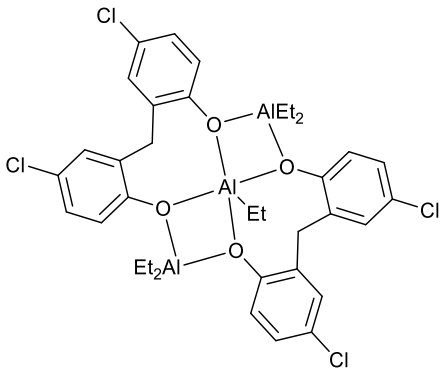

1.29

Figure 1.17. Aluminum bis(phenolate) complexes for CHO/CO_2 copolymerization

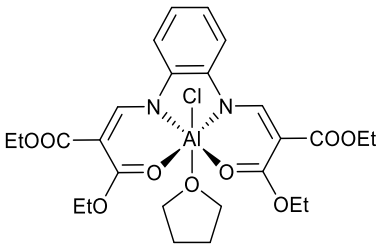

1.30

Figure 1.18. Aluminum-N_2O_2 complex for CHO/CO_2 copolymerization

An aluminum calixarene complex (**1.31**, Figure 1.19) has also been studied in homopolymerization of CHO and PO and related ROCOP with CO_2.[82] NMR data (^{27}Al) were consistent with a 5-coordinate Al centre and therefore, the complex was proposed to be rigid with the Al in a distorted trigonal bipyramidal environment. Reactions were carried out without co-catalyst over several days at either 35 or 70 °C and 61 bar CO_2 in toluene. Low conversions (30%) were obtained but very good selectivity (86%) for oligo(ether-carbonate) (M_n = 1930 Da) was achieved with CHO after 11 days at 35 °C. Selectivity dropped slightly (83%) when the reaction temperature was increased to 70 °C but this is not unusual in ROCOP reactions. The role of the Al-bound chloride in ring-opening was confirmed using elemental analysis and $^{13}C\{^1H\}$ NMR spectroscopy on the copolymer.

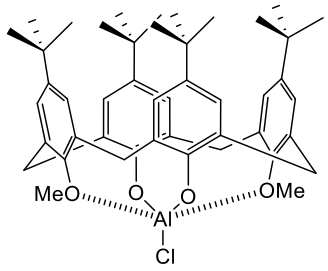

1.31

Figure 1.19. Aluminum calixarene for homopolymerization of CHO and copolymerization with CO_2

In 2013, the Kerton group provided an overview of aluminum systems able to copolymerize epoxides and CO_2.[83] This review established the need for more research into the area of aluminum-catalyzed copolymerization, since lower activities and generally low carbonate linkages have shifted the focus to other metals in copolymerization. Accordingly, they briefly studied aluminum amino-phenolate complexes (**1.32a–b**, Figure 1.20) in

copolymerization of CHO/CO_2 (the primary focus of the paper was ROP of ε-CL).[84] Using **1.32b** in the presence or absence of 1 equiv PPNCl, no copolymer or cyclic carbonate was detected after 24 h at 60 °C and 40 bar CO_2. On the other hand, **1.32a** converted 67% CHO monomer to a copolymer containing 54% carbonate linkages after 16 h, albeit with poor dispersity ($Đ$ = 3.16). This difference in reactivity between **1.32a** and **1.32b** was attributed to the facile coordination of the outer-sphere oxygen atom in **1.32a** which displaces the chloride to allow ring-opening of the coordinated CHO. In **1.32b**, stereochemical nitrogen inversion would be needed for the outer-sphere NMe group to coordinate to aluminum and thus provide the necessary nucleophilic chloride ion for ring-opening the epoxide.

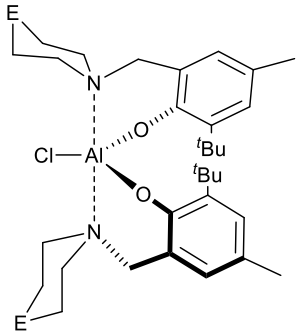

1.32a E = O
1.32b E = NMe

Figure 1.20. Aluminum amino-phenolate complexes for CHO/CO_2 copolymerization

1.8.6 Aluminum Catalysts for LO/CO_2 Copolymerization

Some of the most significant results in aluminum catalyzed ROCOP have been achieved using aluminum amino-tris(phenolate) complexes (**1.33a–c**, Figure 1.21).[22, 85] These complexes are some of the very few catalyst systems reported to date able to efficiently perform ROCOP of LO/CO_2. While structurally similar to CHO, LO is more

challenging to ring-open due to the methyl group which poses a steric hindrance to catalysts which might bind this epoxide; these aluminum complexes are able to switch between 5- and 6-coordinate geometries to allow LO binding. Preliminary screening of a 40/60 *cis*/*trans* mixture of LO indicated **1.33b**/PPNBr to be the most active catalyst system with PPNCl giving slightly lower conversions under identical conditions. Pure *cis* or *trans* LO were copolymerized using **1.33b**/PPNCl system at various ratios. They observed faster reactivity of the *cis* isomer and this phenomenon was studied *in silico* using DFT. Copolymerization of CHO/CO_2 and terpolymerization of LO/CHO/CO_2 were further investigated using the **1.33b**/PPNCl system. With a 0.5 mol% aluminum loading (0.5 equiv PPNCl), copolymerization of CHO/CO_2 proceeded to 77% conversion after 48 h at optimized conditions of 40 °C and 15 bar CO_2. The copolymer obtained was a strictly alternating polycarbonate with an M_n of 11.9 kDa and $Đ$ = 1.49. Under identical reaction conditions, terpolymerizations were performed with various ratios of CHO and *cis*-LO. A clear preference for CHO insertion was observed, e.g. at 1:1 ratio, 75% conversion to a copolymer containing 69% CHO units was obtained. The % carbonate linkages decreased slightly as the *cis*-LO/CHO ratio was increased, from 99% in the strictly alternating PCHC to 93% in the copolymer comprised solely of *cis*-LO and CO_2. Molecular weights decreased as well, reaching a minimum of 3.6 kDa in the CHO:*cis*-LO 1:2 mixture. Kinetic studies *via* ^{1}H NMR spectroscopy indicated that as the terpolymerization proceeds the insertion of *cis*-LO becomes more favoured, giving a gradient terpolymer.

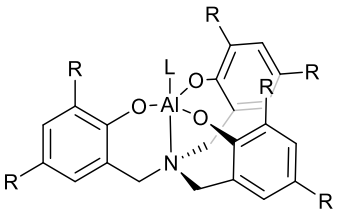

1.33a R = H, no L
1.33b R = Me, L = THF
1.33c R = Cl, L = THF

Figure 1.21. Aluminum amino-tris(phenolate) complexes for copolymerization of LO/CO_2

1.9 Metal Catalysts for ε-Caprolactone Polymerization

A wide variety of metal complexes have been studied as catalysts for ROP of ε-CL. These have been reviewed by Labet and Thielemans[26] and Arbaoui and Redshaw[25]. More recently, cationic complexes for these reactions have been reviewed by Sarazin and Carpentier.[30] High activities have been attained for both neutral and cationic systems, with rare earth metals achieving exceptional activities according to the activity scale introduced by Arbaoui and Redshaw. In the context of Green Chemistry, a shift towards catalysts based on non-toxic, abundant, and inexpensive metals is desirable, including those that can operate in an immortal fashion. Recently, *s* block metal systems have achieved very high activities for ROP of ε-CL.

Kol and co-workers reported a highly active magnesium complex (**1.34b**, Figure 1.22) for homopolymerization and block copolymerization of ε-CL and lactide.[86] The related chloride complex **1.34a** was essentially inactive for ε-CL polymerization. **1.34b**, which contained a nucleophilic HMDS group, was reactive towards benzyl alcohol (and consequently, ε-CL). Polymerizations were carried out in CH_2Cl_2 at room temperature in

the presence of BnOH. With 300 equiv ε-CL, full conversion was reached within 45 seconds ($M_{n,calcd}$ = 34 kDa; M_n 28 kDa), although the dispersity was quite broad ($Đ$ = 1.54) which was attributed to the extremely fast rate of propagation compared to initiation. High efficiencies were also observed under immortal conditions.

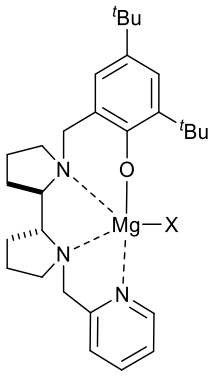

1.34a X = Cl
1.34b X = $N(SiMe_3)_2$

Figure 1.22. Magnesium complexes for homopolymerization and block copolymerization of ε-CL and lactide

Lichtenberg and co-workers investigated sodium aminotroponiminate (ATI) complexes (**1.35a–f**, Scheme 1.11) for ROP of ε-CL including sodium sodiate and mixed-metal potassium sodiate compounds that are accessible *via* ligand-induced disproportionation.[87] Polymerizations were carried out in THF at −30 °C. The increased nucleophilicity of the $[Na(ATI)_2]^-$ anion compared to neutral [Na(ATI)] yielded a more efficient catalyst and **1.35f** could convert 2500 equiv of ε-CL to PCL within 1 minute. Although the $ATI^{Ph/iPr}$ complexes were less active than $ATI^{iPr/iPr}$ complexes, their molecular weight control was excellent ($Đ$ = 1.14–1.35). Lower ε-CL/catalyst ratios or replacement of THF with toluene (when the catalyst was toluene-soluble) dramatically lowered

dispersities. These catalysts are the most efficient alkali metal systems that have been reported to date. NMR studies indicated that deprotonation of ε-CL by the ATI ligand initiates the polymerization rather than nucleophilic attack of ATI at the carbonyl group.

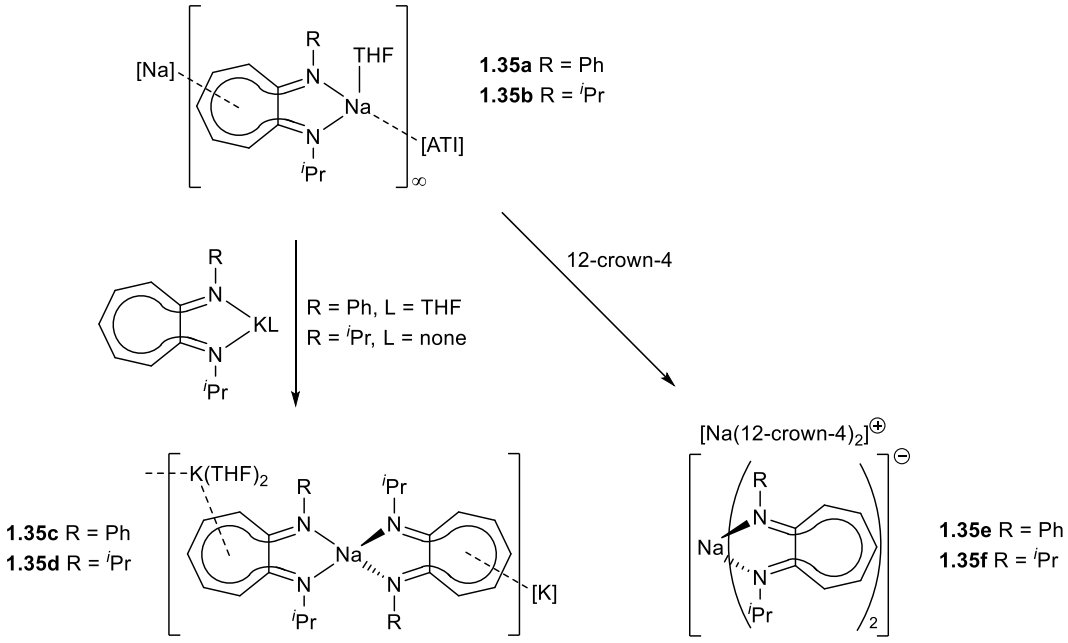

Scheme 1.11. Synthesis of sodium aminotroponiminate complexes for ROP of ε-CL

1.9.1 Aluminum Catalysts Based on N,O ligands for ROP of ε-CL

Lee *et al.* reported a series of aluminum Schiff base complexes (**1.36a–f** and **1.37a–d**, Figure 1.23) for ε-CL polymerization, paying particular attention to the effect of reducing the ring size from a 6- to 5-membered ring structure.[88] Polymerizations were approximately 2–3 fold faster with 5-membered structures (**1.36a–f**), and remarkably shorter induction periods were observed. Both effects are believed to be due to the open coordination space around the Al centre in 5-membered structures, which allows easy access for ε-CL and

benzyl alcohol coordination. DFT calculations showed these findings to be a product of geometric constraints and not electronic effects.

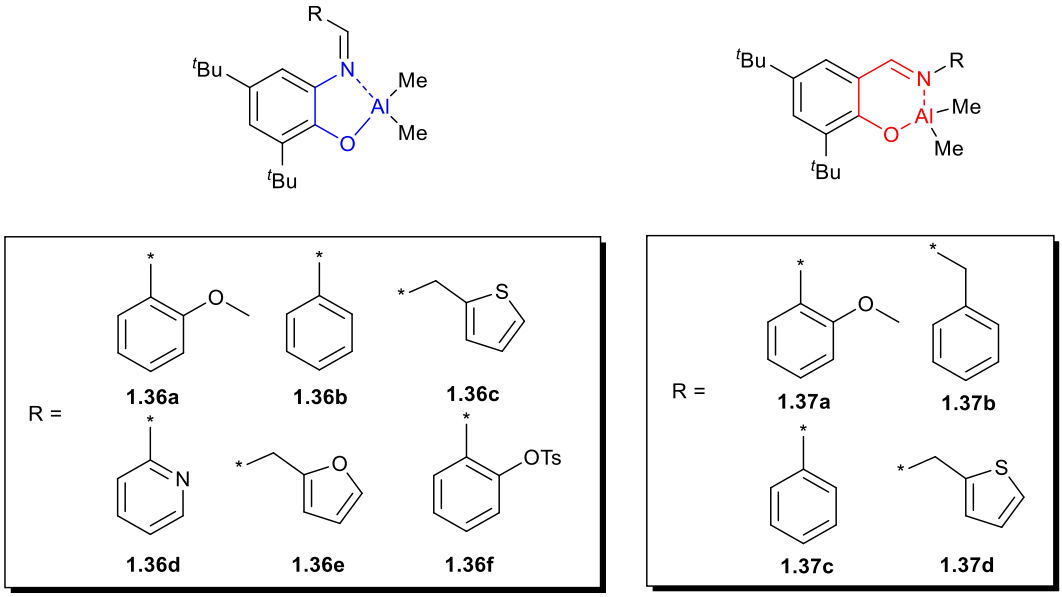

Figure 1.23. Aluminum Schiff base complexes for ROP of ε-CL

Johnstone and co-workers synthesized mono and bimetallic aluminum complexes (**1.38e–f** and **1.39a–f**, Figure 1.24) containing a piperazine backbone and tested their efficacies in ε-CL polymerization.[89] Polymerizations were run in toluene at 60 °C for 24 h. The bimetallic complex **1.38e** proved to be the most active catalyst, affording 68% conversion, while the monometallic methoxide **1.39a** furnished 47% conversion. The remaining complexes (**1.39b–c** and **1.39e–f**) afforded 12–29% conversion, except for **1.39d** which was inactive. Non-linearity was observed in the polymer molecular weight growth over time, thus these polymerizations do not exhibit living character (no dispersity or molecular weight data were reported otherwise).

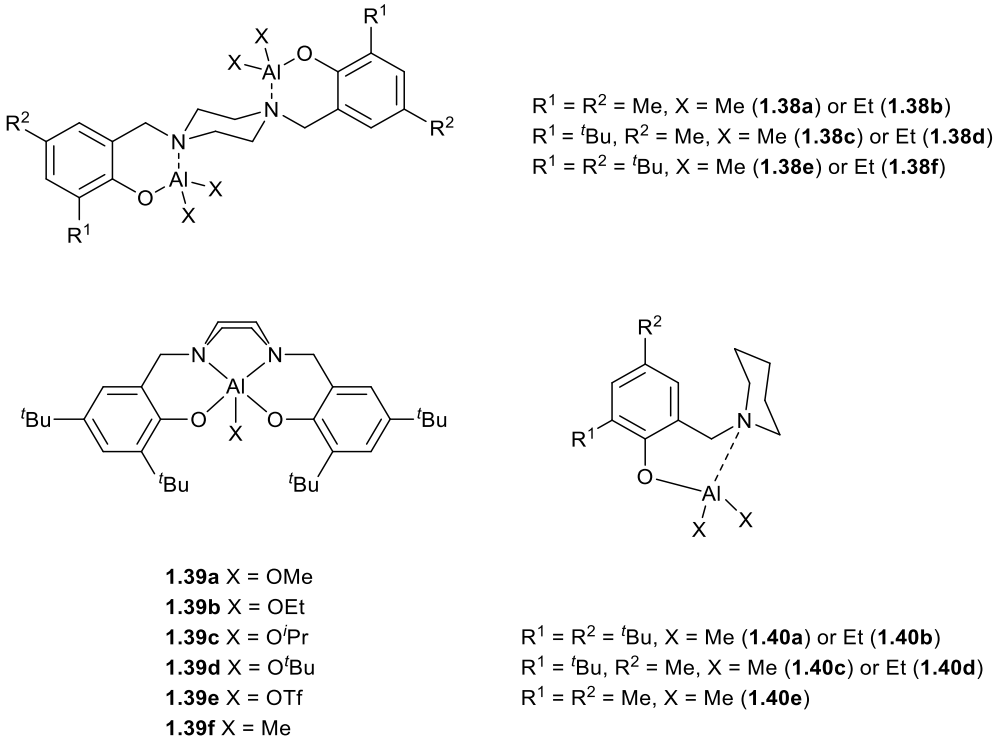

Figure 1.24. Mono and bimetallic aluminum amino-phenolate complexes for ROP of ε-CL

Building on these findings, Yao's group reported a more in-depth study in ROP of ε-CL comparing mono and bimetallic aluminum complexes (**1.38a–f** and **1.40a–e**, Figure 1.24).[90-91] The monometallic analogues (**1.40a–e**) of the piperazine bimetallic complexes were prepared with amino-phenolate ligands containing a piperidinyl donor at the *ortho* position. Polymerizations were run in the presence and absence of EtOH in toluene. At 70 °C in the absence of co-initiator, the monometallic systems **1.40a–e** were significantly less active (TOF 5.4–16 h^{-1}) than their bimetallic counterparts **1.38a–f** (TOF 17–46 h^{-1}). The PCL obtained exhibited broad dispersities ($Đ$ = 1.47–2.04) indicating poor control of polymerization. Kinetic studies at various temperatures focused on the most active

bimetallic complex **1.38d** and its monometallic analogue **1.40d**. The apparent polymerization rate constant was 2–8 times higher for **1.38d** compared to **1.40d** over the temperature range of 50–90 °C, and Eyring analyses showed this was due to the higher Gibbs energy barrier for polymerization initiated by **1.40d**. Thus, a cooperative effect of two aluminum centres was proposed.

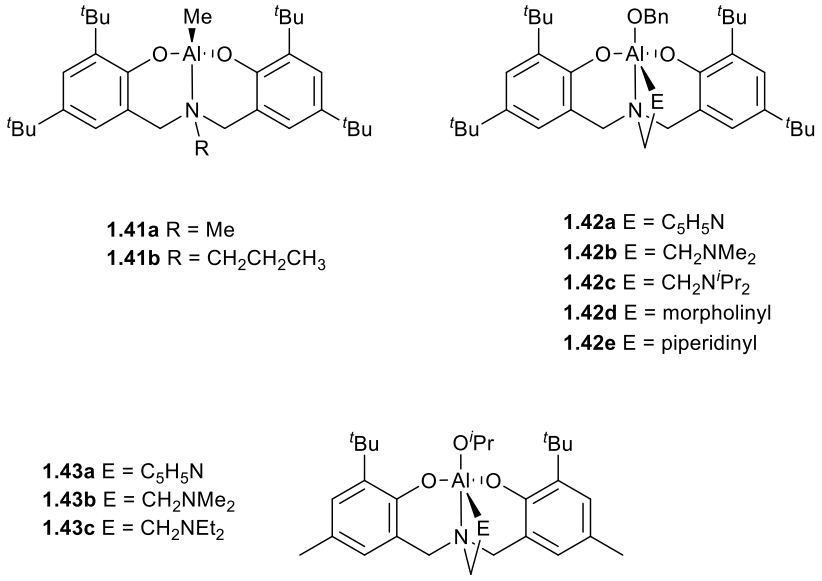

Figure 1.25. Aluminum amino-bis(phenolate) complexes for ROP of ε-CL

The group of Huang reported four-coordinate aluminum amino-bis(phenolate) complexes (**1.41a–b**, Figure 1.25) for ε-CL polymerization.[92] Polymerizations were carried out in toluene at 50 °C in the presence of BnOH. In nearly all cases, quantitative conversion was reached after 15–30 min. The isolated PCLs exhibited narrow dispersities ($Đ$ = 1.04–1.13) and molecular weights determined using NMR spectroscopy were in excellent agreement with the calculated values, supporting a living ROP process.

Shaver and co-workers also investigated a series of aluminum amino-bis(phenolate) complexes (**1.42a–e**, Figure 1.25) for ROP of ε-CL.[93] Polymerizations were conducted in toluene. At 25 °C, the best control was exhibited by **1.42d**, giving a narrow dispersity ($Đ$ = 1.09) and excellent agreement with calculated molecular weights ($M_{n,calcd}$ = 10.1 kDa; M_n 10.6 kDa). The activity of the complexes in increasing order is C_5H_5N (**1.42a**) << NMe_2 (**1.42b**) << morpholinyl (**1.42d**) < N^iPr_2 (**1.42c**) < piperidinyl (**1.42e**). Higher temperature (50 °C) was generally detrimental to activities but the weaker performing complexes (**1.42a–b**) became considerably more active under these conditions.

Phomphrai and co-workers studied a series of aluminum amino-bis(phenolate) complexes (**1.43a–c**, Figure 1.25) for ROP of ε-CL.[94] The complexes were differentiated by the pendent donors, which have different steric and electronic effects. The polymerization activities of the complexes increased in the order pyridyl (**1.43a**) < dimethylamino (**1.43b**) < diethylamino (**1.43c**), with **1.43c** quickly converting 92% ε-CL in 2.5 min (TOF 110 min^{-1}). Good dispersities were obtained ($Đ$ = 1.18–1.30) although the molecular weights diverged considerably from the calculated values for the highly active complex **1.43c** ($M_{n,calcd}$ = 31.5 kDa; M_n 52.1 kDa). Steric effects were believed to be negligible as the aluminum intermediate after ε-CL insertion remains five-coordinate, that is, no stable metallacycle is formed. On the other hand, electronic effects rationalized the observed activity trend, that is, the greater basicity of the pendent donor (basicity order: pyridyl < dimethylamino < diethylamino) promoted the displacement of the nucleophilic alkoxide group.

1.9.2 Cationic Aluminum Catalysts for ROP of ε-Caprolactone

It is worth mentioning that the use of cationic aluminum systems for ROP of cyclic esters and carbonates has been much less studied compared to zinc and alkali metal cations, whereas in ROP of epoxides cationic aluminum complexes have been much more successful. Dagorne and co-workers investigated cationic Al-alkyl and -alkoxide complexes (**1.44–46**, Figure 1.26) for ε-CL polymerization.[95] The presence of ε-CL stabilized **1.44** which otherwise formed complex mixtures or decomposition products if synthesized using $B(C_6F_5)_3$ alone. Polymerizations were performed in CH_2Cl_2 at room temperature or 45 °C. **1.44** and **1.45** were inactive for ROP but did react with one equiv of ε-CL to form stable isolable adducts. In contrast, **1.46** showed good ROP activity, for instance, converting 46% ε-CL within 3 min at 45 °C. The molecular weights were in very good agreement with the calculated values, with fair dispersities ($Đ$ = 1.28–1.53) showing that a fairly well-controlled ROP was taking place.

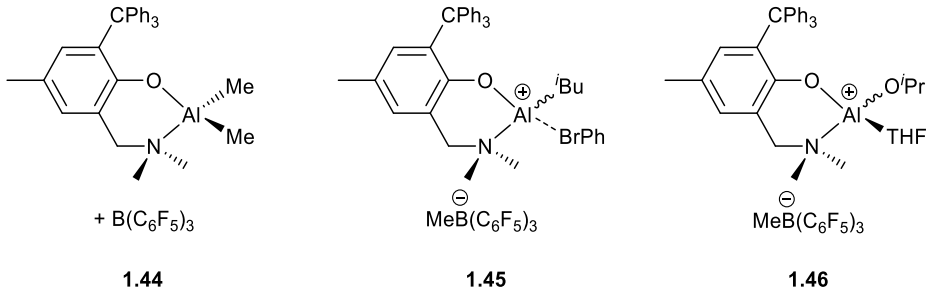

Figure 1.26. Neutral and cationic aluminum complexes for ROP of ε-CL

Very recently, Phomphrai and co-workers prepared neutral and cationic aluminum complexes containing furfuryl pendent donors (**1.47a-b**, **1.47a$^+$[MeB(C$_6$F$_5$)$_3$]**, and **1.47a$^+$[B(C$_6$F$_5$)$_4$]**, Figure 1.27) and compared their abilities for ROP of ε-CL.[96] NMR

studies on the cationic complexes supported a monometallic cation and the labile nature of the pendent donors appeared to stabilize the low-coordinate cationic aluminum. Polymerizations were performed in CH_2Cl_2 at room temperature. For the neutral complexes **1.47a** and **1.47b**, only traces of PCL were observed after extended reaction times, even when BnOH was added to **1.47b**. In contrast, the cationic complexes fared better with BnOH, with **1.47a$^+$[MeB(C$_6$F$_5$)$_3$]** attaining 97% conversion in 2 h, furnishing PCL with good dispersity ($Đ$ = 1.21). The polymerization was slightly slower using **1.47a$^+$[B(C$_6$F$_5$)$_4$]**, possibly since a bulkier anion sterically hinders access to the aluminum centre.

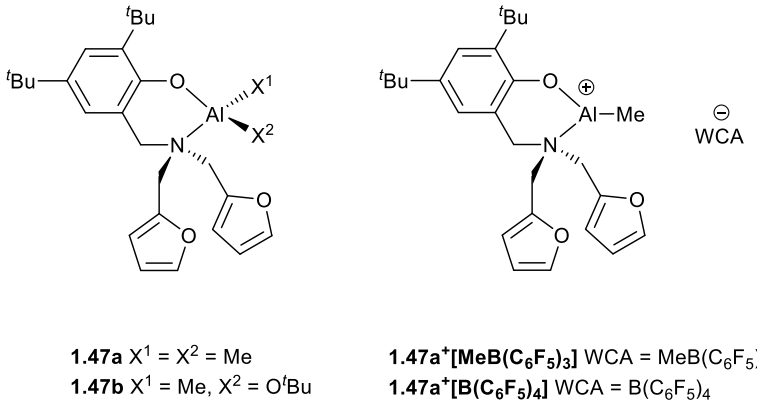

Figure 1.27. Neutral and cationic aluminum complexes for ROP of ε-CL

1.10 Objectives and Outline of the Thesis

The morpholine moiety has been often reported in catalyst structures but little is known about the underlying role it plays in reactivity. The structure-activity relationships of the morpholine group prompted us to examine catalysts containing this moiety in more detail.

In Chapter 2, the catalytic activities of chloro-aluminum complexes toward the ROP of cyclohexene oxide is described. Chapter 3 introduces the synthesis and characterization of a series of cationic aluminum amino-bis(phenolate) complexes bearing a morpholinyl donor. These cations were applied as catalysts in the ROP of ε-caprolactone in the presence of EtOH. Chapter 4 introduces the preparation and characterization of aluminum amino-phenolate complexes bearing various pendent donors. The catalytic activity of these complexes towards the copolymerization of cyclohexene oxide and CO_2 is described.

Bimetallic systems have been frequently been reported for ROCOP of epoxides/CO_2 and impressive activities under atmospheric pressures of CO_2 have been obtained. However, the surface has barely been scratched with respect to bimetallic aluminum systems in this area, which is surprising given that bimetallic aluminum systems are ubiquitous in ROP of epoxides and some of the most impressive systems reported for cycloaddition of PO/CO_2 are bimetallic aluminum salen-oxo complexes. Hence, in Chapter 5, the synthesis and characterization of a bimetallic aluminum amino-bis(phenolate) complex and its monometallic analogue is described. Their catalytic activities towards ROCOP of CHO and CO_2 is investigated. Chapter 6 primarily focuses on the development of more active aluminum systems for ROCOP of CHO and CO_2 including the synthesis of new pro-ligands (or use of linkers) that can accommodate two aluminum centres.

1.11 References

1. M. Lancaster, *Green Chemistry: An Introductory Text*, Royal Society of Chemistry, Cambridge, UK, 2 ed., 2010.
2. P. A. Wilbon, F. Chu and C. Tang, *Macromol. Rapid Commun.*, **2013**, *34*, 8-37.
3. M. F. Costa and M. Barletta, *Environ. Sci.: Processes Impacts*, **2015**, *17*, 1868-1879.
4. J. A. Ivar do Sul and M. F. Costa, *Environ. Pollut.*, **2014**, *185*, 352-364.
5. D. Xanthos and T. R. Walker, *Mar. Pollut. Bull.*, **2017**, *118*, 17-26.
6. G. L. Gregory, E. M. Lopez-Vidal and A. Buchard, *Chem. Commun.*, **2017**, *53*, 2198-2217.
7. M. Hong and E. Y. X. Chen, *Nat. Chem.*, **2015**, *8*, 42-49.
8. X. Zhang, M. Fevre, G. O. Jones and R. M. Waymouth, *Chem. Rev.*, **2018**, *118*, 839-885.
9. J. H. Clark, T. J. Farmer, L. Herrero-Davila and J. Sherwood, *Green Chem.*, **2016**, *18*, 3914-3934.
10. https://newplasticseconomy.org/projects/global-commitment).
11. M. Aresta, A. Dibenedetto and A. Angelini, *Chem. Rev.*, **2014**, *114*, 1709-1742.
12. N. A. Tappe, R. M. Reich, V. D'Elia and F. E. Kühn, *Dalton Trans.*, **2018**, *47*, 13281-13313.
13. T. Sakakura, J.-C. Choi and H. Yasuda, *Chem. Rev.*, **2007**, *107*, 2365-2387.
14. S. Fukuoka, M. Kawamura, K. Komiya, M. Tojo, H. Hachiya, K. Hasegawa, M. Aminaka, H. Okamoto, I. Fukawa and S. Konno, *Green Chem.*, **2003**, *5*, 497-507.
15. A. Yoshino, 1 - Development of the Lithium-Ion Battery and Recent Technological Trends, in *Lithium-Ion Batteries*, ed. G. Pistoia, Elsevier, Amsterdam, 2014, pp. 1-20.
16. M. Taherimehr and P. P. Pescarmona, *J. Appl. Polym. Sci.*, **2014**, *131*, n/a-n/a.
17. Y. Wang and D. J. Darensbourg, *Coord. Chem. Rev.*, **2018**, *372*, 85-100.
18. M. J. L. Tschan, E. Brulé, P. Haquette and C. M. Thomas, *Polym. Chem.*, **2012**, *3*, 836-851.
19. F.-T. Tsai, Y. Wang and D. J. Darensbourg, *J. Am. Chem. Soc.*, **2016**, *138*, 4626-4633.
20. T. Artham and M. Doble, *Macromol. Biosci.*, **2008**, *8*, 14-24.
21. C. M. Byrne, S. D. Allen, E. B. Lobkovsky and G. W. Coates, *J. Am. Chem. Soc.*, **2004**, *126*, 11404-11405.
22. C. Martín and A. W. Kleij, *Macromolecules*, **2016**, *49*, 6285-6295.
23. O. Hauenstein, S. Agarwal and A. Greiner, *Nature Communications*, **2016**, *7*, 11862.
24. M. Winkler, C. Romain, M. A. R. Meier and C. K. Williams, *Green Chem.*, **2015**, *17*, 300-306.
25. A. Arbaoui and C. Redshaw, *Polym. Chem.*, **2010**, *1*, 801-826.
26. M. Labet and W. Thielemans, *Chem. Soc. Rev.*, **2009**, *38*, 3484-3504.
27. A.-L. Brocas, C. Mantzaridis, D. Tunc and S. Carlotti, *Prog. Polym. Sci.*, **2013**, *38*, 845-873.

28. M. I. Childers, J. M. Longo, N. J. Van Zee, A. M. LaPointe and G. W. Coates, *Chem. Rev.*, **2014**, *114*, 8129-8152.
29. J. Herzberger, K. Niederer, H. Pohlit, J. Seiwert, M. Worm, F. R. Wurm and H. Frey, *Chem. Rev.*, **2016**, *116*, 2170-2243.
30. Y. Sarazin and J.-F. Carpentier, *Chem. Rev.*, **2015**, *115*, 3564-3614.
31. A. J. Downs, *Chemistry of Aluminium, Gallium, Indium and Thallium*, Springer Netherlands, 1993.
32. J. Lewinski and A. E. H. Wheatley, *Top. Organomet. Chem.*, **2013**, *41*, 1-58.
33. E. L. Bastos, F. H. Bartoloni and L. C. P. Gonçalves, Acid–Base and Solvation Properties of Metal Phenolates, in *PATAI'S Chemistry of Functional Groups*, ed. Z. Rappoport, 2012, pp. 1-72.
34. E. L. Bastos and C. O. Machado, Recent Advances in Acid–Base and Solvation Properties of Metal Phenolates, in *PATAI'S Chemistry of Functional Groups*, ed. Z. Rappoport, 2017, pp. 1-60.
35. O. Wichmann, R. Sillanpää and A. Lehtonen, *Coord. Chem. Rev.*, **2012**, *256*, 371-392.
36. C. S. Higham, D. P. Dowling, J. L. Shaw, A. Cetin, C. J. Ziegler and J. R. Farrell, *Tetrahedron Lett.*, **2006**, *47*, 4419-4423.
37. F. M. Kerton, S. Holloway, A. Power, R. G. Soper, K. Sheridan, J. M. Lynam, A. C. Whitwood and C. E. Willans, *Can. J. Chem.*, **2008**, *86*, 435-443.
38. K. L. Collins, L. J. Corbett, S. M. Butt, G. Madhurambal and F. M. Kerton, *Green Chem. Lett. Rev.*, **2007**, *1*, 31-35.
39. S. Dagorne, M. Bouyahyi, J. Vergnaud and J.-F. Carpentier, *Organometallics*, **2010**, *29*, 1865-1868.
40. J.-T. Issenhuth, J. Pluvinage, R. Welter, S. Bellemin-Laponnaz and S. Dagorne, *Eur. J. Inorg. Chem.*, **2009**, *2009*, 4701-4709.
41. M.-A. Munoz-Hernandez, M. L. McKee, T. S. Keizer, B. C. Yearwood and D. A. Atwood, *J. Chem. Soc., Dalton Trans.*, **2002**, 410-414.
42. B. Y. Liu, H. Q. Li, C. S. Ha, I. Kim and W. D. Yan, *Macromol. Res.*, **2008**, *16*, 441-445.
43. F. Isnard, M. Lamberti, L. Lettieri, I. D'Auria, K. Press, R. Troiano and M. Mazzeo, *Dalton Trans.*, **2016**, *45*, 16001-16010.
44. W. Li, H. Ouyang, L. Chen, D. Yuan, Y. Zhang and Y. Yao, *Inorg. Chem.*, **2016**, *55*, 6520-6524.
45. J. Wei, M. N. Riffel and P. L. Diaconescu, *Macromolecules*, **2017**, *50*, 1847-1861.
46. X. Sheng, W. Wu, Y. Qin, X. Wang and F. Wang, *Polym. Chem.*, **2015**, *6*, 4719-4724.
47. C. Martín, G. Fiorani and A. W. Kleij, *ACS Catal.*, **2015**, *5*, 1353-1370.
48. M. North, R. Pasquale and C. Young, *Green Chem.*, **2010**, *12*, 1514-1539.
49. M. W. Lehenmeier, C. Bruckmeier, S. Klaus, J. E. Dengler, P. Deglmann, A. K. Ott and B. Rieger, *Chem. Eur. J.*, **2011**, *17*, 8858-8869.
50. D. J. Darensbourg, J. C. Yarbrough, C. Ortiz and C. C. Fang, *J. Am. Chem. Soc.*, **2003**, *125*, 7586-7591.

51. S. Inoue, H. Koinuma and T. Tsuruta, *J. Polym. Sci., Part B: Polym. Lett.*, **1969**, *7*, 287-292.
52. S. Inoue, H. Koinuma and T. Tsuruta, *Makromol. Chem.*, **1969**, *130*, 210-220.
53. N. Takeda and S. Inoue, *Makromol. Chem.*, **1978**, *179*, 1377-1381.
54. D. J. Darensbourg and M. W. Holtcamp, *Macromolecules*, **1995**, *28*, 7577-7579.
55. M. Cheng, E. B. Lobkovsky and G. W. Coates, *J. Am. Chem. Soc.*, **1998**, *120*, 11018.
56. M. Cheng, D. R. Moore, J. J. Reczek, B. M. Chamberlain, E. B. Lobkovsky and G. W. Coates, *J. Am. Chem. Soc.*, **2001**, *123*, 8738-8749.
57. D. R. Moore, M. Cheng, E. B. Lobkovsky and G. W. Coates, *Angew. Chem. Int. Ed.*, **2002**, *41*, 2599-2602.
58. D. R. Moore, M. Cheng, E. B. Lobkovsky and G. W. Coates, *J. Am. Chem. Soc.*, **2003**, *125*, 11911-11924.
59. E. N. Jacobsen, *Acc. Chem. Res.*, **2000**, *33*, 421-431.
60. D. J. Darensbourg, *Chem. Rev.*, **2007**, *107*, 2388-2410.
61. D. J. Darensbourg, R. M. Mackiewicz, J. L. Rodgers, C. C. Fang, D. R. Billodeaux and J. H. Reibenspies, *Inorg. Chem.*, **2004**, *43*, 6024-6034.
62. D. J. Darensbourg, R. M. Mackiewicz and D. R. Billodeaux, *Organometallics*, **2005**, *24*, 144-148.
63. C. M. Kozak, K. Ambrose and T. S. Anderson, *Coord. Chem. Rev.*, **2018**, *376*, 565-587.
64. K. Nakano, T. Kamada and K. Nozaki, *Angew. Chem. Int. Ed.*, **2006**, *45*, 7274-7277.
65. M. R. Kember, P. D. Knight, P. T. R. Reung and C. K. Williams, *Angew. Chem. Int. Ed.*, **2009**, *121*, 949-951.
66. A. Buchard, M. R. Kember, K. G. Sandeman and C. K. Williams, *Chem. Commun.*, **2011**, *47*, 212-214.
67. M. R. Kember, A. J. P. White and C. K. Williams, *Inorg. Chem.*, **2009**, *48*, 9535-9542.
68. M. R. Kember and C. K. Williams, *J. Am. Chem. Soc.*, **2012**, *134*, 15676-15679.
69. M. R. Kember, F. Jutz, A. Buchard, A. J. P. White and C. K. Williams, *Chem. Sci.*, **2012**, *3*, 1245-1255.
70. M. R. Kember, A. J. P. White and C. K. Williams, *Macromolecules*, **2010**, *43*, 2291-2298.
71. F. Jutz, A. Buchard, M. R. Kember, S. B. Fredriksen and C. K. Williams, *J. Am. Chem. Soc.*, **2011**, *133*, 17395-17405.
72. P. K. Saini, C. Romain and C. K. Williams, *Chem. Commun.*, **2014**, *50*, 4164-4167.
73. C. Chatterjee and M. H. Chisholm, *Inorg. Chem.*, **2011**, *50*, 4481-4492.
74. W. Wu, X. Sheng, Y. Qin, L. Qiao, Y. Miao, X. Wang and F. Wang, *J. Polym. Sci., Part A: Polym. Chem.*, **2014**, *52*, 2346-2355.
75. X. Sheng, Y. Wang, Y. Qin, X. Wang and F. Wang, *RSC Adv.*, **2014**, *4*, 54043-54050.
76. T. Sârbu and E. J. Beckman, *Macromolecules*, **1999**, *32*, 6904-6912.
77. D. J. Darensbourg and D. R. Billodeaux, *Inorg. Chem.*, **2005**, *44*, 1433-1442.

78. H. Sugimoto, H. Ohtsuka and S. Inoue, *J. Polym. Sci., Part A: Polym. Chem.*, **2005**, *43*, 4172-4186.
79. T. A. Zevaco, J. Sypien, A. Janssen, O. Walter and E. Dinjus, *Catal. Today*, **2006**, *115*, 151-161.
80. T. A. Zevaco, J. K. Sypien, A. Janssen, O. Walter and E. Dinjus, *J. Organomet. Chem.*, **2007**, *692*, 1963-1973.
81. M. A. Fuchs, C. Altesleben, T. A. Zevaco and E. Dinjus, *Eur. J. Inorg. Chem.*, **2013**, *2013*, 4541-4545.
82. W. Kuran, T. Listos, M. Abramczyk and A. Dawidek, *J. Macromol. Sci. A*, **1998**, *35*, 427-437.
83. N. Ikpo, J. C. Flogeras and F. M. Kerton, *Dalton Trans.*, **2013**, *42*, 8998-9006.
84. N. Ikpo, S. M. Barbon, M. W. Drover, L. N. Dawe and F. M. Kerton, *Organometallics*, **2012**, *31*, 8145-8158.
85. L. Peña Carrodeguas, J. González-Fabra, F. Castro-Gómez, C. Bo and A. W. Kleij, *Chem. Eur. J.*, **2015**, *21*, 6115-6122.
86. T. Rosen, I. Goldberg, W. Navarra, V. Venditto and M. Kol, *Angew. Chem. Int. Ed.*, **2018**, *130*, 7309-7313.
87. A. Hanft, M. Jürgensen, R. Bertermann and C. Lichtenberg, *ChemCatChem*, **2018**, *10*, 4018-4027.
88. C.-L. Lee, Y.-F. Lin, M.-T. Jiang, W.-Y. Lu, J. K. Vandavasi, L.-F. Wang, Y.-C. Lai, M. Y. Chiang and H.-Y. Chen, *Organometallics*, **2017**, *36*, 1936-1945.
89. N. C. Johnstone, E. S. Aazam, P. B. Hitchcock and J. R. Fulton, *J. Organomet. Chem.*, **2010**, *695*, 170-176.
90. W. Li, W. Wu, Y. Wang, Y. Yao, Y. Zhang and Q. Shen, *Dalton Trans.*, **2011**, *40*, 11378-11381.
91. L. Chen, W. Li, D. Yuan, Y. Zhang, Q. Shen and Y. Yao, *Inorg. Chem.*, **2015**, *54*, 4699-4708.
92. C.-T. Chen, C.-A. Huang and B.-H. Huang, *Macromolecules*, **2004**, *37*, 7968-7973.
93. E. D. Cross, G. K. Tennekone, A. Decken and M. P. Shaver, *Green Mater.*, **2013**, *1*, 79-86.
94. K. Phomphrai, P. Chumsaeng, P. Sangtrirutnugul, P. Kongsaeree and M. Pohmakotr, *Dalton Trans.*, **2010**, *39*, 1865-1871.
95. S. Dagorne, F. Le Bideau, R. Welter, S. Bellemin-Laponnaz and A. Maisse-François, *Chem. Eur. J.*, **2007**, *13*, 3202-3217.
96. J. Kiriratnikom, S. Chotchatchawankul, S. Haesuwannakij, S. Kiatisevi and K. Phomphrai, *New J. Chem.*, **2018**, *42*, 8374-8383.

1.12 Co-Authorship Statement

This PhD thesis includes results of joint research that have been published in peer reviewed journals in the form of two papers, as follows:

Chapter 2: Ring-opening polymerization of cyclohexene oxide using aluminum amine-phenolate complexes.

Authors: Hart Plommer, Immanuel Reim, and Francesca M. Kerton

Journal: *Dalton Trans.*, **2015**, *44*, 12098–12102.

The principal author (Hart Plommer) contributed to all aspects of the project as the main researcher including performing approximately 80% of all the experiments, collecting and analyzing the data, mentoring undergraduate student intern Immanuel Reim, and writing the first draft of the manuscript.

The co-author (Immanuel Reim) ran approximately 20% of the experiments, helping synthesize Al complexes and run polymerization reactions.

The corresponding author (Dr. Francesca M. Kerton) was the principal investigator and developed the original ideas for the research. She oversaw all aspects of the project including supervision of the principal author (H. P.) and co-author (I. R.), experimental design, data analysis, manuscript revisions and journal submission, and responses to peer reviewer questions and comments.

Chapter 3: Morpholine-Stabilized Cationic Aluminum Complexes and Their Reactivity in Ring-Opening Polymerization of ε-Caprolactone.

Authors: Hart Plommer, Jennifer N. Murphy, Louise N. Dawe, and Francesca M. Kerton

Journal: *Inorg. Chem.*, **2019**, *58*, 5253–5264.

The principal author (Hart Plommer) contributed to all aspects of the project as the main researcher including performing all of the experiments, collecting and analyzing the data, writing the first draft of the manuscript, and addressing peer reviewer questions and comments in subsequent drafts.

The co-author (Jennifer N. Murphy) collected the XRD data and solved the structures for the complexes.

The co-author (Dr. Louise N. Dawe) verified the XRD structure solutions and mentored the co-author (J. N. M.).

The corresponding author (Dr. Francesca M. Kerton) was the principal investigator and developed the original ideas for the research. She oversaw all aspects of the project including supervision of the principal author (H. P.) and co-author (J. N. M.), experimental design, data analysis, manuscript revisions and journal submission, and responses to peer reviewer questions and comments.

In addition, this thesis includes results of joint research that are currently in preparation for publication in a peer reviewed journal, as follows:

Chapter 4: Copolymerization of CHO/CO_2 Catalyzed by Aluminum Amino-Phenolate Complexes

Authors: Hart Plommer, Laura Stein, Jennifer N. Murphy, Nduka Ikpo, Louise N. Dawe, Nelaine Mora-Diez, and Francesca M. Kerton.

The principal author (Hart Plommer) contributed to all aspects of the project as the main researcher including performing approximately 80% of all the experiments, collecting and analyzing the data, mentoring undergraduate student intern Laura Stein, and writing the first draft of the manuscript.

The co-author (Laura Stein) ran approximately 20% of the experiments, helping synthesize Al complexes and run polymerization reactions.

The co-author (Jennifer N. Murphy) collected the XRD data and solved the structures for the complexes.

The co-author (Dr. Nduka Ikpo) synthesized and fully characterized a pro-ligand.

The co-author (Dr. Louise N. Dawe) verified the XRD structure solutions and mentored the co-author (J. N. M.).

The co-author (Dr. Nelaine Mora-Diez) assisted with the computational section.

The corresponding author (Dr. Francesca M. Kerton) was the principal investigator and developed the original ideas for the research. She oversaw all aspects of the project including supervision of the principal author (H. P.) and co-authors (J. N. M. and L.S.), experimental design, data analysis, and manuscript revisions.

CHAPTER 2

Ring-Opening Polymerization of Cyclohexene Oxide Using Aluminum Amino-Phenolate Complexes

Chapter 2. Ring-Opening Polymerization of Cyclohexene Oxide Using Aluminum Amino-Phenolate Complexes

A version of this chapter has been published

Hart Plommer, Immanuel Reim, and Francesca M. Kerton

Dalton Trans., **2015**, *44*, 12098-12102. Themed issue: Earth abundant element compounds in homogeneous catalysis

Some modifications were made to the original paper for inclusion as a chapter in this thesis.

2.1 Introduction

Aluminum is the most abundant of all metals in the earth's crust and its complexes can be used as Lewis acid catalysts or as co-catalysts for a range of reactions.[1-2] In particular, they have found broad applicability as homogeneous catalysts in polymerization processes.[3] Recently, significant attention has been given to their use in ROP reactions of lactide and ε-CL that yield biodegradable polyesters of controlled molecular weight and near uniform dispersity.[4-20] They are also being widely explored as catalysts for reactions of CO_2 with epoxides that yield either polycarbonates or cyclic carbonate products.[21-41] Aluminum species can also be active for polymerizations of PO,[42-48] CHO,[5, 28, 49] and CHO/anhydride[50] and PO/lactide copolymerizations.[51] The areas of polyether synthesis and stereoselective polymerization/copolymerizations of epoxides have recently been

reviewed and provide good overviews of the concepts and possible mechanistic considerations in these reactions.[52-53]

The Kerton group have previously shown that chloro-aluminum complexes of *N*-morpholinyl and *N*-piperazinyl amino-phenolate ligands, including **2.1–2.2** (Scheme 2.1) herein, were active in ROP of ε-CL to yield polymers with the general formula (Cl{ε-CL}$_n$OH) i.e. containing chloride end groups.[54] It was proposed that these reactions proceeded in a similar manner to ROP of trimethylene carbonate using aluminum-salen chloride catalysts,[55] which is to say that reactions proceed *via* insertion into the Al–Cl bond. It was also shown that **2.1** was catalytically active in CHO/CO_2 copolymerization to yield copolymers with a mix of ether and carbonate linkages i.e. poly(ether-*co*-carbonates).[54] Because of the relatively large number of ether linkages in these polymers, an investigation into the first step in this process was pursued, namely, the reaction of CHO with aluminum chloride complexes.

2.2 Results and Discussion

Complexes **2.1** and **2.2** are easily prepared in near quantitative yields *via* alkane elimination reactions of diethylaluminum chloride with 2 equiv of the corresponding protio ligand (Scheme 2.1). Attempts to investigate the interaction of one equivalent of CHO with the aluminum complexes on an NMR scale in a range of solvents were unsuccessful due to the fluxional nature of the complexes. Therefore, larger amounts of CHO were added to samples and it was discovered that polyether forms.

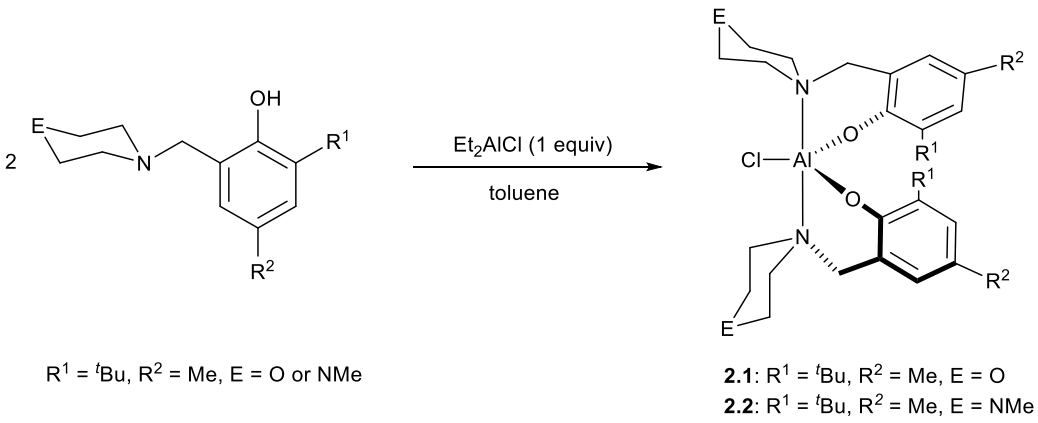

R^1 = ^{t}Bu, R^2 = Me, E = O or NMe

2.1: R^1 = ^{t}Bu, R^2 = Me, E = O
2.2: R^1 = ^{t}Bu, R^2 = Me, E = NMe

Scheme 2.1. Synthesis of aluminum amino-phenolate complexes **2.1–2.2**

2.3 Polymerization of CHO

ROP of CHO was carried out using complexes **2.1** and **2.2** (Table 2.1) in the absence of solvent at room temperature. In most cases, polymerization occurred rapidly to yield a viscous monomer-polymer mixture that could no longer be stirred magnetically. For **2.2** however, the polymerizations were much slower, leading to less viscous solutions even after extended reaction times. This indicates that the nature of the outer-sphere heteroatom in the *N*-containing heterocycle has a significant effect on these reactions. Differences in reactivity between **2.1** and **2.2** were also seen in ROP of ε-CL and CHO/CO_2 copolymerizations.[54]

Table 2.1. Polymerization of CHO using **2.1–2.3**[a]

Entry	Complex	[CHO]/[Al]	t (min)	Conv. (%) [% yield]	M_n[b,c] × 10^3	$Đ$[b]	TOF (min^{-1})
1	**2.1**	100000/1	60	15 [13]	500	1.17	250
2	**2.1**	1000/1	1	58 [53]	180	1.20	580
3	**2.2**	1000/1	50	15 [6]	–	–	3
4	**2.2**	200/1	30	16 [3]	76.2	1.15	1
5	**2.3**	10000/1	1260	<1%	–	–	–
6	**2.3**	1000/1	45	29	262	1.36	6
7	**2.3**	500/1	25	49	255	1.21	10
8	**2.3**	200/1	2	56	125	1.12	56
9[d]	**2.3**	500/1	40	66	110	1.08	8

[a] Reactions were performed neat at room temperature in the absence of solvent unless otherwise indicated in an inert atmosphere workstation. Conversions determined by ^{1}H NMR spectroscopy. Isolated yields indicated in square brackets. [b] Determined by GPC equipped with a multi-angle light scattering detector. [c] In Da. [d] Reaction performed in the presence of 160 μL toluene. Note, 7% conversion was obtained after 18 h in 5 mL toluene.

In an effort to determine the important structural features of active complexes, **2.3** was prepared (Scheme 2.2). Amino-bis(phenolate) aluminum-alkyl and -alkoxide complexes similar to **2.3** have been prepared previously and used for ROP of lactide.[56-57] **2.3** showed good activity in ROP of CHO and using small amounts of toluene a higher conversion and less disperse polymer could be obtained compared to the neat reactions (entries 9 and 7). In contrast to **2.1**, catalyst loadings could not be reduced past 0.1 mol%.

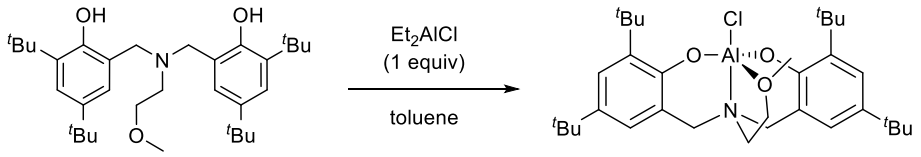

H_2[**L1**] **2.3**

Scheme 2.2. Synthesis of aluminum amino-bis(phenolate) complex **2.3**

The activities of these aluminum amino-phenolate complexes are clearly dependent on the nature of the ligand. Since the maximum conversion of CHO that can be attained during neat polymerization depends on the molecular weight of PCHO produced and the ability of CHO to solvate the catalyst and polymer, TOFs are the most practical way to compare the catalysts. The conversion of 1000 equiv of CHO was much quicker for **2.1** than **2.2** and **2.3** (Table 2.1, entries 2–3 and 6) and TOF values are an order of magnitude higher for **2.1**. The observed reactivity trend for complexes **2.1–2.3** is in the order **2.1** >> **2.3** > **2.2**. This implies that, although chloro complexes of both monoanionic and dianionic amino-phenolate ligands give rise to active species, there is a more complex relationship between ligand structure and reactivity at play that warrants further investigation. Control polymerizations were performed using two simple chloro-aluminum reagents under similar reaction conditions to those employed with **2.1–2.3**. $AlCl_3$ (0.5 mol%) or Et_2AlCl (0.25 mol%) gave TOFs (min^{-1}) of 4 and 160, respectively, and a maximum M_n of 32.0 kDa with relatively narrow dispersities (~1.3). These are significantly lower activities and molecular weights than achieved using **2.1** at similar loadings.

To avoid gelation and potentially increase conversions, some solution polymerizations with **2.1** were attempted using CH_2Cl_2, toluene or THF as reaction media. Reaction rates

were significantly reduced and for a 200:1 ratio of CHO: **2.1** in 5 mL solvent conversions of 28% (CH_2Cl_2), 18% (toluene) and <1% (THF) were obtained after 20 h. The latter may be due to THF preferentially coordinating to the Al centre over CHO. Darensbourg and Chung have recently reinvestigated the basicities of a range of ethers and esters,[58] and this statement is in agreement with the reported pK_b values. A difference in reactivity for ROP reactions in CH_2Cl_2 and toluene was also observed by Martínez *et al.*[49] in their study of multinuclear Al complexes for CHO polymerizations, e.g. 96% yield in CH_2Cl_2 and 75% yield in toluene. They found that the addition of benzenesulfonyl chloride to toluene improved activities, reaching similar conversions to those performed in CH_2Cl_2 with no chloride additive. This suggests that the chloride group is important in these ROP reactions.

Of note is the very low loadings of **2.1** that could be used, 0.001 mol% relative to CHO (Table 2.1, entry 1), giving low conversion (15%) of CHO but yielding a polymer with very high M_n (500 kDa) and uniform dispersity. The only catalysts reported to date for CHO polymerization that can produce such high molecular weight polymers (albeit at longer reaction times) are group 4 benzotriazole-phenolate complexes, which could achieve M_n values of up to 980 kDa.[59] Other systems reported that give PCHO with high molecular weights include the rare earth catalysts of Cui and co-workers[60] that attain M_n up to 147 kDa with a dispersity of 2.38, as well as the Zn and Mg catalysts prepared by Bochmann and co-workers[61] that achieve up to 380 kDa with a dispersity of 3.8. It should be noted that previous authors invariably report M_n determined *via* GPC calibrated with polystyrene standards, and therefore some care must be taken in making direct comparisons with the results based on multi-angle light scattering reported herein.

2.4 Attempted ROP of Other Epoxides

The polymerization of various other epoxides (PO, styrene oxide, LO, and epichlorohydrin) was attempted using **2.1–2.3** (Table F.1). In all cases, including microwave heated reactions conducted at 60 °C with propylene oxide and at 130 °C with LO, no polymer was detected by ^{1}H NMR. Catalysts for ROP of CHO containing a range of other metals such as iron,[62] zinc, magnesium,[61] uranium,[63-64] titanium, zirconium, and halfnium[59] are able to polymerize a number of different epoxides (e.g. PO, epichlorohydrin). Therefore, it was somewhat surprising that **2.1** could not polymerize any of the other monomers studied. It is well known that the ring-opening reactions of CHO are more facile than PO. It has been suggested that this is due to the release of extra strain energy upon polymerizing the bicyclic CHO monomer,[65] but more recently others have shown that the strain energies of CHO and PO are essentially the same.[66] This is also reflected by nearly identical enthalpies of polymerization: −96.7 kJ mol^{-1} for CHO[67] and −94.5 kJ mol^{-1} for PO (calculated using thermodynamic data in the NIST chemistry webbook). Therefore, differences in reactivity must be due to kinetic effects and thus determination of reaction pathways computationally would aid in discerning the differences observed experimentally. One possible reason for the differences in epoxide reactivity is steric i.e. the CHO monomer is slimmer, due to its bicyclic nature, than the other monomers studied,[63] and this means it can coordinate to the metal centre more readily prior to ring-opening by a nucleophile.

2.5 Polymer Analyses

MALDI-TOF mass spectra were obtained on the polymers in order to identify end-groups, as no phenolate or other end groups were seen in their ^{1}H NMR spectra. It has been reported that laser desorption techniques induce significant fragmentation of polyethers and consequently only small oligomers are seen when using this technique,[51] but these methods have been useful in identifying chloride end groups in polyethers and copolymers. The MALDI-TOF spectrum of the PCHO formed using **2.3** (Table 2.1, entry 9), Figure B.1, is described here. The spectrum shows two prominent series of peak distributions with a mass difference between them of 36 Da, which corresponds to the mass of HCl. Successive peak distributions of either series are separated by 98 Da which equals the mass of the CHO monomer. These data are consistent with the formation of sodium adducts of both cyclic PCHO ($\{CHO\}_n \cdot Na^+$) [e.g. n = 8, m/z 807.58 (expt), m/z 807.52 (calcd)] and PCHO chains, the latter being capped with hydroxyl and chloride end groups ($Cl\{CHO\}_nH \cdot Na^+$) [e.g. n = 8, m/z 843.55 (expt), m/z 843.50 (calcd)]. Since HCl was unable to catalyze these reactions under identical conditions, the identification of a chloride end group confirms the role of the chloride ligand in ring-opening of the epoxide. In previous research, PCL containing chloride end groups could be made with complex **2.2**.[54]

The polymers obtained with **2.1–2.3** were analyzed by DSC. Glass transition temperatures obtained were 68–69 °C, in agreement with values found for PCHO by Kim *et al*.,[68] who polymerized CHO to give PCHO with M_n in the range of 12.4 to 24.9 kDa. No exotherm corresponding to a crystallization process could be observed on cooling, indicating that these polymers are amorphous. The stereochemistry of the PCHO was

analyzed *via* ^{1}H and $^{13}C\{^{1}H\}$ NMR spectroscopy (Figures A.1–A.2). No stereocontrol was achieved in these polymerizations, as three peaks at δ 3.53, 3.44, and 3.37 in the ^{1}H NMR spectra were observed corresponding to the methine protons are characteristic of syndiotactic (*rr*), heterotactic (*rm* and *mr*), and isotactic (*mm*) triads. The atactic nature of the polymer was also confirmed by the presence of three broad peaks at δ 78.8, 77.7, and 75.6 (methine carbons) in the $^{13}C\{^{1}H\}$ NMR spectra. The stereochemistry is in accordance with the finding of others using similar achiral Al catalysts.[28, 49]

2.6 Kinetic Investigations

Kinetic studies on the ROP of CHO using **2.2** were carried out under neat conditions using a co-axial NMR tube containing $CDCl_3$ for locking. The slower reactivity of this catalyst meant it was a practical choice for NMR monitoring. These studies show that the polymerization is first-order in [Al], indicated by the linear relationship between k_{obs} and [**2.2**] (Figure 2.1). The slope of this graph gives a propagation rate of 0.0568 M^{-1} min^{-1}. More studies are needed to determine whether the reactions proceed *via* a monometallic (intramolecular) or bimetallic (intermolecular) mechanism. Namely, whether the chloride initiator originates on the same Al centre as the coordinated CHO or on a neighbouring complex. For recently reported ROP of epoxides using $[UO_2Cl_2(THF)_3]$ as a catalyst,[64] an intermolecular process is favoured and we think that a similar mechanism is at work in our catalyst system.

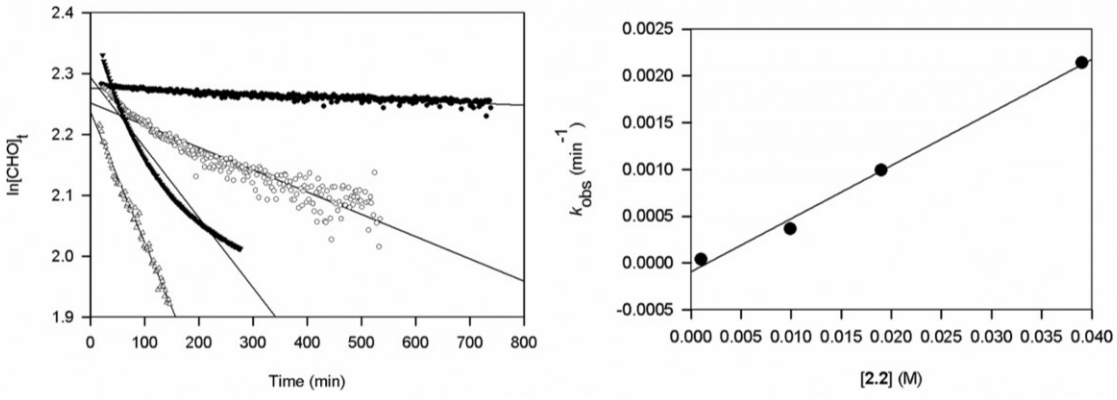

Figure 2.1. Plots of $\ln[CHO]_t$ against time at catalyst loadings 0.01 (●), 0.1 (○), 0.2 (▼) and 0.4 (Δ) mol% using **2.2** (left) and k_{obs} (min^{-1}) against [**2.2**] (M) (right)

2.7 Conclusions

In summary, it has been shown that amino-phenolate complexes of aluminum containing ancillary chloride ligands are active catalysts for ROP of CHO under neat conditions. In some cases, very low catalyst loadings (0.001%) can be used and high molecular weight amorphous polymers (M_n up to 500 kDa) are obtained. The reactions are generally inhibited in the presence of solvents, especially THF, and are first order in [Al]. The reactions are initiated by nucleophilic attack of the coordinated epoxide by a chloride anion, as evidenced by MALDI-TOF analysis of the resulting polymers. Further studies are needed to unequivocally determine whether the reaction proceeds *via* a monometallic or bimetallic process, and to determine the extent of reactivity across a wider range of aluminum amino-phenolate species.

2.8 Experimental Section

2.8.1 General Considerations

All experiments involving metal complexes were carried out under nitrogen atmosphere in an inert atmosphere workstation. Ligands were prepared according to literature procedures.[69-71] Synthesis of **2.1** and **2.2** has been reported previously.[54] Epoxides were dried over CaH_2, distilled, and stored under nitrogen. Elemental analyses were performed by Canadian Microanalytical Service Ltd., Delta, BC, Canada. ^{1}H and $^{13}C\{^{1}H\}$ NMR spectra were recorded on a Bruker Avance 300 or 500 MHz spectrometer at 25 °C and are referenced internally to residual signals of the solvent. Kinetic studies were performed on a Bruker Avance 500 MHz spectrometer using a co-axial NMR tube and $CDCl_3$ as the lock solvent. Polymer GPC data was collected from a setup consisting of a miniDawn TREOS light scattering detector, a Viscostar-II viscometer, and an Optilab T-rEX differential refractive index detector (Wyatt Technology) connected to an Agilent Infinity 1260 HPLC system equipped with a ResiPore 250×4.6 mm column. Samples were prepared in $CHCl_3$ at a typical concentration of 2 mg/mL, filtered, and analyzed at a flow rate of 0.3 mL/min and 25 °C. Molecular weights were calculated using a dn/dc value of 0.0795 mL/g (obtained from standard calibration analyses by injecting known concentrations of PCHO in $CHCl_3$ directly into the refractive index detector). DSC data were collected on a Mettler Toledo DSC1 Star^{e} System with a scanning rate of 10 °C/min and nitrogen gas flow of 50 mL/min. Samples were heated from 25 to 100 °C three times in order to eliminate the difference in sample history and all glass transition temperatures were taken from the third heating cycle. Polymer samples were analyzed by MALDI-TOF

MS using an Applied Biosystems 4800 TOF-TOF mass spectrometer, with spectra recorded in reflectron mode. The matrix was 2,5-dihydroxybenzoic acid, with tetrahydrofuran as the solvent. Spectra were modelled using mMass software (www.mmass.org). Microwave reactions were carried out using a Biotage Initiator microwave reactor with sealed 2 mL vials.

2.8.2 Typical ROP Procedure

A desired amount of catalyst was weighed into a vial and epoxide (CHO, PO, styrene oxide, LO, or epichlorohydrin) was added with stirring. For lower catalyst loadings, the use of a standardized solution of the catalyst in toluene was necessary to accurately measure out known amounts of catalyst, followed by removal of the toluene *via* vacuum prior to epoxide addition. Reactions were typically terminated once they were unable to be stirred further, by removing the vial from the glovebox and opening it to air. A small amount was taken for ^{1}H NMR analysis to determine conversion of epoxide monomer to polymer. The crude polymer was dissolved in $CHCl_3$ (or CH_2Cl_2), precipitated from cold MeOH acidified with a small amount of 1 M HCl, and isolated by suction filtration or centrifugation. Finally, the polymer was dried in a vacuum oven to yield the PCHO that was analyzed by GPC and DSC.

2.8.3 Synthetic Procedures

[$O_2NO^{tBu,tBu}$]AlCl (**2.3**). In a glovebox at room temperature, 2.10 g (4.10 mmol) of H_2[**L1**] was added to an Erlenmeyer flask and dissolved in dry toluene (20 mL). To this a solution of Et_2AlCl (25% w/w in toluene; 0.495 g, 4.10 mmol) was added dropwise while rapidly stirring. The reaction was allowed to stir for two hours, after which the toluene was

removed *in vacuo*. The resulting fluffy solid was washed with 5 mL pentane and dried under vacuum, yielding **2.3** as a colourless solid. Yield: 2.34 g, 100%. Anal. Calcd for $C_{33}H_{51}AlClNO_3$: C, 69.27; H, 8.98; N, 2.45. Found: C, 69.28; H, 8.99; N, 2.40. ^{1}H NMR (C_7D_8, 300 MHz, 298 K) δ 7.53 (2H, d, Ar*H*), 6.73 (2H, d, Ar*H*), 3.45 (3H, s, OC*H*$_3$), 3.26 (2H, d, $^2J_{HH}$ =13 Hz, Ar–C*H*$_2$–N), 3.10 (2H, d, $^2J_{HH}$ =13 Hz, Ar–C*H*$_2$–N), 2.60 (2H, t, N–C*H*$_2$–CH$_2$), 1.96 (2H, t, CH$_2$–C*H*$_2$–O), 1.73 (s, 18H, Ar–C{C*H*$_3$}$_3$), 1.39 (s, 18H, Ar–C{C*H*$_3$}$_3$); ^{13}C{^{1}H} NMR (C_7D_8, 75 MHz, 298 K) δ 155.6, 140.1, 139.9, 124.9, 123.7, 120.6 (Ar*C*), 68.6 (N–*C*H$_2$–CH$_2$), 64.0 (O*C*H$_3$), 58.4 (Ar–*C*H$_2$–N), 48.5 (CH$_2$–*C*H$_2$–O), 35.5 (Ar–*C*{CH$_3$}$_3$), 34.4 (Ar–*C*{CH$_3$}$_3$), 32.0 (Ar–C{*C*H$_3$}$_3$), 29.9 (Ar–C{*C*H$_3$}$_3$).

2.9 References

1. M. R. Mason, Aluminum: Organometallic Chemistry, in *Encyclopedia of Inorganic Chemistry*, eds. R. B. King, R. H. Crabtree, C. M. Lukehart, D. A. Atwood and R. A. Scott, John Wiley & Sons, Ltd, 2006.
2. J. Lewinski and A. E. H. Wheatley, *Top. Organomet. Chem.*, **2013**, *41*, 1-58.
3. S. Dagorne and C. Fliedel, *Top. Organomet. Chem.*, **2013**, *41*, 125-171.
4. M. H. Chisholm, J. C. Gallucci, K. T. Quisenberry and Z. Zhou, *Inorg. Chem.*, **2008**, *47*, 2613-2624.
5. B. Liu, H. Li, C.-S. Ha, I. Kim and W. Yan, *Macromol. Res.*, **2008**, *16*, 441-445.
6. H. Du, A. H. Velders, P. J. Dijkstra, J. Sun, Z. Zhong, X. Chen and J. Feijen, *Chem. Eur. J.*, **2009**, *15*, 9836-9845.
7. K. Phomphrai, P. Chumsaeng, P. Sangtrirutnugul, P. Kongsaeree and M. Pohmakotr, *Dalton Trans.*, **2010**, *39*, 1865-1871.
8. A. D. Schwarz, Z. Chu and P. Mountford, *Organometallics*, **2010**, *29*, 1246-1260.
9. M.-H. Thibault and F.-G. Fontaine, *Dalton Trans.*, **2010**, *39*, 5688-5697.
10. C. Bakewell, R. H. Platel, S. K. Cary, S. M. Hubbard, J. M. Roaf, A. C. Levine, A. J. P. White, N. J. Long, M. Haaf and C. K. Williams, *Organometallics*, **2012**, *31*, 4729-4736.
11. M. Bouyahyi, T. Roisnel and J.-F. Carpentier, *Organometallics*, **2012**, *31*, 1458-1466.
12. M. Lamberti, I. D'Auria, M. Mazzeo, S. Milione, V. Bertolasi and D. Pappalardo, *Organometallics*, **2012**, *31*, 5551-5560.
13. W. Alkarekshi, A. P. Armitage, O. Boyron, C. J. Davies, M. Govere, A. Gregory, K. Singh and G. A. Solan, *Organometallics*, **2013**, *32*, 249-259.
14. X. Liu, C. Jian, D. Yu, J. Zhang, N. Tang, C. Wang and J. Wu, *Inorg. Chem. Commun.*, **2013**, *36*, 206-211.
15. L. Postigo, M. d. C. Maestre, M. E. G. Mosquera, T. Cuenca and G. Jimenez, *Organometallics*, **2013**, *32*, 2618-2624.
16. K. Bakthavachalam, A. Rajagopal and N. Dastagiri Reddy, *Dalton Trans.*, **2014**, *43*, 14816-14823.
17. M. J. Go, S. H. Kim, Y. Y. Kang, H.-R. Park, Y. Kim and J. Lee, *Inorg. Chem. Commun.*, **2014**, *44*, 139-142.
18. S.-Y. Hsu, C.-H. Hu, C.-Y. Tu, C.-H. Lin, R.-Y. Chen, A. Datta and J.-H. Huang, *Eur. J. Inorg. Chem.*, **2014**, *2014*, 1965-1973.
19. C. Romain, C. Fliedel, S. Bellemin-Laponnaz and S. Dagorne, *Organometallics*, **2014**, *33*, 5730-5739.
20. H. Kampova, E. Riemlova, J. Klikarova, V. Pejchal, J. Merna, P. Vlasak, P. Svec, Z. Ruzickova and A. Ruzicka, *J. Organomet. Chem.*, **2015**, *778*, 35-41.
21. W. Kuran, T. Listos, M. Abramczyk and A. Dawidek, *J. Macromol. Sci. A*, **1998**, *35*, 427-437.
22. J. H. Jung, M. Ree and T. Chang, *J. Polym. Sci., Part A: Polym. Chem.*, **1999**, *37*, 3329-3336.
23. T. Sârbu and E. J. Beckman, *Macromolecules*, **1999**, *32*, 6904-6912.

24. M. H. Chisholm and Z. Zhou, *J. Am. Chem. Soc.*, **2004**, *126*, 11030-11039.
25. H. Sugimoto, H. Ohtsuka and S. Inoue, *J. Polym. Sci., Part A: Polym. Chem.*, **2005**, *43*, 4172-4186.
26. T. A. Zevaco, A. Janssen, J. Sypien and E. Dinjus, *Green Chem.*, **2005**, *7*, 659-666.
27. J. Melendez, M. North and R. Pasquale, *Eur. J. Inorg. Chem.*, **2007**, 3323-3326.
28. T. A. Zevaco, J. K. Sypien, A. Janssen, O. Walter and E. Dinjus, *J. Organomet. Chem.*, **2007**, *692*, 1963-1973.
29. M. North and R. Pasquale, *Angew. Chem. Int. Ed*, **2009**, *48*, 2946-2948.
30. W. Clegg, R. W. Harrington, M. North and R. Pasquale, *Chem. Eur. J.*, **2010**, *16*, 6828-6843.
31. C. Chatterjee and M. H. Chisholm, *Inorg. Chem.*, **2011**, *50*, 4481-4492.
32. K. Nishioka, H. Goto and H. Sugimoto, *Macromolecules*, **2012**, *45*, 8172-8192.
33. M. North, P. Villuendas and C. Young, *Tetrahedron Lett.*, **2012**, *53*, 2736-2740.
34. D. Tian, B. Liu, Q. Gan, H. Li and D. J. Darensbourg, *ACS Catal.*, **2012**, *2*, 2029-2035.
35. M. A. Fuchs, C. Altesleben, T. A. Zevaco and E. Dinjus, *Eur. J. Inorg. Chem.*, **2013**, *2013*, 4541-4545.
36. N. Ikpo, J. C. Flogeras and F. M. Kerton, *Dalton Trans.*, **2013**, *42*, 8998-9006.
37. C. J. Whiteoak, N. Kielland, V. Laserna, E. C. Escudero-Adan, E. Martin and A. W. Kleij, *J. Am. Chem. Soc.*, **2013**, *135*, 1228-1231.
38. J. A. Castro-Osma, C. Alonso-Moreno, A. Lara-Sánchez, J. Martínez, M. North and A. Otero, *Catal. Sci. Technol.*, **2014**, *4*, 1674.
39. S. H. Kim, D. Ahn, M. J. Go, M. H. Park, M. Kim, J. Lee and Y. Kim, *Organometallics*, **2014**, *33*, 2770-2775.
40. X. Sheng, Y. Wang, Y. Qin, X. Wang and F. Wang, *RSC Adv.*, **2014**, *4*, 54043-54050.
41. C. J. Whiteoak, N. Kielland, V. Laserna, F. Castro-Gómez, E. Martin, E. C. Escudero-Adán, C. Bo and A. W. Kleij, *Chem. Eur. J.*, **2014**, *20*, 2264-2275.
42. M. Akatsuka, T. Aida and S. Inoue, *Macromolecules*, **1994**, *27*, 2820-2825.
43. M. H. Chisholm and D. Navarro-Llobet, *Macromolecules*, **2002**, *35*, 2389-2392.
44. W. Braune and J. Okuda, *Angew. Chem. Int. Ed.*, **2003**, *42*, 64-68.
45. L. Tang, E. P. Wasserman, D. R. Neithamer, R. D. Krystosek, Y. Cheng, P. C. Price, Y. He and T. J. Emge, *Macromolecules*, **2008**, *41*, 7306-7315.
46. J.-T. Issenhuth, J. Pluvinage, R. Welter, S. Bellemin-Laponnaz and S. Dagorne, *Eur. J. Inorg. Chem.*, **2009**, *2009*, 4701-4709.
47. S. Dagorne, M. Bouyahyi, J. Vergnaud and J.-F. Carpentier, *Organometallics*, **2010**, *29*, 1865-1868.
48. N. Nakata, Y. Saito and A. Ishii, *Organometallics*, **2014**, *33*, 1840-1844.
49. G. Martínez, S. Pedrosa, V. Tabernero, M. E. G. Mosquera and T. Cuenca, *Organometallics*, **2008**, *27*, 2300-2305.
50. E. H. Nejad, C. G. W. van Melis, T. J. Vermeer, C. E. Koning and R. Duchateau, *Macromolecules*, **2012**, *45*, 1770-1776.
51. M. H. Chisholm, D. Navarro-Llobet and W. J. Simonsick, Jr., *Macromolecules*, **2001**, *34*, 8851-8857.

52. A.-L. Brocas, C. Mantzaridis, D. Tunc and S. Carlotti, *Prog. Polym. Sci.*, **2013**, *38*, 845-873.
53. M. I. Childers, J. M. Longo, N. J. Van Zee, A. M. LaPointe and G. W. Coates, *Chem. Rev.*, **2014**, *114*, 8129-8152.
54. N. Ikpo, S. M. Barbon, M. W. Drover, L. N. Dawe and F. M. Kerton, *Organometallics*, **2012**, *31*, 8145-8158.
55. D. J. Darensbourg, P. Ganguly and D. Billodeaux, *Macromolecules*, **2005**, *38*, 5406-5410.
56. C.-T. Chen, C.-A. Huang and B.-H. Huang, *Dalton Trans.*, **2003**, 3799-3803.
57. Z. Tang and V. C. Gibson, *Eur. Polym. J.*, **2006**, *43*, 150-155.
58. D. J. Darensbourg and W.-C. Chung, *Polyhedron*, **2013**, *58*, 139-143.
59. S. Pappuru, E. R. Chokkapu, D. Chakraborty and V. Ramkumar, *Dalton Trans.*, **2013**, *42*, 16412-16427.
60. D. Cui, M. Nishiura and Z. Hou, *Macromolecules*, **2005**, *38*, 4089-4095.
61. Y. Sarazin, M. Schormann and M. Bochmann, *Organometallics*, **2004**, *23*, 3296-3302.
62. E. Ertürk, M. A. Tezeren, T. Tilki, T. Erdogan and A. C. Gören, *Polym. Int.*, **2012**, *61*, 795-799.
63. R. J. Baker and A. Walshe, *Chem. Commun.*, **2012**, *48*, 985-987.
64. J. Fang, A. Walshe, L. Maron and R. J. Baker, *Inorg. Chem.*, **2012**, *51*, 9132-9140.
65. Z. Liu, M. Torrent and K. Morokuma, *Organometallics*, **2002**, *21*, 1056-1071.
66. M. W. Lehenmeier, C. Bruckmeier, S. Klaus, J. E. Dengler, P. Deglmann, A.-K. Ott and B. Rieger, *Chem. Eur. J.*, **2011**, *17*, 8858.
67. F. Andruzzi, L. Shaofeng, G. Pilcher and F. Heatley, *Makromol. Chem.*, **1987**, *188*, 2643-2650.
68. B. Y. Liu, H. Q. Li, C. S. Ha, I. Kim and W. D. Yan, *Macromol. Res.*, **2008**, *16*, 441-445.
69. E. Y. Tshuva, S. Groysman, I. Goldberg, M. Kol and Z. Goldschmidt, *Organometallics*, **2002**, *21*, 662-670.
70. N. Ikpo, L. N. Saunders, J. L. Walsh, J. M. B. Smith, L. N. Dawe and F. M. Kerton, *Eur. J. Inorg. Chem.*, **2011**, *2011*, 5347-5359.
71. F. M. Kerton, S. Holloway, A. Power, R. G. Soper, K. Sheridan, J. M. Lynam, A. C. Whitwood and C. E. Willans, *Can. J. Chem.*, **2008**, *86*, 435-443.

CHAPTER 3

Morpholine Stabilized Cationic Aluminum Complexes and their Reactivity in Ring-Opening Polymerization of ε-Caprolactone

Chapter 3. Morpholine Stabilized Cationic Aluminum Complexes and their Reactivity in Ring-Opening Polymerization of ε-Caprolactone

A version of this chapter has been published

Hart Plommer, Jennifer N. Murphy, Louise N. Dawe, and Francesca M. Kerton

Inorg. Chem., **2019**, *58*, 5253–5264.

Some modifications were made to the original paper for inclusion as a chapter in this thesis.

3.1 Introduction

Cationic complexes typically demonstrate high activities in catalytic reactions such as ROP of polar heteroatom-containing monomers such as epoxides and cyclic esters (e.g. lactide and ε-CL, producing polylactide (PLA) and PCL, respectively).[1-3] PLA, PCL, and their copolymers with other monomers have wide-ranging applications in health and drug design due to their biocompatibility and biodegradation properties.[4-6]

Morpholinyl-containing metal complexes (Figure 3.1) are of interest since the outer-sphere oxygen offers the possibility to tune the electron density on the metal centre, which can have a stabilizing effect when cations are generated. This donor competes with oxygen-containing monomers that coordinate to aluminum and this influences the course of polymerization. Cationic four-coordinate aluminum complexes for ROP of PO, lactide, and ε-CL have been studied by Dagorne and co-workers,[7] and the Kerton group have

investigated ROP of ε-CL and ROCOP of CHO/CO_2 using neutral aluminum amino-phenolate complexes.[8] It was proposed that the hemilabile nature of the morpholinyl group allowed the facile displacement of an aluminum-bound chloride to initiate the copolymerization of CHO and CO_2. Shaver and co-workers surveyed aluminum amino-bis(phenolate) complexes containing different pendant donors for ROP of *rac*-lactide and ε-CL.[9] They found the morpholinyl pendant donor afforded a high degree of control when applied to both monomers, but this control was lost at higher temperatures with ε-CL.

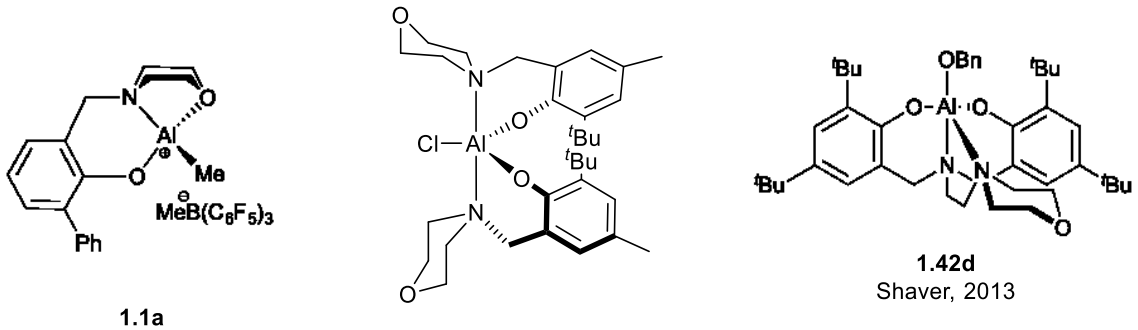

1.1a
Dagorne, 2009

2.1
Kerton, 2012

1.42d
Shaver, 2013

Figure 3.1. Aluminum-morpholinyl catalysts for ROP of cyclic esters and epoxides.

Based upon the earlier research employing morpholinyl amino-phenolate metal complexes,[7-13] including the excellent results in ROP of CHO reported in Chapter 2, the question arose as to whether species containing such a structural motif could be considered a privileged class of ligand for polymerization of polar monomers including ε-CL and epoxides. Furthermore, Stradiotto and co-workers have found that morpholinyl-containing phosphines provide exceptionally stable and active catalyst systems for cross-coupling and other important reactions in organic synthesis,[14-17] giving further credence to the privileged

role that morpholine can play in stabilizing catalytic intermediates. In this chapter, the synthesis and characterization of a family of cationic aluminum complexes with various counterions and their application as initiators for well-controlled ROP of ε-CL is reported. Computational studies, using experimental data as a starting point, were also performed to evaluate the degree of stabilization provided by chelation of the morpholine donor.

3.2 Results and Discussion

In order to prepare a series of closely related cationic species, the neutral aluminum chloride complex **3.1** (Scheme 3.1) was prepared to allow subsequent chloride ion abstraction to yield cationic species with potential activity towards ROP of ε-CL.

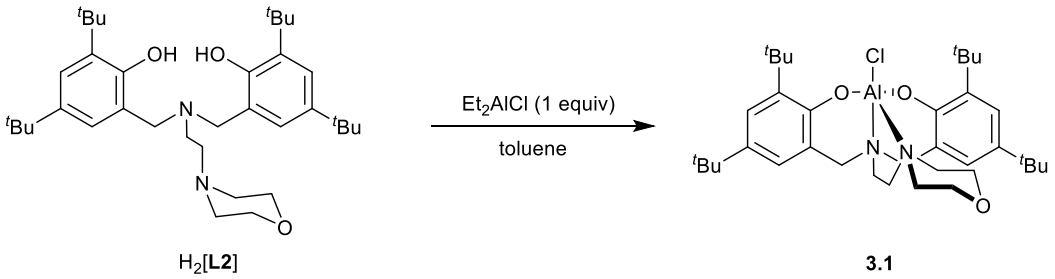

Scheme 3.1. Synthesis of aluminum amino-bis(phenolate) complex **3.1**

X-ray structural analysis of **3.1** confirmed the connectivity within the complex and monodentate (N) coordination of the morpholine group to Al (Figure C.1), but data were not of sufficient quality to provide accurate bond lengths and angles. The fluxionality within the morpholine group gives broad ^{1}H NMR resonances in the methylene region at room temperature (Figure A.3). Lowering the temperature allows coupling patterns to appear at 243 K and assignment of the different proton environments (Figures A.6–A.7).

Heptane washings of **3.1** containing residual Et_2AlCl reagent formed crystals on standing. Upon X-ray analysis these showed formation of an ionic species **3.2** produced *via* abstraction of chloride by excess diethylaluminum chloride reagent and simultaneous coordination of the outer-sphere morpholinyl oxygen (Figure C.2). This was particularly surprising since the fixed boat-like conformation adopted by the morpholinyl ring is expected to be energetically unfavourable compared to the chair conformation, in line with theoretical calculations that predict a stabilization energy of 25.1 kJ/mol for the chair conformers of morpholine.[18] We probed this coordination phenomenon using density functional theory (DFT) calculations at the B97D3/6-311G(d,p)/LANL2DZ level of theory. Cation geometries (Figure 3.2) displaying bidentate (**NO**) and monodentate (**N2**) coordination of the morpholine group were first optimized in the gas phase using atomic coordinates obtained from X-ray diffraction. The **N1** geometry (Figure 3.2) was obtained from **NO** by translating O_{morph} onto the opposite side of the morpholine ring (away from the Al centre). The gas phase structures were then optimized in $CHCl_3$ solution with the SMD solvent model to account for solvent effects. The calculated Gibbs energies in solution indicate that **NO** is 21.1 kJ/mol more stable than the **N1** conformer. If the morpholine group is positioned similarly to neutral **3.1**, the energy increases slightly by 0.7 kJ/mol (**N2**). These stabilities provide a rationale for why only **NO** is observed experimentally in solution (in the absence of coordinating reagents such as ε-CL, vide infra) and in the solid-state structures of the cationic complexes reported herein.

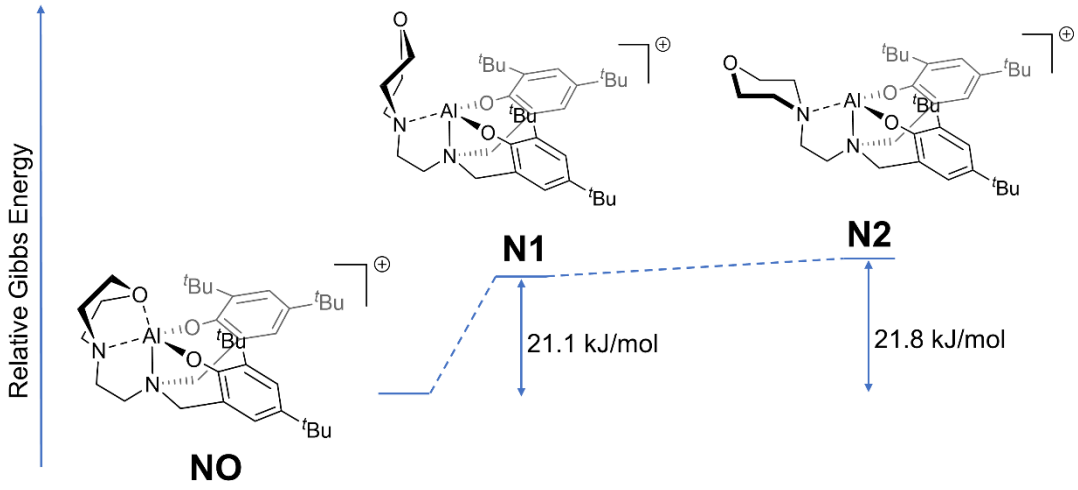

Figure 3.2. Gibbs energy profile showing the **NO**, **N1**, and **N2** geometries of the Al cation optimized in $CHCl_3$ solution at the B97D3/6-311G(d,p)/LANL2DZ level of theory

This observation of a cationic species led us to synthesize a series of cationic complexes by halide abstraction reactions of **3.1** with one equiv of anhydrous Lewis acid (Scheme 3.2).

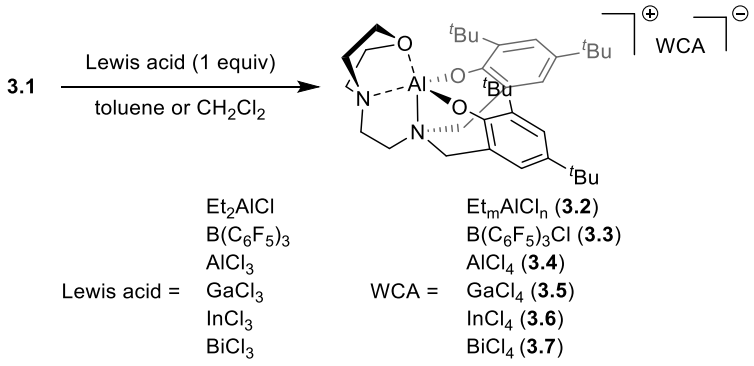

Scheme 3.2. Synthesis of cationic aluminum amino-bis(phenolate) complexes containing morpholinyl donors and various weakly coordinating anions.

Typically, halide abstraction reactions proceeded readily at room temperature and a colorless precipitate formed within minutes in toluene. Notably, the gram scale synthesis of **3.2** led to an intractable mixture composed of ca. 50% of the cation, along with unidentifiable species that likely form *via* ligand scrambling reactions and Schlenk equilibria (see Figure A.8). These data are consistent with the unexpected $[EtAlCl_3]^-$ anion observed crystallographically (instead of $[Et_2AlCl_2]^-$). It is not uncommon for ligand scrambling to occur in alkyl- and chloroaluminum species leading to a mixture of species at equilibrium.[19-20] Where Et_2AlCl exists as a dimer in the solid state and non-polar solvents, the exchange of bridging groups with terminally located groups may play a role in formation of anions other than $[Et_2AlCl_2]^-$ upon chloride abstraction.[21] The weaker Lewis acid BPh_3 was unable to abstract the chloride on the basis of ^1H and ^{11}B NMR (Figures A.23–A.24) illustrating the range of Lewis acidity needed to affect the abstraction. Attempts to prepare a Ge^{IV} chlorometallate analogue also failed, both on a preparative scale and NMR scale. Halide abstraction reactions have been successful using $GeCl_4$ and BPh_3 in other systems,[22-23] which shows that the ideal choice of halide abstractor will be dependent on the nature of the initial chloride reagent. Attempted metathesis reactions of **3.1** with $LiB(C_6F_5)_4$ were challenging due to insoluble nature of the product and so the complex formed was not isolated. However, ROP of CL was attempted *in situ* using the LiCl containing reaction mixture (vide infra). Preliminary experiments showed that **3.3** could be made on an NMR scale in toluene-d_8 (see Figures A.9–A.10), however, attempts to scale up the reaction and isolate a product were unsuccessful. Therefore, most efforts focused on complexes **3.4–3.7**.

Complexes **3.4–3.7** were characterized in most cases by elemental analyses and ^{1}H, ^{13}C{^{1}H}, COSY, HSQC, and as appropriate, ^{27}Al and ^{71}Ga NMR spectroscopy, as well as ESI-MS and MALDI-TOF MS analyses. Complexes **3.2**, **3.5**, and **3.6** were structurally characterized by X-ray diffraction methods (Figures 3.3 and C.2–C.3). The ^{1}H and ^{13}C{^{1}H} NMR shifts of the cationic complexes **3.4–3.7** are nearly identical since the only variable is the WCA which has little, if any, effect on the aluminum-containing cation in solution, and this was also seen in subsequent reactivity studies. Therefore, the tetrachlorogallate complex **3.5** will be discussed as representative of the group. In the ^{1}H NMR spectrum (Figure A.14), two doublets corresponding to the aromatic protons are observed at 7.32 and 6.96 ppm which have shifted to higher frequency from 7.27 and 6.83 ppm for the neutral complex **3.1**. A diagnostic shift indicative of the formation of the aluminum cations is seen for the two methylene protons adjacent to the oxygen in the morpholinyl donor from 3.66 to 5.09 ppm. The four methylene protons adjacent to the aromatic rings resonate as two doublets at 4.04 and 3.90 ppm since coordination of the tripodal nitrogen to the aluminum centre gives rise to diastereotopic environments. Moreover, in the ^{13}C{^{1}H} NMR spectrum of **3.1** (Figure A.4) a very broad resonance at 52.1 ppm corresponding to the two carbons bonded to nitrogen within the morpholinyl ring becomes a sharp resonance at 51.1 ppm in **3.5** once the cation is formed (Figure A.15). The broadness of this ^{13}C{^{1}H} resonance in **3.1** is due to *N*-inversion, which is slow on an NMR time-scale. For **3.5**, a NOESY experiment showed that the *ortho tert*-butyl group resonating at 1.36 ppm resides near the two methylene protons (5.09 ppm) of morpholinyl ring adjacent to the coordinated oxygen (but not the two methylene protons at 4.22 ppm located on the opposite face of the

morpholinyl ring) (Figure A.18). 2D COSY and HSQC experiments corroborate the peak assignments within spectra of **3.5** (Figures A.16–A.17).

Single crystals of complexes **3.2**, **3.5**, and **3.6** could be grown at −30 °C in non-coordinating solvents and the resulting X-ray structures confirmed the chelating coordination mode of the morpholine group. Crystallographic and structure refinement data can be found in Table C.1. Most cationic 5-coordinate aluminum complexes are dimeric or contain external donors such as ether[24] or amine-containing solvents, which moderates the reactivity of these species. To the best of our knowledge, **3.2**, **3.5**, and **3.6** represent the first crystallographically characterized aluminum complexes containing a morpholinyl donor coordinated to the metal centre through both heteroatoms. The steric balance also plays an important role in stabilizing **3.2–3.7** as others typically observe a dimerization upon halide abstraction, for example, Atwood's synthesis of aluminum salpen and salophen dications.[25] Herein, the outer-sphere oxygen of the morpholine coordinates to aluminum and the *tert*-butyl groups are sufficiently bulky, thus preventing dimerization from occurring. In our structures, the bond lengths and angles are similar to each other, as expected, and are in the range typical for Al-phenolate and Al-amino complexes.[26-27] In most cases, five-coordinate aluminum complexes containing phenolate ligands are trigonal bipyramidal in geometry (geometry index, τ = 1).[28-29] **3.2**, **3.5**, and **3.6** are extremely distorted from both the ideal trigonal bipyramidal or square based pyramidal geometries typical for five-coordinate species. **3.2** and **3.6** have τ = 0.54 while **3.5** has τ = 0.55. Structurally authenticated coordination of the morpholine group in a bidentate fashion is rare. There are two examples of this with palladium, and one with calcium.[10, 30-31] In the

calcium structure, the bite angle formed at the metal with the morpholinyl donors is highly strained at 59.01°. In the palladium examples, the O_{morph}–Pd–N_{morph} angles have an average value of 69.83°. In **3.2**, the O_{morph}–Al–N_{morph} angle is 72.77(12)° and in **3.5** and **3.6**, the same angle is 72.88(11) and 72.84(10)°, respectively. This suggests that the bonding of the morpholinyl to the metal in the current example is less strained due to the size of the metal atom. However, further analyses would be needed to fully understand the differences in bonding in these examples.

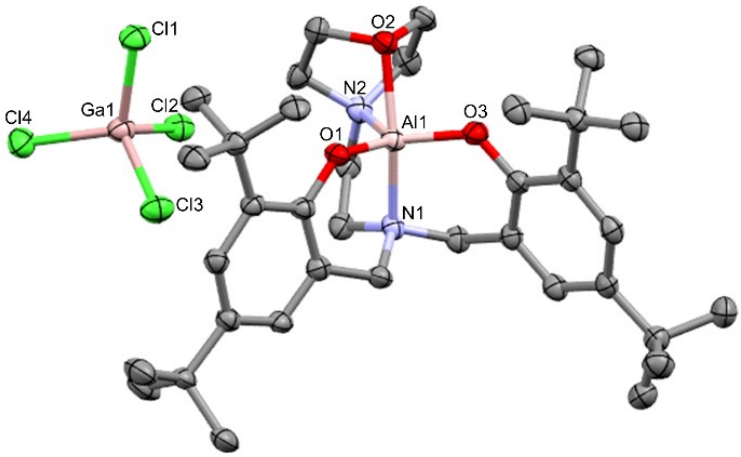

Figure 3.3 Molecular structure and partial numbering of **3.5** (thermal ellipsoids drawn at 50% probability; H atoms and three co-crystallized toluene molecules excluded for clarity). Selected bond distances (Å) and angles (°): Al(1)–O(1), 1.725(2); Al(1)–O(2), 2.022(3); Al(1)–O(3), 1.735(3); Al(1)–N(1), 1.995(3); Al(1)–N(2), 1.994(3); O(1)–Al(1)–O(2), 94.77(11); O(1)–Al(1)–O(3), 124.90(12); O(1)–Al(1)–N(1), 97.68(12); O(1)–Al(1)–N(2), 116.62(13); O(3)–Al(1)–O(2), 90.06(11); O(3)–Al(1)–N(1), 97.85(12); O(3)–Al(1)–N(2), 117.19(13); N(1)–Al(1)–O(2), 157.66(12); N(2)–Al(1)–O(2), 72.88(11); N(2)–Al(1)–N(1), 84.95(12).

3.3 Polymerization of ε-CL

Solution polymerizations in $CHCl_3$, in the absence or presence of *tert*-BuOH, proceeded slowly over the course of many days to give viscous reaction mixtures (Table 3.1, entries 1 and 2, respectively). The narrow dispersity ($Đ$ = 1.09) obtained *via* GPC indicated that **3.5** alone provided some degree of control over the polymerization, though the experimental molecular weights were significantly higher than the calculated values. In the presence of *tert*-BuOH, higher temperature (70 °C) increased catalyst activity significantly (Table 3.1, entry 3 vs. 2). End group analyses of the crude reaction mixture (Table 3.1, entry 2) did not show resonances for *tert*-butyl ester, however, the high molecular weight polymers produced here (M_n >> 25 kDa) would not yield visible end group signals *via* ^{1}H NMR due to an inherent loss of resolution.[32] Moreover, the possibility that cyclic PCL is formed cannot be ruled out. That is, ε-CL could insert into the Al–OPh bond or become ring-opened by a nucleophilic ligand group (e.g. amine within the morpholinyl ring). Such mechanisms have been proposed as the initiation step for various metal phenolate complexes in the absence of a protic co-initiator.[12, 33-36] This is consistent with the ^{1}H and HSQC NMR spectra of an equimolar mixture of **3.5** and ε-CL, which shows that ε-CL breaks up the bidentate coordination of the morpholine group (Figures A.29–A.30). However, resonances characteristic of insertion into the Al–OPh bond were not observed such as the $^{13}C\{^1H\}$ NMR signal for the hypothetical phenyl ester (~170 ppm). In the current studies, the ε-CL ester $^{13}C\{^1H\}$ resonance at 176 ppm shifts to 187 ppm once ε-CL coordinates to Al. It is clear from GPC data that oligomeric, low molecular

Table 3.1. Polymerization of ε-CL using morpholinyl amino-phenolate aluminum complexes[a]

Entry	Cat.	[ε-CL]/ [Al]/[Co-init.]	T (°C)	Time (h)	Conv. (%)	$M_{n,calcd}$[f,h] × 10^3	M_n[g,h] × 10^3	$Đ$[g]
1	**3.5**	200/1/0	20	168	45	10.3	135	1.09
2[b]	**3.5**	200/1/1	20	168	57	13.1	217	2.78
3[b]	**3.5**	200/1/1	70	2	17	3.95	45.6	1.01
4[c]	**3.5**	200/1/1	70	2	>99	22.9	2.79	1.03
5[c]	**3.5**	200/1/2	70	2	99	11.3	1.92	1.04
6[c]	**3.1**	200/1/1	20	6.5	99	22.6	26.8	1.05
7[c]	**3.4**	200/1/1	20	20	41	9.36	10.6	1.00
8[c]	**3.5**	200/1/1	20	20	50	11.5	11.0	1.02
9[c]	**3.5**	200/1/2	20	20	71	8.22	8.29	1.02
10	**3.5**	200/1/0	100	1.33	59	13.5	105	1.24
11[d]	**3.5**	200/1/1	20	20	>99	22.9	164	1.46
12[d]	**3.5**	200/1/1	20	10	81	18.6	113	1.07
13[d]	**3.5**	200/1/2	20	20	89	10.2	44.4	1.01
14[e]	**3.5**	200/1/1	20	22	32	7.42	6.82	1.01
15[e]	**3.5**	100/1/1	20	6	24	2.86	3.18	1.03
16[c]	**3.5**	1000/1/10	20	10	3	0.39	–	–
17[c]	**3.6**	200/1/1	20	20	54	12.3	11.3	1.01
18[c]	**3.6**	200/1/2	20	20	67	7.77	8.27	1.01
19[e]	**3.7**	200/1/1	20	2.67	92	21.1	24.8	1.04
20[c]	**1**/Li(B_6F_5)	200/1/1	20	20	0	–	–	–

[a] Polymerizations were run in $CHCl_3$ solution, $[ε\text{-CL}]_0$ = 1.7 M. [b] *tert*-BuOH [c] EtOH [d] Glycidol [e] Glycerol carbonate, reactions performed in THF. [f] Calculated from [ε-CL]/[Co-init.] × 114.14 × conv. %/100 + molecular weight (co-initiator), except for entries 1 and 10, which were calculated from [ε-CL] × 114.14 × conv. %/100. [g] Determined by triple detection GPC in THF. [h] In Da.

weight cyclic PCL is not being generated, a product of backbiting reactions frequently observed by others.[4, 37-38] It should be noted that any protic impurities in the reagents could

act as a co-initiator leading to the observed activities and high molecular weight polymer although the ε-CL was carefully dried and stored under inert atmospheric conditions.

As the results using *tert*-BuOH were unexceptional, I primarily focused on EtOH in this thesis as its decreased steric demands should yield higher activities. Conversion of 200 equiv ε-CL at 20 °C using **3.5** in the presence of 1 or 2 equiv EtOH gave living character, with experimental M_n values in excellent agreement with those calculated, and dispersities close to unity (Table 3.1, entries 8–9). Higher temperatures allowed reactions to achieve quantitative conversion in short reaction times and the resulting polymers had dispersities close to 1.0, but experimental M_n values were significantly lower than those expected (Table 3.1, entries 4–5). This may be due to intramolecular or intermolecular transesterification reactions taking place once most monomer has been consumed and is commonly observed for cyclic ester polymerizations at higher temperatures.[4, 39-43] Although cationic species are often more active than their neutral counterparts, **3.1** was highly efficient compared to **3.5** (Table 3.1, entry 6 vs. 8). It is noteworthy that the cationic complexes retain some activity, given the chelating properties of the morpholine group. As a related neutral morpholine alkoxy complex had already been studied in detail,[10] I did not pursue further reactions using **3.1** as I was more interested in the reactivities of the cationic series and the role their respective anions might play in the polymerization process. Focusing on the group 13 WCAs, the activity trend follows $InCl_4^- \sim GaCl_4^- > AlCl_4^-$ (Table 3.1, entries 7–8 and 17). ^{27}Al NMR studies (vide infra) indicate that the $AlCl_4^-$ is degraded in the presence of EtOH and this may explain the decrease in activity for this system compared to Ga and In. ^{1}H NMR resonances of the crude reaction mixtures and the purified

polymers showed CH_2OH (3.64 ppm) and ethyl ester (4.12 ppm) end groups, consistent with EtOH acting as a co-initiator.

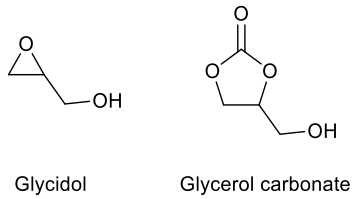

Figure 3.4. Functional co-initiators

Glycidol and glycerol carbonate (Figure 3.4) were explored as co-initiators to yield reactive end groups that could furnish new, diverse polymers. **3.5** was inactive for ROP of glycidol, suggesting it might be an ideal catalyst that would leave the epoxy ring intact for further functionalization following ε-CL polymerization (Figure A.39). Glycidol increased the reaction rate significantly with **3.5**, reaching quantitative conversion in the same amount of time required for **3.5**/EtOH to reach 50% conversion, (Table 3.1, entry 11 vs. 8). Doubling the concentration of glycidol both decreased the activity and molecular weight of the resulting polymer (Table 3.1, entry 13 vs. 11). Irrespective of the glycidol concentration, the molecular weights of the isolated PCLs were four to seven times higher than the calculated values. Howdle's group also observed molecular weights significantly higher than expected in related ROP reactions and attributed this phenomenon to selectivity of the enzyme for hydroxyl-terminated polymer rather than hydroxyl of glycidol, leading to a non-linear decrease in M_n as glycidol concentration increased.[44] In the present case, a bimetallic mechanism could be proposed where the epoxy end group of one PCL chain coordinates to another Al centre and thus decreases the number of available monomer

coordination sites at Al, reducing the number of active catalyst species and thereby increasing M_n. Glycerol carbonate was less reactive compared with glycidol when coupled with **3.5**, converting about 1/3 as much monomer over a similar time period (Table 3.1, entry 14 vs. 11). This might be due to the THF used as a co-solvent to accurately dispense small quantities of glycerol carbonate. THF would compete with the carbonate and morpholinyl oxygen groups for coordination to aluminum. In agreement with this proposal, increasing the concentration of glycerol carbonate five-fold led to a steep loss in activity (ca. 1% conversion after 5 h). A similar trend was seen for a polymerization run with a ten-fold excess of EtOH i.e. immortal conditions (Table 3.1, entry 16). I propose that excess EtOH coordinates to Al and blocks ε-CL from coordinating, which agrees with the stronger Lewis basicity of EtOH compared to ε-CL.[45] This will be discussed in more detail in the NMR section (vide infra).

Due to the insoluble nature of complex **3.7** in many solvents (such as $CHCl_3$ used in most polymerization reactions performed herein), its efficacy for ROP of ε-CL was only tested in the presence of glycerol carbonate (in minimal THF). Under these conditions, **3.7** proved to be highly efficient compared to **3.5** (TOF 69 vs. 3 h^{-1}) and afforded a polymer with narrow dispersity and M_n slightly higher than the theoretical value (Table 3.1, entry 19 vs. 14). Preliminary experiments using the cation paired with the bulky tetrakis(pentafluorophenyl)borate anion showed no activity over the course of 20 h (Table 3.1, entry 20). This lack of activity is likely due to the insoluble nature of this complex. In general, the cationic complexes described herein in the presence of EtOH are poorly active at room temperature (TOF <10 h^{-1}) for ε-CL polymerization according to the activity scale

reported by Arbaoui and Redshaw,[4] but provide good dispersity and M_n control. A lower coordinate cationic Al-isopropoxide complex reported by Dagorne's group is more efficient (room temperature; TOF = 120 h^{-1}), but broader dispersities were observed.[46] Other aluminum complexes are much more efficient; for example, the introduction of electron-withdrawing substituents to phenoxy imines has yielded good activities (TOF up to 530 h^{-1}).[47]

Using **3.5** in the presence of EtOH, excellent control of polymer chain length over time is achieved, with excellent agreement of M_n (GPC) with M_n (calcd) and dispersity consistently 1.01 or less (Figure 3.5). It is worth noting that some reactions exhibited a high molecular weight shoulder (M_n 51–460 kDa) in their GPC traces, which amounted to less than 5% of the PCL sample. This could be due to incomplete conversion of the catalyst to the active species or mass transfer limitations encountered at high monomer conversion.

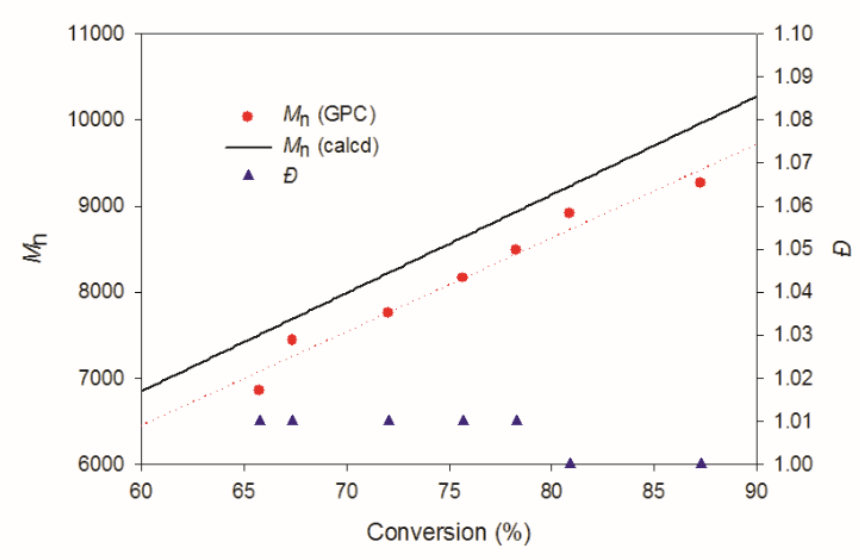

Figure 3.5. Dependence of M_n and $Đ$ on conversion of ε-CL, [ε-CL]/[**3.5**]/[EtOH] = 200/1/2

3.4 Mechanistic Studies

Detailed NMR studies of **3.5** with the co-initiators were undertaken to identify the catalytically active ROP species.

3.4.1 Reaction with EtOH

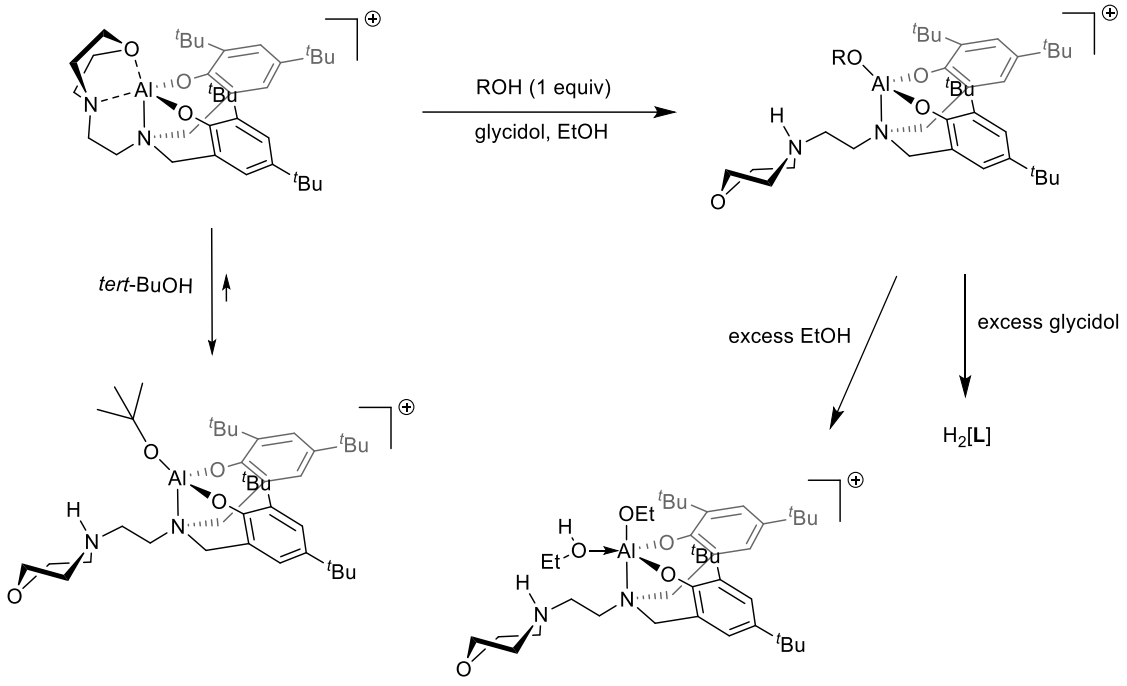

Scheme 3.3. Reactivity of alcohol co-initiators with **3.5** (counteranion omitted for clarity)

An equimolar solution of **3.5**/EtOH showed a peak at 12.06 ppm in the ^{1}H NMR spectrum, shifting to 13.36 (resp. 13.52 and 13.60) ppm when 2 (resp. 5 and 10) equiv EtOH are added (Figure A.31), suggesting that the ligand is protonated and Al–OEt is formed. It is worth noting that these signals are significantly downfield from those assigned to the phenolic protons of the proligand, which appear at 9.26 ppm.[9] This suggests the phenolate oxygens still coordinate to the Al centre and possibly amine protonation is

occurring, which Dagorne *et al.* observed in ^{1}H NMR (11.40 ppm) for their aluminum cations on addition of *iso*-PrOH.[46] For the equimolar solution, a triplet that corresponds to the methyl protons within the ethoxide group bound to Al resonates at 1.51 ppm (Figure A.32); no resonance corresponding to the adjacent methylene protons could be clearly identified). With 2 equiv EtOH, a species that was more easily interpreted *via* ^{1}H NMR spectroscopy was generated, likely due to occupation of the vacant site at Al by EtOH upon displacement of the morpholinyl oxygen (see Figures A.33 and A.35). A ^{1}H–^{15}N HSQC experiment showed a correlation between the proton at 13.36 ppm and a nitrogen atom resonating at 49.2 ppm which is within the range expected for a tertiary ammonium nitrogen atom, confirming the protonation of the morpholinyl nitrogen (Figure A.36). Moreover, the COSY spectrum showed that this proton couples with adjacent methylene protons (Figure A.34). The tetrachlorogallate ^{71}Ga NMR resonance remains at 251–252 ppm (Figure A.37), suggesting it plays no role in the catalysis and confirming the catalytic role of the cationic aluminum species. In contrast, addition of excess EtOH to the tetrachloroaluminate complex led to the disappearance of the tetrachloroaluminate ^{27}Al NMR resonance at 104 ppm (Figure A.38), coincident with the formation of a colorless precipitate. The stable nature of the tetrachlorogallate anion compared to the tetrachloroaluminate was part of the reasoning for focusing my polymerization efforts on **3.5**.

3.4.2 Reaction with Glycidol, Glycerol Carbonate, or *tert*-BuOH

Reaction of 1 equiv *tert*-BuOH with **3.5** also protonates the morpholinyl nitrogen. However, the reaction does not quantitatively form the product, with a small amount of **3.5**

still present after 2 equiv *tert*-BuOH have been added. On the other hand, glycidol protonates the morpholinyl nitrogen, but addition of excess glycidol leads to protonation of the phenolate groups and thus allows the pro-ligand to reform. There is no clear evidence that glycerol carbonate protonates the morpholinyl nitrogen, as multiple deshielded resonances including a broad resonance at 9.1 ppm appear in the ^{1}H NMR spectra. The reactivity of **3.5** with the co-initiators is summarized in Scheme 3.3.

3.5 Kinetic Studies

Kinetic investigations were undertaken by taking aliquots of the reaction mixtures at appropriate intervals and conversion was determined *via* ^{1}H NMR spectroscopy. Activation parameters calculated by Eyring analyses are listed in Table 3.2 (see Figures D.3–D.5 for kinetic plots). The large, negative $\Delta S^{\ddagger}$ values are indicative of an ordered transition state.[30] The $\Delta H^{\ddagger}$ is comparable to that obtained for a morpholinyl aluminum amino-phenolate system with a benzyloxide nucleophile and indium catalysts for ROP of lactide.[8, 48] The results from kinetic and NMR studies support a coordination-insertion mechanism initiated by transfer of an ethoxide nucleophile from Al to ε-CL, followed by oxygen-acyl bond cleavage. Coordination-insertion is a commonly observed pathway for metal complexes in ROP of ε-CL. [49-51]

Table 3.2. Activation parameters for ε-CL polymerization initiated by aluminum complexes **3.5** and **3.6**

Catalyst system	$\Delta H^{\ddagger}$ (kJ/mol)	$\Delta S^{\ddagger}$ (J/mol K)	$\Delta G^{\ddagger}$ (kJ/mol)[a]
3.5/EtOH	57(4)	−117(13)	91
3.6/EtOH	58(3)	−110(11)	91

[a] T = 25 °C

3.6 Polymer Analyses

MALDI-TOF MS spectra of PCL produced using **3.6**/EtOH are shown in Figure 3.6. One peak distribution with peaks separated by 114 Da which corresponds to the mass of ε-CL are observed. The distribution is composed of sodiated PCL chains capped with hydroxyl and ethyl ester end groups ($HO[\varepsilon\text{-}CL]_mEt{\cdot}Na^+$) [e.g. m = 37, *m/z* = 4291.54 (expt), 4291.56 (calcd)].

Representative DSC traces for PCL produced with **3.5** in the presence and absence of EtOH are shown in Figures E.1–E.2 and the corresponding melting temperature, enthalpy of fusion, and calculated weight percent crystallinity are summarized in Table E.1. No glass transitions were observed at low temperature due to inherent sensitivity of the instrument used. The crystallinity values are higher for the PCL produced in the presence of EtOH, which is indicative of a more controlled polymerization taking place.

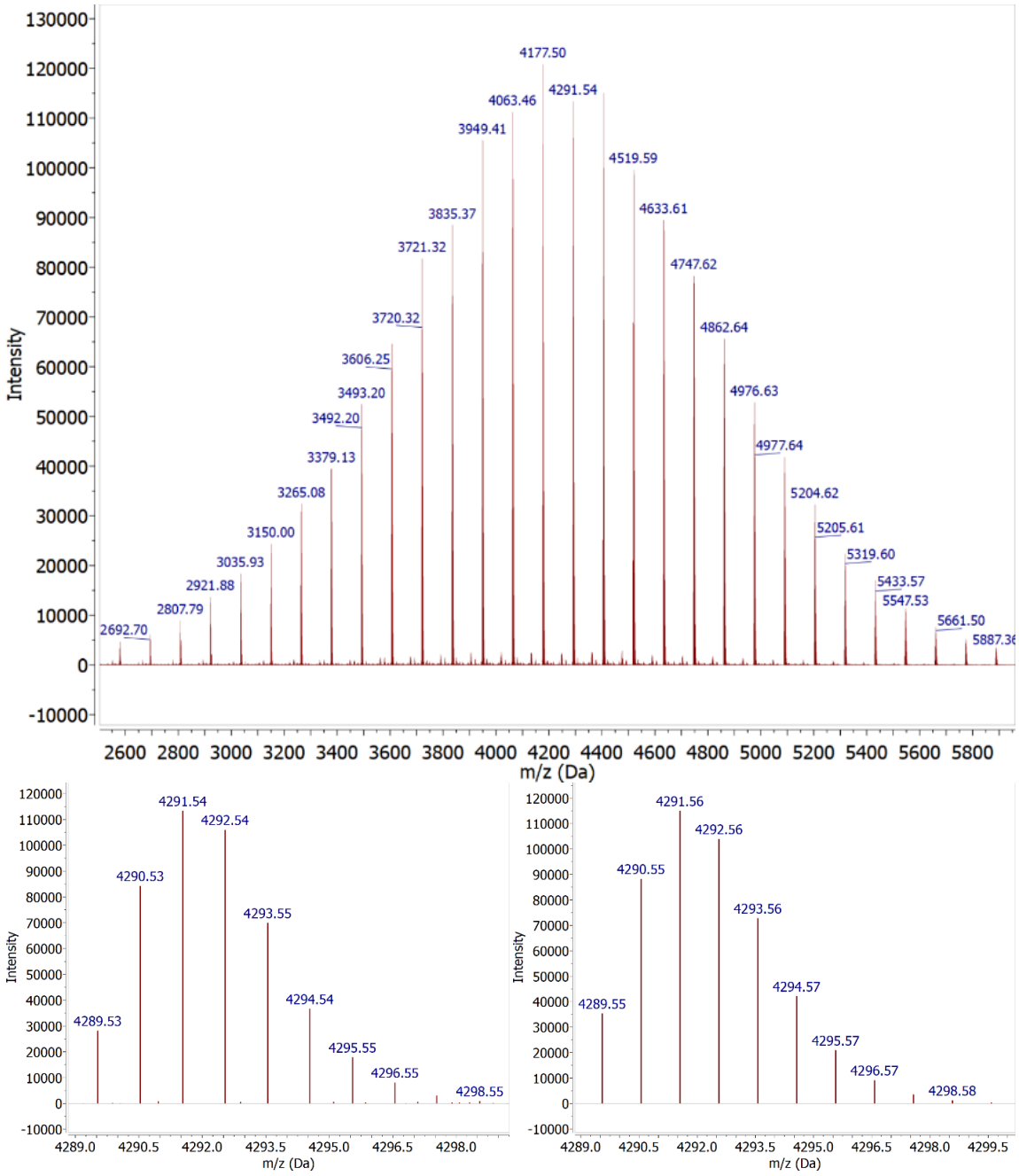

Figure 3.6. MALDI-TOF mass spectra of PCL produced with **3.6**/EtOH (top) showing expanded experimental (bottom left) and theoretical (bottom right) regions

3.7 Polymerization of Lactide

The ability of **3.5** to polymerize lactide was of interest, since catalysts that polymerize ε-CL are sometimes unable to perform ROP of lactide (and vice-versa) due to the relative stabilities of intermediates including the 5-membered metallacycle formed from lactide ring-opening.[52-53] ROP of ε-CL is governed chiefly by electronics whereas for lactide it is highly affected by sterics. The *rac*-lactide polymerizations reported here were highly diluted compared with ε-CL polymerizations due to the lower solubility of lactide in $CHCl_3$. Using **3.5** in the absence or presence of EtOH at room temperature, no polymer could be obtained after extended reaction times (Table 3.3, entries 1 and 3). However, trace peaks in the ^1H NMR spectrum appeared suggesting the formation of a new species, therefore, the inactivity of **3.5** towards ROP of *rac*-lactide was probed further by NMR studies on a mixture containing equimolar amounts of *rac*-lactide and **3.5** in $CDCl_3$. In direct contrast to ε-CL which easily perturbed the cation structure in the absence of co-initiator, the ^1H spectrum indicated that *rac*-lactide does not bind to the aluminum centre nor is it ring-opened, since the methylene proton resonance remains at 5.08 ppm, overlapping with the lactide methine proton signal (Figure A.25). However, addition of 1 equiv EtOH to this **3.5**/lactide solution produced peaks consistent with formation of an Al-lactate cation through ring-opening insertion of lactide into the Al–OEt bond (Figures A.26–A.28). Key ^1H and $^{13}C\{^1H\}$ resonances of the Al-lactate could be assigned. IR spectroscopy of this Al-lactate species showed $\nu_{C=O}$ bands at 1753 and 1678 cm^{-1} which correspond to the non-coordinated and coordinated carbonyl groups. This cation is unreactive towards further ring-opening reactions with *rac*-lactide and ε-CL (Table 3.3,

entry 2), in contrast to the Al-lactate cation reported by Dagorne and coworkers which polymerized ε-CL but not lactide.[46] Like Dagorne, I believe this Al-lactate cationic species is unreactive due to formation of a highly stable 5-membered metallacycle chelate and the bulky *tert*-butyl groups of the ancillary ligand may also play a role. No direct correlation of Lewis basicity to monomer reactivity could be made since the morpholinyl oxygen is more basic than cyclic esters.[45] Conducting lactide polymerization in the melt gave 17% conversion after 20 h (Table 3.3, entry 6) whereas in solution at 70 °C no polymer was observed after 18 h (Table 3.3, entry 5). Unfortunately, the polymer produced exhibited a broad dispersity, which is characteristic of an uncontrolled polymerization taking place.

Table 3.3. Attempted ROP of *rac*-lactide using complexes **3.5** and **3.6**[a]

Entry	Cat.	[Lactide]/[Al]/[EtOH]	T (°C)	Time (h)	Conv. (%)	M_n[b,c]	$Đ$[b]
1	**3.5**	200/1/0	20	72	–	–	–
2	**3.5**	200/1/1 + 500 equiv ε-CL	20	96	–	–	–
3	**3.5**	200/1/1	20	20	–	–	–
4	**3.6**	70/1/2	20	120	–	–	–
5	**3.5**	200/1/1	70	20	–	–	–
6	**3.5**	200/1/1	120	18	17	10700	3.15

[a] General Conditions: Al catalyst (4.9 mg, 6.1 μmol), EtOH (0.36 μL, 6.1 μmol), 5.00 mL of a *rac*-lactide solution (1.9319 g/50.00 mL $CHCl_3$). [b] Determined by triple detection GPC in THF. [c] In Da.

3.8 Conclusions

In summary, several cationic aluminum complexes were prepared *via* halide abstraction. In the presence of alcohols, **3.4** was not stable due to decomposition of the anion. The anions in **3.5** and **3.6** did not undergo alcoholysis and these complexes could

perform ROP of ε-CL with excellent control over molecular weight and dispersity of PCLs, but were less active than related neutral and cationic systems in the literature. Their controlled nature suggests such cationic species have potential as catalysts for related polymerizations and copolymerizations including carbonylative copolymerizations of epoxides. The unusual stability of the morpholinyl bidentate coordination to Al is supported by theoretical calculations. The stabilizing character of the morpholinyl ligand class is expected to offer privileged access to new complex architectures, which will have profound consequences on reactivity. Future studies will focus on di- and tri-block copolymer synthesis using the carbonate-terminated PCL reported herein. Further work is needed to study steric and electronic effects related to the morpholinyl-ligand structure, and to prepare related cationic complexes containing innocent (unreactive) anions, e.g. $[B(Ar)_4]^-$, through exploration of different synthetic pathways.

3.9 Experimental Section

3.9.1 General Considerations

Unless otherwise stated, all manipulations were done under an atmosphere of dry, oxygen-free nitrogen using Schlenk techniques or an MBraun Labmaster glovebox. All solvents were degassed using freeze-pump-thaw cycles. THF was distilled from sodium/benzophenone ketyl. $CHCl_3$ was refluxed and distilled over P_2O_5. Toluene, heptane, pentane, and CH_2Cl_2 were purified with an MBraun Manual Solvent Purification System. Deuterated solvents were purchased from Cambridge Isotope Laboratories, Inc. and dried over CaH_2 before use. Glycidol was dried over CaH_2 for 24 h at room temperature, distilled under reduced pressure, and stored in the glovebox freezer (*N.B.*

Glycidol distillation should be carried out behind a safety shield). ε-CL was dried over CaH_2 overnight and distilled under reduced pressure. *rac*-Lactide was purchased from Alfa Aesar, dried over Na_2SO_4 in THF, and recrystallized. EtOH was dried over CaH_2 and distilled. Triphenylborane was purchased from Gelest, recrystallized from Et_2O, and sublimed under vacuum. Tris(pentafluorophenyl)borane was purchased from Strem and used as received. Synthesis of H_2[**L2**] was performed using H_2O as the solvent instead of MeOH as previously reported[9], followed by recrystallization from $CHCl_3$/MeOH. Elemental analytical data were collected by Guelph Chemical Laboratories, Inc., Guelph, ON, Canada. ^1H and $^{13}C\{^1H\}$ NMR spectra were recorded on a Bruker Avance 300 or 500 MHz spectrometer at 25 °C (unless otherwise stated) and referenced internally to residual signals of the solvent. ^{11}B, ^{27}Al, and ^{71}Ga NMR spectra were acquired on a Bruker Avance 300 MHz spectrometer at 25 °C and referenced externally to $BF_3{\cdot}OEt_2$, $Al_2(SO_4)_3$ in D_2O, or $Ga(NO_3)_3$ in D_2O, respectively. All NMR experiments involving ^{11}B were carried out using quartz NMR tubes to eliminate interference from boron-containing glass. MALDI-TOF mass spectra were acquired on a Bruker ultrafleXtreme MALDI-TOF/TOF MS system running in reflectron mode at Bruker Daltonics, Billerica, MA, USA or a Waters MALDI SYNAPT G2-Si system running in resolution mode at Waters Corporation, Beverly, MA, USA. Polymers were mixed in a 4:1 (matrix:polymer) ratio in THF with 2,5-dihydroxybenzoic acid as the matrix and spotted. Complexes were mixed in a 2:1 (matrix:complex) ratio in CH_2Cl_2 with anthracene as the matrix, spotted on a plate in the glovebox, and transported in an air-tight bag. ESI mass spectra were acquired on an Agilent 6230 TOF LC/MS and processed with MassHunter workstation software. The ESI capillary

voltage was maintained at 3500 V. In a glovebox, samples were dissolved in dry MeCN at 0.5 mg/mL and filtered through 0.2 μm syringe filters and analyzed immediately. DSC data were collected on a Mettler Toledo DSC1 Star^e System with a scanning rate of 10 °C/min and nitrogen gas flow of 50 mL/min. Samples were heated from −70 to 150 °C three times to eliminate the difference in sample history and all melting temperatures were taken from the third heating cycle. Polymer molecular weight determination was performed on a GPC setup consisting of an Agilent Infinity HPLC, Wyatt Technologies triple detection (miniDAWN TREOS light scattering, ViscoStar-II viscometer, and Optilab T-rEX refractive index detectors), and two Phenogel columns (10^3 Å and 10^4 Å, 300 × 4.6 mm) with THF as eluent. Samples were prepared at a concentration of 4 mg/mL, filtered through 0.2 μm syringe filters, and run at 0.3 mL/min. Chromatograms were processed using Astra 6 software (Wyatt Technologies) using a dn/dc value of 0.075 mL/g for PCL in THF reported[44] in the literature. For polylactide in THF, a dn/dc value of 0.049 mL/g was used.[54] Microwave polymerizations were performed using a Biotage Initiator microwave reactor. Infrared spectra were recorded on a Bruker Alpha FTIR spectrometer with single-bounce diamond ATR accessory in the range of 4000–400 cm^{-1}.

3.9.2 Typical Procedure for ε-CL Polymerization

$CHCl_3$ (109 μL) solutions of Al catalyst (13.7 mg, 17.1 μmol) and EtOH (0.996 μL, 17.1 μmol) were transferred to a vial using a glass syringe and stirred briefly. 2.00 mL of a ε-CL solution (9.7485 g/50.00 mL $CHCl_3$) was added *via* pipette and the clear colorless solution was stirred for the allotted time. After the vial was removed from the glovebox, an NMR aliquot was taken (in $CDCl_3$) to determine conversion and the polymer was

precipitated immediately with cold MeOH and stored in the freezer overnight. After centrifugation, the solution phase was decanted and polymer was dried *in vacuo* to yield a white powder which was analyzed by GPC.

3.9.3 Typical Procedure for Lactide Polymerization

$CHCl_3$ (39 μL) solutions of Al catalyst (4.9 mg, 6.1 μmol) and EtOH (0.36 μL, 6.1 μmol) were transferred to a vial using a glass syringe and stirred briefly. 5.00 mL of a *rac*-lactide solution (1.9319 g/50.00 mL $CHCl_3$) was added *via* pipette and the solution stirred for the allotted time. After the vial was removed from the glovebox, an NMR aliquot was taken in $CDCl_3$ to determine conversion. For melt polymerization (120 °C), volatiles were removed *in vacuo* prior to heating in an oil bath.

3.9.4 Computational Details

Calculations were carried out using the Gaussian 09 software package.[55] The B97-D3 dispersion-corrected functional[56-58] was employed. The 6-311G(d,p) basis set[59-60] was used for C, H, N, and O atoms. The LANL2DZ basis set[61] and associated relativistic effective core pseudopotential were used for Al and Cl atoms. Solvent effects for $CHCl_3$ were introduced using the SMD model[62] during geometry optimizations and frequency calculations.

3.9.5 Synthetic Procedures

$[N_2O_3]^{tBu,tBu}AlCl$ (**3.1**). A solution of diethylaluminum chloride (25% w/w in toluene; 1.38 g, 11.5 mmol) was added dropwise to a stirred solution of H_2[**L2**] (6.18 g, 10.9 mmol) in toluene and stirred for 2 h. Volatiles were removed in vacuo and the residue was washed

with 30 mL heptane and 2×20 mL pentane to furnish a colorless crystalline solid after drying. Crystals of **3.1** could be grown from a concentrated CH_2Cl_2 solution upon standing at room temperature. Yield: 6.70 g, 97.9%. ^{1}H NMR ($CDCl_3$, 300 MHz, 298 K) δ 7.27 (2H, d, Ar*H*), 6.83 (2H, d, Ar*H*), 3.82 (4H, t, Ar–C*H*$_2$–N), 3.66 (4H, br s, N–CH$_2$–C*H*$_2$–O), 3.48 (2H, t, N–C*H*$_2$–CH$_2$–morph), 2.4–4.8 (4H, br s, N–C*H*$_2$–CH$_2$–O), 2.82 (2H, s, N–CH$_2$–C*H*$_2$–morph), 1.46 (18H, s, Ar–C{C*H*$_3$}$_3$), 1.27 (18H, s, Ar–C{C*H*$_3$}$_3$). ^{13}C{^{1}H} NMR ($CDCl_3$, 75 MHz, 298 K) δ 155.4, 140.0, 139.1, 124.4, 123.3, 119.8 (Ar*C*), 60.5 (Ar–*C*H$_2$–N), 59.1 (N–CH$_2$–*C*H$_2$–O), 52.1 (N–*C*H$_2$–CH$_2$–O), 48.6 (N–*C*H$_2$–CH$_2$–morph), 47.6 (N–CH$_2$–*C*H$_2$–morph), 35.1, 34.3 (Ar–*C*{CH$_3$}$_3$), 31.9, 29.7 (Ar–C{*C*H$_3$}$_3$). Anal. Calcd for $C_{36}H_{56}AlClN_2O_3$: C, 68.93; H, 9.00; 4.47. Found: C, 68.68; H, 8.84; N, 4.36. MS (MALDI-TOF) *m/z* (%, ion): 591.4095 (100, [Al[**L2**]]$^+$). HRMS (ESI/Q-TOF) *m/z*: [Al[**L2**]]$^+$ Calcd for $C_{36}H_{56}AlN_2O_3$ 591.4106; Found 591.4128.

{[N_2O_3]^{tBu,tBu}Al}$^+$ {Et$_m$AlCl$_n$}$^-$ (**3.2**). A solution of diethylaluminum chloride (25% w/w in toluene; 0.240 g, 1.99 mmol) was added dropwise to a stirred solution of **3.1** (1.20 g, 1.92 mmol) in toluene (7 mL). After 30 min stirring all volatiles were removed under vacuum. The residue was recrystallized from pentane at –30 °C to yield a colorless solid, **3.2**. Yield: 0.512 g, 35.8%. ^{1}H NMR ($CDCl_3$, 300 MHz, 298 K) δ 7.34 (2H, d, Ar*H*), 6.95 (2H, d, Ar*H*), 5.08 (2H, q, N–CH$_2$–C*H*$_2$–O), 4.25 (2H, overlapping q, N–CH$_2$–C*H*$_2$–O), 4.06 (2H, d, Ar–C*H*$_2$–N), 3.90 (2H, overlapping d, Ar–C*H*$_2$–N), 3.83 (2H, overlapping q, N–C*H*$_2$–CH$_2$–O), 3.74 (2H, overlapping t, N–CH$_2$–C*H*$_2$–morph), 3.57 (2H, q, N–C*H*$_2$–CH$_2$–O), 3.27 (2H, t, N–C*H*$_2$–CH$_2$–morph), 1.35–1.45 (18H, m, Ar–C{C*H*$_3$}$_3$), 1.29 (18H, s, Ar–C{C*H*$_3$}$_3$), 1.00–1.25 (6H, three sets of t, (C*H*$_3$–CH$_2$)$_m$–AlCl$_n^-$), −0.10–0.18 (4H, m,

(CH_3–CH_2)$_m$–$AlCl_n^-$). X-ray quality crystals of **3.2** were obtained from the heptane washings obtained during the isolation of **3.1** (which contained residual Et_2AlCl). The heptane washings gave colorless crystals upon standing at room temperature.

{[N_2O_3]^{tBu,tBu}Al}$^+$ {B(C_6F_5)$_3$Cl}$^-$ (**3.3**). Prepared on an NMR scale with **3.1** (47.6 mg, 75.9 μmol) and tris(pentafluorophenyl)borane (39.3 mg, 76.8 μmol) in toluene-d_8 (0.7 mL) giving a colorless solution. ^{1}H NMR (toluene-d_8, 300 MHz, 298 K) δ 7.44 (2H, d, Ar*H*), 6.82 (2H, d, Ar*H*), 4.39 (2H, q, N–CH_2–CH_2–O), 3.36 (2H, d, Ar–CH_2–N), 3.26 (2H, d, Ar–CH_2–N), 3.05 (2H, q, N–CH_2–CH_2–O), 2.54 (2H, overlapping t, N–CH_2–CH_2–morph), 2.50 (2H, overlapping q, N–CH_2–CH_2–O), 2.36 (2H, q, N–CH_2–CH_2–O), 2.23 (2H, t, N–CH_2–CH_2–morph), 1.37 (18H, s, Ar–C{CH_3}$_3$), 1.30 (18H, s, Ar–C{CH_3}$_3$).^{13}C{^{1}H} NMR (toluene-d_8, 75 MHz, 298 K) δ 152.5, 142.8, 138.9, 125.8, 124.9, 119.7 (Ar*C*), 67.3 (N–CH_2–*C*H_2–O), 57.0 (Ar–*C*H_2–N), 50.3 (N–*C*H_2–CH_2–O), 48.9 (N–CH_2–*C*H_2–morph), 47.6 (N–*C*H_2–CH_2–morph), 35.1, 34.4 (Ar–*C*{CH_3}$_3$), 31.6, 30.4 (Ar–C{*C*H_3}$_3$).

{[N_2O_3]^{tBu,tBu}Al}$^+$ {$AlCl_4$}$^-$ (**3.4**). $AlCl_3$ (0.326 g, 2.44 mmol) was added to a stirred toluene (20 mL) solution of **3.1** (1.58 g, 2.52 mmol). After 3 min, a colorless solid precipitated from solution. The solution was decanted and the solid washed with heptane (2×10 mL) and pentane (2×10 mL) and dried under vacuum. Yield: 1.79 g, 96.3%. ^{1}H NMR ($CDCl_3$, 300 MHz, 298 K) δ 7.34 (2H, d, Ar*H*), 6.98 (2H, d, Ar*H*), 5.10 (2H, q, N–CH_2–CH_2–O), 4.23 (2H, q, N–CH_2–CH_2–O), 4.05 (2H, d, Ar–CH_2–N), 3.91 (2H, d, Ar–CH_2–N), 3.70 (2H, overlapping t, N–CH_2–CH_2–morph), 3.70 (2H, overlapping q, N–CH_2–CH_2–O), 3.57 (2H, q, N–CH_2–CH_2–O), 3.29 (2H, t, N–CH_2–CH_2–morph), 1.39 (18H, s, Ar–C{CH_3}$_3$), 1.29 (18H, s, Ar–C{CH_3}$_3$). ^{13}C{^{1}H} NMR ($CDCl_3$, 75 MHz, 298 K) δ

152.4, 142.5, 138.7, 125.5, 125.0, 119.6 (Ar*C*), 68.0 (N–CH_2–*C*H_2–O), 57.5 (Ar–*C*H_2–N), 51.1 (N–*C*H_2–CH_2–O), 49.6 (N–CH_2–*C*H_2–morph), 48.5 (N–*C*H_2–CH_2–morph), 35.1, 34.4 (Ar–*C*{CH_3}$_3$), 31.7, 30.4 (Ar–C{*C*H_3}$_3$). ^{27}Al NMR ($CDCl_3$, 78 MHz, 298 K) δ 104.27 (s, *Al*Cl_4^-). Anal. Calcd for $C_{36}H_{56}Al_2Cl_4N_2O_3$: C, 56.85; H, 7.42; N, 3.68. Found: C, 57.11; H, 7.20; N, 3.39. HRMS (ESI/Q-TOF) *m/z*: $[AlCl_4]^-$ Calcd for $AlCl_4$ 168.8539; Found 168.8532.

{$[N_2O_3]^{tBu,tBu}$Al}$^+$ {$GaCl_4$}$^-$ (**3.5**). This compound was prepared in the same manner as above with **3.1** (1.58 g, 2.52 mmol) and $GaCl_3$ (0.455 g, 2.58 mmol) as starting materials and washed with heptane (2×10 mL) and once with 10 mL pentane. Obtained as a colorless solid. Yield: 2.05 g, 100%. Crystals suitable for single-crystal X-ray analysis could be grown from a CH_2Cl_2/toluene solution at –30 °C. ^{1}H NMR ($CDCl_3$, 300 MHz, 298 K) δ 7.32 (2H, d, Ar*H*), 6.96 (2H, d, Ar*H*), 5.09 (2H, q, N–CH_2–C*H*$_2$–O), 4.22 (2H, q, N–CH_2–C*H*$_2$–O), 4.04 (2H, d, Ar–C*H*$_2$–N), 3.90 (2H, d, Ar–C*H*$_2$–N), 3.71 (2H, overlapping t, N–CH_2–C*H*$_2$–morph), 3.71 (2H, overlapping q, N–C*H*$_2$–CH_2–O), 3.56 (2H, q, N–C*H*$_2$–CH_2–O), 3.28 (2H, t, N–C*H*$_2$–CH_2–morph), 1.38 (18H, s, Ar–C{C*H*$_3$}$_3$), 1.28 (18H, s, Ar–C{C*H*$_3$}$_3$). ^{13}C{^{1}H} NMR ($CDCl_3$, 75 MHz, 298 K) δ 152.4, 142.5, 138.8, 125.6, 125.0, 119.5 (Ar*C*), 68.0 (N–CH_2–*C*H_2–O), 57.5 (Ar–*C*H_2–N), 51.1 (N–*C*H_2–CH_2–O), 49.7 (N–CH_2–*C*H_2–morph), 48.6 (N–*C*H_2–CH_2–morph), 35.1, 34.4 (Ar–*C*{CH_3}$_3$), 31.7, 30.4 (Ar–C{*C*H_3}$_3$). ^{71}Ga NMR ($CDCl_3$, 92 MHz, 298 K) δ 251.9 (br s, *Ga*Cl_4^-). Anal. Calcd for $C_{36}H_{56}AlCl_4GaN_2O_3$: C, 53.82; H, 7.03; N, 3.49. Found: C, 54.07; H, 6.85; N, 3.39. MS (MALDI-TOF) *m/z* (%, ion): 210.7867 (100, $[GaCl_4]^-$). HRMS (ESI/Q-TOF) *m/z*:

$[GaCl_4]^-$ Calcd for $GaCl_4$ 210.7988; Found 210.8011. $[Al[\mathbf{L2}]]^+$ Calcd for $C_{36}H_{56}AlN_2O_3$ 591.4106; Found 591.4114.

$\{[N_2O_3]^{tBu,tBu}Al\}^+ \{InCl_4\}^-$ (**3.6**). $InCl_3$ (0.567 g, 2.56 mmol), **3.1** (1.72 g, 2.73 mmol), and toluene (ca. 100 mL) were combined in an ampoule and heated at reflux for 48 h yielding a pale-yellow solution. Concentrating this solution precipitated the product as a colorless solid. The solution was decanted and the solid washed with pentane (3×10 mL) and dried in vacuo. Yield: 1.96 g, 90.2%. Crystals suitable for single-crystal X-ray analysis could be grown from a CH_2Cl_2/toluene solution at –30 °C. ^{1}H NMR ($CDCl_3$, 300 MHz, 298 K) δ 7.32 (2H, d, Ar*H*), 6.93 (2H, d, Ar*H*), 5.09 (2H, q, N–CH_2–C*H*$_2$–O), 4.20 (2H, m, N–CH_2–C*H*$_2$–O), 4.02 (2H, d, Ar–C*H*$_2$–N), 3.87 (2H, d, Ar–C*H*$_2$–N), 3.70 (2H, overlapping t, N–CH_2–C*H*$_2$–morph), 3.70 (2H, overlapping q, N–C*H*$_2$–CH_2–O), 3.56 (2H, q, N–C*H*$_2$–CH_2–O), 3.25 (2H, t, N–C*H*$_2$–CH_2–morph), 1.37 (18H, s, Ar–C{C*H*$_3$}$_3$), 1.27 (18H, s, Ar–C{C*H*$_3$}$_3$). ^{13}C{^{1}H} NMR ($CDCl_3$, 75 MHz, 298 K) δ 152.4, 142.6, 138.8, 125.6, 125.0, 119.5 (Ar*C*), 68.1 (N–CH_2–*C*H_2–O), 57.6 (Ar–*C*H_2–N), 51.3 (N–*C*H_2–CH_2–O), 49.7 (N–CH_2–*C*H_2–morph), 48.6 (N–*C*H_2–CH_2–morph), 35.1, 34.4 (Ar–*C*{CH_3}$_3$), 31.7, 30.4 (Ar–C{*C*H_3}$_3$). Anal. Calcd for $C_{36}H_{56}AlCl_4InN_2O_3$: C, 50.96; H, 6.65; N, 3.30. Found: C, 51.17; H, 6.57; N, 3.21. HRMS (ESI/Q-TOF) *m/z*: $[InCl_4]^-$ Calcd for $InCl_4$ 256.7762; Found 256.7784. $[Al[\mathbf{L2}]]^+$ Calcd for $C_{36}H_{56}AlN_2O_3$ 591.4106; Found 591.4105.

$\{[N_2O_3]^{tBu,tBu}Al\}^+ \{BiCl_4\}^-$ (**3.7**). **3.1** (1.84 g, 2.94 mmol) was dissolved in ca. 30 mL toluene in a 100 mL ampoule and $BiCl_3$ (0.903 g, 2.86 mmol) was added directly to the stirring solution. The resulting suspension was heated to reflux overnight to dissolve unreacted $BiCl_3$. The toluene phase was decanted, and the precipitate washed with toluene

(2×20 mL) and pentane (2×20 mL) and dried under vacuum to yield a colorless solid. Yield: 2.36 g, 87.3%. ^{1}H NMR (C_5D_5N, 300 MHz, 298 K) δ 7.46 (2H, d, Ar*H*), 7.16 (2H, obscured by residual toluene, Ar*H*), 4.32 (2H, d, Ar–C*H*$_2$–N), 4.16 (2H, m, Ar–C*H*$_2$–N), 3.54 (4H, t, N–CH$_2$–C*H*$_2$–O), 3.30 (2H, t, N–C*H*$_2$–CH$_2$–morph), 2.57 (2H, t, N–CH$_2$–C*H*$_2$–morph), 2.21 (4H, overlapping s, N–C*H*$_2$–CH$_2$–O), 1.40 (s, 18H, Ar–C{C*H*$_3$}$_3$), 1.25 (s, 18H, Ar–C{C*H*$_3$}$_3$). ^{13}C{^{1}H} NMR (C_5D_5N, 75 MHz, 298 K) δ 156.46, 140.46, 138.19, 122.55 (two resonances absent; Ar*C*), 67.6 (N–CH$_2$–*C*H$_2$–O), 56.6 (Ar–*C*H$_2$–N), 55.1 (N–*C*H$_2$–CH$_2$–O), 50.8 (N–CH$_2$–*C*H$_2$–morph), 50.0 (N–*C*H$_2$–CH$_2$–morph), 35.3, 35.0 (Ar–*C*{CH$_3$}$_3$), 32.6, 30.4 (Ar–C{*C*H$_3$}$_3$). Anal. calcd for $C_{36}H_{56}AlCl_4BiN_2O_3$: C, 45.87; H, 5.99; N, 2.97. Found: C, 45.83; H, 5.97; N, 2.77. HRMS (ESI/Q-TOF) *m/z*: $[BiCl_4]^-$ Calcd for $BiCl_4$ 350.8528; Found 350.8553. [Al[**L2**]]$^+$ Calcd for $C_{36}H_{56}AlN_2O_3$ 591.4106; Found 591.4123.

3.5 + 2 equiv EtOH. ^{1}H NMR ($CDCl_3$, 300 MHz, 298 K) δ 13.36 (1H, s, N*H*–CH$_2$–CH$_2$–O), 7.27 (2H, d obscured by $CDCl_3$ peak, Ar*H*), 6.91 (2H, d, Ar*H*), 4.19 (2H, q, O–C*H*$_2$–CH$_3$), 4.08 (2H, overlapping d, NH–CH$_2$–C*H*$_2$–O), 4.02 (2H, overlapping q, CH$_3$–C*H*$_2$–OH), 3.83 (4H, br s, Ar–C*H*$_2$–N), 3.71 (2H, t, NH–CH$_2$–C*H*$_2$–O), 3.30 (2H, overlapping s, N–CH$_2$–C*H*$_2$–morph), 3.27 (2H, overlapping d,), 3.15 (1H, overlapping s, CH$_3$–CH$_2$–O*H*), 3.13 (2H, s, N–C*H*$_2$–CH$_2$–morph), 2.89 (2H, q, NH–C*H*$_2$–CH$_2$–O), 1.47 (3H, t, O–CH$_2$–C*H*$_3$), 1.40 (18H, s, Ar–C{C*H*$_3$}$_3$), 1.35 (3H, t, C*H*$_3$–CH$_2$–OH), 1.28 (18H, s, Ar–C{C*H*$_3$}$_3$). ^{13}C{^{1}H} NMR ($CDCl_3$, 75 MHz, 298 K) δ 153.5, 141.2, 137.0, 124.7, 120.6 (Ar*C*), 64.4 (NH–CH$_2$–*C*H$_2$–O), 61.4 (O–*C*H$_2$–CH$_3$), 61.1 (Ar–*C*H$_2$–N), 59.1 (CH$_3$–C*H*$_2$–OH), 53.7 (N–CH$_2$–*C*H$_2$–morph), 53.1 (N–*C*H$_2$–CH$_2$–morph), 51.7 (NH–*C*H$_2$–CH$_2$–

O), 35.0, 34.3 (Ar–*C*{CH_3}$_3$), 31.8, 29.8 (Ar–C{*C*H_3}$_3$), 20.3 (*C*H_3–CH_2–OH), 17.7 (O–CH_2–*C*H_3).

3.5 + 1 equiv ε-CL. ^{1}H NMR ($CDCl_3$, 300 MHz, 298 K) δ 7.27 (2H, d, Ar*H*), 6.93 (2H, d, Ar*H*), 4.77 (2H, s, Al–O=C(O)(C*H*$_2$)$_5$), 4.05 (2H, t, N–CH_2–C*H*$_2$–O), 3.95 (2H, d, Ar–C*H*$_2$–N), 3.84 (2H, d, Ar–C*H*$_2$–N), 3.78 (2H, d, N–CH_2–C*H*$_2$–O), 3.70 (2H, overlapping t, N–CH_2–C*H*$_2$–morph), 3.69 (2H, overlapping t, N–C*H*$_2$–CH_2–O), 3.18 (2H, s, Al–O=C(O)(C*H*$_2$)$_5$), 2.98 (2H, t, N–C*H*$_2$–CH_2–morph), 2.76 (2H, d, N–C*H*$_2$–CH_2–O), 2.13 (2H, overlapping resonance, Al–O=C(O)(C*H*$_2$)$_5$), 2.07 (2H, overlapping resonance, Al–O=C(O)(C*H*$_2$)$_5$), 2.04 (2H, overlapping resonance, Al–O=C(O)(C*H*$_2$)$_5$), 1.37 (18H, s, Ar–C{C*H*$_3$}$_3$), 1.26 (18H, s, Ar–C{C*H*$_3$}$_3$). ^{13}C{^{1}H} NMR ($CDCl_3$, 75 MHz, 298 K) δ 187.2 (Al–O=*C*(O)$(CH_2)_5$), 153.3, 141.3, 137.5, 124.7, 124.4, 119.8 (Ar*C*), 75.9 (Al–O=C(O)(*C*H$_2$)$_5$), 60.5 (N–CH_2–*C*H_2–O), 58.3 (Ar–*C*H_2–N), 52.4 (N–*C*H_2–CH_2–O), 48.3 (N–CH_2–*C*H_2–morph), 47.9 (N–*C*H_2–CH_2–morph), 35.8 (Al–O=C(O)(*C*H$_2$)$_5$), 35.1, 34.2 (Ar–*C*{CH_3}$_3$), 31.7, 29.8 (Ar–C{*C*H_3}$_3$), 28.2, 27.7, 22.4 (Al–O=C(O)(*C*H$_2$)$_5$).

3.5 + 1 equiv EtOH + 1 equiv *rac*-lactide. ^{1}H NMR ($CDCl_3$, 300 MHz, 298 K) δ 7.29 (1H, d, Ar*H*), 7.26 (1H, overlapping d, Ar*H*), 6.99 (1H, d, Ar*H*), 6.92 (1H, d, Ar*H*), 5.58 (1H, q, Al–O–C*H*–C=O), 4.81 (1H, q, O–C*H*–COOEt), 4.34 (2H, br s), 4.32 (2H, m, C(O)OC*H*$_2$–CH_3), 4.20 (1H, d), 4.18 (1H, overlapping resonance), 4.05 (1H, d), 2.96–3.77 (11H, overlapping methylene resonances), 2.86 (1H, q), 1.79 (Al–O–CH(C*H*$_3$)–C=O), 1.66 (O–CH(C*H*$_3$)–COOEt), 1.36 (18H, s, Ar–C{C*H*$_3$}$_3$), 1.35 (3H, t, C(O)OCH$_2$–C*H*$_3$), 1.31 (9H, s, Ar–C{C*H*$_3$}$_3$), 1.28 (9H, s, Ar–C{C*H*$_3$}$_3$). ^{13}C{^{1}H} NMR ($CDCl_3$, 75 MHz, 298 K) δ 187.0 (*C*=O$_{\text{lactate chelate}}$), 167.8 (*C*=O$_{\text{ethyl ester}}$), 154.19, 154.16, 140.8, 140.5, 137.8, 137.3,

124.6, 124.5, 124.3, 124.2, 120.6, 120.4 (Ar*C*), 74.2 (Al–O–*C*H–C=O), 68.2 (O–*C*H–COOEt), 64.4, 64.1, 62.5 (C(O)O*C*H_2–CH_3), 62.1, 60.6, 53.9, 53.3, 52.5, 51.4, 35.0, 34.9, 34.3 (Ar–*C*{CH_3}$_3$), 31.82, 31.79, 29.5, 29.4 (Ar–C{*C*H_3}$_3$), 22.0 (O–CH(*C*H_3)–COOEt), 17.1 (Al–O–CH(*C*H_3)–C=O), 14.1 (C(O)OCH_2–*C*H_3). FT-IR ($CHCl_3$): 1753 ($C{=}O_{ethyl\ ester}$), 1678 ($C{=}O_{lactate\ chelate}$) cm^{-1}.

Preparation of Glycerol Carbonate. Cr^{III} amino-phenolate catalyst[63] (56.3 mg, 135 μmol) and $PPNN_3$ (79.3 mg, 137 μmol) were stirred in CH_2Cl_2 solution for 15 minutes, then CH_2Cl_2 was removed *in vacuo.* The residue was dissolved in glycidol (5.00 g, 67.5 mmol) and directly injected into a pre-dried pressure vessel and immediately pressurized to 40 bar CO_2. The vessel was heated at 60 °C for 48 h, cooled to room temperature, and depressurized to yield a viscous green solution. An aliquot taken for NMR analysis in CD_3OD showed quantitative conversion and the crude product was subjected to Kugelrohr distillation (0.25 mmHg, bp 130 °C), giving the pure product as a colourless viscous liquid. ^1H and $^{13}C\{^1H\}$ NMR data were in agreement with the scientific literature.

3.9.6 NMR Scale Reactions

ε-CL binding study: **3.5** (19.5 mg, 24.3 μmol) and ε-CL (2.77 mg, 24.3 μmol, $CHCl_3$ solution) were dissolved in $CDCl_3$ (0.7 mL) in a J. Young NMR tube, then analyzed *via* ^1H NMR.

Lactide binding study: **3.5** (21.0 mg, 26.1 μmol) and lactide (3.77 mg, 26.1 μmol, $CHCl_3$ solution) were dissolved in $CDCl_3$ (0.7 mL) in a J. Young NMR tube, then analyzed *via* ^1H NMR.

3.9.7 Kinetic Studies

For room temperature polymerizations, the procedure is identical to the typical procedure and aliquots were taken periodically and dissolved in $CDCl_3$ outside the glovebox. For the plot of M_n vs. Conversion vs. $Đ$, NMR samples were prepped for GPC analysis by evaporating the $CDCl_3$ and THF was added directly to dissolve the polymer sample. For higher temperature polymerizations, a Teflon-valved 20 mL ampoule was used with a programmable hotplate. Catalyst/EtOH and ε-CL solutions were equilibrated at the set temperature prior to mixing.

3.9.8 Crystallography

Single crystals of **3.1**, **3.2**, **3.5**, and **3.6** were mounted on low-temperature diffraction loops and measured on a Rigaku Saturn CCD area detector with graphite-monochromated Mo-Kα radiation. Using Olex2,[64] the structures were solved with the ShelXS[65] structure solution program using Direct Methods (**3.1**) and ShelXT[66] structure solution program using Intrinsic Phasing (**3.5–3.6**) or Direct Methods (**3.2**). Refinement was done with the ShelXL[67] refinement package using least squares minimisation. For **3.2**, data was processed as a two component twin, however, the second component was very small (less than 8% of all reflections) and had a high R_{int}. Inclusion of the second component *via* hklf5 did not yield satisfactory model refinement values (R_1 lower 23% was not achieved for I>2 σ I). Hence, the second twin contributions were omitted in the final reported structure. The Platon SQUEEZE[68] procedure was used to account for unresolved lattice solvent disorder in **3.1** and **3.2**.

3.10 References

1. S. Dagorne and D. A. Atwood, *Chem. Rev.*, **2008**, *108*, 4037-4071.
2. S. Dagorne and R. Wehmschulte, *ChemCatChem*, **2018**, *10*, 2509-2520.
3. Y. Sarazin and J.-F. Carpentier, *Chem. Rev.*, **2015**, *115*, 3564-3614.
4. A. Arbaoui and C. Redshaw, *Polym. Chem.*, **2010**, *1*, 801-826.
5. M. Schappacher, M. Le Hellaye, R. Bareille, M.-C. Durrieu and S. M. Guillaume, *Macromol. Biosci.*, **2010**, *10*, 60-67.
6. M. Tang, M. Purcell, J. A. M. Steele, K.-Y. Lee, S. McCullen, K. M. Shakesheff, A. Bismarck, M. M. Stevens, S. M. Howdle and C. K. Williams, *Macromolecules*, **2013**, *46*, 8136-8143.
7. J.-T. Issenhuth, J. Pluvinage, R. Welter, S. Bellemin-Laponnaz and S. Dagorne, *Eur. J. Inorg. Chem.*, **2009**, *2009*, 4701-4709.
8. N. Ikpo, S. M. Barbon, M. W. Drover, L. N. Dawe and F. M. Kerton, *Organometallics*, **2012**, *31*, 8145-8158.
9. E. D. Cross, G. K. Tennekone, A. Decken and M. P. Shaver, *Green Mater.*, **2013**, *1*, 79-86.
10. V. Poirier, T. Roisnel, J.-F. Carpentier and Y. Sarazin, *Dalton Trans.*, **2009**, 9820-9827.
11. L. Wang, M. Bochmann, R. D. Cannon, J.-F. Carpentier, T. Roisnel and Y. Sarazin, *Eur. J. Inorg. Chem.*, **2013**, *2013*, 5896-5905.
12. N. Ikpo, C. Hoffmann, L. N. Dawe and F. M. Kerton, *Dalton Trans.*, **2012**, *41*, 6651-6660.
13. N. Ikpo, L. N. Saunders, J. L. Walsh, J. M. B. Smith, L. N. Dawe and F. M. Kerton, *Eur. J. Inorg. Chem.*, **2011**, *2011*, 5347-5359.
14. S. M. Crawford, C. A. Wheaton, V. Mishra and M. Stradiotto, *Can. J. Chem.*, **2018**, *96*, 578-586.
15. M. A. MacLean, C. A. Wheaton and M. Stradiotto, *Can. J. Chem.*, **2018**, *96*, 712-721.
16. C. A. Wheaton and M. Stradiotto, *Can. J. Chem.*, **2013**, *91*, 755-762.
17. R. J. Lundgren, K. D. Hesp and M. Stradiotto, *Synlett*, **2011**, *2011*, 2443-2458.
18. H. Zhan, Y. Hu, P. Wang and J. Chen, *RSC Adv.*, **2017**, *7*, 6179-6186.
19. B. Gilbert, Y. Chauvin, H. Olivier and F. Di Marco-Van Tiggelen, *J. Chem. Soc., Dalton Trans.*, **1995**, 3867-3871.
20. Y. Vestfried, O. Chusid, Y. Goffer, P. Aped and D. Aurbach, *Organometallics*, **2007**, *26*, 3130-3137.
21. C. Elschenbroich and A. Salzer, *Organometallics: A Concise Introduction*, Wiley, 1992.
22. V. Kelsen, C. Vallée, E. Jeanneau, C. Bibal, C. C. Santini, Y. Chauvin and H. Olivier-Bourbigou, *Organometallics*, **2011**, *30*, 4284-4291.
23. P. N. Bartlett, C. Y. Cummings, W. Levason, D. Pugh and G. Reid, *Chem. Eur. J.*, **2014**, *20*, 5019-5027.
24. S. Dagorne, M. Bouyahyi, J. Vergnaud and J.-F. Carpentier, *Organometallics*, **2010**, *29*, 1865-1868.

25. M.-Á. Muñoz-Hernández, B. Sannigrahi and D. A. Atwood, *J. Am. Chem. Soc.*, **1999**, *121*, 6747-6748.
26. W. Su, J. Kobayashi, A. Ellern, T. Kawashima and J. G. Verkade, *Inorg. Chem.*, **2007**, *46*, 7953-7959.
27. W. Su, Y. Kim, A. Ellern, I. A. Guzei and J. G. Verkade, *J. Am. Chem. Soc.*, **2006**, *128*, 13727-13735.
28. A. W. Addison, T. N. Rao, J. Reedijk, J. van Rijn and G. C. Verschoor, *J. Chem. Soc., Dalton Trans.*, **1984**, 1349-1356.
29. B. Lian, H. Ma, T. P. Spaniol and J. Okuda, *Dalton Trans.*, **2009**, 9033-9042.
30. P. G. Alsabeh, R. J. Lundgren, R. McDonald, C. C. C. Johansson Seechurn, T. J. Colacot and M. Stradiotto, *Chem. Eur. J.*, **2013**, *19*, 2131-2141.
31. P. G. Alsabeh, R. McDonald and M. Stradiotto, *Organometallics*, **2012**, *31*, 1049-1054.
32. J. U. Izunobi and C. L. Higginbotham, *J. Chem. Educ.*, **2011**, *88*, 1098-1104.
33. C. E. Willans, M. A. Sinenkov, G. K. Fukin, K. Sheridan, J. M. Lynam, A. A. Trifonov and F. M. Kerton, *Dalton Trans.*, **2008**, 3592-3598.
34. H. E. Dyer, S. Huijser, A. D. Schwarz, C. Wang, R. Duchateau and P. Mountford, *Dalton Trans.*, **2008**, 32-35.
35. K. C. Hultzsch, T. P. Spaniol and J. Okuda, *Organometallics*, **1997**, *16*, 4845-4856.
36. M. Haddad, M. Laghzaoui, R. Welter and S. Dagorne, *Organometallics*, **2009**, *28*, 4584-4592.
37. P. Fei and S. Zhiquan, *J. Appl. Polym. Sci.*, **2007**, *106*, 1828-1835.
38. W. A. Munzeiwa, B. Omondi and V. O. Nyamori, *Polyhedron*, **2017**, *138*, 295-305.
39. S. O. Ojwach, T. T. Okemwa, N. W. Attandoh and B. Omondi, *Dalton Trans.*, **2013**, *42*, 10735-10745.
40. P. Dubois, I. Barakat, R. Jerome and P. Teyssie, *Macromolecules*, **1993**, *26*, 4407-4412.
41. M. K. Samantaray, V. Katiyar, D. Roy, K. Pang, H. Nanavati, R. Stephen, R. B. Sunoj and P. Ghosh, *Eur. J. Inorg. Chem.*, **2006**, *2006*, 2975-2984.
42. X. Wang, K. Liao, D. Quan and Q. Wu, *Macromolecules*, **2005**, *38*, 4611-4617.
43. A.-C. Albertsson and I. K. Varma, *Biomacromolecules*, **2003**, *4*, 1466-1486.
44. J. Zhou, W. Wang, S. Villarroya, K. J. Thurecht and S. M. Howdle, *Chem. Commun.*, **2008**, 5806-5808.
45. C. Laurence and J. F. Gal, *Lewis Basicity and Affinity Scales: Data and Measurement*, Wiley, 2009.
46. S. Dagorne, F. Le Bideau, R. Welter, S. Bellemin-Laponnaz and A. Maisse-François, *Chem. Eur. J.*, **2007**, *13*, 3202-3217.
47. N. Iwasa, S. Katao, J. Liu, M. Fujiki, Y. Furukawa and K. Nomura, *Organometallics*, **2009**, *28*, 2179-2187.
48. A. F. Douglas, B. O. Patrick and P. Mehrkhodavandi, *Angew. Chem. Int. Ed.*, **2008**, *47*, 2290-2293.
49. H. R. Kricheldorf, G. Behnken, G. Schwarz and J. Kopf, *Macromolecules*, **2008**, *41*, 4102-4107.

50. J. Cayuela, V. Bounor-Legaré, P. Cassagnau and A. Michel, *Macromolecules*, **2006**, *39*, 1338-1346.
51. H.-T. Sheng, H. Zhou, H.-D. Guo, H.-M. Sun, Y.-M. Yao, J.-F. Wang, Y. Zhang and Q. Shen, *J. Organomet. Chem.*, **2007**, *692*, 1118-1124.
52. R. K. Dean, A. M. Reckling, H. Chen, L. N. Dawe, C. M. Schneider and C. M. Kozak, *Dalton Trans.*, **2013**, *42*, 3504-3520.
53. K. Phomphrai, P. Chumsaeng, P. Sangtrirutnugul, P. Kongsaeree and M. Pohmakotr, *Dalton Trans.*, **2010**, *39*, 1865-1871.
54. S. A. Saba, B. Lee and M. A. Hillmyer, *ACS Macro Lett.*, **2017**, *6*, 1232-1236.
55. Gaussian 09, Revision D.01, M. J. Frisch, G. W. Trucks, H. B. Schlegel, G. E. Scuseria, M. A. Robb, J. R. Cheeseman, G. Scalmani, V. Barone, B. Mennucci, G. A. Petersson, H. Nakatsuji, M. Caricato, X. Li, H. P. Hratchian, A. F. Izmaylov, J. Bloino, G. Zheng, J. L. Sonnenberg, M. Hada, M. Ehara, K. Toyota, R. Fukuda, J. Hasegawa, M. Ishida, T. Nakajima, Y. Honda, O. Kitao, H. Nakai, T. Vreven, J. J. A. Montgomery, J. E. Peralta, F. Ogliaro, M. Bearpark, J. J. Heyd, E. Brothers, K. N. Kudin, V. N. Staroverov, T. Keith, R. Kobayashi, J. Normand, K. Raghavachari, A. Rendell, J. C. Burant, S. S. Iyengar, J. Tomasi, M. Cossi, N. Rega, J. M. Millam, M. Klene, J. E. Knox, J. B. Cross, V. Bakken, C. Adamo, J. Jaramillo, R. Gomperts, R. E. Stratmann, O. Yazyev, A. J. Austin, R. Cammi, C. Pomelli, J. W. Ochterski, R. L. Martin, K. Morokuma, V. G. Zakrzewski, G. A. Voth, P. Salvador, J. J. Dannenberg, S. Dapprich, A. D. Daniels, O. Farkas, J. B. Foresman, J. V. Ortiz, J. Cioslowski and D. J. Fox, Gaussian, Inc., Wallingford, CT, 2013.
56. A. D. Becke, *J. Chem. Phys.*, **1997**, *107*, 8554-8560.
57. H. L. Schmider and A. D. Becke, *J. Chem. Phys.*, **1998**, *108*, 9624-9631.
58. S. Grimme, S. Ehrlich and L. Goerigk, *J. Comput. Chem.*, **2011**, *32*, 1456-1465.
59. R. Krishnan, J. S. Binkley, R. Seeger and J. A. Pople, *J. Chem. Phys.*, **1980**, *72*, 650-654.
60. A. D. McLean and G. S. Chandler, *J. Chem. Phys.*, **1980**, *72*, 5639-5648.
61. W. R. Wadt and P. J. Hay, *J. Chem. Phys.*, **1985**, *82*, 284-298.
62. A. V. Marenich, C. J. Cramer and D. G. Truhlar, *J. Phys. Chem. B*, **2009**, *113*, 6378-6396.
63. K. Ambrose, Ph.D Thesis, *Cobalt and Chromium Amino-bis(phenolate) Complexes for Epoxide Homopolymerization and Copolymerization with Carbon Dioxide*, Memorial University of Newfoundland, 2019.
64. O. V. Dolomanov, L. J. Bourhis, R. J. Gildea, J. A. K. Howard and H. Puschmann, *J. Appl. Cryst.*, **2009**, *42*, 339-341.
65. G. M. Sheldrick, *Acta Cryst.*, **2008**, *A64*, 112-122.
66. G. M. Sheldrick, *Acta Cryst.*, **2015**, *A71*, 3-8.
67. G. M. Sheldrick, *Acta Cryst.*, **2015**, *C71*, 3-8.
68. A. L. Spek, *Acta Cryst.*, **2015**, *C71*, 9-18.

CHAPTER 4

Copolymerization of CHO/CO_2 Catalyzed by Aluminum Amino-Phenolate Complexes

Chapter 4. Copolymerization of CHO/CO_2 Catalyzed by Aluminum Amino-Phenolate Complexes

4.1 Introduction

Aluminum is desirable for catalytic reactions as it is cheap, earth-abundant, and a relatively non-toxic metal. Aluminum complexes for epoxide/CO_2 copolymerization have been reviewed with focus on PO and CHO.[1] Strides have been made in this area, with Zevaco and co-workers reporting an Al-N_2O_2 system (**1.30**, Figure 4.1) that is active at low pressures of CO_2.[2] The Kerton group previously reported aluminum amino-phenolate complexes that, in the absence of co-catalyst, showed promising incorporation of CO_2 (up to 54%) into the polycarbonate[3] and as shown in Chapter 2, the morpholinyl variant was highly active in ROP of CHO. These activities were attributed to the outer-sphere oxygen atom, which was proposed to promote chloride initiation *via* an intermolecular mechanism. Inspired by these highly active polymerization results, we prepared a simplified aluminum amino-bis(phenolate) complex **3.1** (Figure 4.1) which was subsequently utilized in cationic form in living ROP of ε-CL, outlined in Chapter 3.

It is important to establish structure-activity relationships to understand how the pendent donor in aluminum amino-phenolate complexes influences the aluminum electronics and hence reactivity. In this chapter, the ROCOP of CHO/CO_2 using two series of monometallic aluminum complexes will be presented.

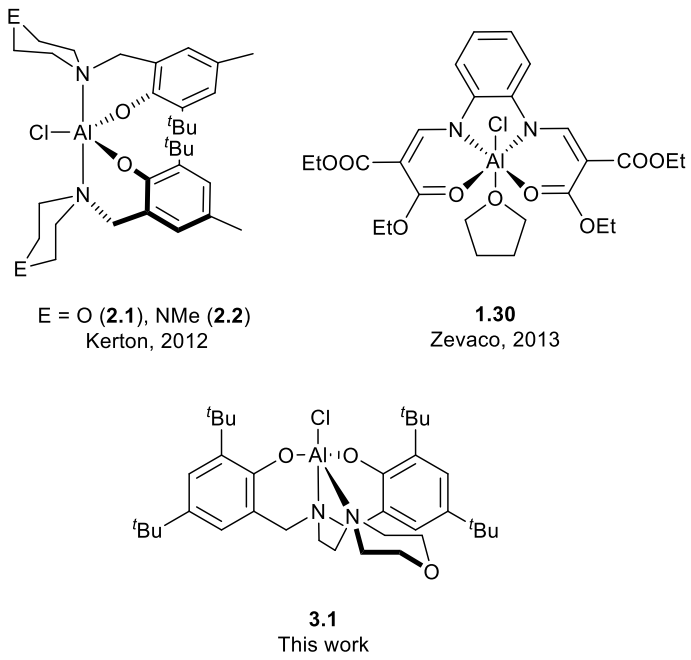

Figure 4.1. Aluminum complexes used in ROP and ROCOP

4.2 Results and Discussion

The two series of complexes described in this chapter are primarily distinguished by the steric and electronic properties of the pendent donor. This is a morpholine group in **3.1** but in **4.1** and **4.2** (Figure 4.2) it is a dimethylamino group. The pK_aH values for the truncated donors, trimethylamine (9.76) and *N*-methylmorpholine (7.41), were considered to assess which is a stronger donor to aluminum.[4] According to these values, the dimethylamino group is a stronger pendent donor (base) than the morpholine group, meaning that the aluminum centre in **3.1** should be more electropositive (Lewis acidic) than in **4.1**.

4.3 Complex Syntheses

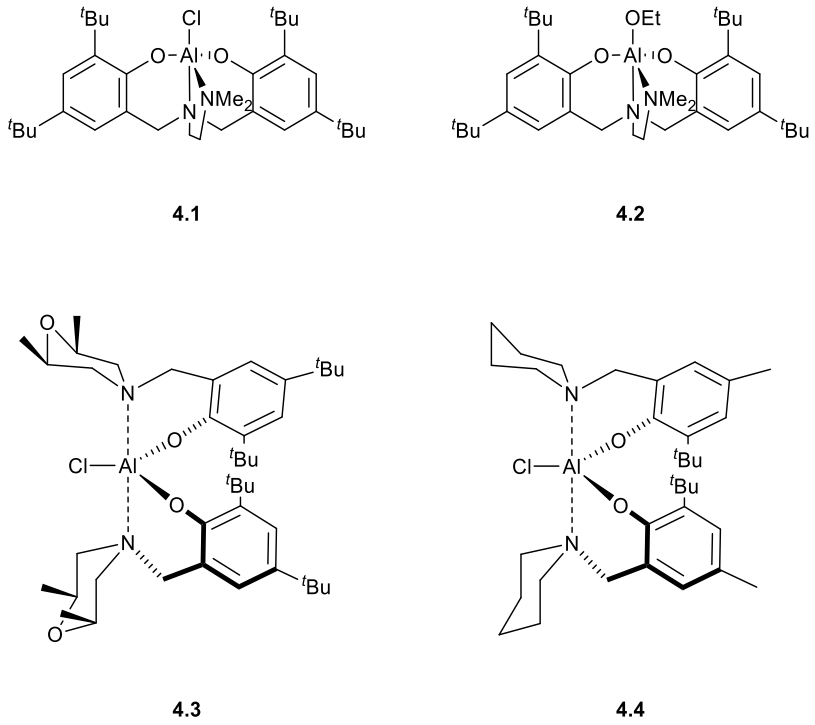

Figure 4.2. Structures of complexes **4.1–4.4**

Aluminum chloride complexes, **3.1**, **4.1**, **4.3** and **4.4** (Figure 4.2), were synthesized by alkane elimination reactions between 1 or 2 equiv of pro-ligand with diethylaluminum chloride in toluene. The insoluble nature of **4.1** in toluene necessitated reflux after aluminum reagent had been added to ensure all aluminum reagent had reacted. **4.2** (Figure 4.2) was prepared by refluxing the pro-ligand with a slight excess of $Al(OEt)_3$ in toluene. The complexes were isolated in 52–100% yield as colourless solids. The complexes were soluble in CH_2Cl_2 and toluene (except **4.1**). They were characterized by NMR spectroscopy (^1H, $^{13}C\{^1H\}$, and ^1H–^1H and ^1H–^{13}C correlations; see Figures A.42–A.55) and elemental

analyses. The ^{1}H NMR spectra confirmed the formation of monometallic aluminum complexes.

Complexes **4.1**, **4.3**, and **4.4** were structurally characterized by X-ray diffraction methods and the crystallographic data are summarized in Table C.2. **4.1** (Figure C.4) adopts a distorted trigonal bipyramidal geometry (τ = 0.80) which is essentially identical to that of the analogous ^{t}Bu, methyl phenolate complex (τ = 0.77), which has been reported previously.[5] The molecular structures of **4.3** and **4.4** are shown in Figures **4.3** and **4.4**, respectively, along with selected bond distances and angles. **4.3** and **4.4** each contain two bidentate ligands coordinated to the metal centre and adopt an almost ideal trigonal bipyramidal geometry (geometry indices, τ = 0.94 and 0.93, respectively). The amino-phenolate ligands are coordinated to the aluminum centre in a bidentate fashion, with the nitrogen atoms occupying the axial positions and the chloride and phenolate oxygen donors coordinated in the equatorial positions. This coordination presents two six-membered puckered rings (C_3NAlO). An alkyl aluminum analogue of **4.4** has been prepared previously, and in the solid state has only one piperidinyl bound to the Al centre.[6] The outer-sphere oxygens in **4.3** are orientated away from the Al centre, which was also seen for **2.2**.[3] Notably, the Al–Cl bond lengths are significantly smaller in **4.3** and **4.4** (ca. 2.20 Å) compared to **3.1** and **4.1** (ca. 2.25 Å) and Phomphrai proposed this resulted from axial coordination of chlorine[5].

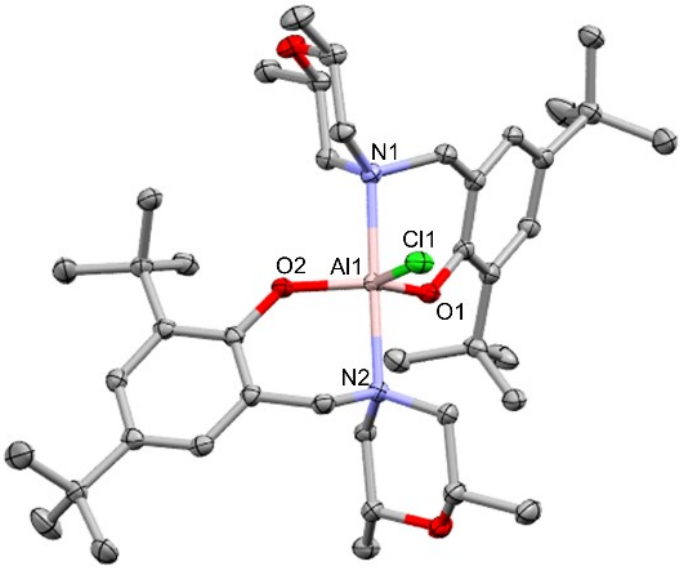

Figure 4.3. Molecular structure and partial numbering of **4.3** (thermal ellipsoids drawn at 50% probability; H atoms excluded for clarity). Selected bond distances (Å) and angles (°): Cl(1)–Al(1), 2.1986(7); Al(1)–O(1), 1.7673(13); Al(1)–O(2), 1.7666(13); Al(1)–N(1), 2.1303(15); Al(1)–N(2), 2.1319(15); O(1)–Al(1)–Cl(1), 119.71(5); O(1)–Al(1)–N(1), 89.55(6); O(1)–Al(1)–N(2), 90.28(6); O(2)–Al(1)–Cl(1), 118.15(5); O(2)–Al(1)–O(1), 122.14(6); O(2)–Al(1)–N(1), 90.91(6); O(2)–Al(1)–N(2), 90.16(6); N(1)–Al(1)–Cl(1), 89.35(5); N(1)–Al(1)–N(2), 178.83(6); N(2)–Al(1)–Cl(1), 89.72(5).

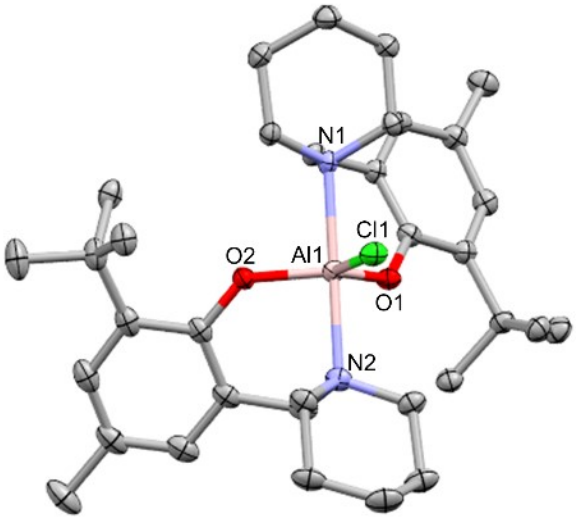

Figure 4.4. Molecular structure and partial numbering of **4.4** (thermal ellipsoids drawn at 50% probability; H atoms and one co-crystallized toluene molecule excluded for clarity). Selected bond distances (Å) and angles (°): Cl(1)–Al(1), 2.2043(9); Al(1)–O(1), 1.7724(17); Al(1)–O(2), 1.7716(17); Al(1)–N(1), 2.120(2); Al(1)–N(2), 2.120(2); O(1)–Al(1)–Cl(1), 122.26(6); O(1)–Al(1)–N(1), 91.11(8); O(1)–Al(1)–N(2), 90.33(8); O(2)–Al(1)–Cl(1), 119.42(6); O(2)–Al(1)–O(1), 118.32(8); O(2)–Al(1)–N(1), 90.59(8); O(2)–Al(1)–N(2), 89.52(8); N(1)–Al(1)–Cl(1), 88.65(6); N(2)–Al(1)–Cl(1), 89.82(6); N(2)–Al(1)–N(1), 178.30(8).

4.4 Catalytic Results

Complexes **3.1** and **4.1–4.2** were screened as catalysts for the copolymerization of CHO/CO_2 using standard optimized conditions (40 bar CO_2, 60 °C, [Al]/[CHO]: 1/500) which allows for direct comparison with other reported systems such as **2.1**.[3] In the absence of co-catalyst, complexes **3.1** and **4.1–4.2** furnished copolymers with a low percentage of carbonate linkages (<15%) (Table 4.1, entries 1–3). Addition of co-catalyst dramatically altered the conversion and selectivity of the copolymerization. Notably, addition of 1 equiv PPNCl to **3.1** selectively formed purely alternating PCHC (Table 4.1, entry 4). This is remarkable since the high Lewis acidity of aluminum generally yields significant

percentages of ether linkages in the resulting copolymer.[1] Other aluminum catalyst systems which achieve purely alternating PCHC include Zevaco's Al-N_2O_2 catalyst[2] and Darensbourg's Al-salens,[7] coupled with various co-catalysts. It is critical to mix catalyst and co-catalyst together in a solvent (typically followed by solvent evaporation) prior to CHO addition rather than directly adding CHO to a catalyst and co-catalyst mixture, as aluminum systems are often highly active for CHO homopolymerization, and pre-mixing allows a nucleophile-catalyst adduct to form that slows down the rate of homopolymerization.[8]

4.4.1 Effect of Pendent Donor

The dimethylamino-containing complex, **4.1**, converts roughly the same amount of CHO at identical conditions as **3.1**, which contains a morpholine group (Table 4.1, entry 5 vs. 4). However, with **4.1** the selectivity for copolymer is poor (63%) with the other 37% of the product mixture being *cis*-CHC. Given that **3.1** and **4.1** adopt distorted trigonal bipyramids with similar geometric indices, the electronic effect of donor basicity or steric congestion at the metal may play a significant role in the copolymerization outcome. Although the solid state structures herein show essentially identical steric hindrances of the pendent donors, the fluxionality of the morpholine donor would result in a reduced propagation rate (i.e. effectively blocking the coordination of a CHO molecule), which is consistent with slightly lower CHO conversions compared to **4.1** (also see: Table 4.1, entry 11 vs. 7). However, the effect is minimal, suggesting the sterics do not significantly influence the conversion.

Table 4.1. Copolymerization of CHO/CO_2 catalyzed by **3.1** and **4.1–4.2**

Entry	Cat.	Cocat.	[Al]/[Cocat.] /[CHO]	T (°C)	Conv. (%)	% copolymer[d]	% CO_3[e]	M_n[f,g] $\times 10^3$	$Đ$[f]
1	**3.1**	–	1/0/500	60	87	>99	13	24.2	3.58
2	**4.1**	–	1/0/500	60	44	>99	4	24.3	1.76
3	**4.2**	–	1/0/500	60	12	>99	14	8.33	1.58
4	**3.1**	PPNCl	1/1/500	60	8	>99	>99	ND	ND
5	**4.1**	PPNCl	1/1/500	60	11	63	>99	ND	ND
6	**3.1**	PPNCl	1/1/500	70	17	89	>99	5.44	1.02
7	**3.1**	PPNCl	1/1/500	80	31	92	>99	7.19	1.05
8[a]	**3.1**	PPNCl	1/1/500	80	18	89	>99	6.41	1.04
9	**3.1**	DMAP	1/1/500	80	17	93	70	5.47	1.09
10	**3.1**	$PPNN_3$	1/1/500	80	38	92	>99	6.68	1.07
11	**4.1**	PPNCl	1/1/500	80	36	49	>99	6.41	1.05
12	**4.1**	$PPNN_3$	1/1/500	80	32	81	>99	6.38	1.08
13	**4.2**	PPNCl	1/1/500	80	25	55	>99	4.54	1.02
14[b,c]	**3.1**	PPNCl	1/1/500	90	72	10	>99	ND	ND
15[b,c]	**4.1**	PPNCl	1/1/500	90	79	14	>99	ND	ND

Reaction conditions unless otherwise noted: 24 h, 40 bar CO_2. [a] 10 bar CO_2 [b] 19 h reactions [c] Co-solvent: 5 mL CH_2Cl_2 [d] Selectivity was determined by ^{1}H NMR spectral deconvolution of the overlapping copolymer and cyclic peaks at 4.6 ppm. [e] Determined by relative integration of the carbonate (4.6 ppm) and ether (3.3–3.5 ppm) regions in ^{1}H NMR. [f] Determined by triple detection GPC in THF. [g] In Da. ND: Copolymer was not isolated in sufficient quantity for analyses.

On the other hand, the lower basicity of the nitrogen donor in the morpholine group would lead to a less electronically saturated (more Lewis acidic) aluminum centre. A higher Lewis acidity would have a stronger electrostatic attraction with the negatively charged carbonate group, preventing it from dissociating to backbite and form cyclic carbonate.

This proposal is explored further in theoretical studies (vide infra). Furthermore, the NMR studies in Chapter 3 indicated slow *N*-inversion of the morpholine group was taking place at ambient conditions and well-resolved ^{1}H NMR resonances were obtained on cooling of the sample to −30 °C, consistent with fluxionality of the morpholine group. Broadened NMR resonances were also observed by Shaver and co-workers with the analogous benzyloxide complex and they came to a similar conclusion.[9] Consequently, the obtained X-ray structure is not representative of the solution-state at room and elevated temperatures considered in the present study. *N*-inversion would (partially) dissociate the morpholine group, furnishing an even more Lewis acidic Al centre.

4.4.2 Effect of Temperature

Elevated temperatures were important for increasing the conversion of CHO monomer. For **3.1**/PPNCl, increasing the temperature from 60 to 70 °C doubled the conversion and strictly alternating PCHC was obtained with 89% selectivity (Table 4.1, entry 6). A further increase to 80 °C again doubled the conversion to 31% and excellent selectivity was still maintained (Table 4.1, entry 7). However, at 90 °C the selectivity switched towards CHC, with only 10% copolymer (Table 4.1, entry 14). Under these conditions, CH_2Cl_2 was used as a co-solvent to alleviate potential mass transfer issues encountered with high concentrations of copolymer formation, which never materialized. The presence of CH_2Cl_2 did not appear to impact the conversion of CHO, however, it should be noted that these reactions were done in a 100 mL vessel with an increased surface area for CO_2 dissolution. The optimal temperature (80 °C) for copolymerization with **3.1**/PPNCl is identical to that seen with Williams' dizinc catalyst.[10]

In the case of **4.1**/PPNCl, a similar increase in conversion was encountered on increasing temperature from 60 to 80 °C (Table 4.1, entries 5 and 11). However, the selectivity towards PCHC formation dropped from 63 to 49%, whereas the decrease in selectivity over the same temperature range using **3.1**/PPNCl was only 7% (Table 4.1, entries 4 and 7). Decreases in selectivity upon increasing temperature are unsurprising as CHC formation becomes more favourable at higher temperatures, however, these data demonstrate that the ligand system in **3.1** can better tune product selectivity than **4.1**.

4.4.3 Effect of Nucleophilic Axial Ligand

4.1 is expected to be more electrophilic (i.e. more Lewis acidic) than **4.2** according to Lewis base binding studies on Al-Cl and Al-OEt porphyrinato complexes carried out by Chisholm and Chatterjee.[11] This can explain the lower conversion rates afforded by **4.2**/PPNCl (Table 4.1, entry 13 vs. 11), since a less Lewis acidic aluminum would not activate the CHO monomer as easily. The poor selectivities toward PCHC formation of **4.2**/PPNCl analogous to **4.1**/PPNCl (55 and 49%, respectively) suggests that chloride initiation (from the added co-catalyst) is taking place in both cases to give a structure amenable to backbiting. However, given that the presence of two different initiating groups (ethoxide and chloride) complicates the mechanistic proposal for the **4.2**/PPNCl catalytic system, attention was focused on the chloride complexes for the remainder of reactions performed.

4.4.4 Effect of Co-catalyst

When DMAP was used in place of PPNCl with **3.1**, the percent of carbonate linkages decreased to 70% (Table 4.1, entry 9). This may be due to the "trapping" of CO_2 by DMAP,

leading to an Al-bound carbamate possessing altered reactivity with CHO/CO_2. Related aluminum systems do not show a decline in carbonate linkages on addition of DMAP,[2, 7] suggesting the morpholinyl group may play a role by hindering access to the aluminum centre, or the formation of a stable Al-DMAP species. The pK_aH value for DMAP[12] (9.60) is two orders of magnitude greater than that for *N*-methylmorpholine (7.41), suggesting that DMAP displacement of the coordinated morpholine group should be favourable from an enthalpic perspective.

The substitution of PPNCl with $PPNN_3$ co-catalyst furnished different results. **3.1**/$PPNN_3$ gave slightly higher conversion and identical selectivity for copolymer as with PPNCl (Table 4.1, entry 10 vs. 7). The combination of **4.1** and $PPNN_3$ converted 32% of CHO with 81% selectivity for copolymer (Table 4.1, entry 12). This selectivity is significantly higher than that obtained with PPNCl co-catalyst (Table 4.1, entry 11), while the conversion is similar. Backbiting of the carbonate group would be less favourable with an azide chain end. The azide anion could either directly ring-open the activated epoxide or alternatively, substitute a chloride *via* an alkyl halide substitution S_N2 type reaction.

4.4.5 Effect of Pressure

With **3.1**/PPNCl, reducing the CO_2 pressure four-fold from 40 to 10 bar approximately halved the CHO conversion (Table 4.1, entry 8 vs. 7), while the selectivity for copolymer remained stable and no ether linkages were observed. A similar pressure effect on conversion was observed by Martinez and co-workers in their study of Zn scorpionate complexes, but they also observed reduced selectivity for copolymer at the same time.[13]

4.4.6 Effect of Outer-Sphere Donor in Amino-Phenolate Systems

The excellent activities of our previously reported amino-phenolate aluminum systems **2.1–2.2** in ROP of CHO prompted us to look more closely at the effect of the outer-sphere donors on reactivity in these types of complexes. The installation of methyl groups in **4.3** make the ethereal oxygens too hindered to coordinate to a metal centre and therefore the most important effects to consider when comparing **4.3** and **4.4** are steric hindrance and the basicity of the nitrogen donor. In the absence of co-catalyst, **4.3** and **4.4** selectively produce copolymers with a low percentage (<7%) of carbonate linkages (Table 4.2, entries 1–2). The addition of a co-catalyst dramatically changes the selectivity of the catalysts towards cyclic carbonate: **4.3**/PPNCl is 50% selective for copolymer (Table 4.2, entry 2) whereas **4.4**/PPNCl is totally selective for CHC (Table 4.2, entry 4 and 5 vs. 2).

Table 4.2. Copolymerization of CHO/CO_2 catalyzed by **4.3–4.4**[a]

Entry	Cat.	[Al]/[PPNCl] /[CHO]	T (°C)	Conv. (%)	% copolymer[b]	% CO_3[c]	M_n[d,e] $\times 10^3$	$Đ$[d]
1	**4.3**	1/0/500	60	47	>99	1	106	1.94
2	**4.4**	1/0/500	60	58	>99	6	24.0	3.77
3	**4.3**	1/1/500	60	10	50	>99	ND	ND
4	**4.4**	1/1/500	60	7	<1	–	–	–
5	**4.4**	1/1/500	80	21	<1	–	–	–

[a] Reaction conditions: 24 h, 40 bar CO_2. [b] Selectivity was determined by ^{1}H NMR spectral deconvolution of the overlapping copolymer and cyclic peaks at 4.6 ppm. [c] Determined by relative integration of the carbonate (4.6 ppm) and ether (3.3–3.5 ppm) regions in ^{1}H NMR. [d] Determined by triple detection GPC in THF. [e] In Da. ND: Copolymer was not isolated in sufficient quantity for analyses.

This change in selectivity phenomenon was also observed for the Zevaco group's tetrahedral Al-bis(phenolate) complexes when coupled with PPNCl.[14] Some In and Al-

salen complexes have also showed a similar trend.[7, 15] For the Al-salens, it was proposed that *tert*-butyl or H substituents on the phenolate rings decreased the electrophilicity of the Al centre leading to negligible reactivity or significant amounts of cyclic carbonate.[7] Therefore, in the present case, it may be that **4.4** is more electronically unsaturated compared to **4.3**. In **4.3**, the morpholine oxygens would withdraw electron density from the nitrogen donors, leading to a less basic N donor in **4.3** compared with **4.4** that contains more basic N donors (pK_aH *N*-methylpiperidine = 10.08).[4] A more electronically saturated aluminum centre would be consistent with detachment of the Al-bound carbonate species to easily backbite on itself, forming CHC. In other words, the aluminum centre in **4.4** is less Lewis acidic rendering it more prone to backbiting. However, the theoretical studies (vide infra) suggest that the Lewis acidities on Al are similar and other effects such as sterics take precedence.

4.4.7 Comparison of Complexes 3.1, 4.1, 4.3–4.4

At 40 bar and 60 °C with 1 equiv PPNCl, **3.1**, **4.1**, and **4.3–4.4** all have similar activities, each converting about 10% CHO to products. Whereas **3.1** has excellent selectivity for copolymer, **4.3** is only 50% selective (Table 4.2, entry 2 vs. Table 4.1, entry 2), comparable to the 49% selectivity obtained by **4.1**. Only traces of *trans*-CHC are produced in these copolymerizations, indicating that the backbiting pathway must proceed through a metal-free or metal bound backbiting of the carbonate anion to produce *cis*-CHC with good selectivity. The small quantities of *trans*-CHC are unlikely to be produced under high CO_2 pressures but are favoured under low CO_2 pressures, i.e. during reactor depressurization as noted by Chisholm and Chatterjee.[11]

4.5 Literature Comparison

Table 4.3. Reported Al catalyst systems for CHO/CO_2 copolymerization[a]

Entry	Ref	Cat.	Cocat.	T (°C)	Conv. (%)	% copolymer	% CO_3	M_n[d] ×10^3	$Đ$
1	This work	**3.1**	PPNCl	60	8	>99	>99	ND	ND
2		**3.1**	PPNCl	80	31	92	>99	7.19	1.05
3		**3.1**	–	60	87	>99	13	24.2	3.58
4[b]	3	**2.1**	–	60	66.7	>99	54.0	29.0	3.16
5		**2.1**	PPNCl	60	–	–	–	–	–
6[c]	2	**1.30**	PPNCl	80	[96]	>99	98	12.8	1.63

[a] Reaction conditions unless otherwise noted: [Al]/[PPNCl]/[CHO] = 1/1/500, 24 h, 40 bar CO_2. Isolated yield indicated within square brackets. [b] 16 h [c] 20 h, 50 bar CO_2. [d] In Da.

It is important to compare the catalysts reported herein to other aluminum catalysts (Table 4.3) reported in the literature. While highly selective towards copolymer formation, **3.1** is significantly less active than other reported catalyst systems for CHO/CO_2 copolymerization. For instance, Zevaco's **1.30**/PPNCl system yields 97% PCHC after 20 h at 50 bar and 80 °C, significantly higher compared to 31% conversion attained by **3.1**/PPNCl using identical catalyst loading (Table 4.3, entry 4). However, the former yielded a relatively disperse copolymer whereas **3.1** produces copolymer with narrow dispersities ($Đ$ = 1.02–1.09) indicating that the latter is a more controlled catalyst system. These differences in reactivity are most likely due to the stronger Lewis acidity of the aluminum in Zevaco's complex. At 40 bar and 60 °C for 16 h, **2.1** selectively converts 66.7% CHO monomer to copolymer having a broad dispersity ($Đ$ = 3.16) and 54.0%

carbonate linkages.[3] The copolymer obtained from **3.1** under identical conditions (but longer time) contained significantly lower carbonate linkages (13%) but exhibited a very similar dispersity ($Đ$ = 3.58) and molecular weight.

Aluminum complexes that are highly active for cycloaddition of aliphatic epoxides with CO_2 generally perform poorly (or not at all) when converting CHO to polymer, which is a challenging internal epoxide to form CHC from selectively. For example, North and co-workers' **[Al-salen]$_2$O** complex (Figure 4.5) fails to produce any CHC or PCHC from CHO/CO_2 although it is highly efficient in converting PO/CO_2 to PC at ambient conditions.[16] A selection of aluminum complexes from the literature are reported in Table 4.4 along with **4.4**. It is worth noting that cycloaddition is commonly promoted with excess co-catalyst and two of the reported systems follow this practice (Table 4.4, entries 2–3) whereas **4.4** and the bimetallic heteroscorpionate catalyst **Al$_2${heterosc.}** (Figure 4.5) do not (Table 4.4, entries 1, 4). The Al-tris(phenolate) **1.33c** outperforms the other three systems (Table 4.4, entry 2; TOF 34 h^{-1}).[17] While the **Al$_2${phenolate}** catalyst (Figure 4.5) reported by Yao and co-workers has promising activity (TOF 4.3 h^{-1}), the selectivity for cyclic carbonate is poor (Table 4.4, entry 3).[18] This is surprising even though a three-fold excess of TBAB co-catalyst was used. **Al$_2${heterosc.}** could selectively convert 20–37% CHO to CHC (TOF up to 3.1 h^{-1}) depending on the CO_2 pressure used (Table 4.4, entry 4).[19] The activity of **4.4** (Table 4.4, entry 1; TOF 4.4 h^{-1}) is competitive with the bimetallic systems **Al$_2${phenolate}** and **Al$_2${heterosc.}** but is slower than the monometallic **1.33c** by a factor of eight. It is worth noting that the selectivity of **4.4** towards CHC is remarkable given that only a single stoichiometric equivalent (no excess) of PPNCl is necessary.

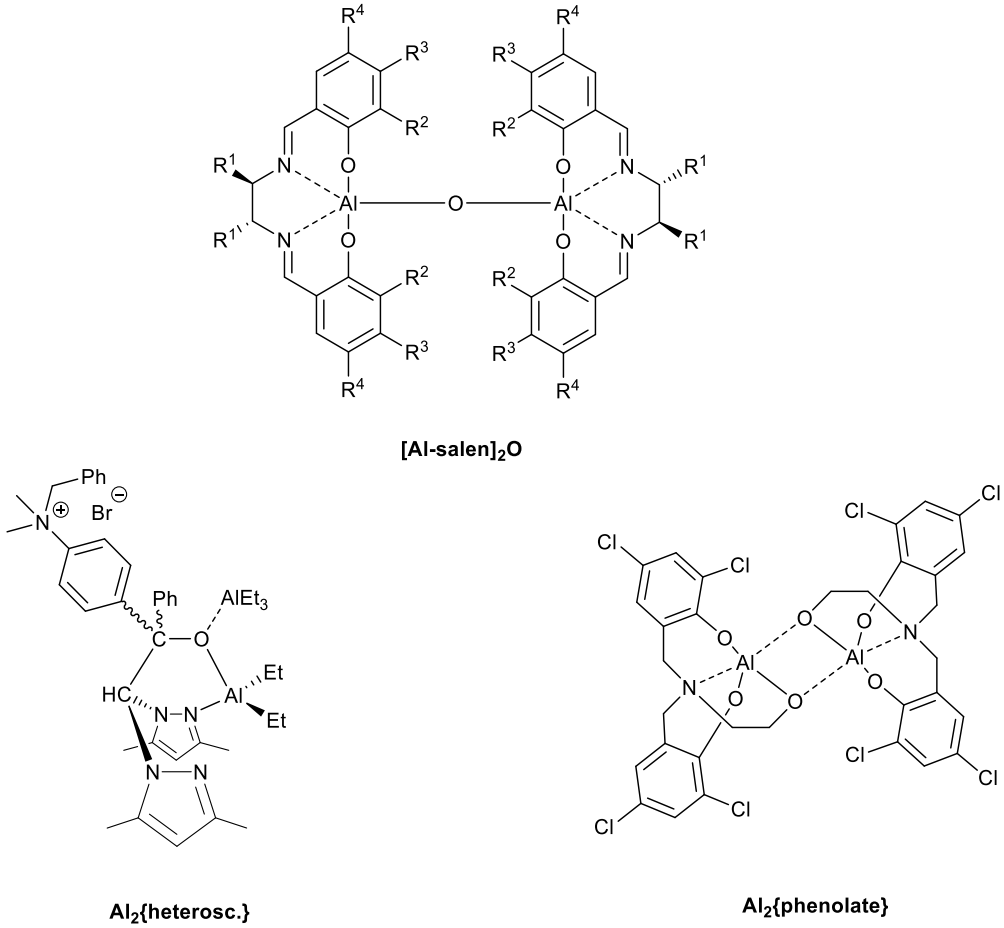

Figure 4.5. Aluminum complexes used in cycloaddition of epoxides/CO_2

Table 4.4. Reported Al catalyst systems for cycloaddition of CHO/CO_2

Entry	Ref	Cat.	Cocat.	T (°C)	P (bar)	Conv. (Yield)	% cyclic
1[a]	this work	**4.4**	PPNCl	80	40	21	>99
2[b]	17	**1.33c**	TBAB	70	10	61	>99
3[c]	18	**Al_2{phenolate}**	TBAB	85	10	(52)	60
4[d]	19	**Al_2{heterosc.}**	Br^-	80	10	20	>99
5[d]		**Al_2{heterosc.}**	Br^-	80	20	37	>99

[a] 0.2 mol% catalyst, 0.2 mol% co-catalyst, 24 h. [b] 0.1 mol% catalyst, 0.5 mol% co-catalyst, 18 h. [c] 0.3 mol% catalyst, 0.9 mol% co-catalyst, 40 h. [d] 0.5 mol% catalyst, 0.5 mol% appended Br^- co-catalyst, 24 h.

4.6 Kinetic Investigations

Focusing on the **3.1**/PPNCl system, kinetic studies were undertaken by monitoring the conversion of CHO to PCHC at 50, 60, 65, and 70 °C by *in situ* IR spectroscopy (Figure D.6). A linear response curve for absorbance with respect to carbonate concentration in CHO has been established, allowing for the calculation of rates directly from absorbance profiles.[20] At 80 °C, signal saturation was reached and this precluded data collection for this temperature. The calculated activation energy for copolymerization from the Arrhenius plot (Figure 4.6) is 149 ± 8 kJ/mol. This value is nearly 100 kJ/mol higher than the reported values for a Cr^{III} amino-bis(phenolate) system[20] (62 kJ/mol) and a Zn Schiff base complex (18 kJ/mol).[21] A high activation energy (96.8 kJ/mol) was also reported by Williams' group for dizinc complex **1.16a**.[10] In Williams' case, a bimetallic mechanism was taking place and the high activation energy was consistent with higher reaction temperatures needed.

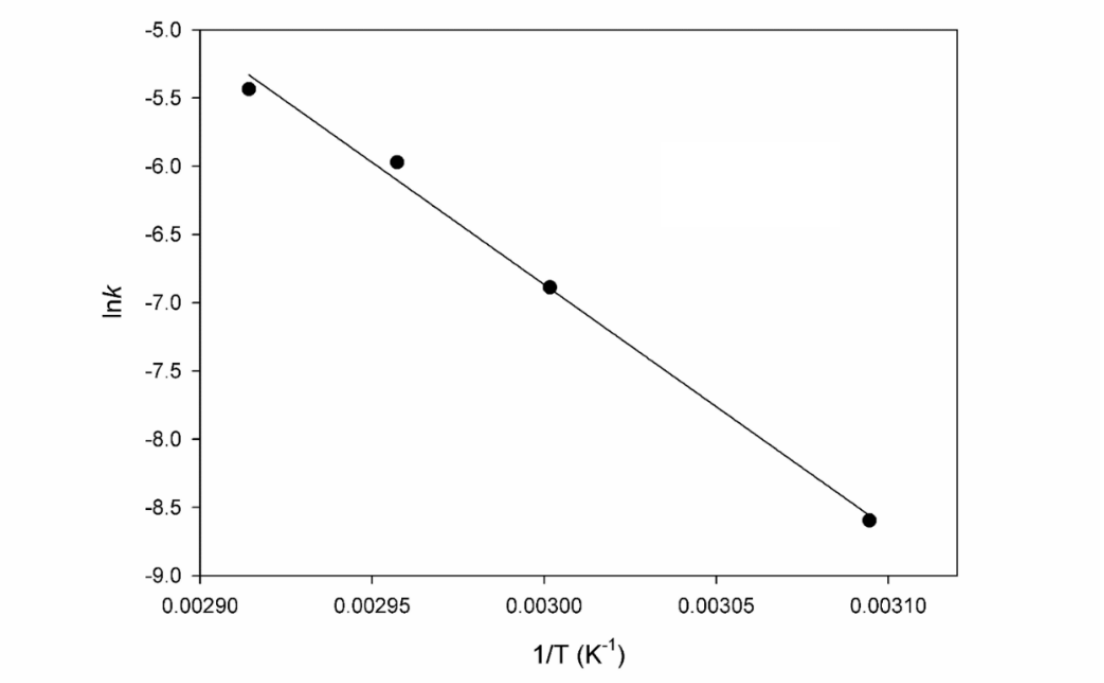

Figure 4.6. Arrhenius plot for the copolymerization of CHO/CO_2 at 40 bar pressure using **3.1**/PPNCl at various temperatures (R^2 = 0.9948)

4.7 DFT Studies

The tunable selectivity of cyclic carbonate vs. copolymer by choice of aluminum catalyst **3.1**, **4.1**, **4.3**, or **4.4** prompted us to investigate these systems on a theoretical basis. While backbiting can take place by a variety of mechanisms, the results attained with the azide co-catalyst strongly suggested that the co-catalyst becomes enchained to the cyclohexane ring by intermolecular initiation, although there is some potential for an azide anion to replace a chloride group. The stereochemistry of the cyclohexene carbonate obtained was predominately *cis* suggesting that backbiting occurs *via* S_N2 attack of Al-bound or Al-free carbonate, outlined in Scheme 4.1.[22] The more loosely bound to the aluminum the carbonate group is, the more likely it will displace the nucleophile enchained

to the cyclohexane ring. Accordingly, the partial atomic charges on the aluminum centres in their Al-carbonate derivatives, and possibly the Al-carbonate bond distances, should correlate with their propensity for backbiting.

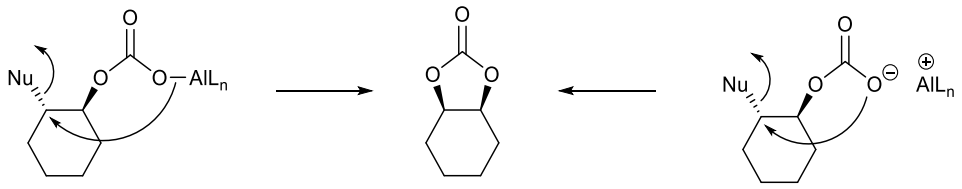

Scheme 4.1. Backbiting of Al-bound and Al-free carbonate to produce *cis*-CHC (Nu = nucleophile)

Although aluminum has been less studied computationally (and experimentally), there are important findings to note from other computational investigations in the field of CHO/CO_2 ROCOP. Luinstra, Rieger, and co-workers investigated Al and Cr^{III}-salen complexes and found that Gibbs energies of carbonate dissociation were approximately half as much for aluminum, explaining the tendency for aluminum complexes to follow metal-free backbiting to form cyclic carbonate.[23] Backbiting barriers for the metal-bound carbonates were essentially identical but considerably higher than the metal-free pathway.

4.7.1 Computational Method Selection and Validation

Kleij's group studied aluminum amino-tris(phenolate) complexes computationally using the B97-D3 functional with LANL2DZ pseudopotentials.[24-25] However, using this methodology, preliminary calculations showed that B97D3 (SMD)/6-311+G(d,p)/ LANL2DZ predicted significantly longer Al–Cl and Al–N bond distances compared to experimental X-ray structures herein. It is worth noting that Darensbourg and Yeung have

benchmarked various computational methods in ROCOP and concluded that the M06 and M06-2X functionals coupled with triple-zeta basis sets give computational results nearly matching high level calculations.[26] Therefore, the hybrid M06 functional (containing Hartree-Fock exchange) was chosen as it describes main group structures well. The SMD solvation model was employed and *tert*-butyl groups were substituted with methyl groups as our systems are quite large. The experimental and calculated bond distances are reported in Table 4.5. There is excellent agreement for Al–Cl, Al–O, and Al–N bond distances although the Al–N(axial) distances deviate from experimental values by approximately 0.06–0.07 Å. One must bear in mind that X-ray data is collected in the solid state at low temperatures while the calculations are in solution.

Table 4.5. Experimental (X-ray) and calculated (M06/6-311+G(d,p)) bond distances of **3.1**, **4.1**, **4.3**, and **4.4**

Cat.	Al–O(phenolate) (Å)		Al–N(axial)[a] (Å)		Al–N(pendent) (Å)		Al–Cl (Å)	
	Expt	Calcd	Expt	Calcd	Expt	Calcd	Expt	Calcd
3.1	1.75 1.75	1.77 1.77	2.10	2.16	2.08	2.07	2.26	2.28
4.1	1.75 1.75	1.77 1.77	2.12	2.19	2.07	2.06	2.25	2.27
4.3	1.77 1.77	1.77 1.77	2.13 2.13	2.13 2.13	–	–	2.20	2.20
4.4	1.77 1.77	1.78 1.78	2.12 2.12	2.15 2.15	–	–	2.20	2.20

[a] In **4.3** and **4.4**, the pendent nitrogen donors also assume axial positions.

With the suitability of the computational method established from a geometric perspective, the partial atomic charges of the pendent nitrogen within the pro-ligands H_2[**L1**] and H_2[**L2**] were calculated with a variety of charge models for validation purposes (see Table F.2). Charge analyses indicated that only Mulliken and CM5 models were able to describe the more negative charge on the dimethylamino pendent compared to the morpholinyl pendent. However, of the two models, only the CM5 model describes the loss of atomic charge once bonded to aluminum. Next, the partial atomic charges were calculated for the hypothetical Al-carbonate complexes and are reported in Table 4.6. Here, the MSK and Mulliken charges on aluminum correlate well with the observed selectivities for copolymer. On the other hand, the CM5, NBO, and DDEC6 models predict identical charges on aluminum centres within the two families of complexes (**3.1**/**4.1** and **4.3**/**4.4**). To summarize, the charge models are inconsistent in their prediction of charges on the aluminum centre.

However, the calculated bond distances (Table 4.6) confirm the pendent donor strength and somewhat explain the experimentally observed selectivities when comparing **3.1** and **4.1**. The calculated Al–N(pendent) bond distances are slightly shorter for **4.1** compared to **3.1** (2.04 vs. 2.08 Å) which agrees with the dimethylamino pendent being a better donor than the morpholinyl pendent. Moreover, the Al–carbonate bond distance is slightly shorter for **3.1** than **4.1** (1.84 vs. 1.85 Å), reflecting the greater electrostatic attraction resulting from a more positively charged aluminum centre. However, the difference is minor and may be negligible. The Al–carbonate bond distance in **4.3** and **4.4** is ca. 0.05 Å shorter than in **3.1** and **4.1** which correlates well with the axial-equatorial Al–Cl bond distance trend

observed computationally and experimentally. However, this means the Al–carbonate bond distance cannot be used as an absolute measure of cyclic carbonate selectivity when comparing different families of complexes. This bond distance comparison is not useful for **4.3** and **4.4**, where identical Al–carbonate bond distances are predicted. The calculated Al–N(pendent) distances in **4.3** and **4.4** are similar (2.14, 2.12 vs. 2.13, 2.13 Å), suggesting that the donor abilities are similar due to the substitution of the morpholinyl groups with methyl groups adjacent to the oxygen atom. This would explain the identical Al–carbonate bond distances in **4.3** and **4.4**. This hints that other factors, such as steric effect of the pendent donor, may be influencing the copolymer selectivities seen herein for **4.3** and **4.4**. However, calculation of the barrier for carbonate dissociation in these two complexes is needed to further support the proposal that the Lewis acidity of these centres are similar. It would also be interesting to calculate a series of aluminum amino-bis(phenolate) complexes with different pendent donors to assess if the bond distance trend seen for **3.1** and **4.1** continued.

Table 4.6. Calculated (M06/6-311+G(d,p)) Al charges and relevant bond distances of Al-carbonate derivatives

Cat.	Mulliken	MSK	CM5	NBO	DDEC6	Al–N(pendent) (Å)	Al–carbonate (Å)
3.1	1.37	1.18	0.48	2.10	1.48	2.08	1.84
4.1	−0.02	1.12	0.47	2.10	1.48	2.04	1.85
4.3	−1.69	0.63	0.49	2.18	1.51	2.14, 2.12	1.81
4.4	−1.69	0.55	0.48	2.18	1.51	2.13, 2.13	1.81

As mentioned earlier, the morpholine group's fluxionality comes into play at ambient and elevated temperatures encountered in this study, but the calculations show static structures at 298.15 K. Molecular dynamic calculations would be needed to get a better understanding of the mobility of this group as a function of temperature. Therefore, the partial atomic charge on the aluminum centre in **3.1** is likely higher than the static charges calculated herein.

4.8 Conclusions

In summary, this combined experimental and theoretical study has shown that the ability of aluminum complexes to form copolymer over cyclic carbonate can be tuned by altering the Lewis acidity of the central aluminum through variation of pendent donors. In the presence of PPNCl, all complexes except **4.4** formed well-controlled catalyst systems that produce strictly alternating copolymer from CHO/CO_2. **3.1** incorporating a morpholine pendent group shows consistently high selectivity for copolymer and promising reactivity at low pressures of CO_2 (10 bar) when coupled with PPNCl, warranting further optimization of this catalyst system. DFT studies attempting to explain these selectivity differences using calculated atomic charges on the aluminum centres were inconsistent. Further computational studies are needed to determine the barrier for carbonate dissociation in these complexes to better understand the difference in selectivity.

4.9 Experimental Section

4.9.1 General Considerations

Unless otherwise stated, all manipulations were done under an atmosphere of dry, oxygen-free nitrogen using Schlenk techniques or an MBraun Labmaster glovebox. All

solvents were degassed using freeze-pump-thaw cycles. Toluene, heptane, pentane, and CH_2Cl_2 were purified with an MBraun Manual Solvent Purification System. Deuterated solvents were purchased from Cambridge Isotope Laboratories, Inc. and dried over CaH_2 before use. Elemental analyses were performed by Guelph Chemical Laboratories, Inc., Guelph, ON, Canada. H[**L5**] was prepared using a modified method with water as the reaction medium instead of EtOH as previously reported.[27] NMR spectra (^1H and $^{13}C\{^1H\}$) were recorded on a Bruker Avance 300 or 500 MHz spectrometer at 25 °C (unless otherwise stated) and referenced internally to residual signals of the solvent. MALDI-TOF mass spectra were acquired on a Bruker ultrafleXtreme MALDI−TOF/TOF MS system running in reflectron mode at Bruker Daltonics, Billerica, MA or an Applied Biosystems 4800 MALDI TOF/TOF Analyzer equipped with a reflectron, delayed ion extraction and high-performance nitrogen laser (200 Hz operating at 355 nm). Complexes were mixed in a 2:1 (matrix:complex) ratio in CH_2Cl_2 with anthracene as the matrix, spotted on a plate in the glovebox, and transported in an airtight bag. Polymer molecular weight determination was performed on a GPC setup consisting of an Agilent Infinity HPLC, Wyatt Technologies triple detection (miniDAWN TREOS light scattering, ViscoStar-II viscometer, and Optilab T-rEX refractive index detectors), and two Phenogel columns (10^3 Å and 10^4 Å, 300 × 4.6 mm) with THF as eluent. Samples were prepared at a concentration of 4 mg/mL, filtered through 0.2 μm syringe filters, and run at 0.3 mL/min. Chromatograms were processed with Astra 6 software (Wyatt Technologies) and dn/dc values used were calculated according to the injected mass and RI detector response, assuming 100% elution from the GPC columns. **3.1** was prepared following the method reported in Chapter 3.

4.9.2 Computational Details

Calculations were carried out using the Gaussian 09 software package. The M06 functional was employed with the 6-311+G(d,p) basis set.[28-30] Solvent effects for CHO were introduced in geometry optimizations, frequency calculations, and single-point calculations (used for charge calculations) using the SMD model[31] with 1-hexanol (ε = 12.51), representative of the simplest epoxide, ethylene oxide. Partial atomic charges were calculated using Gaussian 09 (Mulliken, Merz-Singh-Kollman, CM5, NBO) or the Chargemol program (DDEC6).[32-39]

4.9.3 Crystallography

Single crystals of H[**L4**], **4.1**, **4.3**, and **4.4** were mounted on low-temperature diffraction loops and measured on a Rigaku Saturn CCD area detector with graphite-monochromated Mo-Kα radiation. H[**L4**] was solved using the CrystalStructure[40-41] structure solution program using direct methods and refined with the SHELXL-97 refinement package.[42] Using Olex2,[43] **4.1**, **4.3**, and **4.4** were solved with the ShelXT[44] structure solution program using Intrinsic Phasing and refined with the ShelXL[45] refinement package using least squares minimisation.

4.9.4 Synthetic Procedures

H[**L4**]. Water (80 mL), 2,4-di-*tert*-butylphenol (6.19 g, 30.0 mmol), and formaldehyde (37 wt. % in H_2O, 2.44 mL, 30.0 mmol) were added to a 250 mL round-bottom flask equipped with a stir bar and condenser. 2,6-Dimethylmorpholine (3.70 mL, 30.0 mmol) was added dropwise to the stirred solution. The resulting mixture was heated at reflux for 18 h. H[**L4**] was obtained as a gray solid, which was recrystallized in MeOH to give a

colourless, crystalline solid. Yield: 9.20 g, 92.0%. Crystals suitable for X-ray diffraction were grown from a saturated methanol solution at 0 °C. ^{1}H NMR ($CDCl_3$, 500 MHz, 298 K) δ 10.78 (1H, s, ArO*H*), 7.24 (1H, d, *J* =2.2 Hz, Ar*H*), 6.84 (1H, d, *J* =2.2 Hz, Ar*H*), 3.74 (2H, m, O–C_2H_2{C_2H_6}C_2H_4–N), 3.65 (2H, s, Ar–C*H*$_2$–N), 2.84 (2H, d, *J* = 11.00 Hz , O–C_2H_2{C_2H_6}C*H*$_2$–N), 1.87 (2H, d, *J* = 11.00 Hz , O–C_2H_2{C_2H_6}C*H*$_2$–N), 1.41 (9H, s, Ar–C{C*H*$_3$}$_3$), 1.28 (9H, s, Ar–C{C*H*$_3$}$_3$), 1.17 (6H, d, *J* = 6.3 Hz, O–C_2H_2{C_2H_6}C_2H_4–N). ^{13}C{^{1}H} NMR ($CDCl_3$, 75 MHz, 298 K) δ 154.0, 140.5, 135.4, 123.4, 123.0, 120.0 (Ar*C*), 71.5 (O–C_2H_2{C_2H_6}*C*$_2$H$_4$–N), 62.2 (Ar–*C*H$_2$–N), 58.3 (O–*C*$_2$H$_2${C_2H_6}C_2H_4–N), 34.7, 34.0 (Ar–*C*{CH_3}$_3$), 31.6, 29.5 (Ar–C{*C*H$_3$}$_3$), 18.9 (O–C_2H_2{*C*$_2$H$_6$}C_2H_4–N). MS (MALDI-TOF) *m/z* (%, ion): 332 (100, $[M-H]^+$). Anal. calcd for $C_{21}H_{35}NO_2$: C, 75.63; H, 10.58; N, 4.20. Found: C, 75.61; H, 10.73; N, 4.18. mp 133–135 °C.

[N_2O_2]^{tBu,tBu}AlCl (**4.1**). This compound was prepared with diethylaluminum chloride (25% w/w in toluene; 0.705 g, 5.85 mmol) and H_2[**L3**] (2.46 g, 4.69 mmol) in 20 mL toluene. A colourless solid precipitated from solution before all Et_2AlCl was added so the mixture was heated to dissolution in an evacuated ampoule with an additional 30 mL toluene to ensure all ligand had reacted. After cooling to −30 °C the solution phase was decanted and the solid washed with heptane and pentane and dried under vacuum. Yield: 1.46 g, 53.2%. ^{1}H NMR ($CDCl_3$, 300 MHz, 298 K) δ 7.27 (2H, d, Ar*H*), 6.83 (2H, d, Ar*H*), 3.73 (4H, m, Ar–C*H*$_2$–N), 3.13 (2H, br s, N–C*H*$_2$–CH$_2$–N–{CH_3}$_2$), 2.86 (6H, s, N–{C*H*$_3$}$_2$), 2.81 (2H, br s, C*H*$_2$–N–{CH_3}$_2$), 1.45 (18H, s, Ar–C{C*H*$_3$}$_3$), 1.27 (18H, s, Ar–C{C*H*$_3$}$_3$). ^{13}C{^{1}H} NMR ($CDCl_3$, 75 MHz, 298 K) δ 154.5, 139.9, 139.2, 124.4, 123.5, 120.2 (Ar*C*), 59.3 (Ar–*C*H$_2$–N), 57.0 (N–*C*H$_2$–CH$_2$–N–{CH_3}$_2$), 49.3 (N–{*C*H$_3$}$_2$), 48.9

(CH$_2$–N–{CH$_3$}$_2$), 35.2, 34.3 (Ar–C{CH$_3$}$_3$), 31.9, 29.7 (Ar–C{CH$_3$}$_3$). Anal. Calcd for $C_{34}H_{54}AlClN_2O_2$: C, 69.78; H, 9.30; N, 4.79. Found: C, 69.59; H, 9.53; N, 4.61. MS (MALDI-TOF) *m/z* (%, ion): 584.3689 (2.8, [Al[**L3**]Cl]$^{\bullet+}$), 549.4001 (100, [Al[**L3**]]$^+$).

[N$_2$O$_2$]^{tBu,tBu}AlOEt (**4.2**). Al(OEt)$_3$ (0.629 g, 3.88 mmol) and H$_2$[**L3**] (1.66 g, 3.16 mmol) were combined in an ampoule and the headspace evacuated. The mixture was heated to reflux for 24 h and subsequently all volatiles were removed *in vacuo*. The residue was dissolved in 20 mL toluene and cooled at −30 °C yielding a small amount of precipitate that was discarded. The solution was dried *in vacuo* and washed with 20 mL pentane yielding a colourless solid. Yield: 2.18 g, 100%. ^{1}H NMR (CDCl$_3$, 300 MHz, 298 K) δ 7.24 (2H, d, ArH), 6.81 (2H, d, ArH), 4.15 (2H, q, O–CH_2–CH$_3$), 3.67 (4H, m, Ar–CH_2–N), 2.85 (2H, br s, N–CH_2–CH$_2$–N–{CH$_3$}$_2$), 2.70 (6H, s, N–(CH_3)$_2$), 2.67 (2H, br s, CH_2–N–{CH$_3$}$_2$), 1.46 (18H, s, Ar–C{CH_3}$_3$), 1.28 (18H, s, Ar–C{CH_3}$_3$), 1.22 (3H, t, O–CH$_2$–CH_3). ^{13}C{^{1}H} NMR (CDCl$_3$, 75 MHz, 298 K) δ 155.8, 138.6, 138.1, 123.9, 123.6, 121.0 (ArC), 59.3 (Ar–CH$_2$–N), 58.1 (O–CH$_2$–CH$_3$), 55.7 (N–CH$_2$–CH$_2$–N–{CH$_3$}$_2$), 49.7 (CH$_2$–N–{CH$_3$}$_2$), 49.4 (N–{CH$_3$}$_2$), 35.2, 34.2 (Ar–C{CH$_3$}$_3$), 31.9, 29.8 (Ar–C{CH$_3$}$_3$), 21.2 (O–CH$_2$–CH$_3$). Anal. Calcd for $C_{36}H_{59}AlClN_2O_3$: C, 72.69; H, 10.00; N, 4.71. Found: C, 72.87; H, 9.79; N, 4.48.

[N$_2$O$_2$]^{morph,tBu,tBu}AlCl (**4.3**). This compound was prepared in the same manner as above with diethylaluminum chloride (25% w/w in toluene; 1.26 g, 10.4 mmol) and H[**L4**] (6.03 g, 18.1 mmol). Volatiles were removed in vacuo and the residue washed with heptane and pentane to yield a colourless solid after drying. Crystals suitable for single-crystal X-ray analysis could be grown by slow evaporation of a saturated toluene solution at room

temperature. Yield: 4.82 g, 73.3%. ^{1}H NMR ($CDCl_3$, 300 MHz, 298 K) δ 7.28 (2H, m, ArH), 6.85 (2H, m, Ar*H*), 5.06 (1H, d, Ar–C*H*$_2$–N), 4.92 (1H, d, Ar–C*H*$_2$–N), 4.32 (1H, m, (O–C*H*–CH$_3$), 4.24 (1H, m, O–C*H*–CH$_3$), 4.13 (1H, d, Ar–C*H*$_2$–N), 4.05 (1H, d, Ar–C*H*$_2$–N), 3.81 (1H, overlapping d, N–C*H*$_2$–CH), 3.77 (1H, overlapping m, N–C*H*$_2$–CH), 3.73 (2H, overlapping m, O–C*H*–CH$_3$), 3.19 (3H, overlapping m, N–C*H*$_2$–CH), 3.15 (1H, overlapping t, N–C*H*$_2$–CH), 2.53 (1H, m, N–C*H*$_2$–CH), 2.30 (1H, d, N–C*H*$_2$–CH), 1.48 (18H, s, Ar–C{C*H*$_3$}$_3$), 1.29 (18H, overlapping m, Ar–C{C*H*$_3$}$_3$), 1.27 (3H, overlapping d, O–CH–C*H*$_3$), 1.14 (3H, d, O–CH–C*H*$_3$), 1.02 (3H, d, O–CH–C*H*$_3$), 0.92 (3H, d, O–CH–C*H*$_3$). ^{13}C{^{1}H} NMR ($CDCl_3$, 75 MHz, 298 K) δ 155.42, 155.38, 140.5, 140.3, 137.6, 137.0, 124.5, 124.2, 124.1, 122.1, 121.9 (Ar*C*), 64.91, 64.87, 64.4, 64.1 (O–*C*H–CH$_3$), 55.9, 55.4 (N–*C*H$_2$–CH), 53.9, 53.2 (Ar–*C*H$_2$–N), 51.9, 50.7 (N–*C*H$_2$–CH), 35.2, 35.1, 34.3, 34.2 (Ar–*C*{CH$_3$}$_3$), 31.9, 31.8, 30.3 (Ar–C{*C*H$_3$}$_3$), 19.52, 19.47, 19.3, 19.2 (O–CH–*C*H$_3$). Anal. Calcd for $C_{42}H_{68}AlClN_2O_4$: C, 69.35; H, 9.42; N, 3.85. Found: C, 69.47; H, 9.23; N, 3.92. MS (MALDI-TOF) *m/z* (%, ion): 691.5440 (100, [Al[**L4**]$_2$]$^+$).

[N_2O_2]^{pip,tBu,Me}AlCl (**4.4**). This compound was prepared in the same manner as above with diethylaluminum chloride (25% w/w in toluene; 1.17 g, 9.72 mmol) and H[**L5**] (4.41 g, 16.9 mmol) in 10 mL toluene. After stirring overnight, the solution was placed in the freezer yielding a colourless precipitate. The solution phase was decanted and the precipitate washed with 2 × 20 mL pentane to yield a colourless solid after drying. Crystals suitable for single-crystal X-ray analysis could be grown by slow evaporation of a saturated toluene solution at room temperature. Yield: 2.69 g, 54.7%. ^{1}H NMR ($CDCl_3$, 300 MHz, 298 K) δ 7.08 (2H, m, Ar*H*), 6.77 (2H, m, Ar*H*), 4.87 (1H, d, Ar–C*H*$_2$–N), 4.75 (1H, d,

Ar–C*H*$_2$–N), 4.00 (1H, overlapping d, pipC*H*$_2$), 3.95 (1H, overlapping d, Ar–C*H*$_2$–N), 3.88 (2H, overlapping d and t, Ar–C*H*$_2$–N and pipCH_2), 3.61 (1H, d, pipC*H*$_2$), 3.2–3.5 (3H, three overlapping m, pipC*H*$_2$), 2.78 (1H, d, pipC*H*$_2$), 2.61 (1h, d, pipC*H*$_2$), 2.28 (6H, two overlapping s, Ar–C*H*$_3$), 2.05 (2H, br s, pipC*H*$_2$), 1.80 (2H, br s, pipC*H*$_2$), 1.50 (6H, overlapping m, pipC*H*$_2$), 1.49 (18H, s, Ar–C{C*H*$_3$}$_3$), 1.24 (2H, m, pipC*H*$_2$). ^{13}C{^{1}H} NMR ($CDCl_3$, 75 MHz, 298 K) δ 155.9, 137.5, 128.2, 127.4, 126.0, 123.0 (Ar*C*), 51.5, 51.1 (Ar–*C*H_2–N), 50.6, 49.9, 47.8, 46.6 (pip*C*H_2), 34.6 (Ar–*C*{CH_3}$_3$), 30.0 (Ar–C{*C*H_3}$_3$), 23.5, 22.8 (pip*C*H_2), 20.7 (Ar–C*H*$_3$), 19.0, 18.8, 18.4, 17.9 (pip*C*H_2). Anal. Calcd for $C_{34}H_{52}AlClN_2O_2$: C, 70.02; H, 8.99; N, 4.80. Found: C, 70.06; H, 8.80; N, 5.05.

4.9.5 Typical Copolymerization Procedure

In a vial, Al catalyst (64.0 mg, 102 μmol) and PPNCl (58.5 mg, 102 μmol) were dissolved in approximately 5 mL dichloromethane and stirred for 15 minutes. The clear colourless solution was pumped to dryness yielding a colourless solid, then CHO (5.00 g, 51.0 mmol) was added to the vial, dissolving the residue briefly followed by the formation of a colourless precipitate. The suspension produced was taken up in a plastic syringe fitted with a cannula needle and pierced through a septum-capped vial to prevent air contamination prior to injection. The suspension was injected into the pressure vessel (pre-dried and CO_2-flushed) through an injection port (fitted with a septum) and quickly pressurized to 40 bar CO_2 followed by heating to 60 °C for 24 hours, with stirring. The reactor was then cooled to room temperature and depressurized slowly. An aliquot of the crude product (a colourless viscous solution) was dissolved in $CDCl_3$ and analyzed by ^{1}H NMR to obtain conversion, percent carbonate linkages, and percent polymer (with respect

to cyclic cyclohexene carbonate byproduct). The remaining product was dissolved in a minimal amount of dichloromethane (ca. 50 mL) and polymer precipitated with the addition of cold, HCl-acidified methanol. After storing in the freezer for a few days, the solution phase was decanted and the polymer dried for a few hours on a Schlenk line, then in a vacuum oven overnight at 60 °C. For copolymerizations in the absence of a co-catalyst, the pressure vessel was charged in the glovebox with catalyst (CH_2Cl_2 solution) and volatiles were removed in vacuo. The pressure vessel was sealed, brought out of the glovebox, and flushed with CO_2. CHO was then injected into the vessel following the method described above.

4.10 References

1. N. Ikpo, J. C. Flogeras and F. M. Kerton, *Dalton Trans.*, **2013**, *42*, 8998-9006.
2. M. A. Fuchs, C. Altesleben, T. A. Zevaco and E. Dinjus, *Eur. J. Inorg. Chem.*, **2013**, *2013*, 4541-4545.
3. N. Ikpo, S. M. Barbon, M. W. Drover, L. N. Dawe and F. M. Kerton, *Organometallics*, **2012**, *31*, 8145-8158.
4. H. K. Hall, *J. Am. Chem. Soc.*, **1957**, *79*, 5441-5444.
5. K. Phomphrai, P. Chumsaeng, P. Sangtrirutnugul, P. Kongsaeree and M. Pohmakotr, *Dalton Trans.*, **2010**, *39*, 1865-1871.
6. L. Chen, W. Li, D. Yuan, Y. Zhang, Q. Shen and Y. Yao, *Inorg. Chem.*, **2015**, *54*, 4699-4708.
7. D. J. Darensbourg and D. R. Billodeaux, *Inorg. Chem.*, **2005**, *44*, 1433-1442.
8. T. A. Zevaco, J. K. Sypien, A. Janssen, O. Walter and E. Dinjus, *J. Organomet. Chem.*, **2007**, *692*, 1963-1973.
9. E. D. Cross, G. K. Tennekone, A. Decken and M. P. Shaver, *Green Mater.*, **2013**, *1*, 79-86.
10. F. Jutz, A. Buchard, M. R. Kember, S. B. Fredriksen and C. K. Williams, *J. Am. Chem. Soc.*, **2011**, *133*, 17395-17405.
11. C. Chatterjee and M. H. Chisholm, *Inorg. Chem.*, **2011**, *50*, 4481-4492.
12. I. Kaljurand, A. Kütt, L. Sooväli, T. Rodima, V. Mäemets, I. Leito and I. A. Koppel, *J. Org. Chem.*, **2005**, *70*, 1019-1028.
13. J. Martinez, J. A. Castro-Osma, A. Lara-Sanchez, A. Otero, J. Fernandez-Baeza, J. Tejeda, L. F. Sanchez-Barba and A. Rodriguez-Dieguez, *Polym. Chem.*, **2016**, *7*, 6475-6484.
14. T. A. Zevaco, J. Sypien, A. Janssen, O. Walter and E. Dinjus, *Catal. Today*, **2006**, *115*, 151-161.
15. A. Thevenon, A. Cyriac, D. Myers, A. J. P. White, C. B. Durr and C. K. Williams, *J. Am. Chem. Soc.*, **2018**, *140*, 6893-6903.
16. W. Clegg, R. W. Harrington, M. North and R. Pasquale, *Chem. Eur. J.*, **2010**, *16*, 6828-6843.
17. C. J. Whiteoak, N. Kielland, V. Laserna, E. C. Escudero-Adán, E. Martin and A. W. Kleij, *J. Am. Chem. Soc.*, **2013**, *135*, 1228-1231.
18. P. Gao, Z. Zhao, L. Chen, D. Yuan and Y. Yao, *Organometallics*, **2016**, *35*, 1707-1712.
19. J. Martínez, J. A. Castro-Osma, C. Alonso-Moreno, A. Rodríguez-Diéguez, M. North, A. Otero and A. Lara-Sánchez, *ChemSusChem*, **2017**, *10*, 1175-1185.
20. K. Ni and C. M. Kozak, *Inorg. Chem.*, **2018**, *57*, 3097-3106.
21. Y. Xu, L. Lin, C.-T. He, J. Qin, Z. Li, S. Wang, M. Xiao and Y. Meng, *Polym. Chem.*, **2017**, *8*, 3632-3640.
22. D. J. Darensbourg and S.-H. Wei, *Macromolecules*, **2012**, *45*, 5916-5922.
23. G. A. Luinstra, G. R. Haas, F. Molnar, V. Bernhart, R. Eberhardt and B. Rieger, *Chem. Eur. J.*, **2005**, *11*, 6298-6314.

24. C. J. Whiteoak, N. Kielland, V. Laserna, F. Castro-Gómez, E. Martin, E. C. Escudero-Adán, C. Bo and A. W. Kleij, *Chem. Eur. J.*, **2014**, *20*, 2264-2275.
25. L. Peña Carrodeguas, J. González-Fabra, F. Castro-Gómez, C. Bo and A. W. Kleij, *Chem. Eur. J.*, **2015**, *21*, 6115-6122.
26. D. J. Darensbourg and A. D. Yeung, *Polym. Chem.*, **2014**, *5*, 3949-3962.
27. X. Deng, Y.-M. Guo, M. Du and Y.-Y. Fang, *Acta Crystallographica Section E*, **2001**, *57*, o488-o489.
28. Y. Zhao and D. G. Truhlar, *Theor. Chem. Acc.*, **2008**, *120*, 215-241.
29. R. Krishnan, J. S. Binkley, R. Seeger and J. A. Pople, *J. Chem. Phys.*, **1980**, *72*, 650-654.
30. A. D. McLean and G. S. Chandler, *J. Chem. Phys.*, **1980**, *72*, 5639-5648.
31. A. V. Marenich, C. J. Cramer and D. G. Truhlar, *J. Phys. Chem. B*, **2009**, *113*, 6378-6396.
32. Gaussian 09, Revision D.01, M. J. Frisch, G. W. Trucks, H. B. Schlegel, G. E. Scuseria, M. A. Robb, J. R. Cheeseman, G. Scalmani, V. Barone, B. Mennucci, G. A. Petersson, H. Nakatsuji, M. Caricato, X. Li, H. P. Hratchian, A. F. Izmaylov, J. Bloino, G. Zheng, J. L. Sonnenberg, M. Hada, M. Ehara, K. Toyota, R. Fukuda, J. Hasegawa, M. Ishida, T. Nakajima, Y. Honda, O. Kitao, H. Nakai, T. Vreven, J. J. A. Montgomery, J. E. Peralta, F. Ogliaro, M. Bearpark, J. J. Heyd, E. Brothers, K. N. Kudin, V. N. Staroverov, T. Keith, R. Kobayashi, J. Normand, K. Raghavachari, A. Rendell, J. C. Burant, S. S. Iyengar, J. Tomasi, M. Cossi, N. Rega, J. M. Millam, M. Klene, J. E. Knox, J. B. Cross, V. Bakken, C. Adamo, J. Jaramillo, R. Gomperts, R. E. Stratmann, O. Yazyev, A. J. Austin, R. Cammi, C. Pomelli, J. W. Ochterski, R. L. Martin, K. Morokuma, V. G. Zakrzewski, G. A. Voth, P. Salvador, J. J. Dannenberg, S. Dapprich, A. D. Daniels, O. Farkas, J. B. Foresman, J. V. Ortiz, J. Cioslowski and D. J. Fox, Gaussian, Inc., Wallingford, CT, 2013.
33. Gaussian 09, Revision A.02, M. J. Frisch, G. W. Trucks, H. B. Schlegel, G. E. Scuseria, M. A. Robb, J. R. Cheeseman, G. Scalmani, V. Barone, G. A. Petersson, H. Nakatsuji, X. Li, M. Caricato, A. Marenich, J. Bloino, B. G. Janesko, R. Gomperts, B. Mennucci, H. P. Hratchian, J. V. Ortiz, A. F. Izmaylov, J. L. Sonnenberg, D. Williams-Young, F. Ding, F. Lipparini, F. Egidi, J. Goings, B. Peng, A. Petrone, T. Henderson, D. Ranasinghe, V. G. Zakrzewski, J. Gao, N. Rega, G. Zheng, W. Liang, M. Hada, M. Ehara, K. Toyota, R. Fukuda, J. Hasegawa, M. Ishida, T. Nakajima, Y. Honda, O. Kitao, H. Nakai, T. Vreven, K. Throssell, J. J. A. Montgomery, J. E. Peralta, F. Ogliaro, M. Bearpark, J. J. Heyd, E. Brothers, K. N. Kudin, V. N. Staroverov, T. Keith, R. Kobayashi, J. Normand, K. Raghavachari, A. Rendell, J. C. Burant, S. S. Iyengar, J. Tomasi, M. Cossi, J. M. Millam, M. Klene, C. Adamo, R. Cammi, J. W. Ochterski, R. L. Martin, K. Morokuma, O. Farkas, J. B. Foresman and D. J. Fox, Gaussian, Inc., Wallingford, CT, 2009.
34. R. S. Mulliken, *J. Chem. Phys.*, **1955**, *23*, 1833-1840.
35. U. C. Singh and P. A. Kollman, *J. Comput. Chem.*, **1984**, *5*, 129-145.
36. B. H. Besler, K. M. Merz Jr. and P. A. Kollman, *J. Comput. Chem.*, **1990**, *11*, 431-439.

37. A. V. Marenich, S. V. Jerome, C. J. Cramer and D. G. Truhlar, *J. Chem. Theory Comput.*, **2012**, *8*, 527-541.
38. E. D. Glendening, C. R. Landis and F. Weinhold, *J. Comput. Chem.*, **2013**, *34*, 1429-1437.
39. T. A. Manz and N. G. Limas, *RSC Adv.*, **2016**, *6*, 47771-47801.
40. CrystalStructure 3.7.0: Crystal Structure Analysis Package, Rigaku and Rigaku/MSC, 9009 New Trails Dr. The Woodlands TX 77381 USA, 2000-2005.
41. CRYSTALS Issue 10, D. J. Watkin, C. K. Prout, J. R. Carruthers and P. W. Betteridge, Oxford, UK, 1996.
42. SHELX97, G. M. Sheldrick, 1997.
43. O. V. Dolomanov, L. J. Bourhis, R. J. Gildea, J. A. K. Howard and H. Puschmann, *J. Appl. Cryst.*, **2009**, *42*, 339-341.
44. G. M. Sheldrick, *Acta Cryst.*, **2015**, *A71*, 3-8.
45. G. M. Sheldrick, *Acta Cryst.*, **2015**, *C71*, 3-8.

CHAPTER 5

A Bimetallic Aluminum Catalyst for CHO/CO_2 Copolymerization

Chapter 5. A Bimetallic Aluminum Catalyst for CHO/CO_2 Copolymerization

5.1 Introduction

As described in Chapter 1 and observed for the Al amino-bis(phenolate) complexes reported in Chapter 4, pendent donors are important for modulating the electronic properties of the metal centre responsible for catalysis. With this in mind, Kleij's group has reported "pendent-free" Al amino-tris(phenolate) complexes that are active for copolymerization of LO/CO_2 and cycloaddition of various epoxides with CO_2.[1-3] Inspired by these results and the success of bimetallic zinc and aluminum catalysts developed by North and Williams' group,[4-5] we opted to use simple "pendent-free" amino-bis(phenolate) ligands that chelate one or two aluminum centres. We expected that the metal centres would exhibit a higher Lewis acidity in the absence of a pendent donor leading to higher catalytic activities and high selectivities for polycarbonate.

5.2 Results and Discussion

Complex **5.1** (bimetallic) and **5.2** (monometallic), illustrated in Figure 5.1, were prepared *via* alkane elimination reaction of the corresponding pro-ligand with 1 or 2 equiv Et_2AlCl, respectively, in toluene. The compounds were isolated as colourless solids in 43 and 67% yield and characterized by ^1H and $^{13}C\{^1H\}$ NMR spectroscopy (see Figures A.56–A.60) and elemental analyses. MALDI-TOF mass spectra were in agreement with the theoretical isotope patterns (Figures B.5–B.6). Single crystals of **5.1** and **5.2** suitable for X-ray analysis could be grown by slow evaporation of concentrated solutions at room temperature. To better compare 4-coordinate structures, an alternative geometry index for

4-coordinate compounds (τ_4') has been reported by Okuniewski *et al.*[6] The X-ray structures are illustrated in Figures 5.2 and 5.3 and revealed that the aluminum centres in **5.1** and **5.2** adopt an almost ideal tetrahedral coordination geometry according to the τ_4' values of 0.90 and 0.91, respectively. An identical τ_4' value (0.91) was calculated for the reported monometallic complex containing a methyl group in place of the chloride.[7]

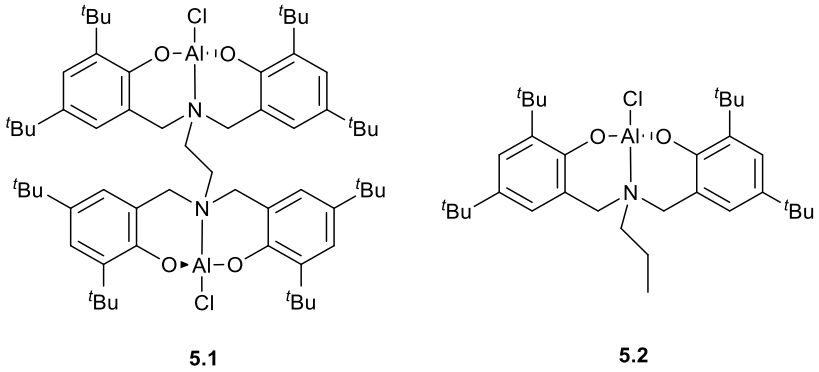

Figure 5.1. Structures of complexes **5.1–5.2**

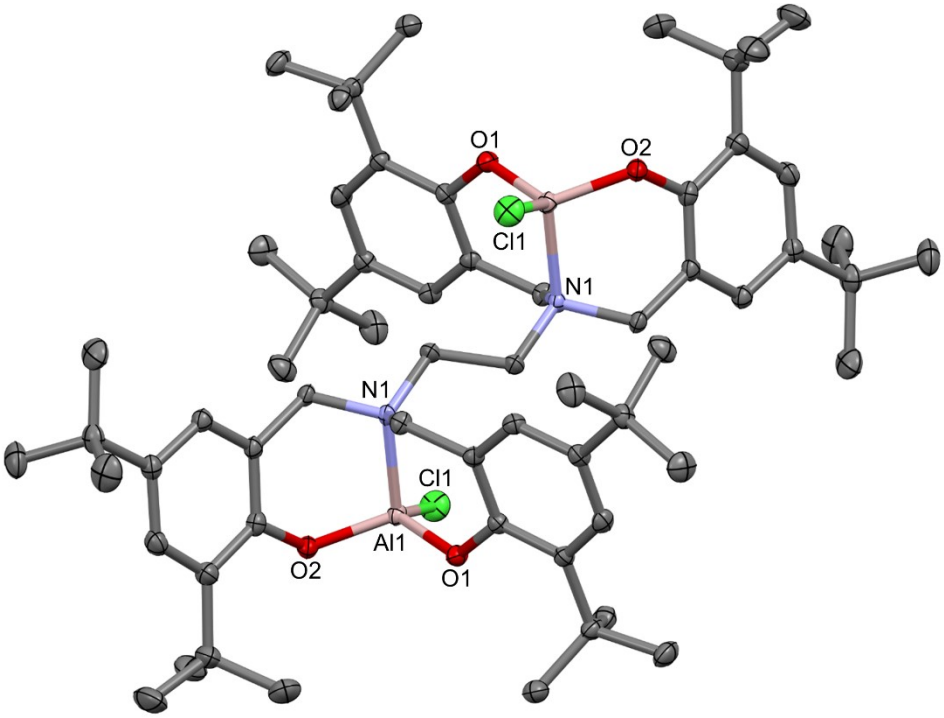

Figure 5.2. Molecular structure and partial numbering of **5.1** (thermal ellipsoids drawn at 50% probability; H atoms and a disordered CH_2Cl_2 molecule excluded for clarity). Selected bond distances (Å) and angles (°): Al(1)–Cl(1), 2.1192(6); Al(1)–O(1), 1.7225(11); Al(1)–O(2), 1.7294(11); Al(1)–N(1), 1.9783(13); O(1)–Al(1)–Cl(1), 115.54(4); O(1)–Al(1)–O(2), 115.54(6); O(1)–Al(1)–N(1), 100.84(5); O(2)–Al(1)–Cl(1), 110.82(4); O(2)–Al(1)–N(1), 102.49(5); N(1)–Al(1)–Cl(1), 110.17(4).

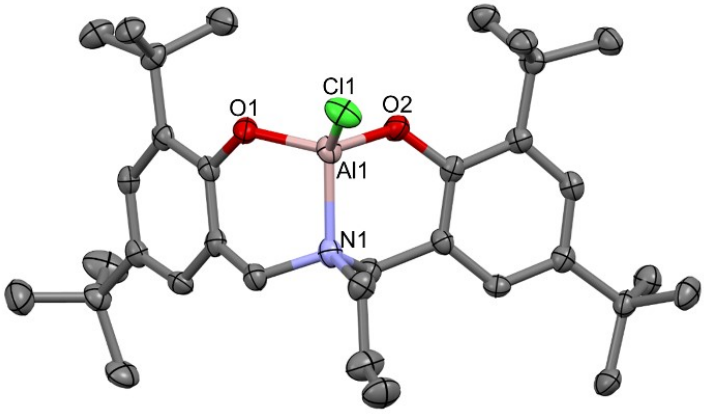

Figure 5.3. Molecular structure and partial numbering of **5.2** (thermal ellipsoids drawn at 50% probability; H atoms and one disordered *tert*-butyl group excluded for clarity). Selected bond distances (Å) and angles (°): Al(1)–Cl(1), 2.1088(16); Al(1)–O(1), 1.718(3); Al(1)–O(2), 1.709(3); Al(1)–N(1), 1.967(4); O(1)–Al(1)–Cl(1), 109.15(12); O(1)–Al(1)–N(1), 101.88(16); O(2)–Al(1)–Cl(1), 112.97(13); O(2)–Al(1)–O(1), 117.86(16); O(2)–Al(1)–N(1), 101.18(16); N(1)–Al(1)–Cl(1), 113.06(13).

5.2.1 Copolymerization of CHO/CO_2

5.1 was initially screened for copolymerization of CHO/CO_2 at 40 bar CO_2 and 60 °C for 24 h in the presence of 2 equiv of PPNCl (1 PPNCl per Al centre) as a co-catalyst. These conditions converted 49% of CHO monomer into strictly alternating polycarbonate, with 85% selectivity for copolymer over cyclic carbonate (Table 5.1, entry 2). While the aluminum complexes reported in Chapter 4 also produce strictly alternating polycarbonate, strictly alternating character is seldom observed with Al catalysts due to the high Lewis acidity of Al that favours consecutive CHO insertions into the growing polymer chain i.e. ether linkages. An improved understanding of the careful balance required to control catalyst reactivity and selectivity has allowed great advances in this area.[8] In the absence

of co-catalyst, **5.1** afforded a copolymer with 8% carbonate linkages and broad dispersity ($Đ$ = 3.06) which highlights the critical role played by careful stoichiometry and choice of co-catalyst in designing catalytic systems (Table 5.1, entry 1). However, reactions utilizing PPNCl did produce varying amounts of *cis*-CHC (only traces of *trans*-CHC were observed). This is due to backbiting reactions which require the presence of an external nucleophile.[9]

Table 5.1. Copolymerization of CHO/CO_2 catalyzed by **5.1–5.2**[a]

Entry	Cat.	[Al]/[PPNCl]/[CHO]	Conv. (%)	% copolymer[c]	% CO_3[d]	M_n[e,f] × 10^3	$Đ$[e]
1	**5.1**	2/0/500	93	>99	8	41.4	3.06
2	**5.1**	2/2/500	48	85	>99	5.86	1.04
3	**5.1**	2/1/500	62	98	19	6.66	1.10
4[b]	**5.1**	2/2/500	45	75	90	4.47	1.02
5	**5.2**	1/0/500	84	>99	11	133	1.27
6	**5.2**	1/1/500	28	92	75	5.58	1.06

[a]Reaction conditions unless otherwise noted: 24 h, 40 bar CO_2, 60 °C. [b] 30 bar CO_2. [c] Selectivity was determined by ^{1}H NMR spectral deconvolution of the overlapping copolymer and cyclic peaks at 4.6 ppm. [d] Determined by relative integration of the carbonate (4.6 ppm) and ether (3.3–3.5 ppm) regions in ^{1}H NMR. [e] Determined by triple detection GPC in THF. [f] In Da.

The optimal CO_2 pressure for copolymerizations with **5.1** was explored further as this may affect catalyst activity and carbonate content within the copolymer, particularly where cooperative bimetallic catalysts operate at low CO_2 pressures. There was an insignificant difference in conversion on decreasing the pressure from 40 to 30 bar (48 vs. 45%) which suggested an independence on [CO_2] over this pressure range (Table 5.1, entry 4 vs. 2). Even so, there was a concomitant increase in formation of ether linkages (10%) within the

copolymer. This slight difference in conversion could be attributed to the relative reactivity rates of an alkoxide vs. carbonate nucleophile. The percentage of ether linkages within the copolymer further increased from 10 to 18% following precipitation in acidified MeOH. This suggests that the high molecular weight fraction contains more ether linkages. DSC thermograms of the copolymers yielded glass transition temperatures of 105.2 and 99.1 °C (Figures E.3 and E.4, respectively). The former value agrees well with literature precedent which show T_g up to 115 °C depending on the molecular weight distribution of pure polycarbonate.[10] On the other hand, the latter value corroborates the percentage of carbonate linkages in the purified copolymer. Most likely, some strictly alternating polycarbonate remained in solution during the precipitation process, giving the lower percent carbonate linkages. Further reducing the CO_2 pressure to 20 bar only produced small amounts of *cis*-CHC (1–4% conversion by NMR). Copolymerization using (−)-LO in the presence and absence of PPNCl was unsuccessful.

Due to the promising reactivity of **5.1** towards PCHC formation, the monometallic analogue **5.2** was tested for copolymerization activity and performed well compared to **5.1** at identical conditions (Table 5.1, entry 6 vs. 2). The selectivity for copolymer increased slightly from 85 to 92%. However, the copolymer contained a lower percentage of carbonate linkages (75 vs. >99%). Considering that there are 2 Al centres in **5.1** and only 1 in **5.2**, we would expect approximately half as much activity from **5.2**, which is the case (48 vs. 28% conversion).

The copolymer produced in the absence of PPNCl (Table 5.1, entry 5) exhibited a bimodal molecular weight distribution, likely due to uncontrolled polymerization of CHO

that occurred prior to CO_2 pressurization. Despite their differences, both **5.1** and **5.2** in the absence of PPNCl do not produce cyclic carbonate. Moreover, the absence of pendent donors in these complexes leads to higher conversions; for example, **5.2** achieves conversions roughly triple that of the aluminum amino-phenolate complexes reported in Chapter 4. Hence, while there seems to be no cooperative bimetallic catalysis at play with respect to activities, the absence of pendent donors is critical for higher activities.

5.3 Polymerization Kinetics

Compared to other catalysts in the area, Al catalysts are generally less active[11] and this makes them ideal for mechanistic studies utilizing *in situ* IR spectroscopy. A linear response curve for absorbance with respect to carbonate concentration in CHO has been established, allowing for the calculation of rates directly from absorbance profiles.[12] The presence of an induction period for PCHC (Table 5.1, entry 2) during the initial 4.5 h of reaction time was remarkable (Figure D.7); moreover, a steady growth of the CHC IR band was observed over this time period. These data suggested that CHC initially formed is subsequently ring-opened to form copolymer. However, we were unable to ring-open either isomer of CHC using **5.1** in the presence or absence of PPNCl (see Figure A.64). The induction period is most likely characterized by a competitive binding between CHO and Al-bound chloride due to their similar metal bond strengths.[13]

5.4 Polymer Analyses

Interestingly, the GPC traces of copolymers obtained with 2 equiv of PPNCl and 30 or 40 bar CO_2 pressure were bimodal. In studies by others, bimodal traces were attributed to chain transfer agents or bifacial propagation and the higher mass fraction typically

exhibited an M_n double that of the lower mass fraction.[14] In the current study, the higher mass fraction is only ca. 700 Da higher than the lower mass fraction M_n, suggesting a different mechanism may be at play. Moreover, these higher mass fractions are small, amounting to approximately 1% (Table 5.1, entry 2) or 8% (Table 5.1, entry 4) of the copolymer sample (mass percent). To probe this further, we analyzed these copolymers by MALDI-TOF mass spectrometry. The MALDI-TOF mass spectra of the strictly alternating copolymer obtained under 40 bar CO_2 pressure contains one distribution with peaks separated by 142 Da corresponding to the mass of the repeating unit (Figure B.7). The peaks correspond to protonated cyclic PCHC ($[CHO{\cdot}CO_2]_m{\cdot}H^+$) [e.g. $m = 41$, $m/z = 5846.0$ (expt), 5846.3 (calcd)] or lithiated chloride-capped linear PCHC chains ($Cl[CHO{\cdot}CO_2]_m[C_6H_{10}]Cl{\cdot}Li^+$) [e.g. $m = 40$, $m/z = 5846.0$ (expt), 5846.1 (calcd)] (Figure B.8). On the other hand, mass spectra of the copolymer obtained under 30 bar CO_2 pressure contains one main distribution and two minor distributions (Figure B.9). Regardless of distribution, each set of successive peaks is separated by 142 Da. The main distribution corresponds to either lithiated cyclic PCHC containing a small number of ether linkages ($[CHO{\cdot}CO_2]_m[CHO]_n{\cdot}Li^+$) [e.g. $m = 25$, $n = 3$, m/z 3856.8 (expt), 3855.2 (calcd)] or protonated cyclic PCHC ($[CHO{\cdot}CO_2]_m[CHO]_n$) [e.g. $m = 24$, $n = 6$, m/z 4000.5 (expt), 4001.5 (calcd)] (Figure B.10). One minor distribution corresponds to lithiated cyclic PCHC ($[CHO{\cdot}CO_2]_m[CHO]_n{\cdot}Li^+$) [e.g. $m = 26$, $n = 2$, m/z 3810.1 (expt), 3811.2 (calcd)]. The other minor distribution corresponds to linear PCHC chains containing two hydroxyl end groups ($HO[CHO{\cdot}CO_2]_m[CHO]_nH{\cdot}Li^+$) [e.g. $m = 25$, $n = 3$, m/z 3872.9 (expt), 3873.2 (calcd)]. These could form *via* chain transfer reactions with cyclohexane diol. The mass

spectrum for copolymer containing a large quantity of ether linkages (Table 5.1, entry 3; Figure B.11) was very similar to spectra obtained for PCHO prepared using aluminum amino-phenolate complexes in Chapter 2 herein.

5.5 Conclusions

In summary, this work has shown that the absence of a pendent group within aluminum complexes renders the complex more reactive towards ROCOP of CHO/CO_2. This may be due to more Lewis acidic aluminum centres as well as an open vacant site for coordination and activation of CHO. For the bimetallic system **5.1**, 1 equiv of PPNCl per aluminum centre and high CO_2 pressure (40 bar) was necessary to obtain a high quantity of carbonate linkages in the copolymer. The linker between the two Al centres was flexible in **5.1** and thus it is not that surprising that **5.1** and **5.2** showed similar reactivity. In contrast, systems that typically show enhanced reactivity (e.g. catalysts prepared in the Williams group outlined in Section 1.8.3) have two metal centres that are held in close proximity to one another.

5.6 Experimental Section

5.6.1 General Considerations

Unless otherwise stated, all manipulations were performed under an atmosphere of dry oxygen-free nitrogen using standard Schlenk techniques or an MBraun Labmaster 130 glovebox. CHO was purchased from Sigma Aldrich and distilled from CaH_2 under N_2. Cyclohexene carbonate prepared by a colleague was vacuum distilled and brought into the glovebox using partial evacuation cycles. All other chemicals were used as received with no further purification. Toluene, heptane, pentane, and CH_2Cl_2 were purified with an

MBraun Manual Solvent Purification System. ^{1}H and $^{13}C\{^{1}H\}$ NMR shifts are reported relative to internal solvent resonances and reported in ppm. The synthesis of the proligand H_2[**L7**] has been reported.[15] The synthesis of the proligand H_4[**L6**] has also been reported[16] and a modified synthesis with water as the medium is reported below. MALDI-TOF mass spectra were acquired on an Applied Biosystems 4800 MALDI TOF/TOF Analyzer equipped with a reflectron, delayed ion extraction and high-performance nitrogen laser (200 Hz operating at 355 nm). Polymers were mixed in a 3:1 (matrix:polymer) ratio in THF with 2,5-dihydroxybenzoic acid as the matrix. Complexes were mixed in a 2:1 (matrix:complex) ratio in CH_2Cl_2 with anthracene as the matrix, spotted on a plate in the glovebox, and transported in an airtight bag. DSC analyses were performed using a Mettler Toledo DSC1 Star^{e} System with a scanning rate of 10 °C/min and nitrogen gas flow of 50 mL/min. Samples were heated from 25 to 180 °C three times to eliminate the difference in sample history and all glass transition temperatures were taken from the third heating cycle.

5.6.2 Crystallography

Single crystals of **5.1** and **5.2** were mounted on low-temperature diffraction loops and measured on a Rigaku Saturn CCD area detector with graphite-monochromated Mo-Kα radiation. Using Olex2,[17] the structure of **5.1** was solved with the ShelXS[18] structure solution program using Direct Methods and refined with the ShelXL[19] refinement package using least squares minimisation. For **5.2**, using Olex2,[17] the structure was solved with the ShelXT[20] structure solution program using Intrinsic Phasing and refined with the ShelXL[19] refinement package using least squares minimisation.

5.6.3 Synthetic Procedures

H_4[**L6**]. Ethylenediamine (1.46 g, 24.3 mmol) was slowly added to a stirring mixture of 2,4-di-*tert*-butylphenol (20.1 g, 97.4 mmol) and formaldehyde (37% w/w aqueous solution; 7.92 g, 97.6 mmol). The mixture was heated to reflux for two days during which a solid beige mass formed. Upon cooling, the aqueous layer was decanted and the solid washed with methanol repeatedly (using heating and sonication) to give a white powder. Recrystallization with $CHCl_3$/MeOH yielded the pure product. Yield: 13.6 g, 59.9%. NMR spectroscopy is in agreement with the literature[16] hence no further analyses are reported here. ^{1}H NMR ($CDCl_3$, 300 MHz) δ 7.81 (4H, br s, Ar–O*H*), 7.19 (4H, d, Ar*H*), 6.88 (4H, d, Ar*H*), 3.58 (8H, s, Ar–C*H*$_2$–N), 2.80 (4H, s, N–C*H*$_2$C*H*$_2$–N), 1.37 (36H, s, Ar–C{C*H*$_3$}$_3$), 1.26 (36H, s, Ar–C{C*H*$_3$}$_3$); ^{13}C{^{1}H} NMR ($CDCl_3$, 75 MHz) δ 152.4, 141.8, 136.1, 125.3, 123.7, 121.6 (Ar*C*), 57.4 (Ar–*C*H$_2$–N), 34.9, 34.3 (Ar–*C*{CH$_3$}$_3$), 31.8, 29.9 (Ar–C{*C*H$_3$}$_3$).

[**L6**]Al_2Cl_2 (**5.1**). A solution of diethylaluminum chloride (25% w/w in toluene; 1.18 g, 9.78 mmol) was added dropwise to a stirred solution of H_4[**L6**] (4.15 g, 4.44 mmol) in toluene (50 mL). Volatiles were removed in vacuo and the residue washed with pentane to yield a colourless solid which was recrystallized from CH_2Cl_2 at room temperature as a colourless crystalline solid. Crystals suitable for single-crystal X-ray analysis could be obtained from this recrystallization setup. Yield: 2.01 g, 42.9%. ^{1}H NMR ($CDCl_3$, 300 MHz, 298 K) δ 7.35 (4H, d, Ar*H*), 6.88 (4H, d, Ar*H*), 5.31 (2H, s, C*H*$_2$Cl$_2$), 3.75 (8H, q, Ar–C*H*$_2$–N), 3.34 (4H, s, N–C*H*$_2$C*H*$_2$–N), 1.45 (36H, s, Ar–C{C*H*$_3$}$_3$), 1.27 (36H, s, Ar–C{C*H*$_3$}$_3$). ^{13}C{^{1}H} NMR ($CDCl_3$, 75 MHz, 298 K) δ 154.0, 142.0, 139.2, 125.9, 124.4,

119.6 (Ar*C*), 58.2 (Ar–*C*H_2–N), 53.6 (*C*H_2Cl_2), 49.3 (N–*C*H_2*C*H_2–N), 35.3, 34.4 (Ar–*C*{CH_3}$_3$), 31.8, 29.7 (Ar–C{*C*H_3}$_3$). MS (MALDI-TOF) *m/z* (%, ion): 1017.3760 (53, $[M-Cl]^+$), 1052.3455 (100, $[M]^{\bullet+}$).

[**L7**]AlCl (**5.2**). This compound was prepared in the same manner as above with diethylaluminum chloride (25% w/w in toluene; 1.09 g, 9.06 mmol) and H_2[**L7**] (4.07 g, 8.20 mmol). Heating overnight at 70 °C gave a yellow-brown solution and volatiles were removed *in vacuo*. The residue was washed with pentane (3 × 20 mL) and dried under vacuum to yield a colourless solid. Yield: 3.06 g, 67.0%. Crystals suitable for single-crystal X-ray analysis could be grown from a concentrated toluene solution at room temperature. ^{1}H NMR ($CDCl_3$, 300 MHz, 298 K) δ 7.39 (2H, d, Ar*H*), 6.96 (2H, d, Ar*H*), 3.98 (4H, q, Ar–C*H*$_2$–N), 3.00 (2H, m, N–C*H*$_2$–CH_2–CH_3), 1.86 (2H, m, N–CH_2–C*H*$_2$–CH_3) 1.50 (18H, s, Ar–C{C*H*$_3$}$_3$), 1.34 (18H, s, Ar–C{C*H*$_3$}$_3$), 0.98 (3H, t, CH_2–C*H*$_3$); ^{13}C{^{1}H} NMR ($CDCl_3$, 75 MHz, 298 K) δ 154.4, 141.2, 138.9, 125.3 124.4, 120.3 (Ar*C*), 56.7 (Ar–*C*H_2–N), 55.8 (N–*C*H_2–CH_2–CH_3), 35.3, 34.3 (Ar–*C*{CH_3}$_3$), 31.8, 29.8 (Ar–C{*C*H_3}$_3$), 14.8 (N–CH_2–*C*H_2–CH_3), 11.6 (–CH_2–*C*H_3). MS (MALDI-TOF) *m/z* (%, ion): 520.3710 (61, $[M-Cl]^+$), 555.3312 (100, $[M]^{\bullet+}$).

5.6.4 Typical Copolymerization Procedure

In a vial, Al catalyst (116 mg, 0.102 mmol) and PPNCl (117 mg, 0.204 mmol) were dissolved in approximately 10 mL dichloromethane and stirred for 15 minutes. The clear colourless solution was pumped to dryness yielding a colourless solid, then CHO (5.01 g, 51.1 mmol) was added to the vial, stirring, to yield a suspension. The suspension was taken up in a plastic syringe fitted with a cannula needle and pierced through a septum-capped

vial to prevent air contamination prior to injection. The suspension was injected into the pressure vessel through an injection port (fitted with a septum) and quickly pressurized to 40 bar CO_2 followed by heating to 60 °C for 24 hours, with stirring. The reactor was then cooled to room temperature and depressurized slowly. An aliquot of the crude product (a colourless syrupy material) was dissolved in $CDCl_3$ and analyzed by ^1H NMR to obtain conversion, percent carbonate linkages, and percent polycarbonate (with respect to cyclic cyclohexene carbonate byproduct). The remaining product was dissolved in a minimal amount of dichloromethane (ca. 50 mL) and polymer precipitated with the addition of cold, HCl-acidified methanol. After storing in the freezer for a few days, the solution phase was decanted and the polymer dried for a few hours on a Schlenk line, then in a vacuum oven overnight at 60 °C. Note: for reactions with CH_2Cl_2 as a co-solvent, the catalyst solution (in CH_2Cl_2) and CHO were injected separately (i.e. catalyst and CHO were not premixed) to avoid polymerization prior to injection.

5.6.5 NMR Scale Reactions

A J. Young Teflon-valved NMR tube was charged with CHC (12.6 mg) and CD_2Cl_2 (ca. 0.6 mL) and a ^1H NMR spectrum was recorded (Figure A.64(a)). A small amount of **5.1** was then added (due to poor solubility of **5.1** in the solvent at room temperature, the exact mass was not known). The headspace was evacuated briefly using a freeze-pump sequence. The tube was immersed in an oil bath at 60 °C for 20 hours, then another ^1H NMR spectrum was recorded (Figure A.64(b)). Finally, a small amount of PPNCl was added to the tube, and after another freeze-pump sequence, the tube was immersed in the

oil bath for a further 4 hours. A final ^{1}H NMR spectrum was then recorded (Figure A.64(c)).

5.7 References

1. L. Peña Carrodeguas, J. González-Fabra, F. Castro-Gómez, C. Bo and A. W. Kleij, *Chem. Eur. J.*, **2015**, *21*, 6115-6122.
2. C. J. Whiteoak, N. Kielland, V. Laserna, F. Castro-Gómez, E. Martin, E. C. Escudero-Adán, C. Bo and A. W. Kleij, *Chem. Eur. J.*, **2014**, *20*, 2264-2275.
3. C. J. Whiteoak, N. Kielland, V. Laserna, E. C. Escudero-Adán, E. Martin and A. W. Kleij, *J. Am. Chem. Soc.*, **2013**, *135*, 1228-1231.
4. W. Clegg, R. W. Harrington, M. North and R. Pasquale, *Chem. Eur. J.*, **2010**, *16*, 6828-6843.
5. M. R. Kember, P. D. Knight, P. T. R. Reung and C. K. Williams, *Angew. Chem. Int. Ed.*, **2009**, *121*, 949-951.
6. A. Okuniewski, D. Rosiak, J. Chojnacki and B. Becker, *Polyhedron*, **2015**, *90*, 47-57.
7. C.-T. Chen, C.-A. Huang and B.-H. Huang, *Macromolecules*, **2004**, *37*, 7968-7973.
8. K. Nishioka, H. Goto and H. Sugimoto, *Macromolecules*, **2012**, *45*, 8172-8192.
9. A. Buchard, M. R. Kember, K. G. Sandeman and C. K. Williams, *Chem. Commun.*, **2011**, *47*, 212-214.
10. M. A. Fuchs, C. Altesleben, T. A. Zevaco and E. Dinjus, *Eur. J. Inorg. Chem.*, **2013**, *2013*, 4541-4545.
11. N. Ikpo, J. C. Flogeras and F. M. Kerton, *Dalton Trans.*, **2013**, *42*, 8998-9006.
12. K. Ni and C. M. Kozak, *Inorg. Chem.*, **2018**, *57*, 3097-3106.
13. D. J. Darensbourg and A. D. Yeung, *Polym. Chem.*, **2015**, *6*, 1103-1117.
14. F. Jutz, A. Buchard, M. R. Kember, S. B. Fredriksen and C. K. Williams, *J. Am. Chem. Soc.*, **2011**, *133*, 17395-17405.
15. F. M. Kerton, S. Holloway, A. Power, R. G. Soper, K. Sheridan, J. M. Lynam, A. C. Whitwood and C. E. Willans, *Can. J. Chem.*, **2008**, *86*, 435-443.
16. C. S. Higham, D. P. Dowling, J. L. Shaw, A. Cetin, C. J. Ziegler and J. R. Farrell, *Tetrahedron Lett.*, **2006**, *47*, 4419-4423.
17. O. V. Dolomanov, L. J. Bourhis, R. J. Gildea, J. A. K. Howard and H. Puschmann, *J. Appl. Cryst.*, **2009**, *42*, 339-341.
18. G. M. Sheldrick, *Acta Cryst.*, **2008**, *A64*, 112-122.
19. G. M. Sheldrick, *Acta Cryst.*, **2015**, *C71*, 3-8.
20. G. M. Sheldrick, *Acta Cryst.*, **2015**, *A71*, 3-8.

CHAPTER 6

Preliminary Studies Towards New Catalyst Systems and Future Work

Chapter 6. Preliminary Studies Towards New Catalyst Systems and Future Work

6.1 Introduction

As mentioned in Chapter 1 and observed for the Al complexes reported in this thesis for CHO/CO_2 copolymerization, Al complexes are generally less active (in the presence of a co-catalyst) than other metals investigated for copolymerization (e.g. Cr and Co). This chapter will outline efforts to synthesize more active aluminum complexes for copolymerization. New ligand frameworks are of interest to provide bimetallic (homo or heterometallic) complexes that exhibit improved activities relative to their monometallic counterparts. These include amino-phenolate ligands that can accommodate two metal centres. Oxo ligands may bridge two metal centres and also lead to more reactive bimetallic catalysts.

6.2 Aluminum-Oxo Complexes

As mentioned in Chapter 4, bimetallic **[Al-salen]$_2$O** complexes prepared by North's group coupled with TBAB offer high activities in the cycloaddition of PO/CO_2 to give PC.[1] These bimetallic complexes are easily prepared by hydrolysis of the corresponding Al-OEt salen complexes in toluene. Having observed evidence for the formation of oxo-bridged aluminum complexes during MALDI-TOF mass spectrometric analyses, I attempted to prepare bimetallic oxo-bridged species by a variety of synthetic methods. These included transmetallation using Ag_2O with chloro-Al complexes under either room temperature or reflux conditions (Scheme 6.1 – **A**), as well as water hydrolysis of Al-OEt complexes (Scheme 6.1 – **B**). These approaches were unsuccessful. For instance, only pro-ligand

resulted from the reaction of excess water with **4.2**. It should be noted that North's group used a large excess of water to form their bimetallic oxo species, whereas Li *et al.* reported using 0.5 equiv water with an amido-Al phenoxide precursor.[2] Therefore, approaches for the formation of bimetallic Al-oxo amino-bis(phenolate) complexes that could be explored further include (1) hydrolysis of the Al-OEt amino-bis(phenolate) precursor with 0.5 equiv water, (2) hydrolysis of the amido-Al amino-bis(phenolate) precursor with 0.5 equiv water, and (3) hydrolysis of the cationic Al amino-bis(phenolate) precursor containing a stable WCA with 0.5 equiv water. It would also be interesting to react the cationic Al amino-bis(phenolate) precursor with a diol such as ethylene glycol to link two aluminum centres.

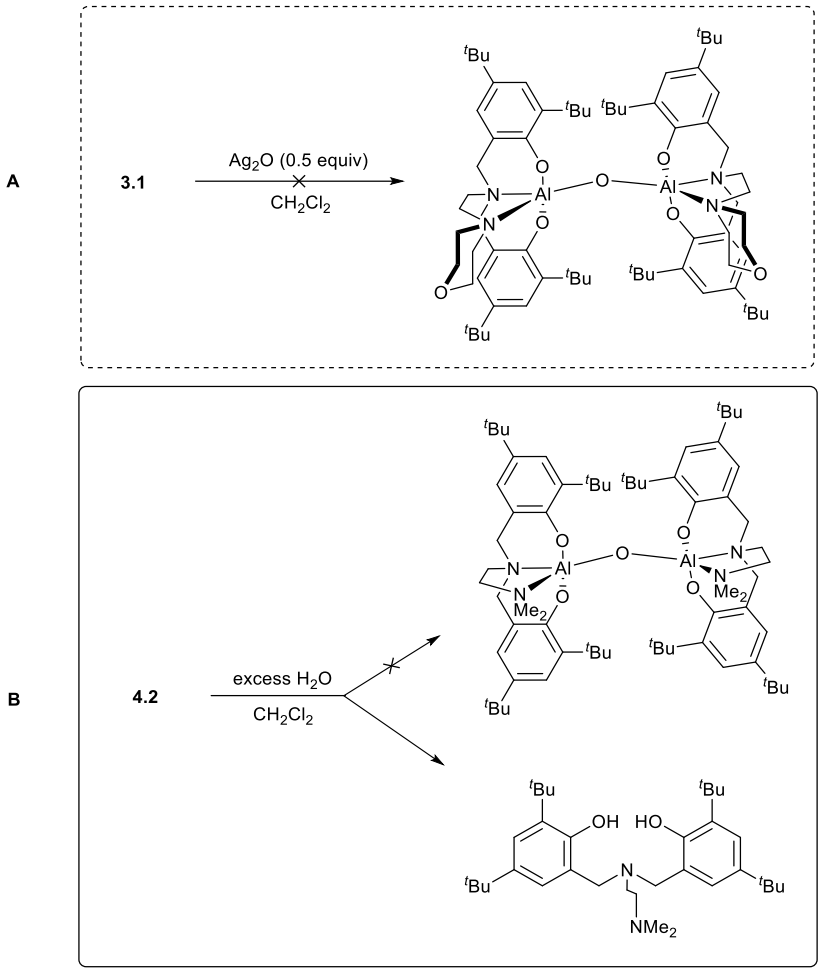

Scheme 6.1. Attempted syntheses of aluminum-oxo complexes

6.3 Mixed-Metal Chromium-Aluminum Systems

Designer Lewis acids such as methylaluminum bis(2,6-di-*tert*-butyl-4-methylphenoxide) (MAD), Figure 6.1, are valuable catalysts for organic transformations.[3] MAD has been used by Nishioka *et al.* to activate CHO towards ring-opening, while still providing sufficient steric bulk to prevent homopolymerization of the CHO.[4] During my research, I was interested to see if MAD could accelerate the rate of reaction observed for two Cr^{III} amino-bis(phenolate) systems (Figure 6.2) reported by Devaine-Pressing *et al.* for

CHO/CO_2 copolymerization.[5-6] These systems give excellent carbonate content in the resulting PCHC but they are less active than other reported Cr^{III} catalyst systems in the area.

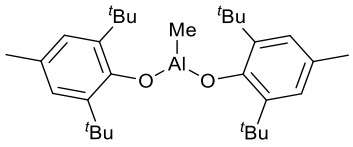

Figure 6.1. Structure of MAD

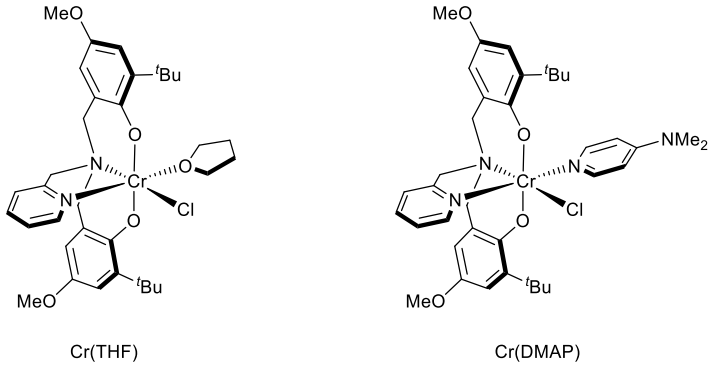

Figure 6.2. Cr^{III} amino-bis(phenolate) catalysts for CHO/CO_2 copolymerization

Initial results utilizing the Cr^{III}/MAD catalyst system are presented in Table 6.1. A copolymer containing only 12.3% carbonate linkages is produced when MAD is used alone (Table 6.1, entry 1). This is a similar result in terms of carbonate linkages when compared to the other aluminum complexes used in ROCOP in this thesis. It should be noted that in the absence of CO_2, homopolymer was formed vigorously upon exothermic addition of MAD to CHO. The most likely reason for this polymerizability in the presence of a sterically bulky Lewis acid, such as MAD, is due to the cationic polymerization of CHO.

Table 6.1. Copolymerization of CHO/CO_2 using Cr catalyst systems and MAD[a]

Entry	Cat.	Co-cat.	[Cat.]/[Co-cat.]/ [MAD]/[CHO]	Conv. (%)[b]	% CO_3[b]	M_n[c,d] × 10^3	$Đ$[c]
1	–	–	0/0/1/500	92.7	12.3	7.16	1.16
2	Cr(THF)	–	1/0/1/500	73.8	25.9	4.73	1.38
3	Cr(THF)	–	1/0/0/500	9.9	36.4	ND	ND
4	Cr(THF)	PPNCl	1/1/1/500	40.9	51.9	3.08	1.66
5	Cr(DMAP)	DMAP	1/1/1/500	40.5	70.6	2.78	2.04
6	Cr(DMAP)	DMAP	1/1/0/500	98.0	>99	9.52	1.10

[a] Reaction conditions: 60 °C, 40 bar CO_2, 24 h, 5 mL CH_2Cl_2. [b] Determined by ^{1}H NMR. [c] Determined by triple detection GPC in THF. [d] In Da. ND: Copolymer was not isolated in sufficient quantity for analyses.

That is, CHO activated by MAD is easily attacked by another molecule of CHO and chain-growth rapidly ensues.

While the M_n and narrow dispersity of 1.16 in the presence of CO_2 are quite reasonable, it is important to note that these copolymers were isolated by CH_2Cl_2/MeOH precipitation, an imprecise purification method according to others,[7] instead of simple quenching and drying *in vacuo*. The latter method would maintain the composition of the polymer in cases with large M_n ranges that contain low molecular weight polymer and oligomers. This became evident in reactions utilizing both Cr^{III} catalyst and MAD, as isolated yields following precipitation dropped sharply coinciding with low M_n values according to GPC (Table 6.1, entries 2, 4–5). The use of CH_2Cl_2 as a diluent did not appear to adversely affect the reactivity of the system, as observed for the aluminum amino-bis(phenolate) systems, probably due to the larger surface area of this reactor.

6.4 Tetra-Amide Ligands

The Kerton group previously worked on synthesis of bis-amide ligands which were easily synthesized by microwave reaction of diethyl malonate and the appropriate amine reagent. I sought to extend this ligand framework to a tetra-amide to accommodate two metals, thereby increasing catalytic activities through cooperative effects frequently seen in the literature for these bimetallic systems. The initial synthetic step (Scheme 6.2) was based on a report by Chen *et al.* who prepared a methylene-bridged tetra(methyl ester) intermediate using paraformaldehyde and KOH.[8] My attempts to isolate the tetra(ethyl ester) using this reaction protocol only yielded the desired product with a contaminating side-product. Chen's group did not isolate and characterize their tetra(methyl ester) intermediate. Therefore, any side-product may have been removed in subsequent reaction steps. Attempts to use the impure tetra(ethyl ester) in the subsequent microwave reaction with primary amines produced solid products but these contained significant impurities according to NMR. While there are options to purify the tetra(ethyl ester) and corresponding tetra-amide, due to limited time and practicality this project was not pursued further.

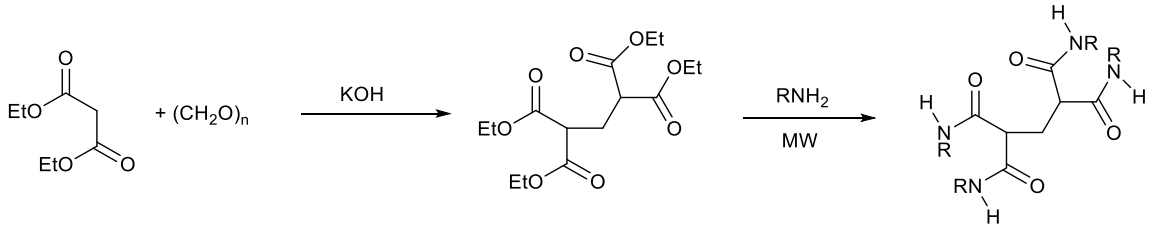

Scheme 6.2. Potential synthetic pathway to tetra-amide ligands

6.5 Salan Ligands

As mentioned previously, metal salen complexes have been widely studied in epoxide/CO_2 copolymerization reactions. However, complexes based on the related salan ligand framework have been less frequently investigated, with primary emphasis on Co and Cr systems.[9-10] Salan ligands are more flexible and electron donating than their salen counterparts. I was interested in preparing salan ligands incorporating piperidinyl or morpholinyl pendent donors at the *ortho* position of the aromatic ring to compare the effect of the outer-sphere heteroatoms on copolymerizations. The attachment of piperidinyl donors at the *ortho* position has some precedent in the copolymerization literature, namely, the Co^{III} salen complex **1.14** containing piperidinyl and piperidinium end-capping arms reported by Nozaki and co-workers.[11] Similarly, the related *N*-methylhomopiperazine donor has been appended to the *ortho* position of an Al-salen complex and found to possess efficient activity for the synthesis of cyclic carbonates from epoxides/CO_2.[12] The *N*-methylhomopiperazinyl group was proposed to function as a co-catalyst that ring-opens the metal-coordinated epoxide.

The synthetic pathway of steps required to reach these ligands is summarized in Scheme 6.3. The first step is a formylation reaction to produce 5-*tert*-butyl-2-hydroxybenzaldehyde. Step 2 involves a Mannich condensation using paraformaldehyde and morpholine or piperidine in the presence of an acid catalyst (glacial acetic acid). Step 3 is an amine condensation to form the salen intermediate. It is worth noting that both salen intermediates have been isolated previously and utilized in metal sulfate extraction studies.[13] Step 4 is a reduction using sodium borohydride followed by acid workup. Given

the abundance of donor groups in these salan ligands (six or eight), there is potential for two Al centres to occupy the ligand framework. While the reaction pathway was ultimately successful for H_2[**L8**] and H_2[**L9**], further optimization of steps 3–4 are needed as a very low percent yield was obtained.

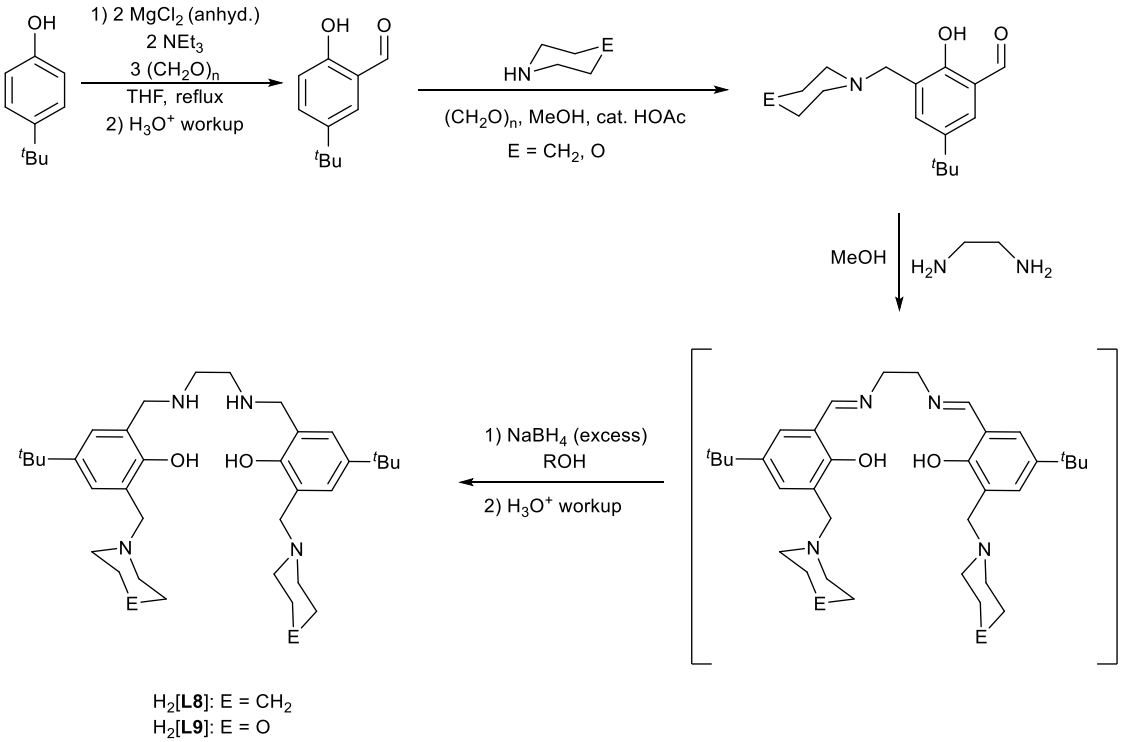

Scheme 6.3. Synthetic pathway to salan ligands H_2[**L8**] and H_2[**L9**]

H_2[**L8**] and H_2[**L9**] were characterized by ^{1}H NMR spectroscopy. Except for the multiplet at 1.61 ppm and the two aromatic doublets at 6.87 and 7.10 ppm, the spectrum for H_2[**L8**] contained singlets at 1.26, 1.48 (broad), 2.49 (broad), 2.81, 3.62, and 3.80 ppm. These peaks integrated to 8, 2 × 2, 18, 4, 8, 4, 4, and 4 protons and were attributed to the CH_2 of the piperidine, CH of the phenol, CH_2 of the piperidine, CH_2 of the piperidine, CH_2

coupling the secondary amine and phenol, and the CH_2 coupling the piperidine and phenol, respectively. The spectrum for H_2[**L9**] contained singlets at 1.26, 2.55, 2.93, 3.68, 3.72 (broad), and 3.89 ppm along with two aromatic doublets at 6.96 and 7.14 ppm. These peaks integrated to 18, 8, 4, 4, 8, 4, and 2 × 2 protons and were attributed to the two ^{t}Bu groups, CH_2 of the morpholine (adjacent to nitrogen), CH_2 of the secondary amine, CH_2 coupling the secondary amine and phenol, another CH_2 of the morpholine (adjacent to oxygen), CH_2 coupling the morpholine and phenol, and the CH of the phenol, respectively. The structures were further confirmed by MALDI-TOF MS and the mass spectra for H_2[**L8**] contained peaks at *m/z* 577 and 579 which are consistent with the molecular weights of the $[M-H]^+$ and $[M+H]^+$ ions. The mass spectra for H_2[**L9**] contained peaks at *m/z* 581 and 583 which are consistent with the molecular weights of the $[M-H]^+$ and $[M+H]^+$ ions.

6.6 Experimental Section

6.6.1 General Considerations

Paraformaldehyde was dried over P_2O_5. Anhydrous magnesium chloride was stored under N_2. Triethylamine was dried over CaH_2 and stored under N_2 prior to use. THF was distilled from sodium/benzophenone ketyl. Both 3-(piperidinylmethyl)-5-*tert*-butylsalicylaldehyde and 3-(morpholinylmethyl)-5-*tert*-butylsalicylaldehyde have been synthesized previously.[14] 3-(piperidinylmethyl)-5-*tert*-butylsalicylaldehyde was synthesized following this literature procedure. An attempted synthesis of 3-(morpholinylmethyl)-5-*tert*-butylsalicylaldehyde "on water" was successful and negated the need for column chromatography but utilized excess amounts of formaldehyde and morpholine. MAD was prepared according to literature procedure.[3] MALDI-TOF mass

spectra were acquired on an Applied Biosystems 4800 MALDI TOF/TOF Analyzer equipped with a reflectron, delayed ion extraction and high-performance nitrogen laser (200 Hz operating at 355 nm). Ligands were mixed in a 1:1 (matrix:ligand) ratio in toluene with anthracene as the matrix.

6.6.2 Typical Copolymerization Procedure

Cr^{III} catalyst (0.0712 g, 102 μmol) and PPNCl (0.0585 g, 102 μmol) were stirred in ca. 5 mL CH_2Cl_2 for ten minutes and volatiles were removed *in vacuo*. CHO (5.00 g, 50.9 mmol) was added to the residue. The Cr/PPNCl/CHO vial septum was pierced with a cannulae needle and transported outside of the glovebox. A CH_2Cl_2 solution of MAD (0.0495 g, 103 μmol) was handled identically. The dry and CO_2-flushed pressure vessel was charged sequentially with the CHO and MAD solutions *via* the injection port and quickly pressurized to the 40 bar CO_2. The reaction was stirred at 60 °C for 24 h. Once complete, the reactor was cooled to room temperature and the vessel slowly depressurized. A small sample was taken for ^{1}H NMR analysis and the remaining mixture was dissolved in CH_2Cl_2 and precipitated with cold, HCl-acidified MeOH and left in a freezer overnight to promote precipitation.

6.6.3 Synthetic Procedures

5-*tert*-butyl-2-hydroxybenzaldehyde. A Schlenk round bottom flask containing 4-*tert*-butylphenol (15.06 g, 100.3 mmol) was evacuated for two hours to remove adventitious moisture and subsequently anhydrous magnesium chloride (19.36 g, 203.3 mmol), THF (150 mL), and triethylamine (20.58 g, 203.4 mmol) were added under N_2. Dry paraformaldehyde (9.35 g, 311 mmol) was added in portions and the resulting mint green

mixture was refluxed under N_2 at 110 °C for 16 hours. The reaction mixture was cooled then quenched with 3M HCl (300 mL). The organics were extracted with diethyl ether (2×300 mL), then washed with water (400 mL) and brine (400 mL) and dried over Na_2SO_4. Filtration of the solution and removal of solvent *in vacuo* yields a brown oil that is redissolved in DCM and filtered through silica gel. A yellow oil (15.44 g, 86.4%) is obtained after drying *in vacuo*. ^{1}H NMR ($CDCl_3$, 300 MHz, 298 K) δ 10.86 (1H, s, Ar–C*H*O), 9.89 (1H, s, Ar–O*H*), 7.55 (2H, m, Ar*H*), 6.93 (1H, d, Ar*H*), 1.33 (9H, s, Ar–C{CH_3}$_3$); ^{13}C{^{1}H} NMR ($CDCl_3$, 125 MHz, 298 K) δ 197.0 (Ar–*C*HO), 159.6, 142.9, 134.9, 129.9, 120.2, 117.4 (Ar*C*), 34.3 (Ar–*C*{CH_3}$_3$), 31.4 (Ar–C{*C*H_3}$_3$).

3-(piperidinylmethyl)-5-*tert*-butylsalicylaldehyde. ^{1}H NMR ($CDCl_3$, 300 MHz, 298 K) δ 10.42 (1H, s, Ar–C*H*O), 7.65 (1H, d, Ar*H*), 7.24 (1H, d, Ar*H*), 3.71 (2H, s, Ar–CH_2–N), 2.55 (4H, br s, N–CH_2–CH_2), 1.66 (4H, m, N–CH_2–CH_2–CH_2), 1.52 (2H, br s, N–CH_2–CH_2–CH_2), 1.28 (9H, s, Ar–C{CH_3}$_3$).

3-(morpholinylmethyl)-5-*tert*-butylsalicylaldehyde. ^{1}H NMR ($CDCl_3$, 300 MHz, 298 K) δ 10.25 (1H, s, Ar–C*H*O), 7.61 (1H, d, Ar*H*), 7.39 (1H, d, Ar*H*), 3.76 (4H, t, N–CH_2–CH_2–O), 3.71 (4H, s, Ar–CH_2–N), 2.58 (4H, t, N–CH_2–CH_2–O), 1.30 (9H, s, Ar–C{CH_3}$_3$).

Salan(piperidine) (H_2[**L8**]). Initial reflux (4 h) of 3-(piperidinylmethyl)-5-*tert*-butylsalicylaldehyde (4.31 g, 15.7 mmol) with ethylenediamine (0.60 mL, 9.0 mmol) in 50 mL MeOH did not fully convert the starting material. A second reflux was performed using the crude product, ethylenediamine (0.3 mL, 4.5 mmol), and 2 g anhydrous $MgSO_4$ in 50 mL MeOH for 2.5 h. The reaction mixture was gravity filtered to remove $MgSO_4$ and

cooled in an ice bath. $NaBH_4$ (1.15 g, 30.4 mmol) was added gradually changing the colour from orange-yellow to colourless/pale beige and the mixture was stirred for 1 h. 4 M HCl was added until pH 3 was reached, then 0.5 M Na_2CO_3 was added to reach pH 8. The organics were extracted with 4 × 50 mL EtOAc and volatiles were removed *in vacuo*. The residue was dissolved in $CHCl_3$/MeOH and stored in a freezer for several months yielding a residue on the sides of the flask. After decantation, the product was dried and isolated as a colourless solid. Yield: 0.43 g, 9.5%. ^{1}H NMR ($CDCl_3$, 300 MHz, 298 K) δ 7.10 (2H, d, Ar*H*) 6.87 (2H, d, Ar*H*), 3.80 (4H, s, Ar–C*H*$_2$–N), 3.62 (4H, s, Ar–C*H*$_2$–N), 2.81 (4H, s, HN–C*H*$_2$–C*H*$_2$–NH), 2.49 (8H, br s, N–C*H*$_2$–CH$_2$–CH$_2$), 1.61 (8H, m, N–CH$_2$–C*H*$_2$–CH$_2$), 1.48 (4H, br s, N–CH$_2$–CH$_2$–C*H*$_2$); 1.26 (18H, s, Ar–C{C*H*$_3$}$_3$). MS (MALDI-TOF) *m/z* (%, ion): 577.4300 (100, $[M-H]^+$), 579.4457 (84, $[M+H]^+$).

Salan(morpholine) (H_2[**L9**]). Ethylenediamine (0.67 g, 11.1 mmol) was added dropwise to a stirred mixture of 3-(morpholinylmethyl)-5-*tert*-butylsalicylaldehyde (5.81 g, 20.9 mmol) and excess anhydrous $MgSO_4$ in 50 mL MeOH. The mixture was brought to reflux for 3 h and then gravity filtered. On cooling, a crystalline solid formed and the solution was left in the freezer overnight. The MeOH phase was decanted and 50 mL EtOH was added. In an ice bath, $NaBH_4$ (3.95 g, 104 mmol) was gradually added turning the yellow suspension colourless. Stirred for a further 1.5 h after addition. 4 M HCl was added until pH 3 was reached, then 0.5 M Na_2CO_3 was added to reach pH 8. The organics were extracted with 2 × 50 mL CH_2Cl_2 and dried over anhydrous Na_2SO_4 overnight. Volatiles were removed *in vacuo* yielding a colourless-pink solid. ^{1}H NMR ($CDCl_3$, 300 MHz, 298 K) δ 7.14 (2H, d, Ar*H*), 6.96 (2H, d, Ar*H*), 3.89 (4H, s, Ar–C*H*$_2$–morph), 3.72 (8H,

overlapping br s, N–CH_2–CH_2–O), 3.68 (4H, overlapping s, Ar–CH_2–NH), 2.93 (4H, s, HN–CH_2–CH_2–NH), 2.55 (8H, br s, N–CH_2–CH_2–O), 1.26 (18H, s, Ar–C{CH_3}$_3$). MS (MALDI-TOF) *m/z* (%, ion): 581.3945 (85, $[M-H]^+$), 583.4087 (100, $[M+H]^+$).

6.7 References

1. W. Clegg, R. W. Harrington, M. North and R. Pasquale, *Chem. Eur. J.*, **2010**, *16*, 6828-6843.
2. C.-Y. Li, D.-C. Liu and B.-T. Ko, *Dalton Trans.*, **2013**, *42*, 11488-11496.
3. S. Saito and H. Yamamoto, *Chem. Commun.*, **1997**, 1585-1592.
4. K. Nishioka, H. Goto and H. Sugimoto, *Macromolecules*, **2012**, *45*, 8172-8192.
5. K. Devaine-Pressing and C. M. Kozak, *ChemSusChem*, **2017**, *10*, 1266-1273.
6. K. Devaine-Pressing, L. N. Dawe and C. M. Kozak, *Polym. Chem.*, **2015**, *6*, 6305-6315.
7. M. A. Fuchs, C. Altesleben, T. A. Zevaco and E. Dinjus, *Eur. J. Inorg. Chem.*, **2013**, *2013*, 4541-4545.
8. X. Pang, R. Duan, X. Li, Z. Sun, H. Zhang, X. Wang and X. Chen, *RSC Adv.*, **2014**, *4*, 57210-57217.
9. B. Li, G.-P. Wu, W.-M. Ren, Y.-M. Wang, D.-Y. Rao and X.-B. Lu, *J. Polym. Sci., Part A: Polym. Chem.*, **2008**, *46*, 6102-6113.
10. D. J. Darensbourg, M. Ulusoy, O. Karroonnirum, R. R. Poland, J. H. Reibenspies and B. Çetinkaya, *Macromolecules*, **2009**, *42*, 6992-6998.
11. K. Nakano, T. Kamada and K. Nozaki, *Angew. Chem. Int. Ed.*, **2006**, *45*, 7274-7277.
12. Y. Ren, O. Jiang, H. Zeng, Q. Mao and H. Jiang, *RSC Adv.*, **2016**, *6*, 3243-3249.
13. R. A. Coxall, L. F. Lindoy, H. A. Miller, A. Parkin, S. Parsons, P. A. Tasker and D. J. White, *Dalton Trans.*, **2003**, 55-64.
14. E. F. DiMauro and M. C. Kozlowski, *Org. Lett.*, **2001**, *3*, 3053-3056.

CHAPTER 7

Conclusions

Chapter 7. Conclusions

7.1 Summary

Polymers based on renewable feedstocks are a highly desirable component of a non-fossil fuel-based economy. Polymeric materials that are industrially processable must exhibit uniform properties, which are characteristic of well-controlled polymerizations. This research aimed to synthesize more active aluminum catalysts given the inexpensive and biocompatible nature of this metal.

Chapter 1 gave an overview of research surrounding the synthesis of PCL and PCHC and summarized the aluminum complexes reported for ROP of ε-CL and copolymerization of epoxides (typically CHO and PO) and CO_2.

Chapter 2 focused on developing structure-activity relationships for ROP of CHO with respect to the outer-sphere donor (O or NMe) of aluminum amino-phenolate complexes. The morpholine variant **2.1** showed very high activities in ROP of CHO compared to the NMe variant **2.2** and a related amino-bis(phenolate) complex **2.3** containing a methoxy donor. MALDI-TOF MS confirmed that the chloride anion was initiating the ROP, but further work is needed to understand the exact initiation steps.

Chapter 3 dealt with the synthesis and characterization of a series of cationic aluminum amino-bis(phenolate) complexes **3.2–3.7** which differed with respect to the weakly coordinating anion present. Some Lewis acids (e.g. BPh_3) were unable to (fully) abstract the chloride (from the neutral complex **3.1**) to generate the cation, illustrating the strength of the Lewis acid required. The activity of the complexes in ROP of ε-CL was dependent

on the stability of the anion. Complexes containing an anion stable to alcohol co-initiator ($[GaCl_4]^-$ and $[InCl_4]^-$) showed living character in polymerizations. Activation parameters ($\Delta H^{\ddagger}$, $\Delta S^{\ddagger}$) were determined by ^1H NMR spectroscopy and combined with MALDI-TOF MS data supported a coordination-insertion mechanism. Theoretical studies showed that the bidentate chelation of the morpholine donor is favourable for stability. While these complexes were quite slow in ROP of ε-CL and entirely inactive for ROP of lactide, there remains further possibilities for their utilization in various catalytic reactions. For example, preliminary studies into ROP of PO using **3.5**/EtOH successfully produced polymer. Further modification of the structure of the cation will undoubtedly lead to interesting results in the future.

In Chapter 4, the synthesis and characterization of aluminum amino-phenolate complexes **4.1–4.4** containing different pendent donors was described. These complexes were tested for their efficacy in CHO/CO_2 copolymerization along with **3.1**. All copolymers produced by the complexes in the presence of PPNCl were strictly alternating PCHC and exhibited narrow dispersities indicating excellent control. An extensive screening of the morpholine variant **3.1**/PPNCl showed that it can maintain ca. 90% selectivity towards the copolymer, even at elevated temperatures. The selectivities of **4.1–4.4** were much poorer and this prompted a theoretical examination of the partial atomic charges of the aluminum in the hypothetical Al-carbonate intermediates. Future work in this area may involve the use of **3.1**/PPNCl in copolymerization of epoxides and cyclic anhydrides which has been relatively untouched with aluminum systems but is increasing in popularity in recent years.[1-5]

Chapter 5 introduced a bimetallic aluminum complex **5.1** and its monometallic analogue **5.2**. The activities of **5.1** were roughly twice as much as **5.2** at identical catalyst loadings, which makes sense as there are two Al centres in **5.1** and one Al centre in **5.2**. Although cooperative effects on activity are commonly seen in bimetallic systems, the linker length in **5.1** is probably too long and flexible to provide the foundation for a bimetallic mechanism and increased activities. Nevertheless, improved activities for the pendent-free systems **5.1** and **5.2** were seen relative to the systems containing pendent donors (**3.1**, **4.1**–**4.4**) described in Chapter 4. Recent years have seen promising results in polymerization of other oxygen containing monomers while using electron-deficient ligand frameworks, therefore, future work could involve introducing electron-withdrawing substituents into the phenolate backbones. Also, continued efforts towards the synthesis of bimetallic aluminum species, where the two metal centres are forced close together, would be worthwhile and should lead to more active catalysts especially if the Al centres are coordinatively unsaturated (i.e. lack pendent stabilizing groups).

Chapter 6 primarily explored pathways to synthesize more active aluminum complexes for copolymerization. For instance, the synthesis and characterization of new ligands such as tetra-amide ligands, or salan ligands appended with morpholine and piperidine pendent donors (H_2[**L8**] and H_2[**L9**]). If the syntheses of H_2[**L8**] and H_2[**L9**] could be further optimized, these ligands could be utilized in the future to continue to explore the outer-sphere donor effect once chelated to a metal such as aluminum. The use of MAD as an epoxide activator in copolymerizations with CHO and Cr^{III} was also touched upon.

Depending on the co-catalyst used, a range of conversions were obtained. However, due to time limitations this project was not explored further.

Overall within this thesis, 14 aluminum amino-phenolate complexes were studied in terms of their reactivity towards ROP and ROCOP reactions. A number of structure-activity relationships were established and significant differences in reactivity were seen when morpholine groups were incorporated into ligand structures. The study of closely related cationic, monometallic, and bimetallic species has allowed a better understanding of reactivity for aluminum complexes for these reactions and will act as a foundation for further research.

7.2 References

1. J. Li, B.-H. Ren, S.-Y. Chen, G.-H. He, Y. Liu, W.-M. Ren, H. Zhou and X.-B. Lu, *ACS Catal.*, **2019**, *9*, 1915-1922.
2. J. Li, B.-H. Ren, Z.-Q. Wan, S.-Y. Chen, Y. Liu, W.-M. Ren and X.-B. Lu, *J. Am. Chem. Soc.*, **2019**, *141*, 8937-8942.
3. E. H. Nejad, C. G. W. van Melis, T. J. Vermeer, C. E. Koning and R. Duchateau, *Macromolecules*, **2012**, *45*, 1770-1776.
4. M. J. Sanford, L. Peña Carrodeguas, N. J. Van Zee, A. W. Kleij and G. W. Coates, *Macromolecules*, **2016**, *49*, 6394-6400.
5. N. J. Van Zee, M. J. Sanford and G. W. Coates, *J. Am. Chem. Soc.*, **2016**, *138*, 2755-2761.

Appendix A: NMR Spectroscopy

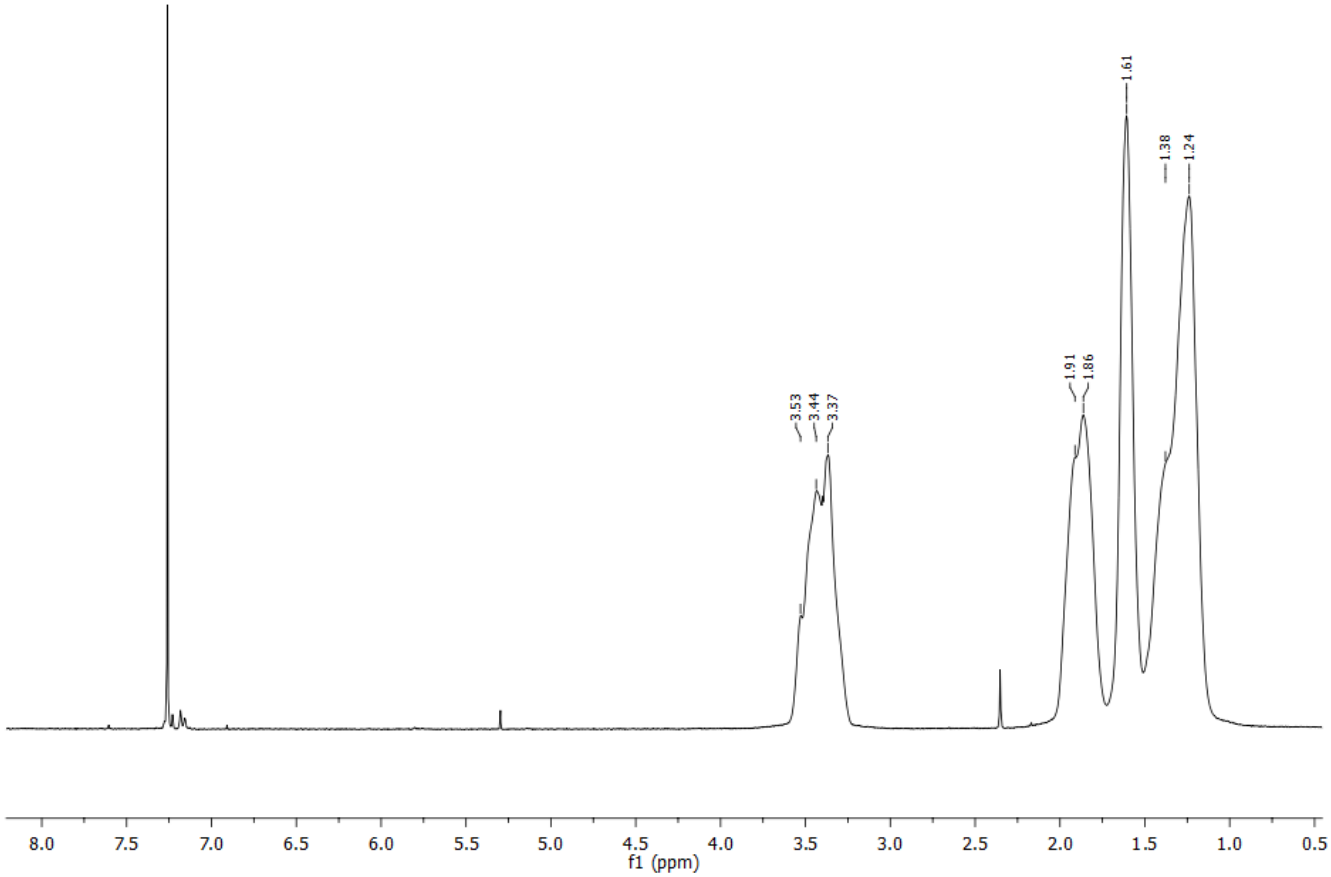

Figure A.1. Typical ^{1}H NMR spectrum of PCHO in $CDCl_3$, 298 K

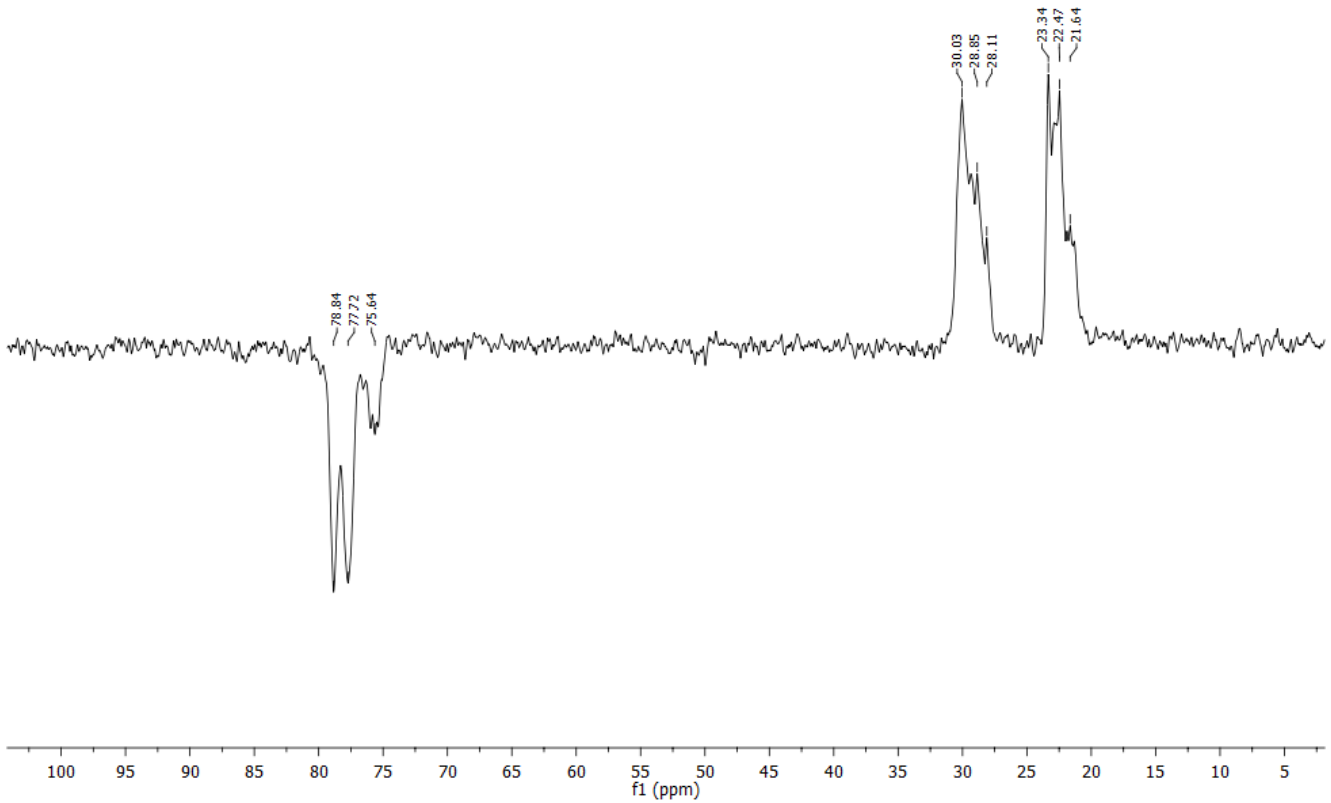

Figure A.2. Typical ^{13}C DEPT-135 NMR spectrum of PCHO in $CDCl_3$, 298 K

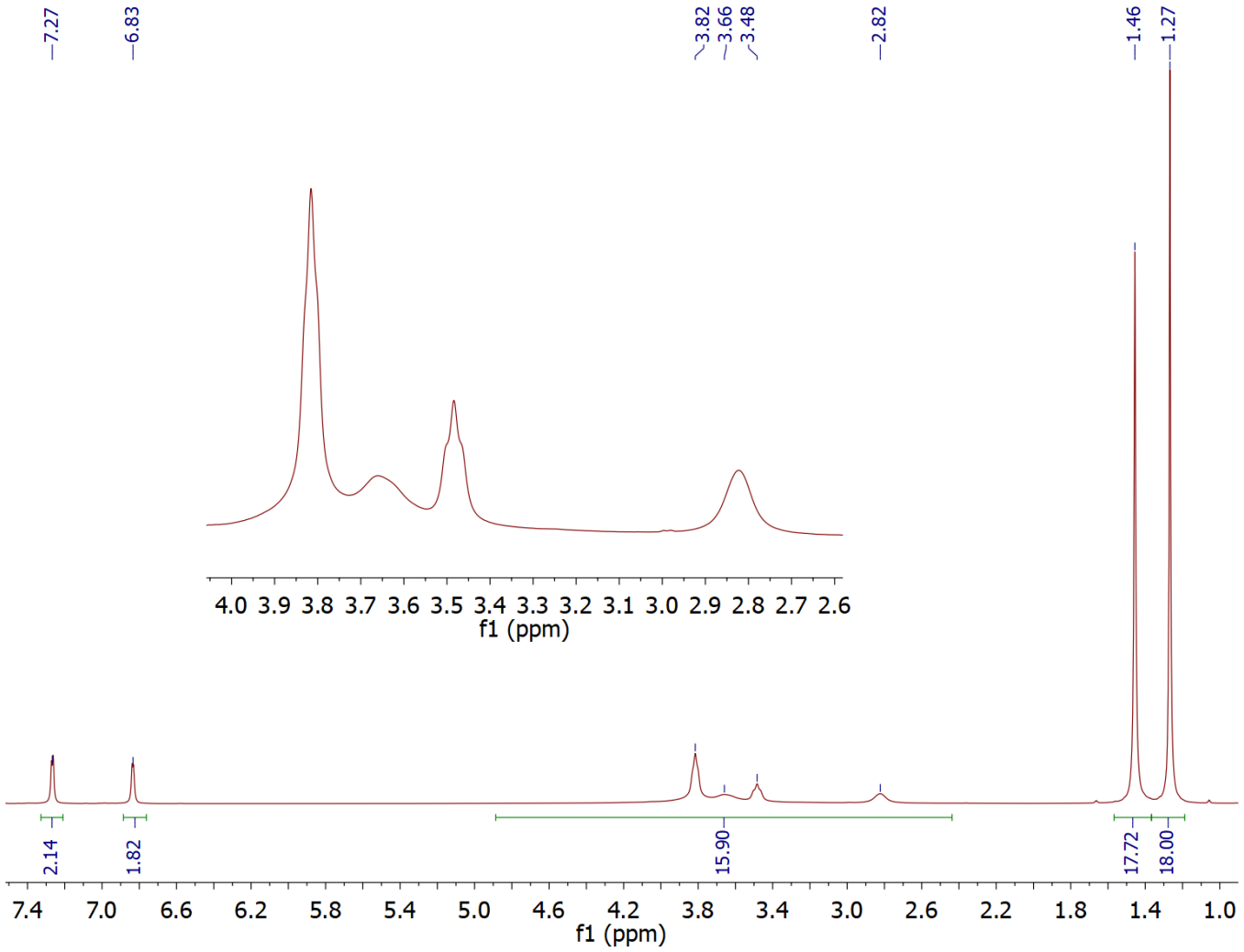

Figure A.3. ^{1}H NMR spectrum of **3.1** in $CDCl_3$, 298 K

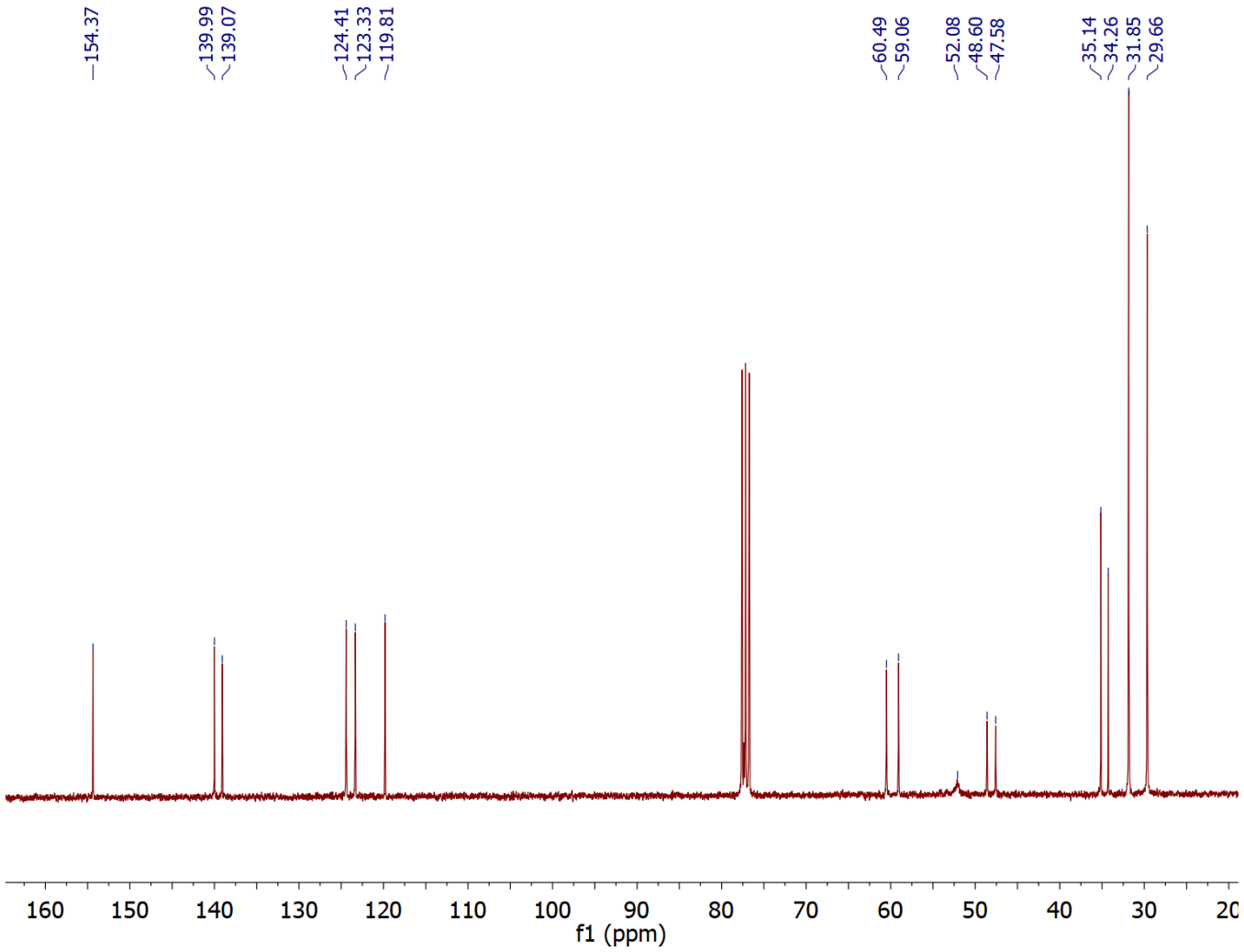

Figure A.4. $^{13}C\{^{1}H\}$ NMR spectrum of **3.1** in $CDCl_3$, 298 K

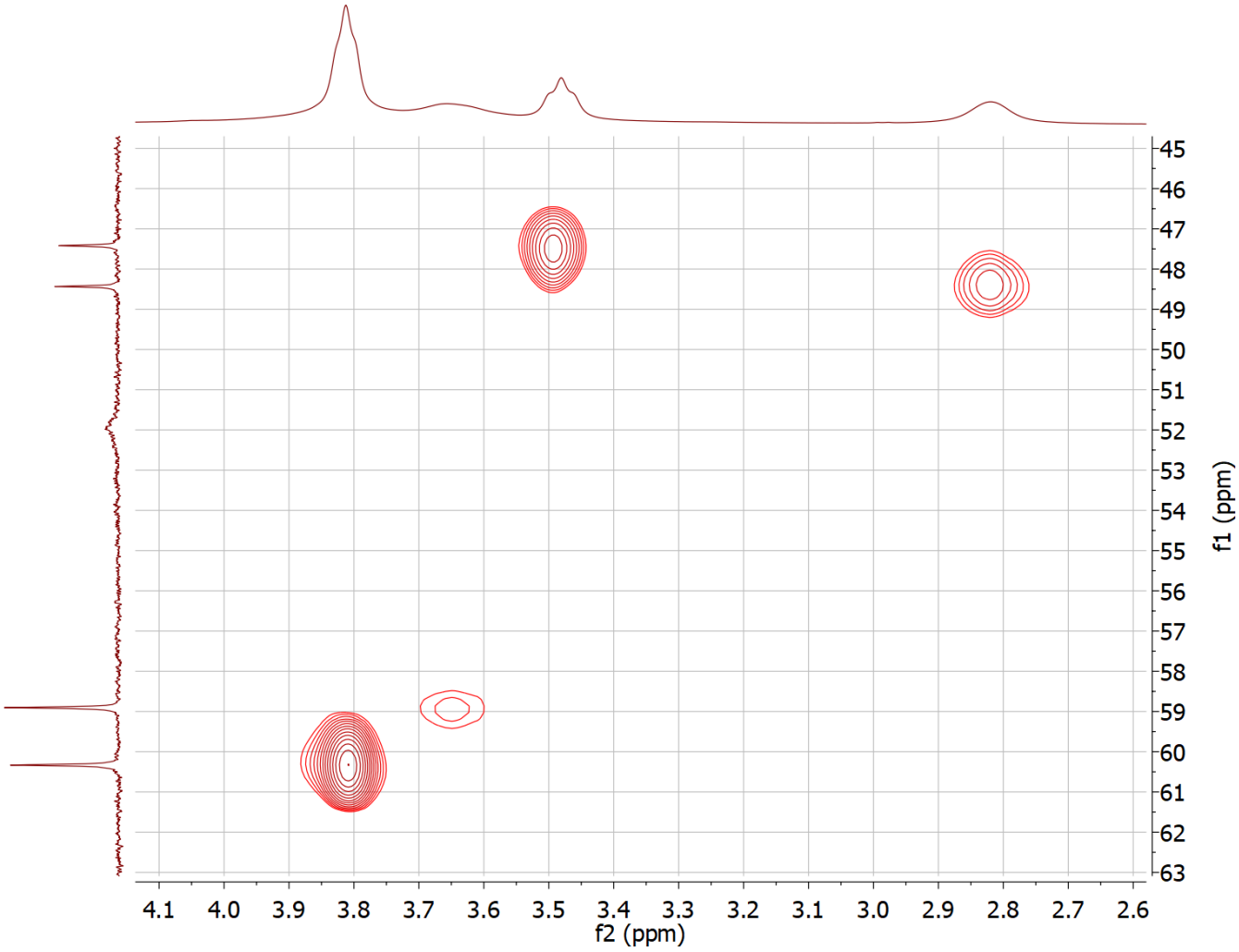

Figure A.5. HSQC spectrum of **3.1** in $CDCl_3$, 298 K

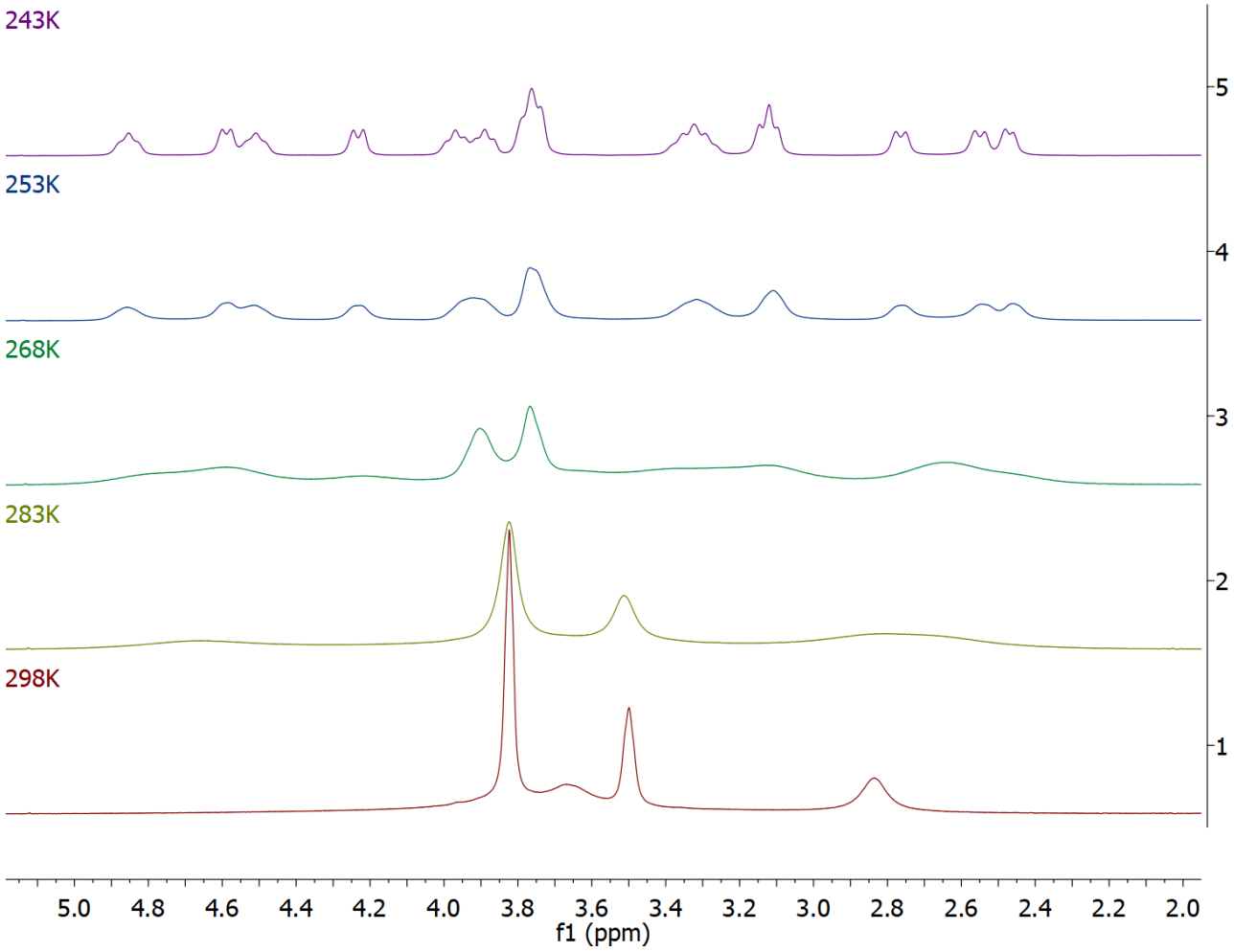

Figure A.6. Variable temperature ^{1}H NMR spectra of **3.1** in $CDCl_3$ (methylene region)

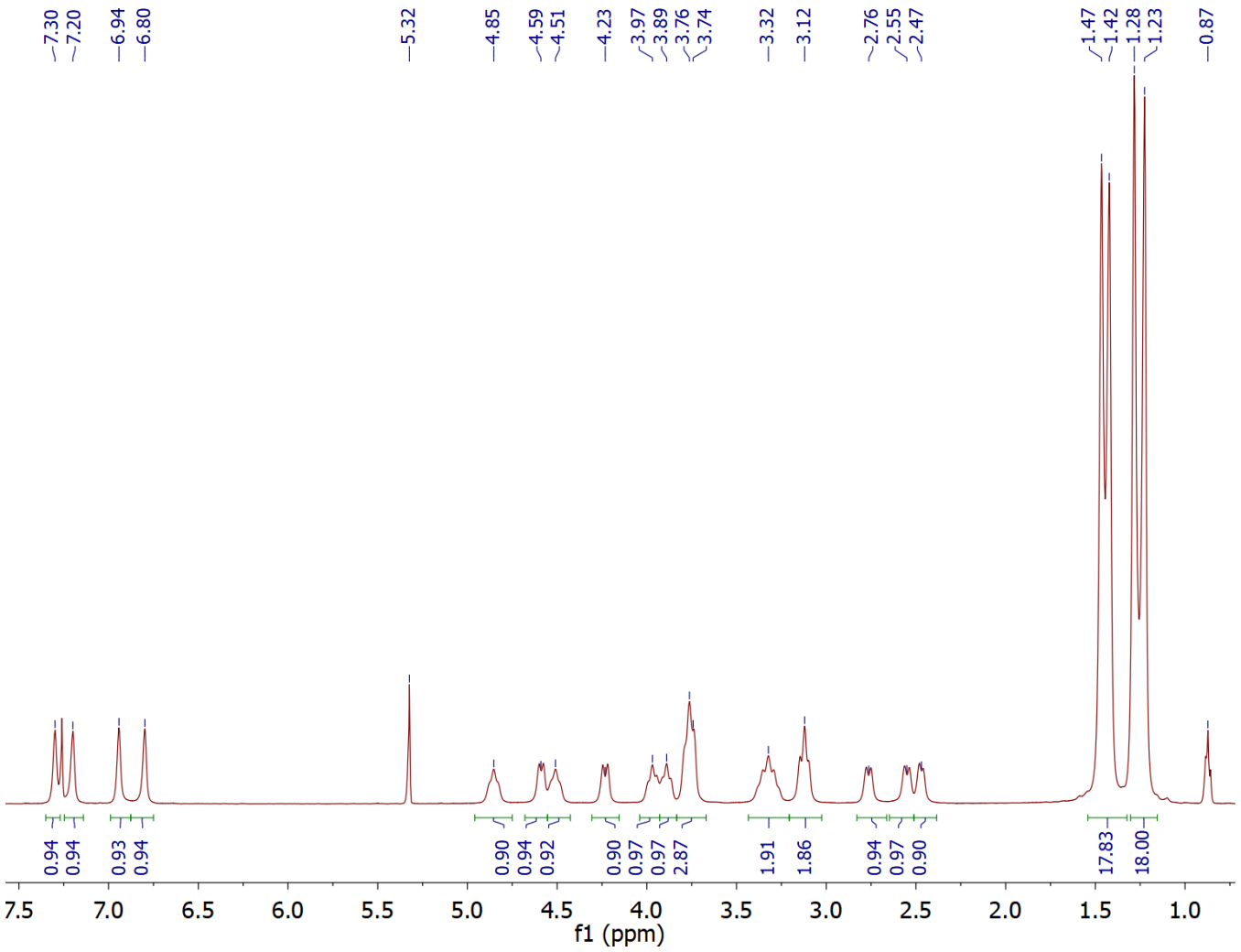

Figure A.7. ^{1}H NMR spectrum of **3.1** in $CDCl_3$, 243 K (residual CH_2Cl_2/heptane resonances at 5.32/0.87 ppm)

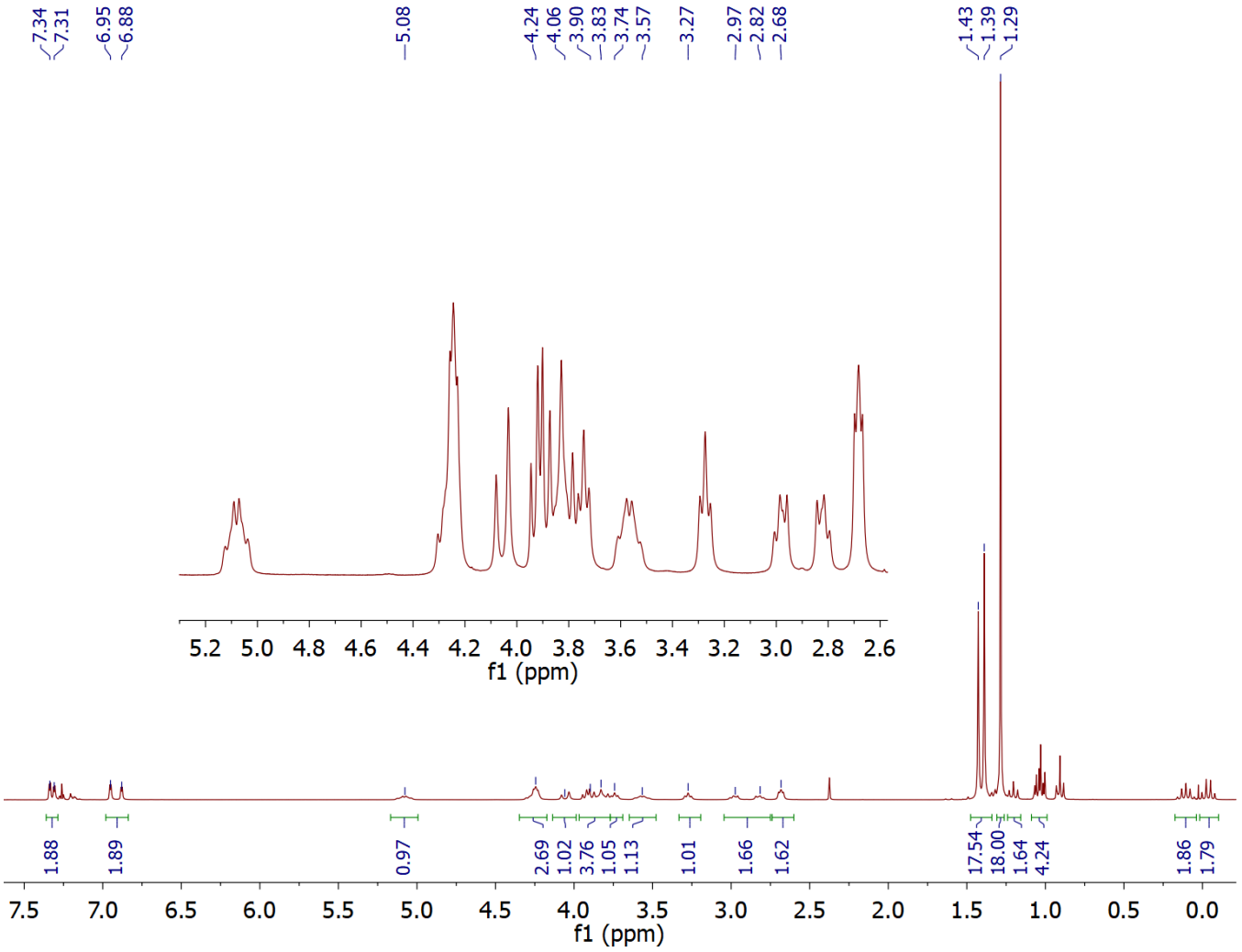

Figure A.8. ^{1}H NMR spectrum of **3.2** in $CDCl_3$, 298 K (residual toluene/pentane resonances at 2.3/0.9 ppm)

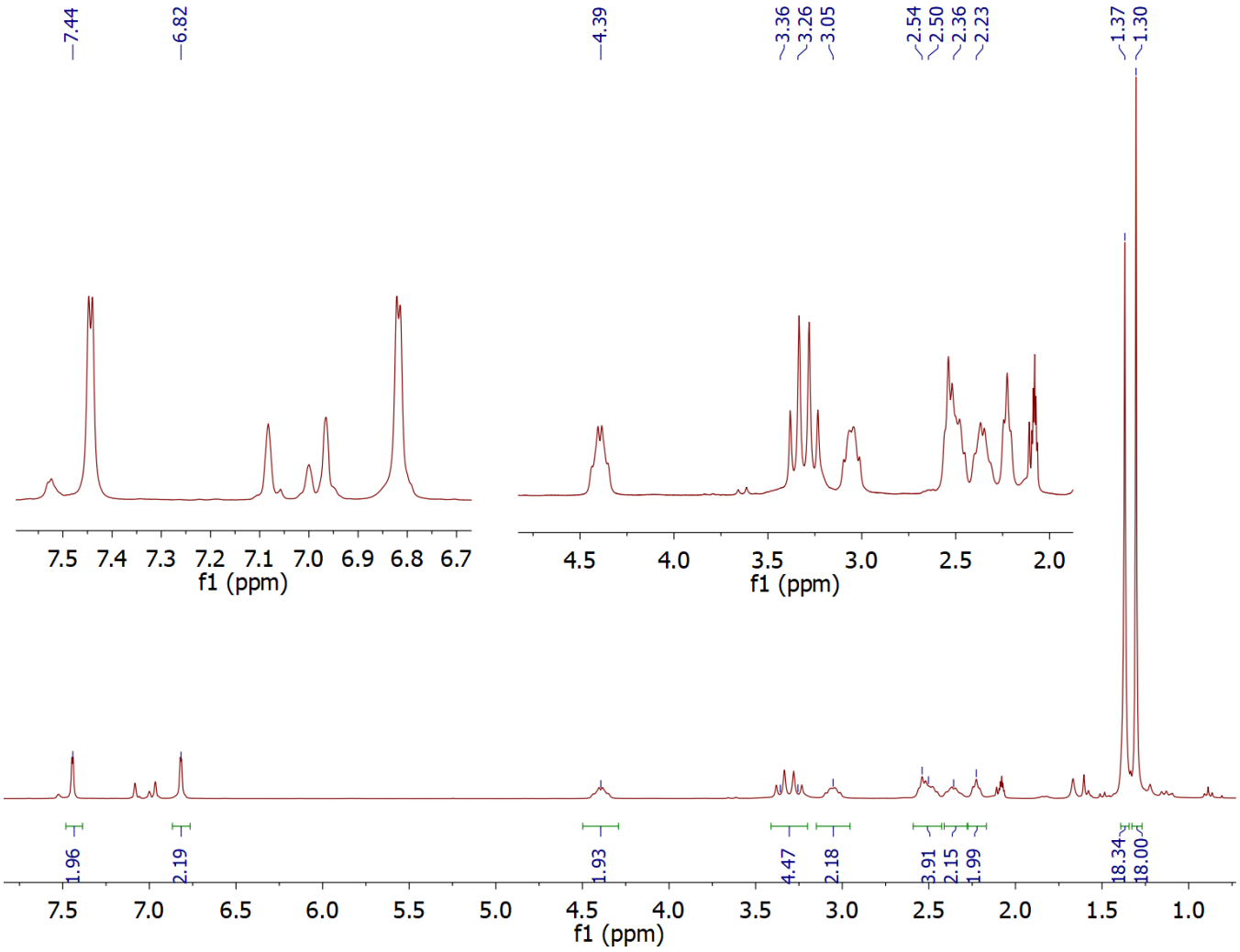

Figure A.9. ^{1}H NMR spectrum of **3.3** in toluene-d_8, 298 K

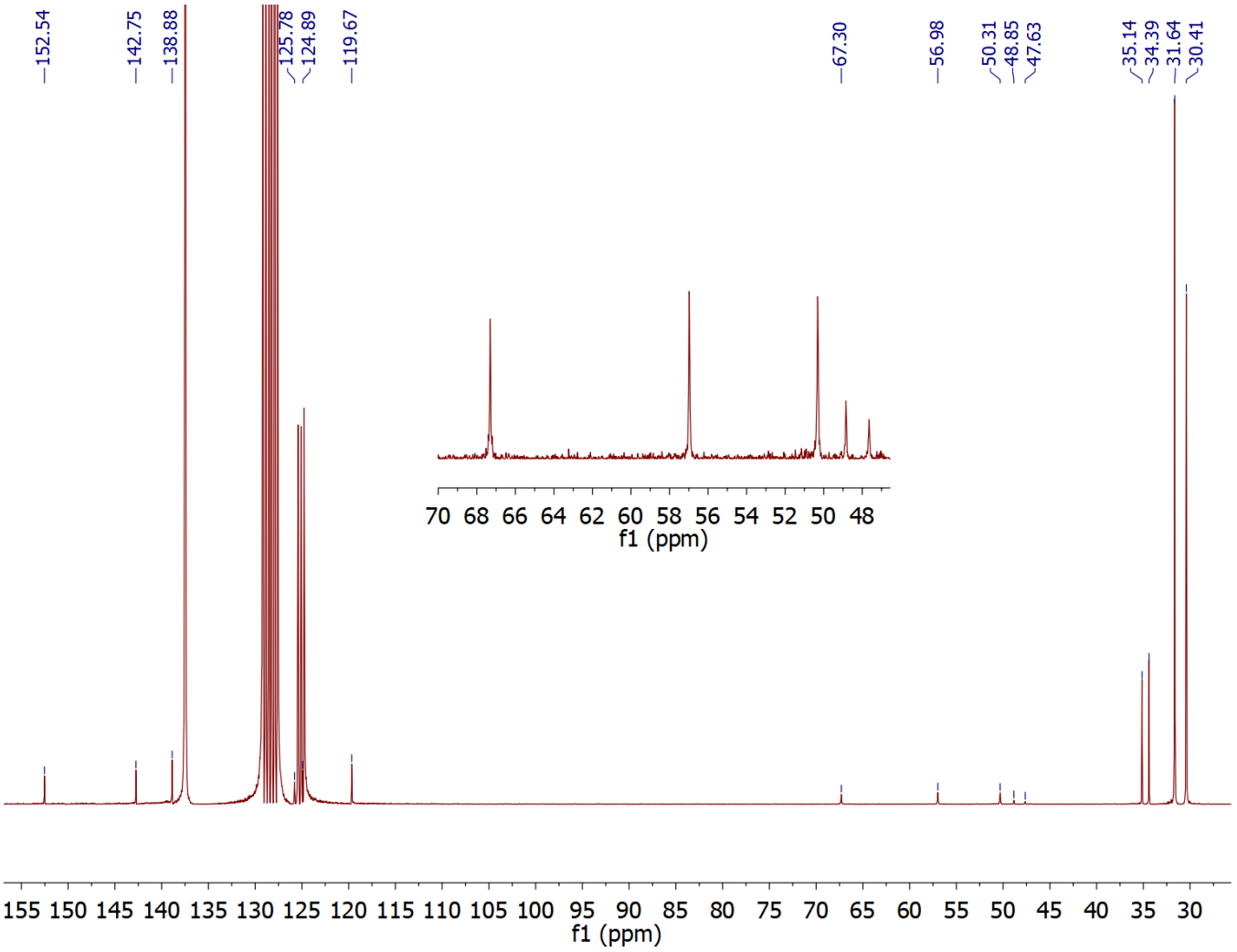

Figure A.10. $^{13}C\{^{1}H\}$ NMR spectrum of **3.3** in toluene-d_8, 298 K

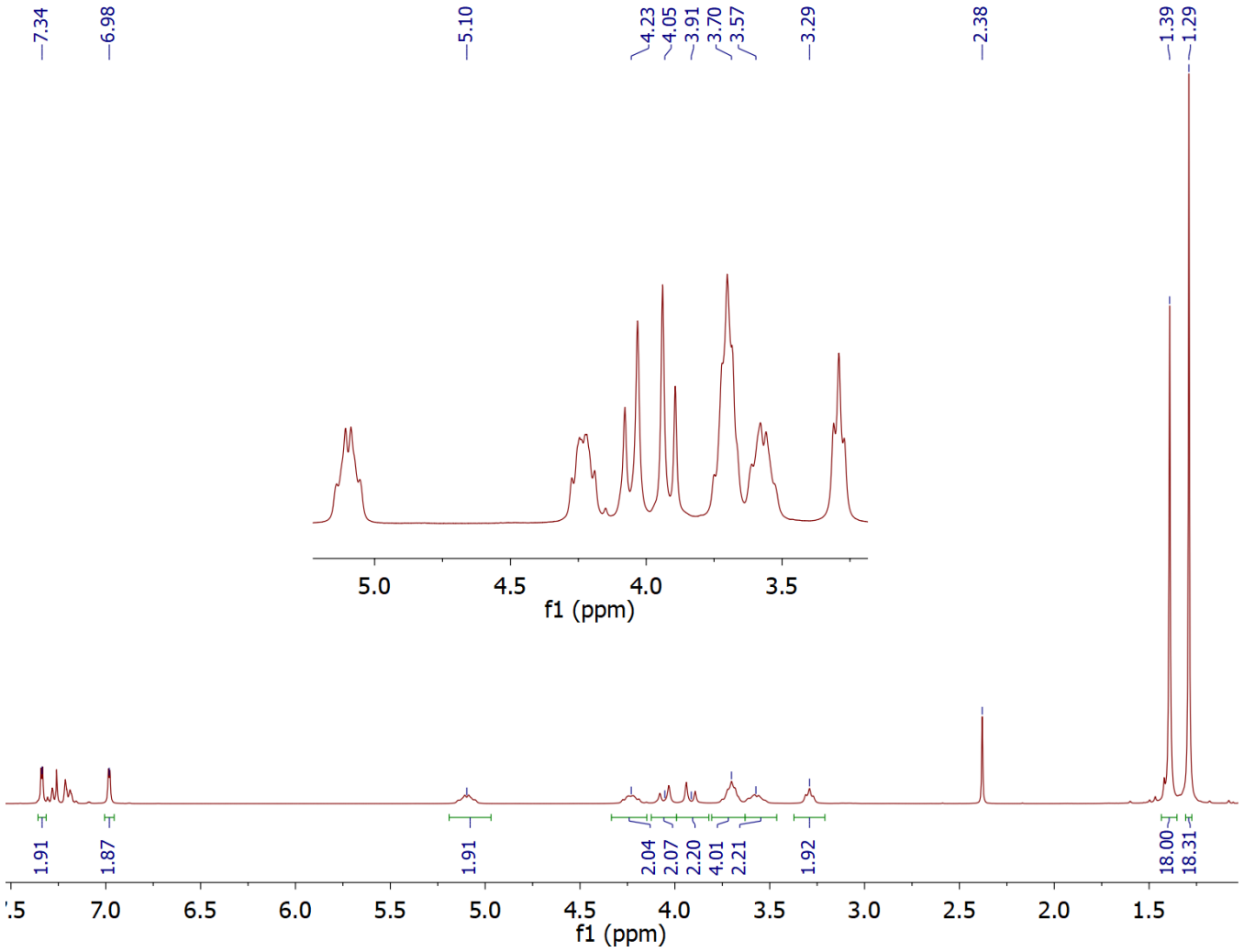

Figure A.11. ^{1}H NMR spectrum of **3.4** in $CDCl_3$, 298 K (residual toluene resonance at 2.38 ppm)

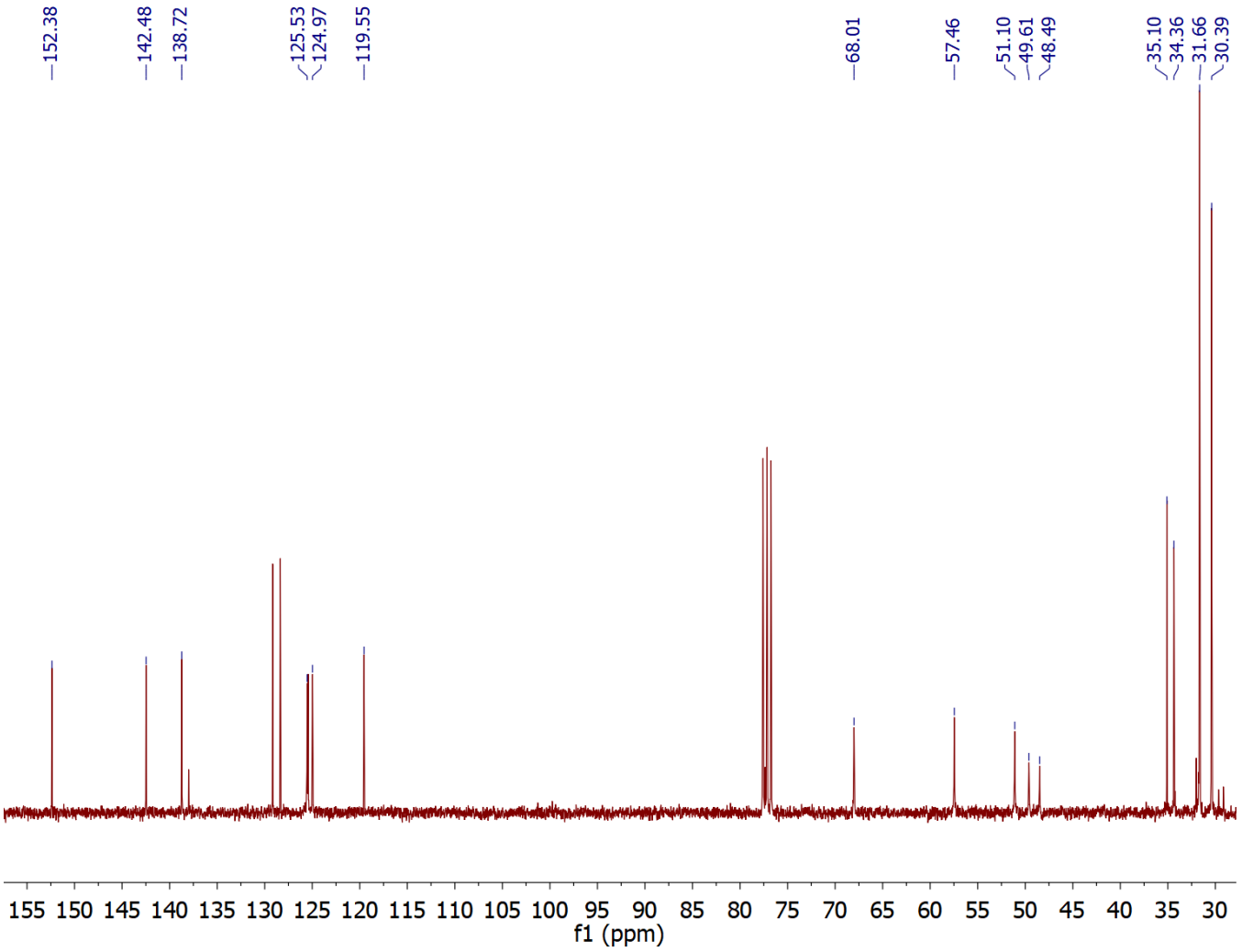

Figure A.12. $^{13}C\{^{1}H\}$ NMR spectrum of **3.4** in $CDCl_3$, 298 K

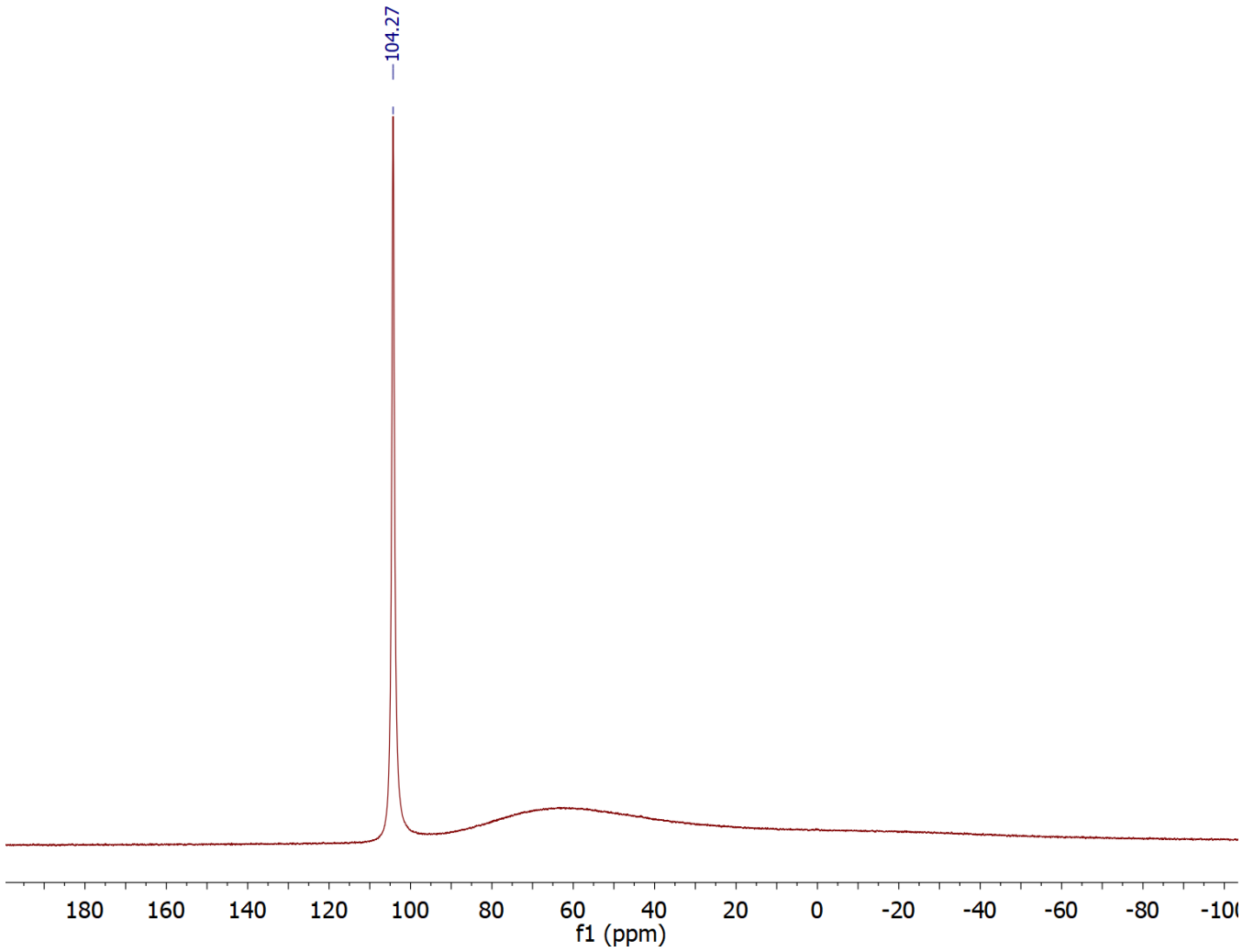

Figure A.13. ^{27}Al NMR spectrum of **3.4** in $CDCl_3$, 298 K (the broad signal at 60 ppm corresponds to the probe background)

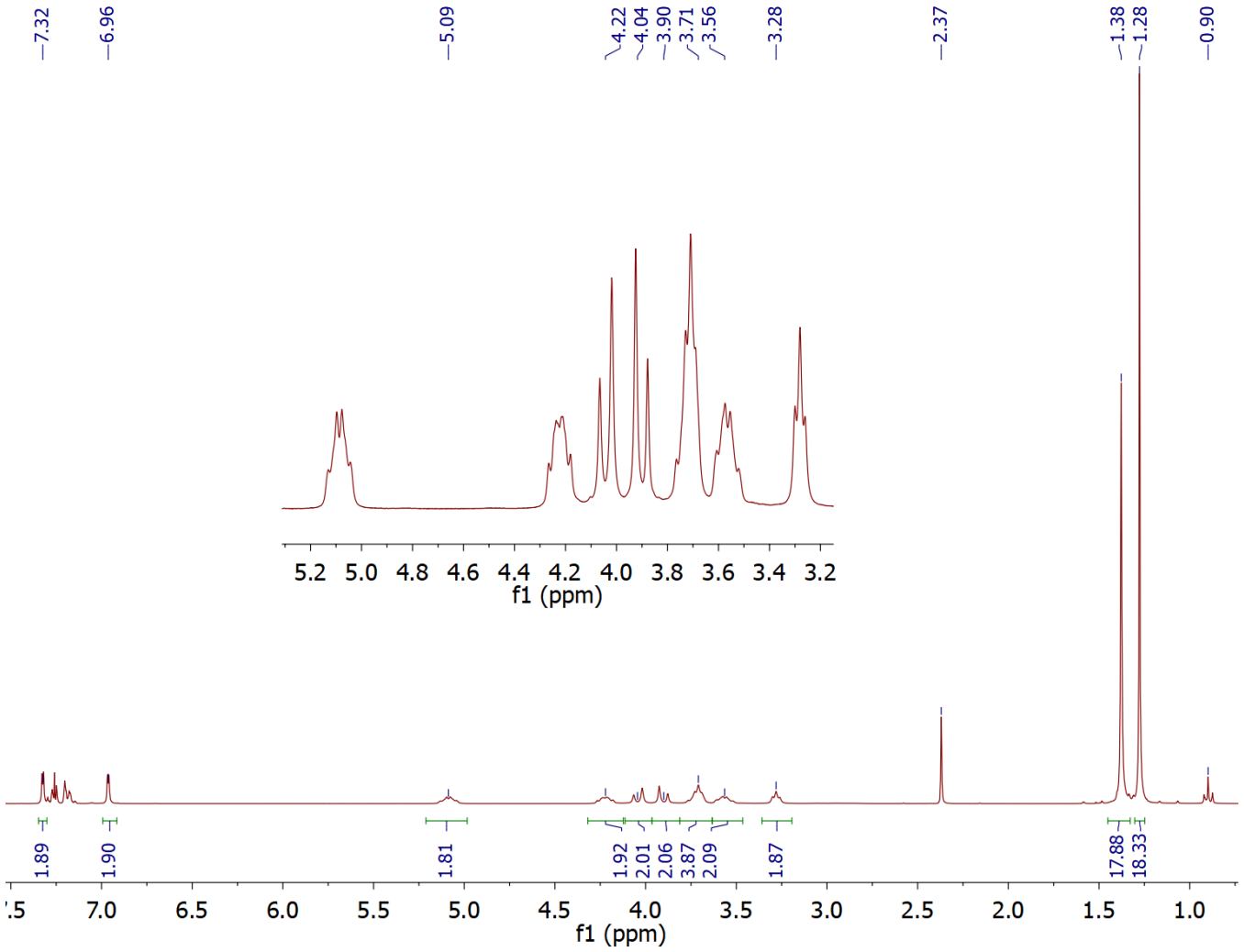

Figure A.14. ^{1}H NMR spectrum of **3.5** in $CDCl_3$, 298 K (residual toluene/heptane resonances at 2.37/0.90 ppm)

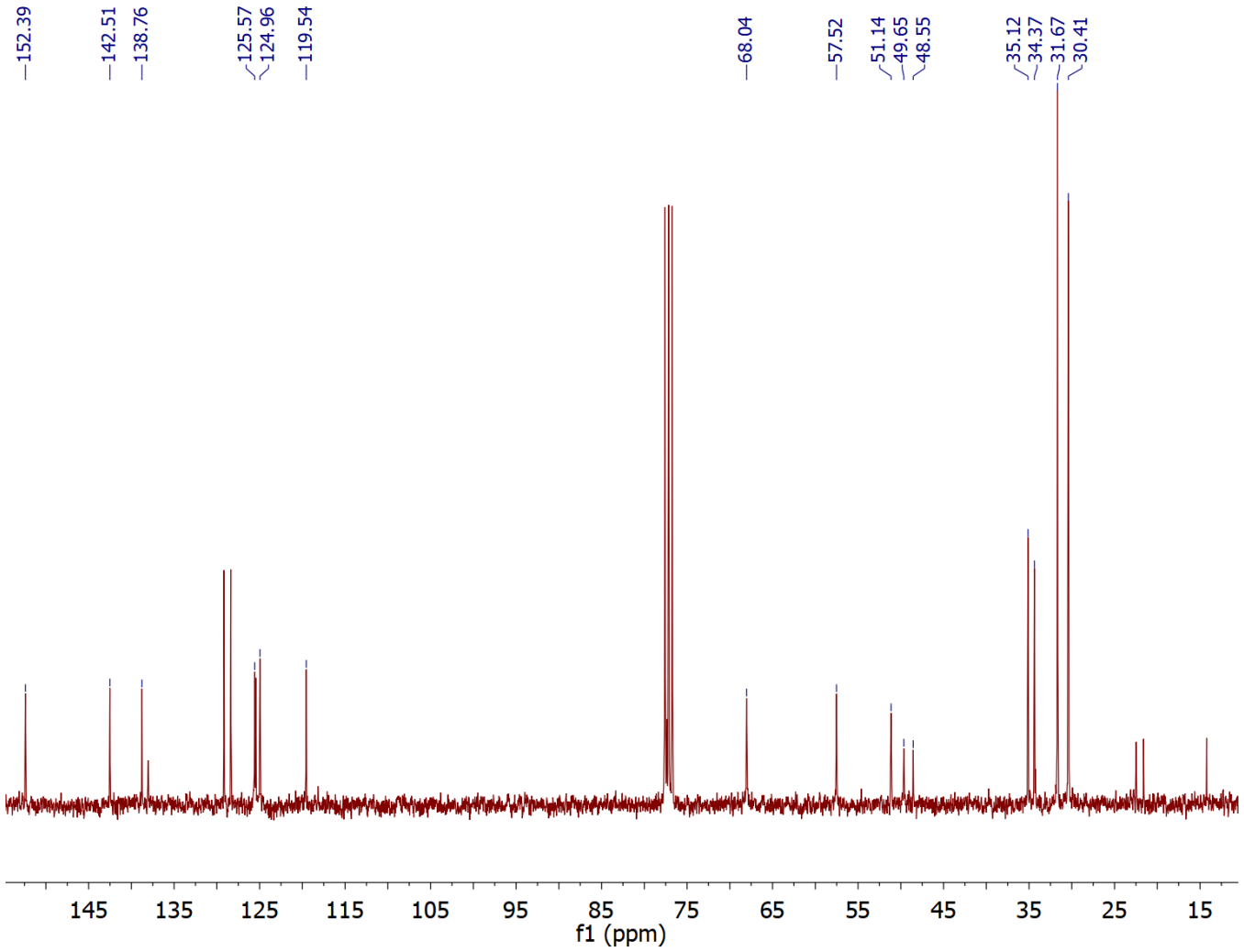

Figure A.15. $^{13}C\{^{1}H\}$ NMR spectrum of **3.5** in $CDCl_3$, 298 K

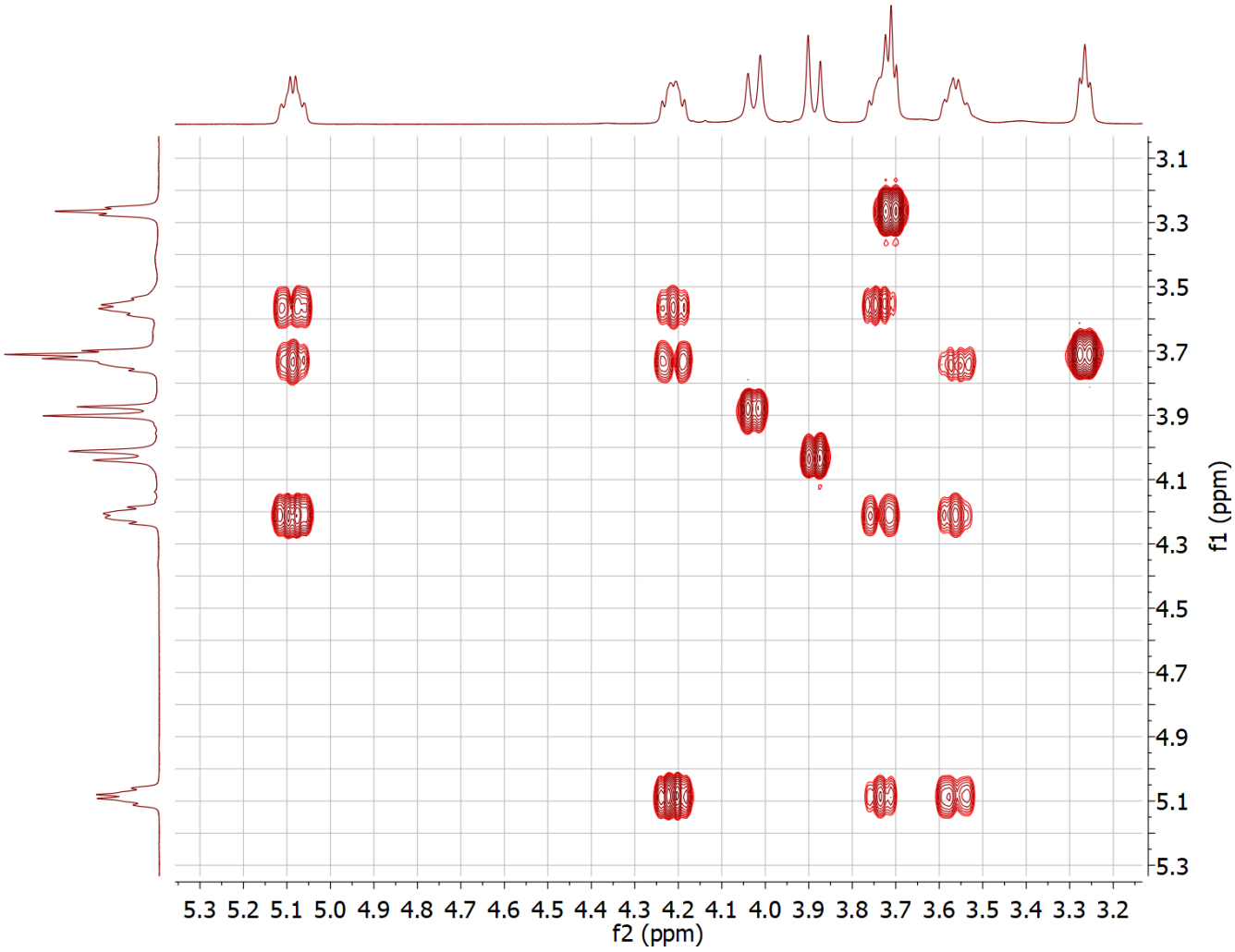

Figure A.16. COSY spectrum of **3.5** in $CDCl_3$, 298 K

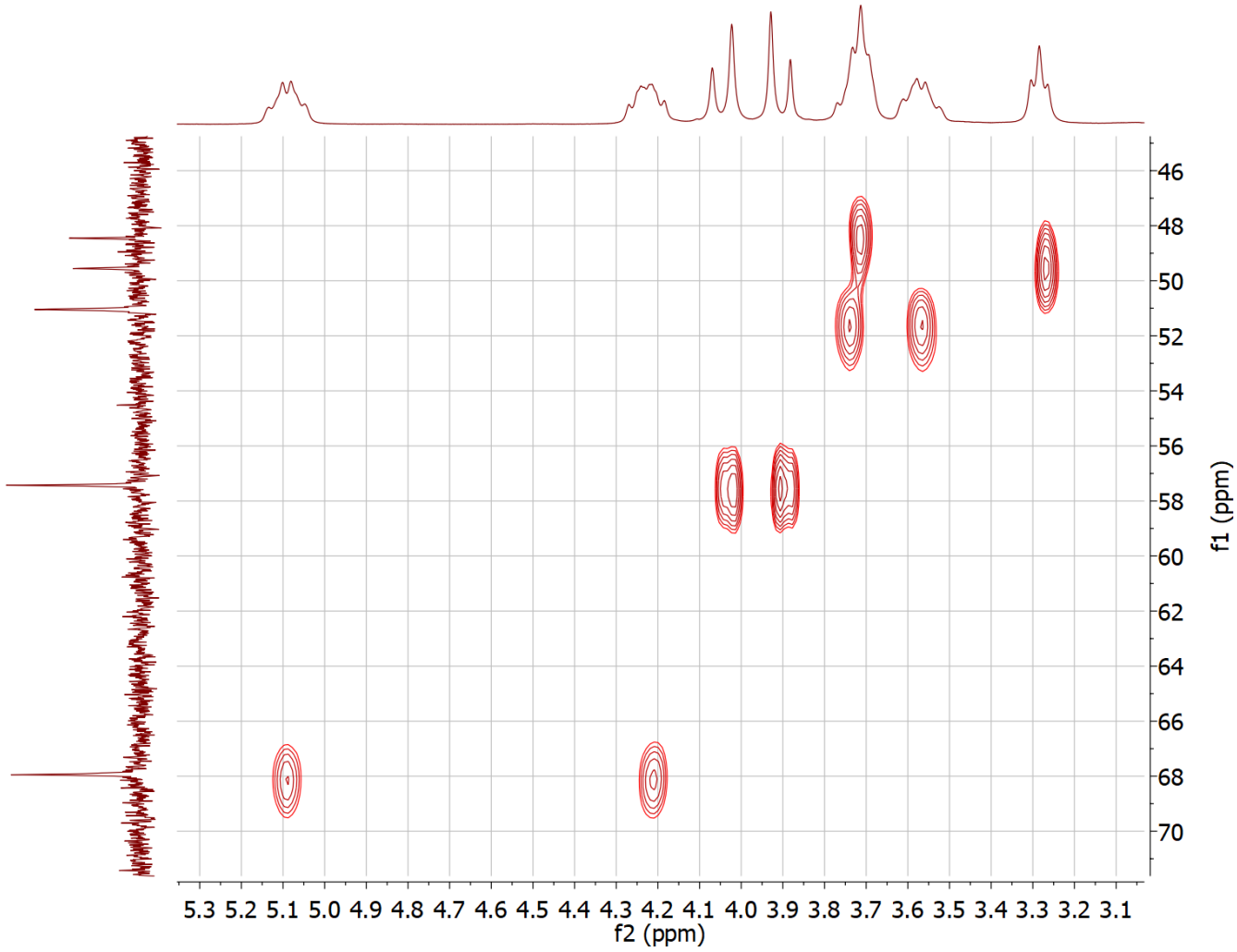

Figure A.17. HSQC spectrum of **3.5** in $CDCl_3$, 298 K

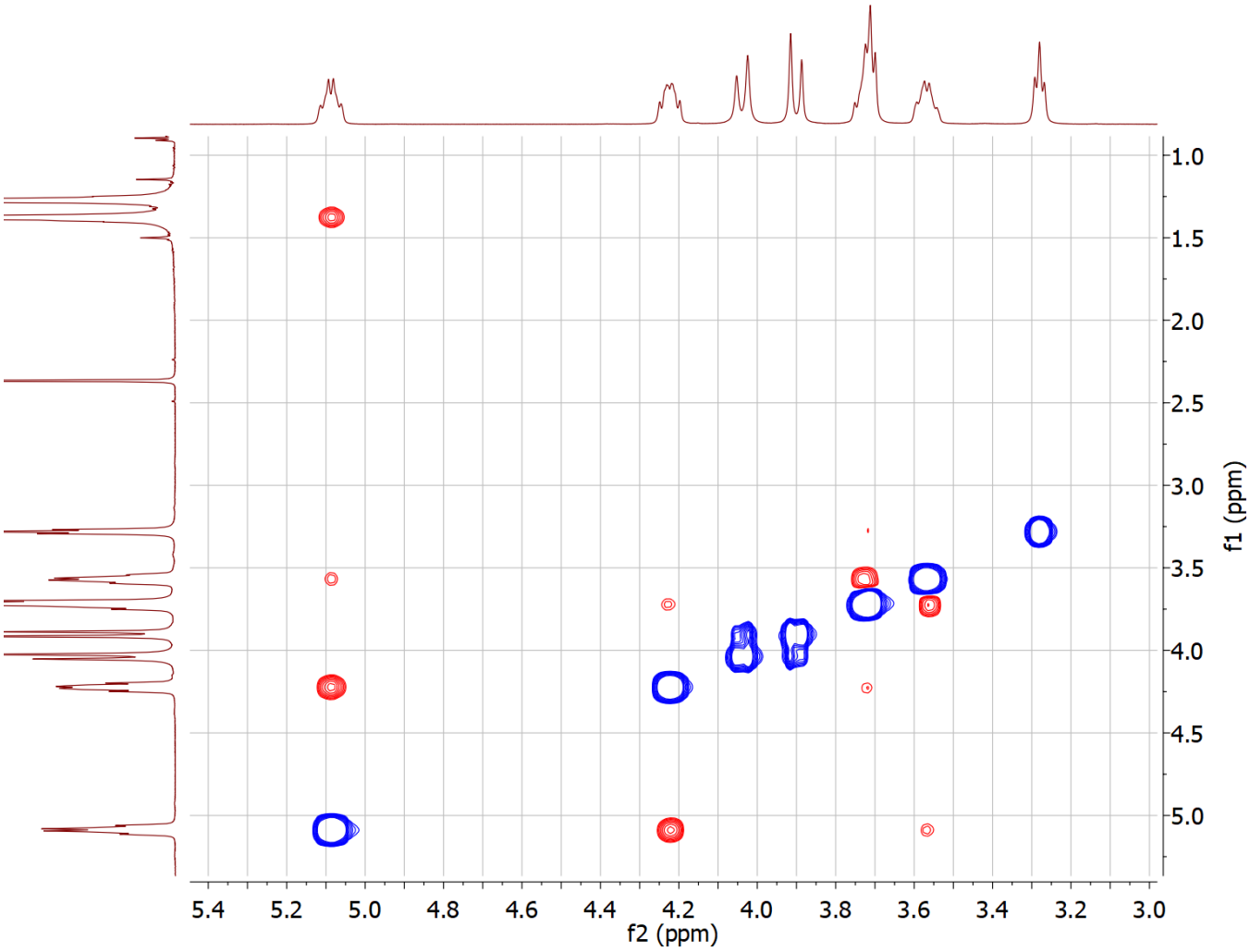

Figure A.18. NOESY spectrum of **3.5** in $CDCl_3$, 298 K

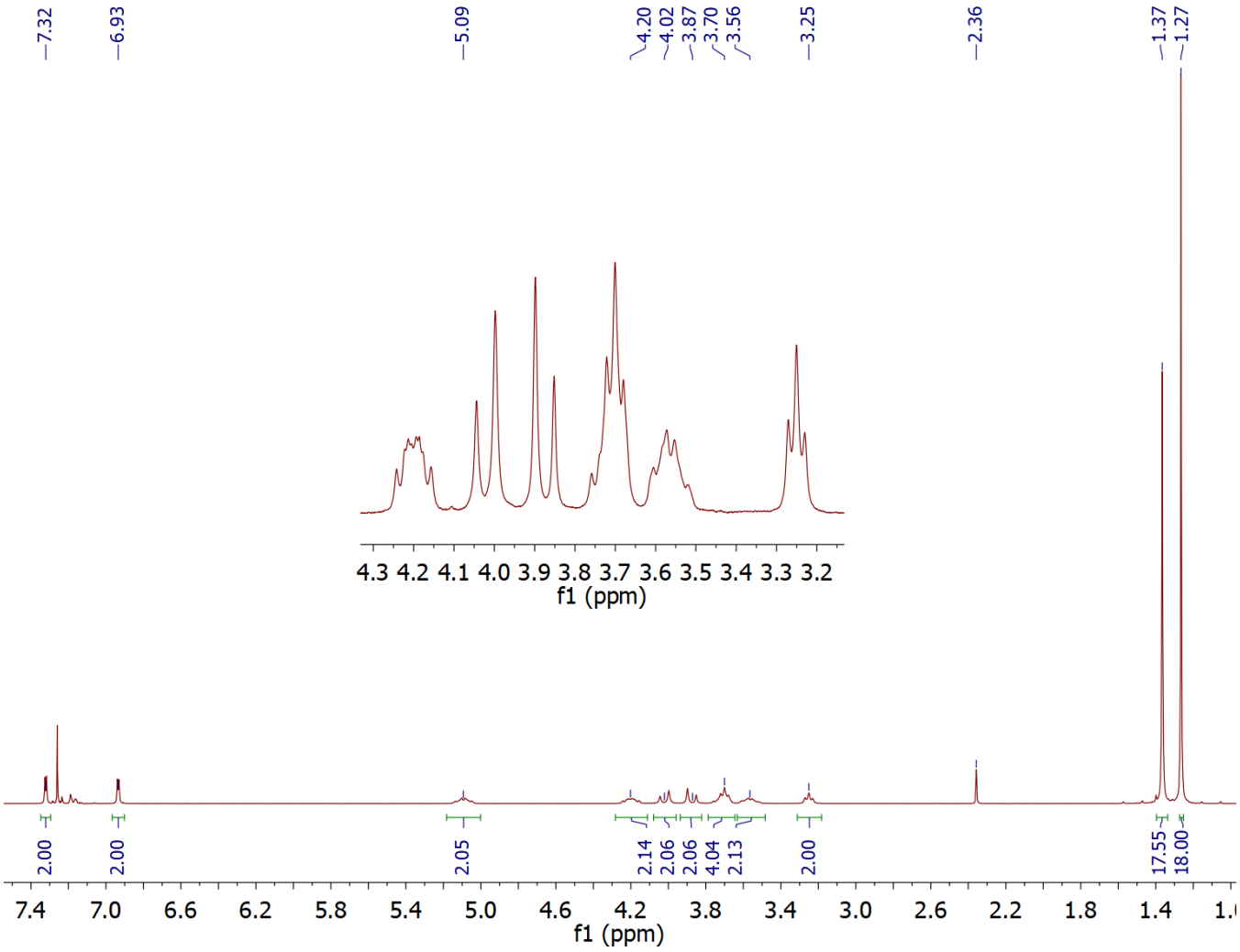

Figure A.19. ^{1}H NMR spectrum of **3.6** in $CDCl_3$, 298 K (residual toluene resonance at 2.36 ppm)

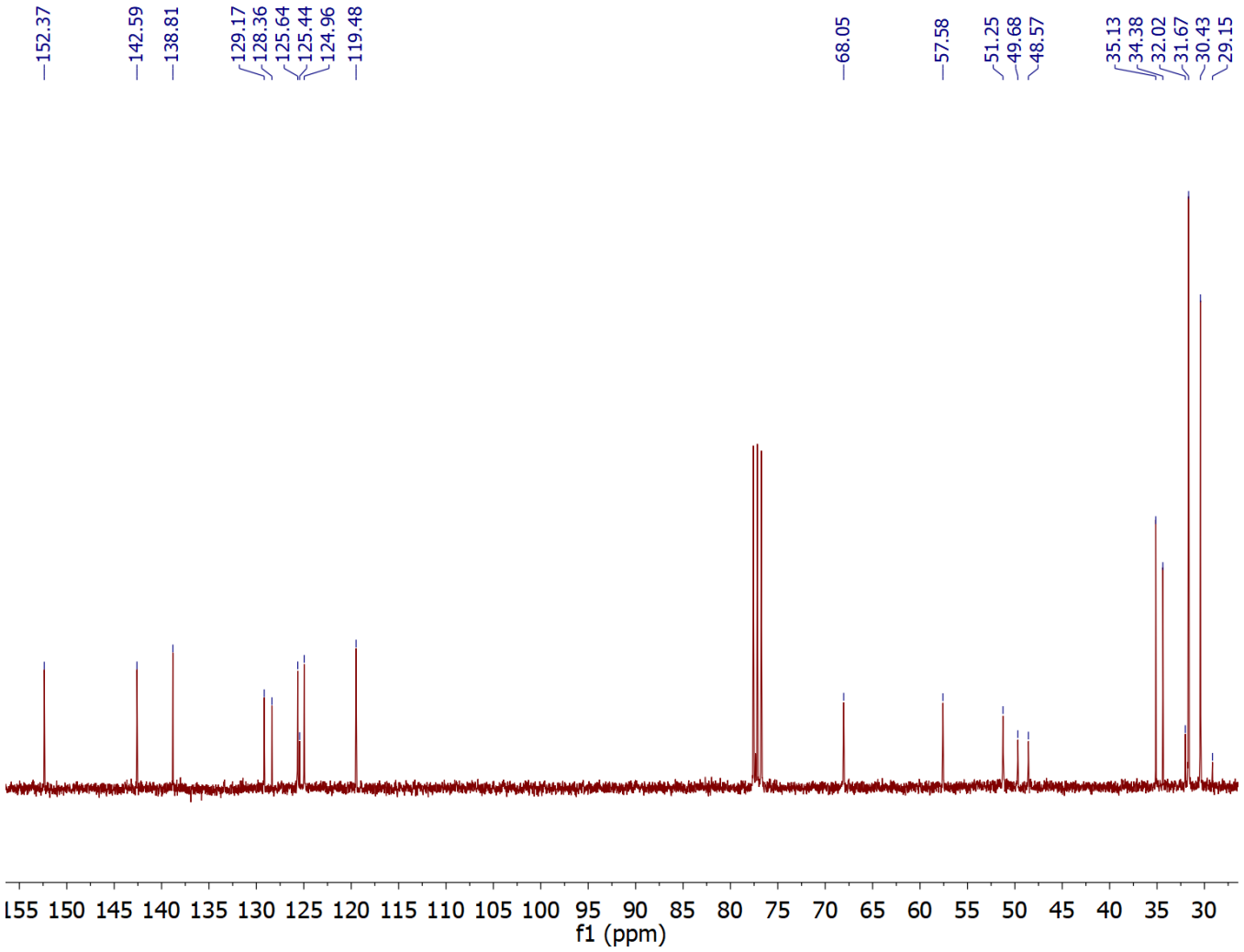

Figure A.20. $^{13}C\{^{1}H\}$ NMR spectrum of **3.6** in $CDCl_3$, 298 K

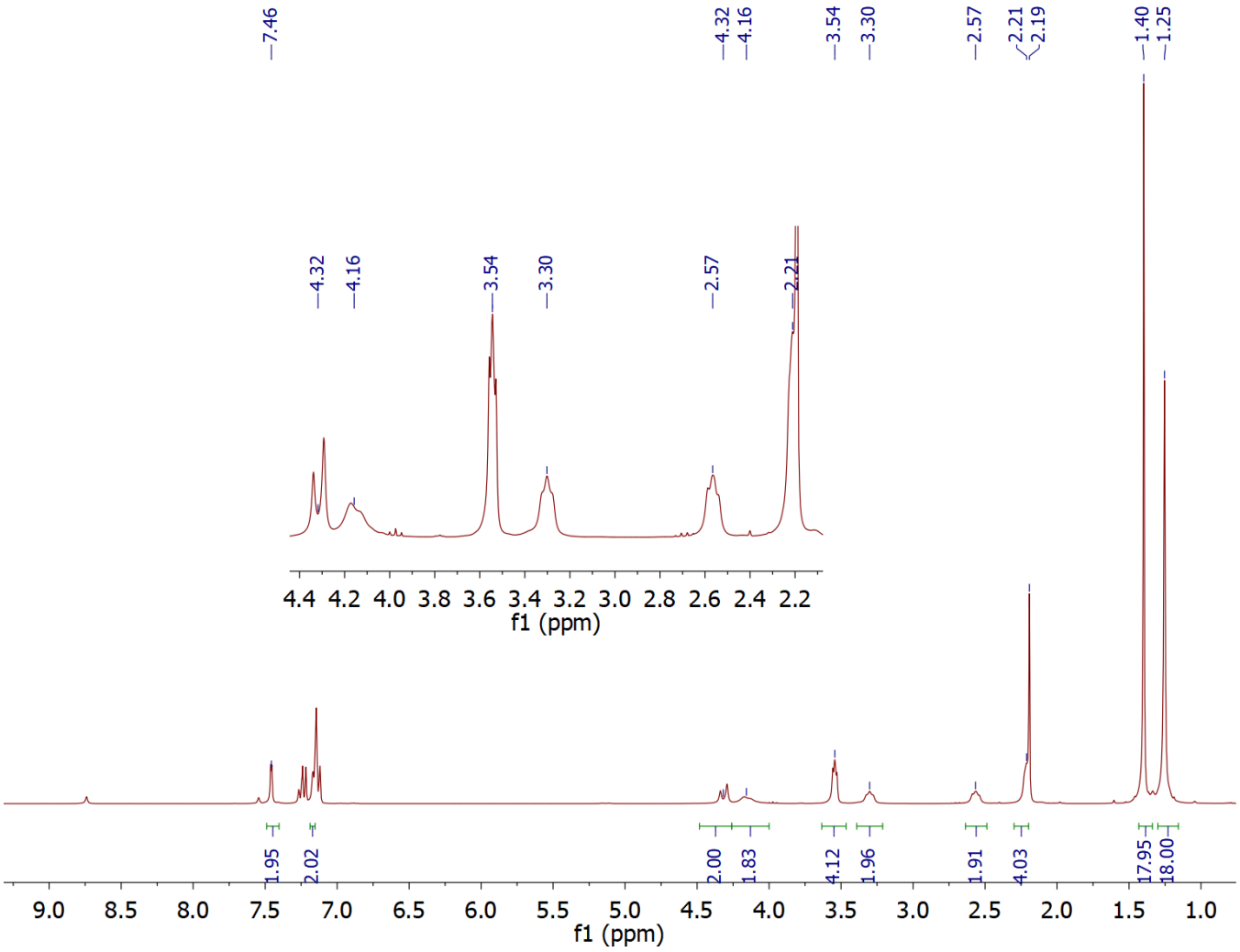

Figure A.21. ^{1}H NMR spectrum of **3.7** in pyridine-d_5, 298 K (residual toluene resonance at 2.19 ppm)

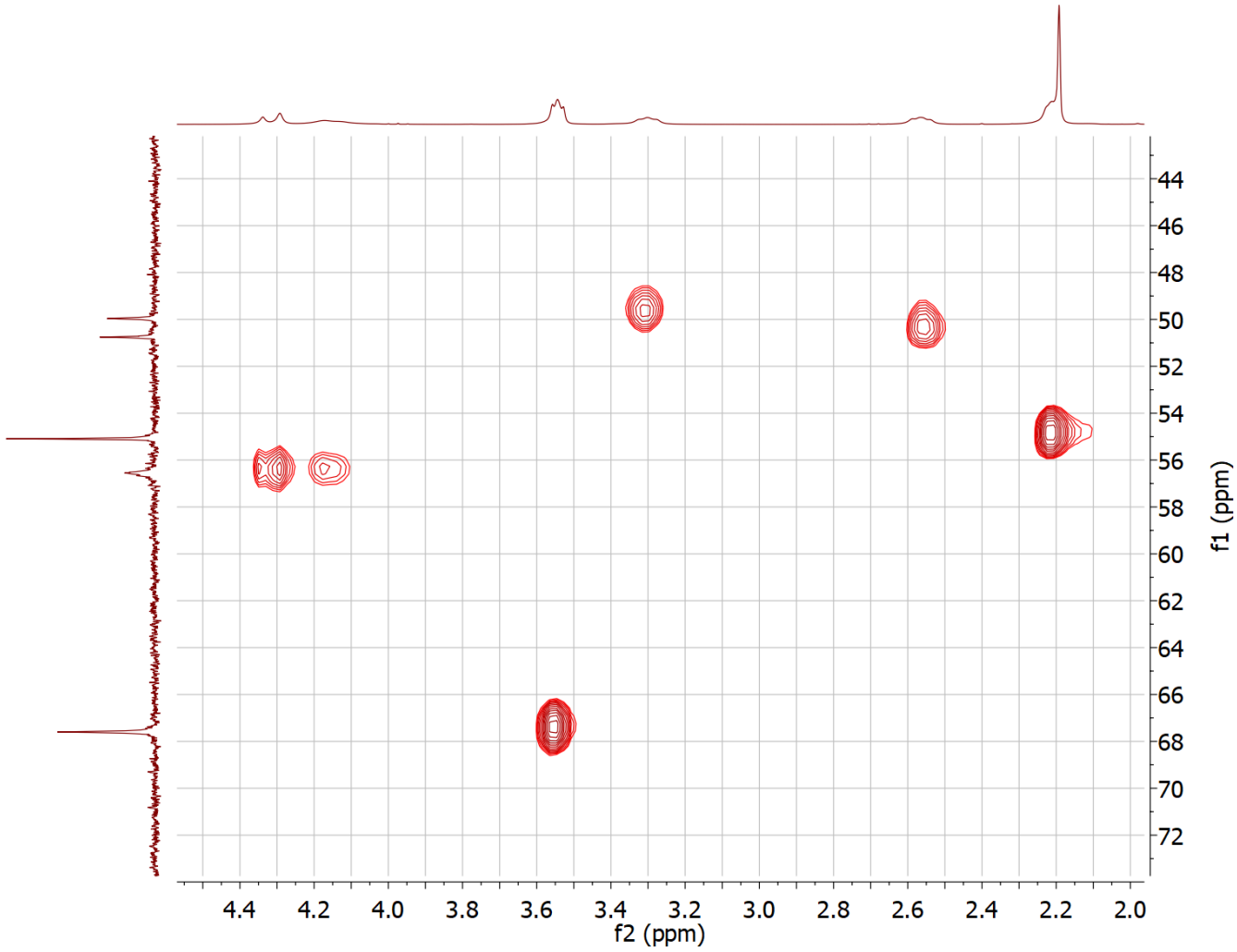

Figure A.22. HSQC spectrum of **3.7** in pyridine-d_5, 298 K

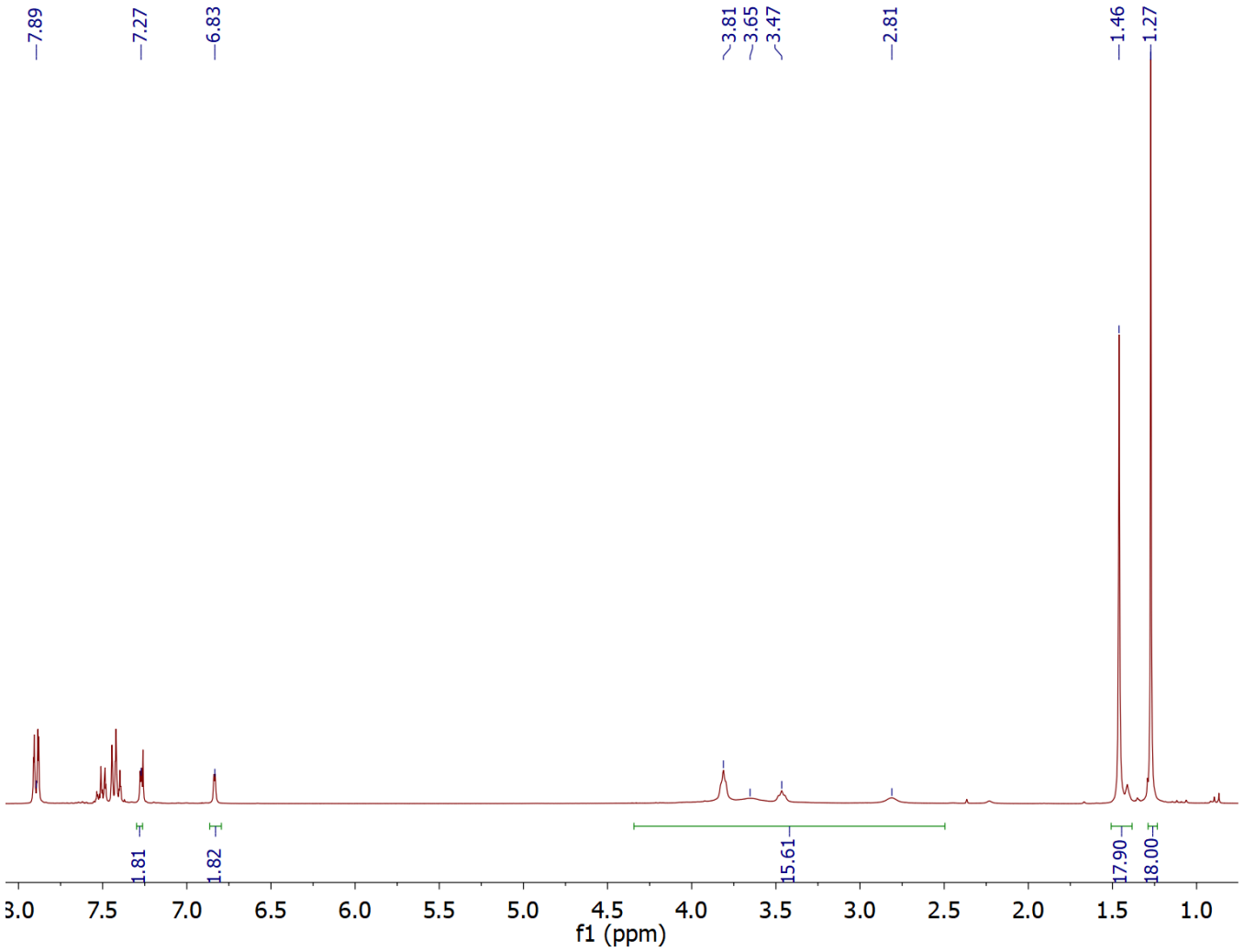

Figure A.23. ^{1}H NMR spectrum of **3.1** + BPh_3 in $CDCl_3$, 298 K

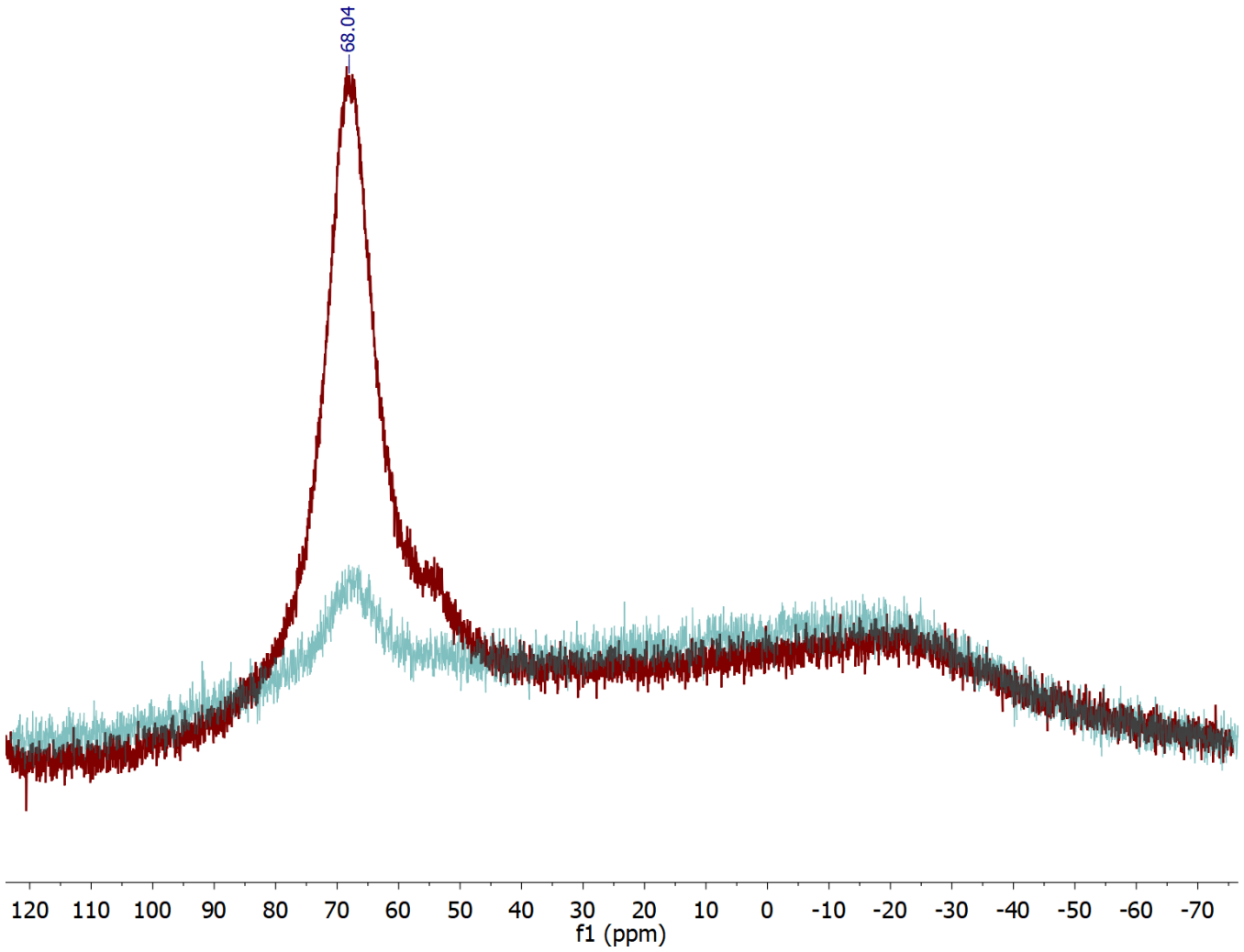

Figure A.24. Overlapped ^{11}B NMR spectra of (a) BPh_3 and (b) **3.1** + BPh_3 in $CDCl_3$, 298 K

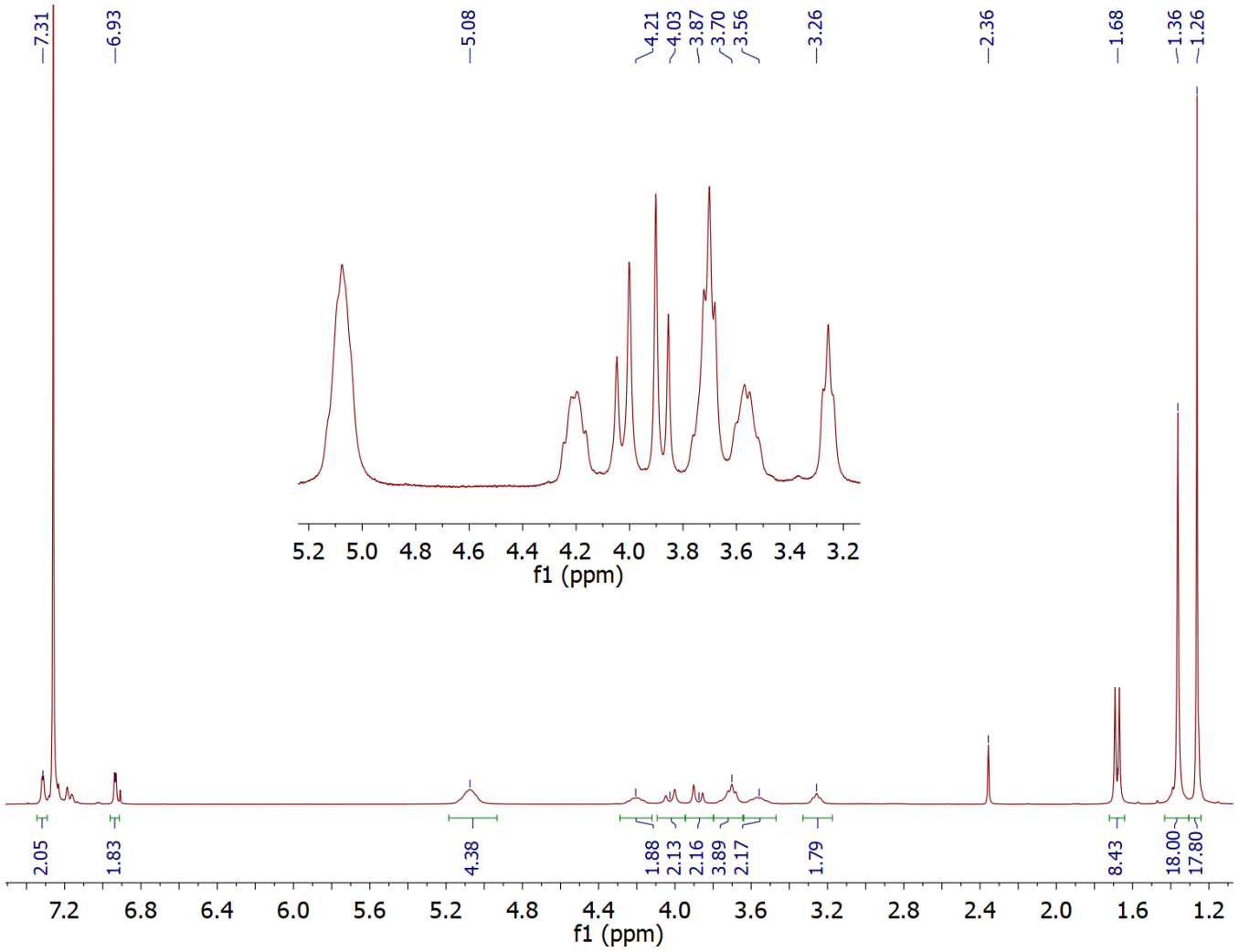

Figure A.25. ^{1}H NMR spectrum of **3.5** + lactide in $CDCl_3$, 298 K (residual toluene resonance at 2.36 ppm)

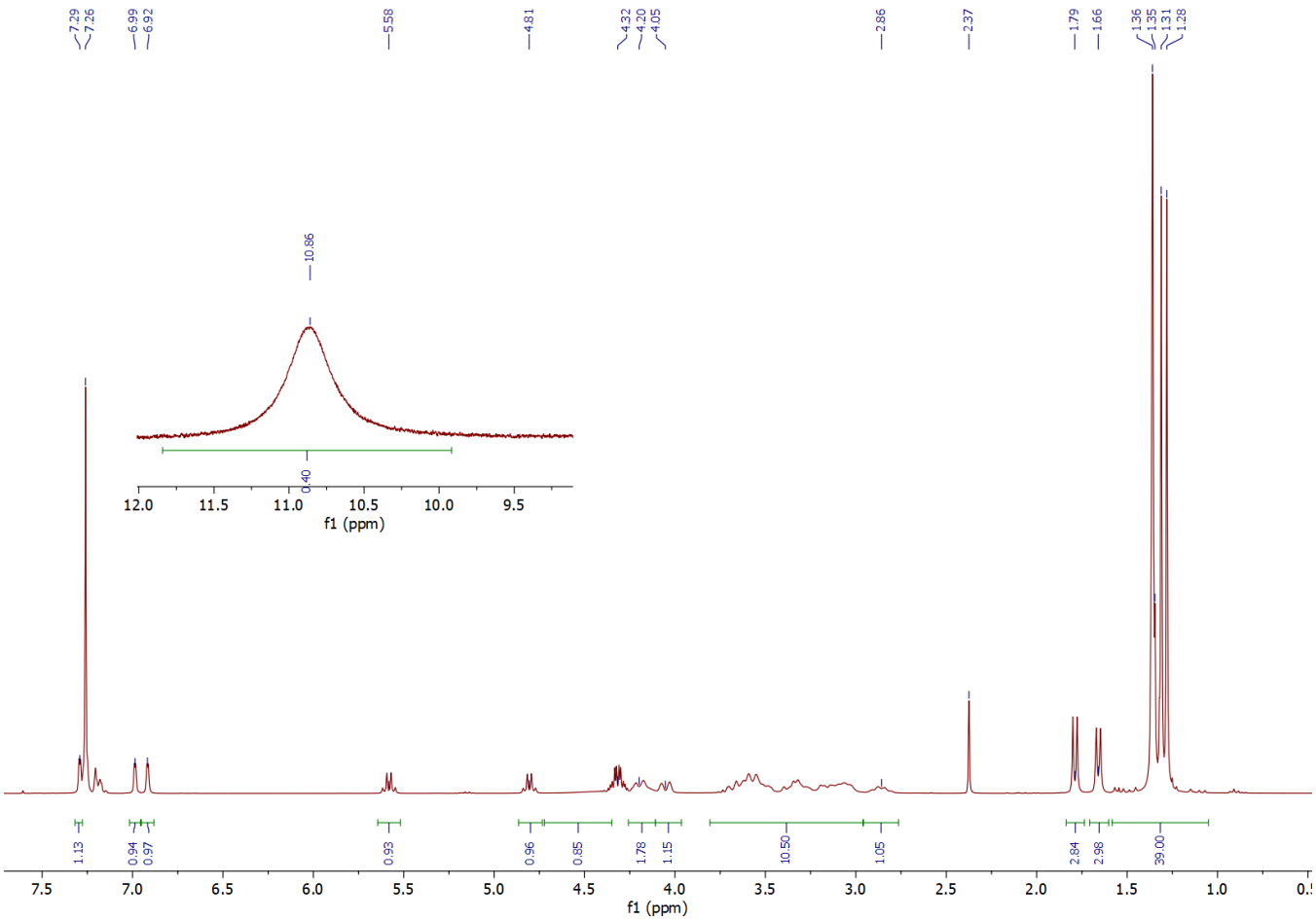

Figure A.26. ^{1}H NMR spectrum of **3.5** + lactide + EtOH in $CDCl_3$, 298 K (residual toluene resonance at 2.37 ppm)

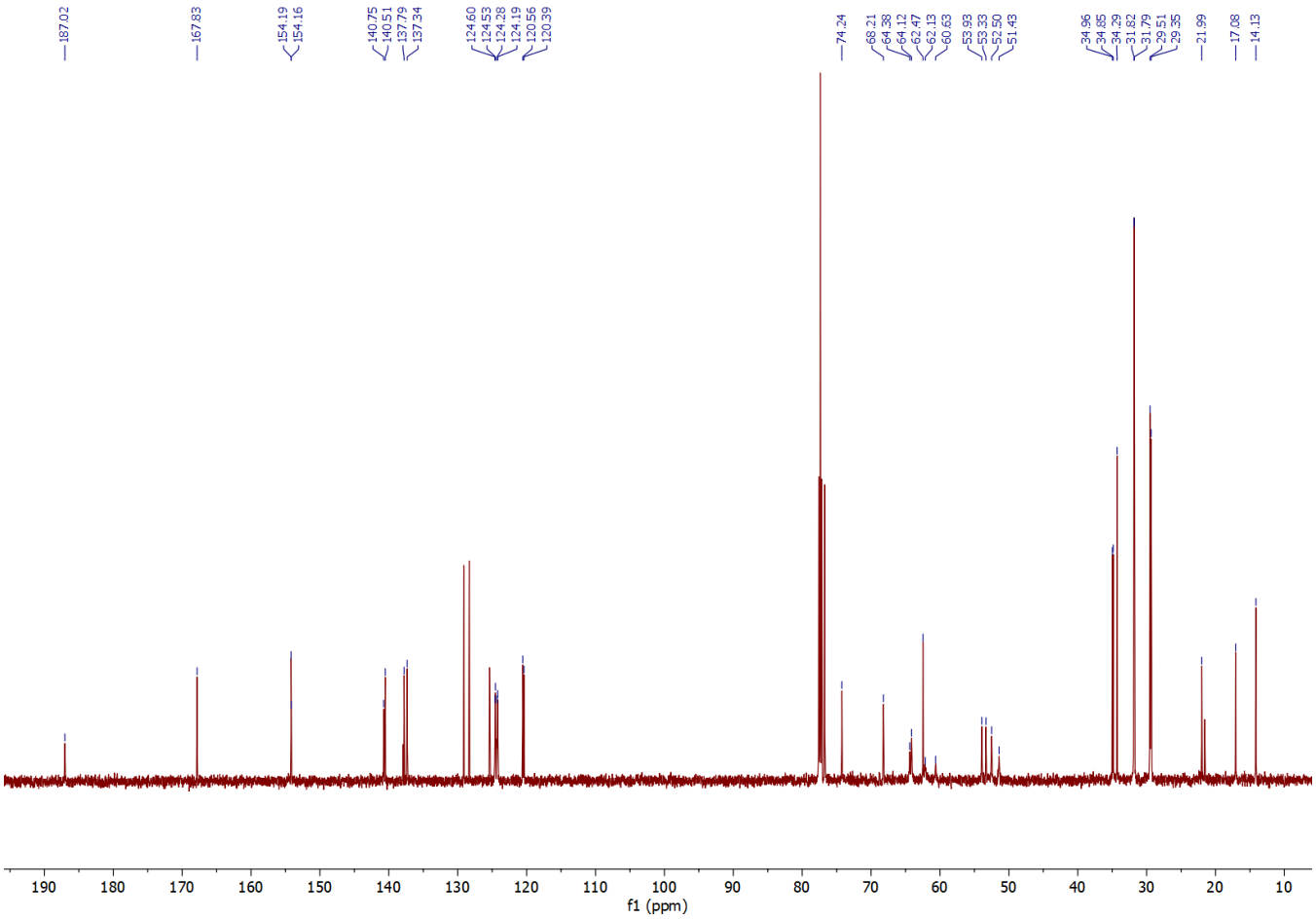

Figure A.27. $^{13}C\{^{1}H\}$ NMR spectrum of **3.5** + lactide + EtOH in $CDCl_3$, 298 K

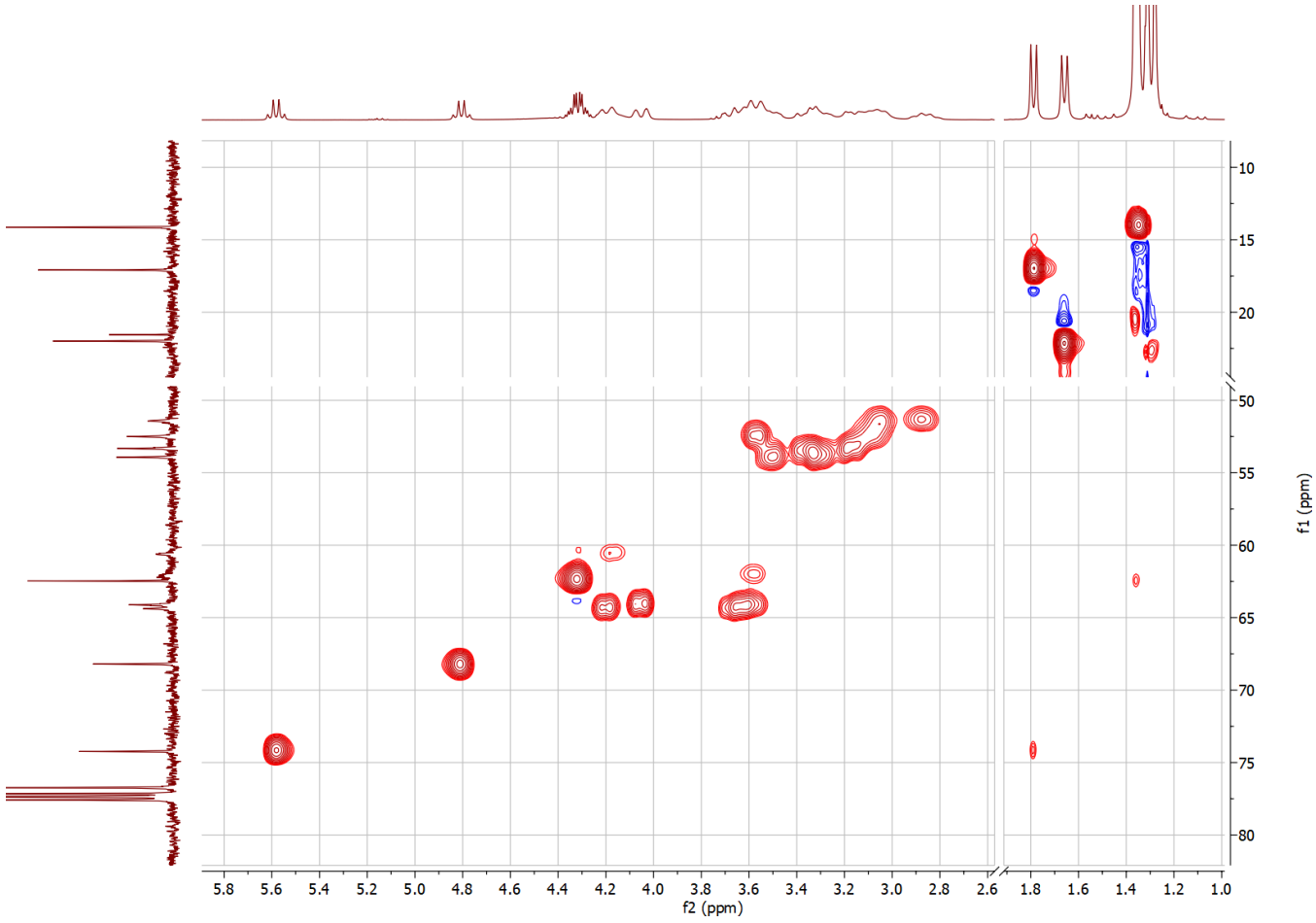

Figure A.28. HSQC spectrum of **3.5** + lactide + EtOH in $CDCl_3$, 298 K

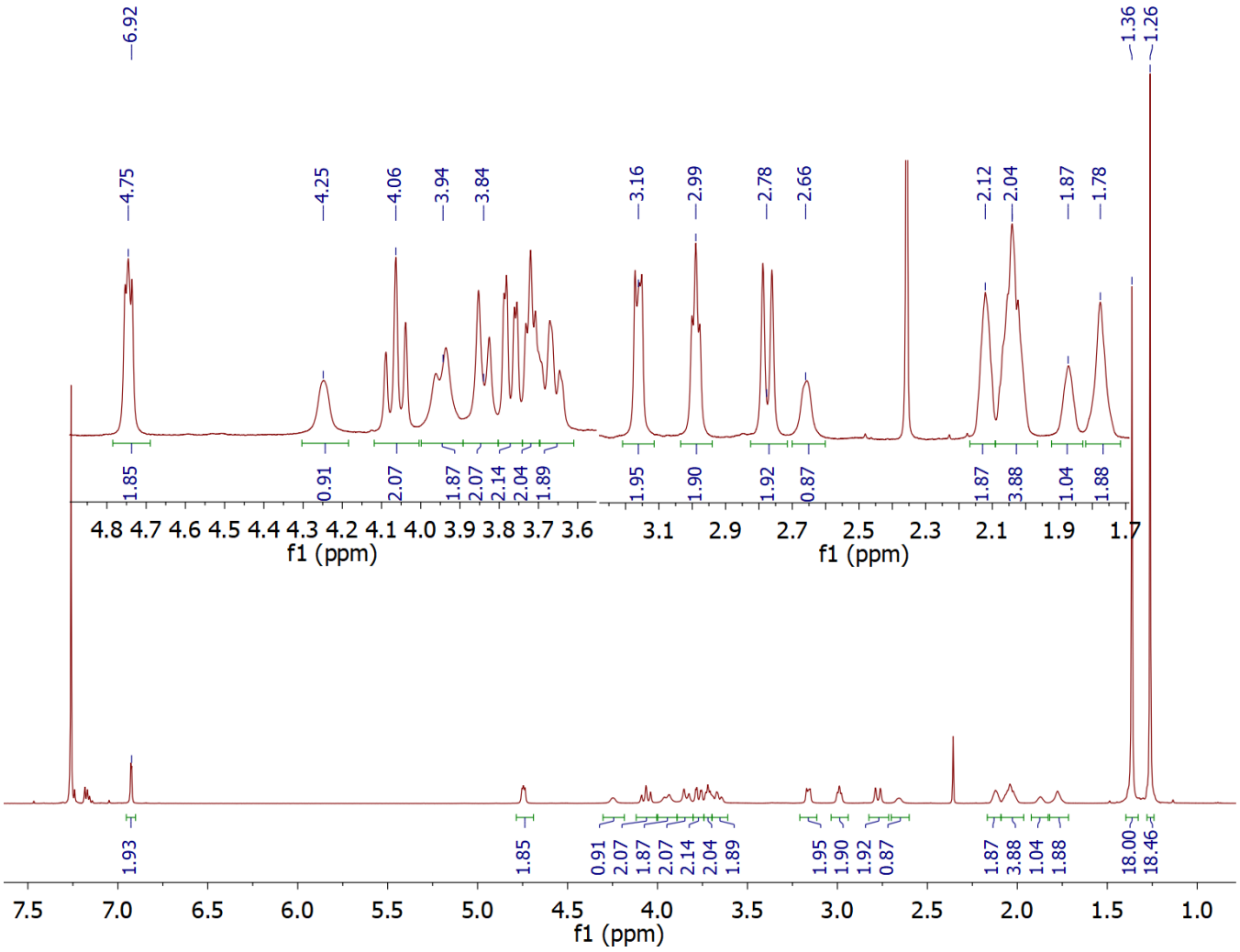

Figure A.29. ^{1}H NMR spectrum of **3.5** + ε-CL in $CDCl_3$, 298 K

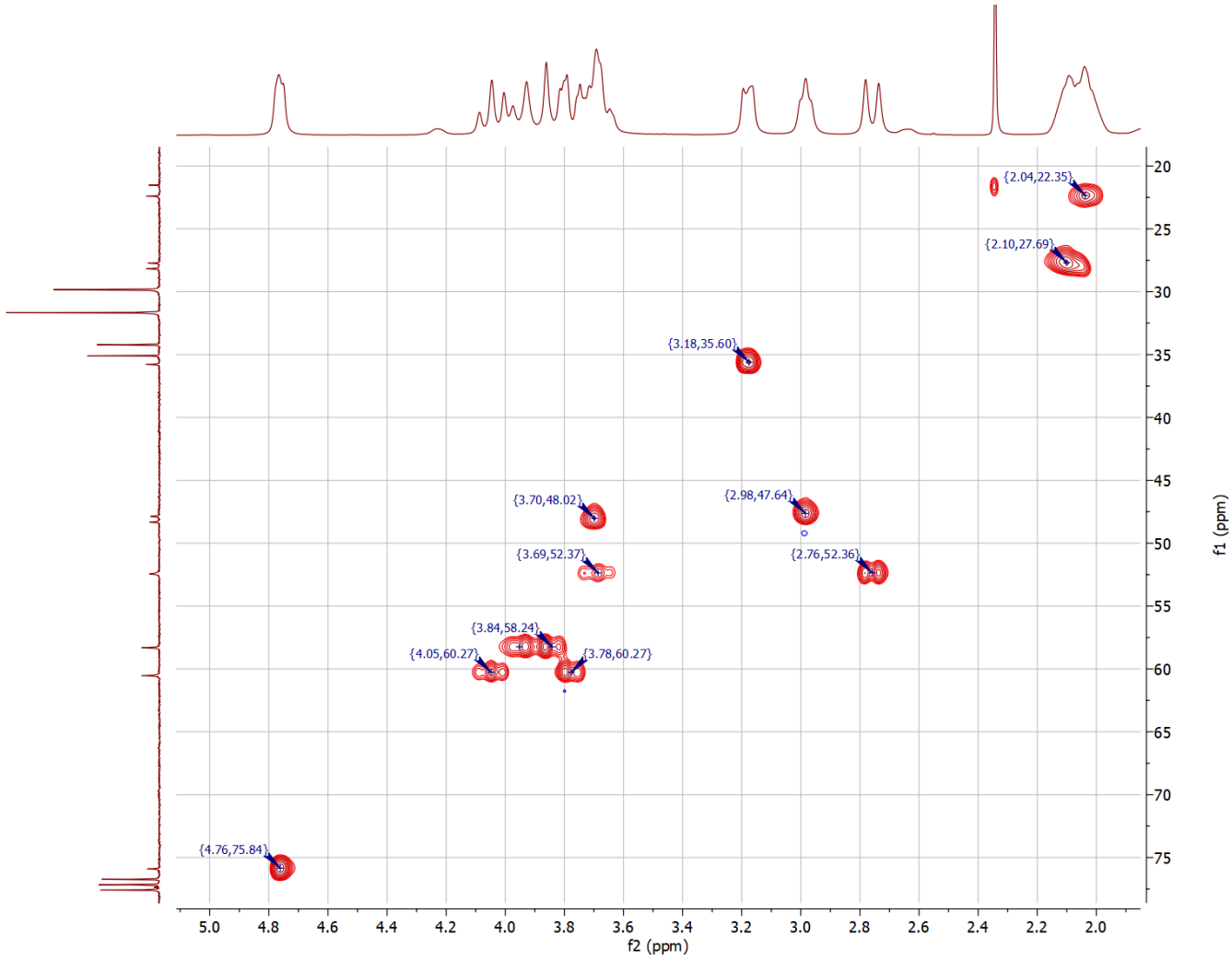

Figure A.30. HSQC spectrum of **3.5** + ε-CL in $CDCl_3$, 298 K

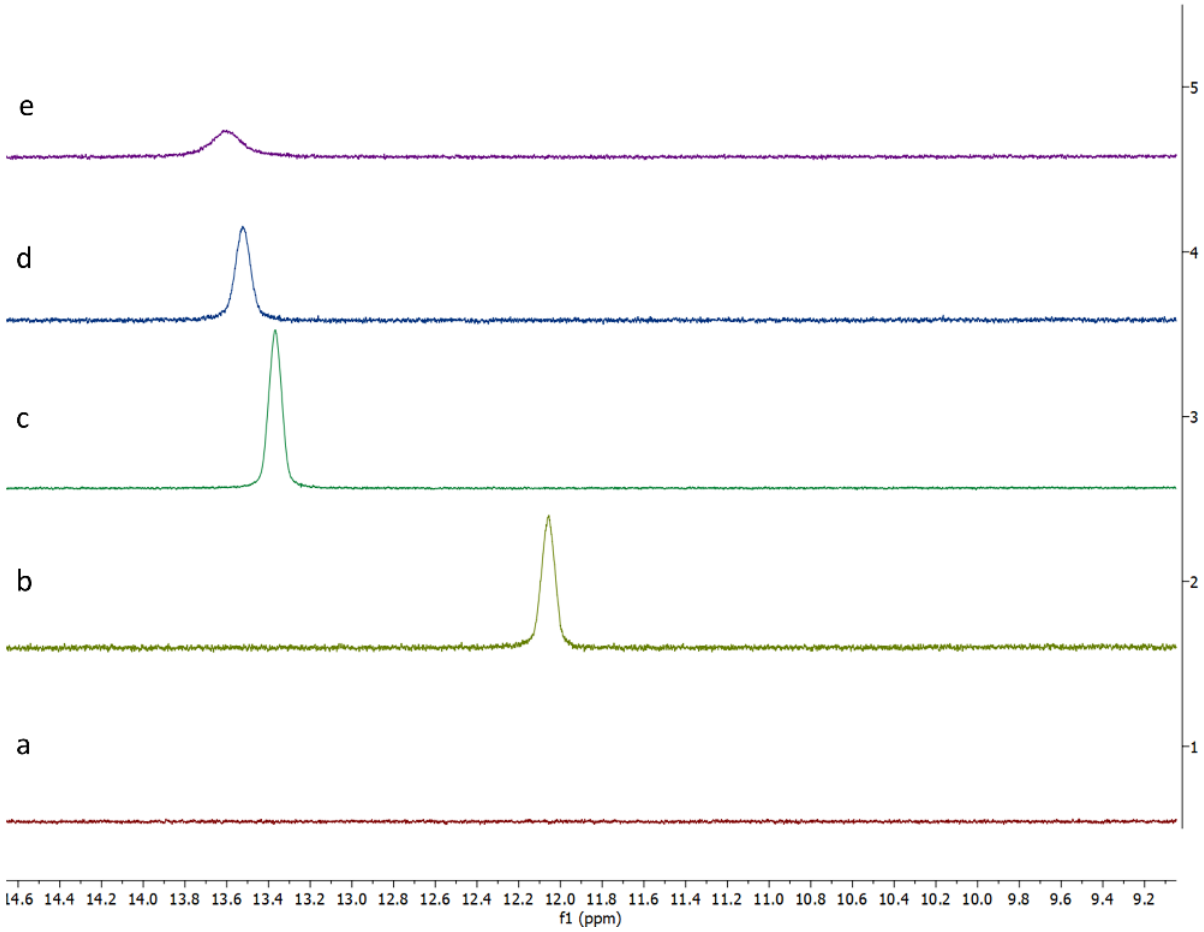

Figure A.31. Expanded ^{1}H NMR spectra of **3.5** ($CDCl_3$, 298 K) after addition of (a) 0 equiv, (b) 1 equiv, (c) 2 equiv, (d) 5 equiv, and (e) 10 equiv EtOH.

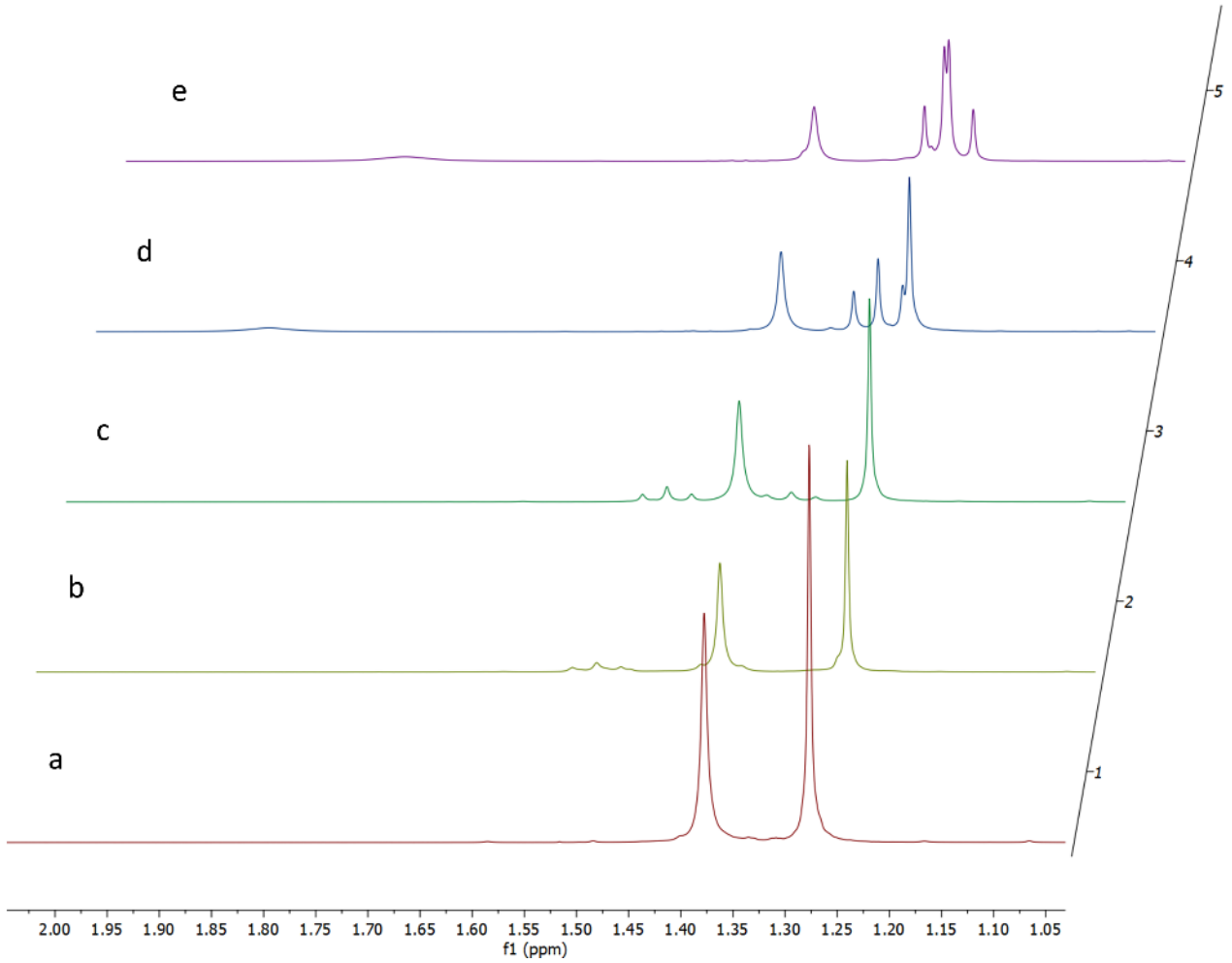

Figure A.32. Expanded ^{1}H NMR spectra of **3.5** ($CDCl_3$, 298K) after addition of (a) 0 equiv, (b) 1 equiv, (c) 2 equiv, (d) 5 equiv, and (e) 10 equiv EtOH.

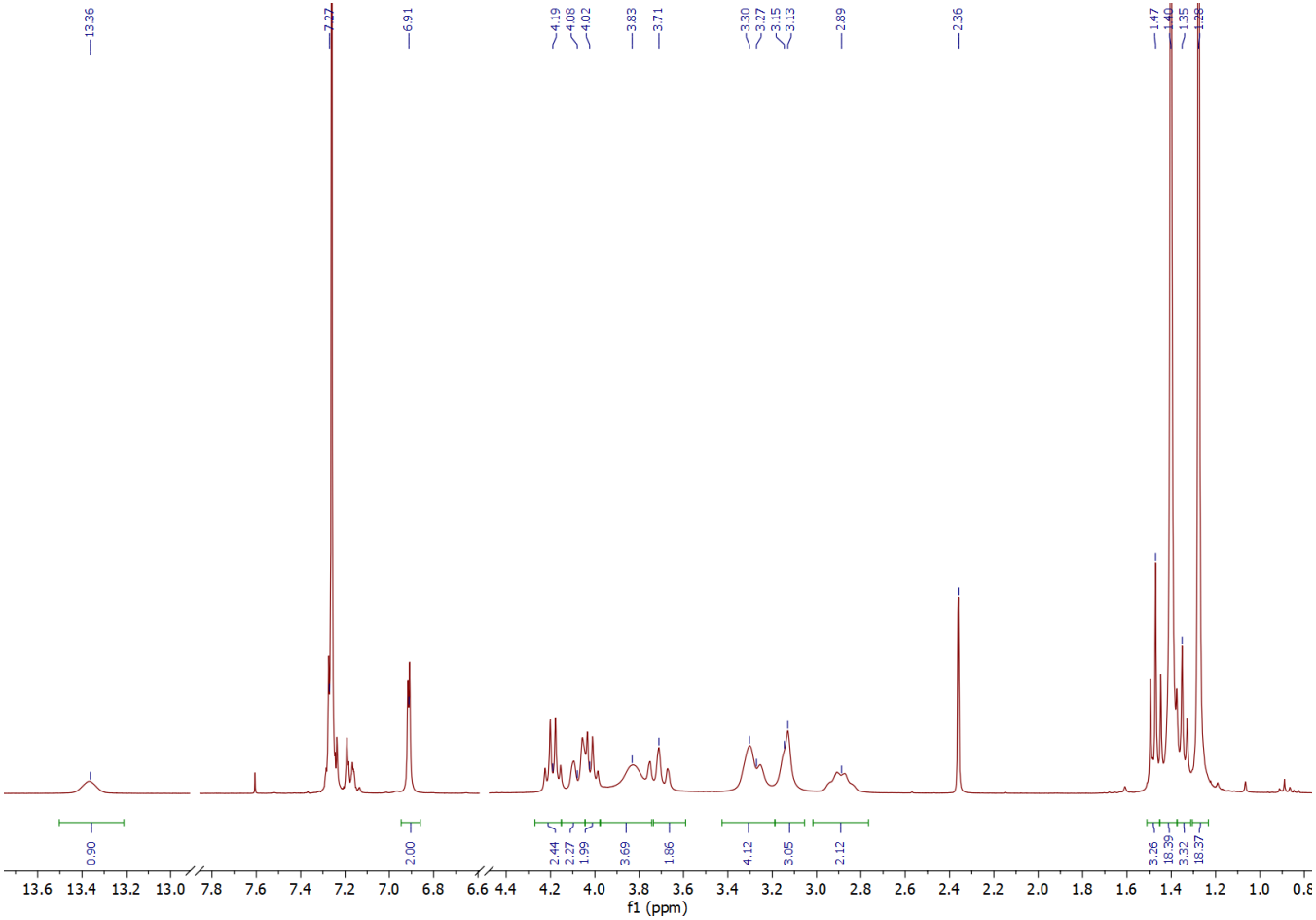

Figure A.33. ^{1}H NMR spectrum of **3.5** + 2 equiv EtOH ($CDCl_3$, 298 K)

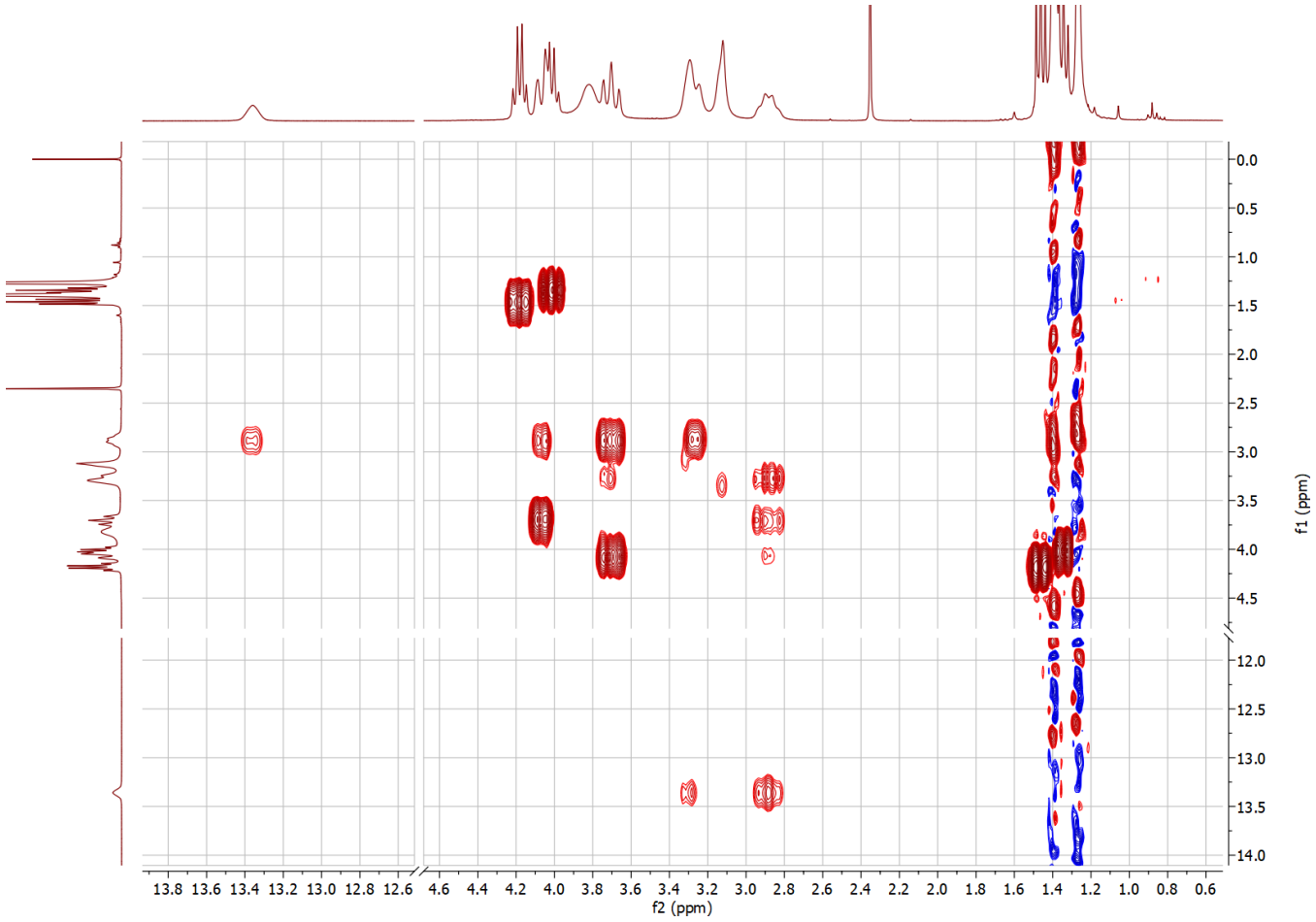

Figure A.34. COSY spectrum of **3.5** + 2 equiv EtOH ($CDCl_3$, 298 K)

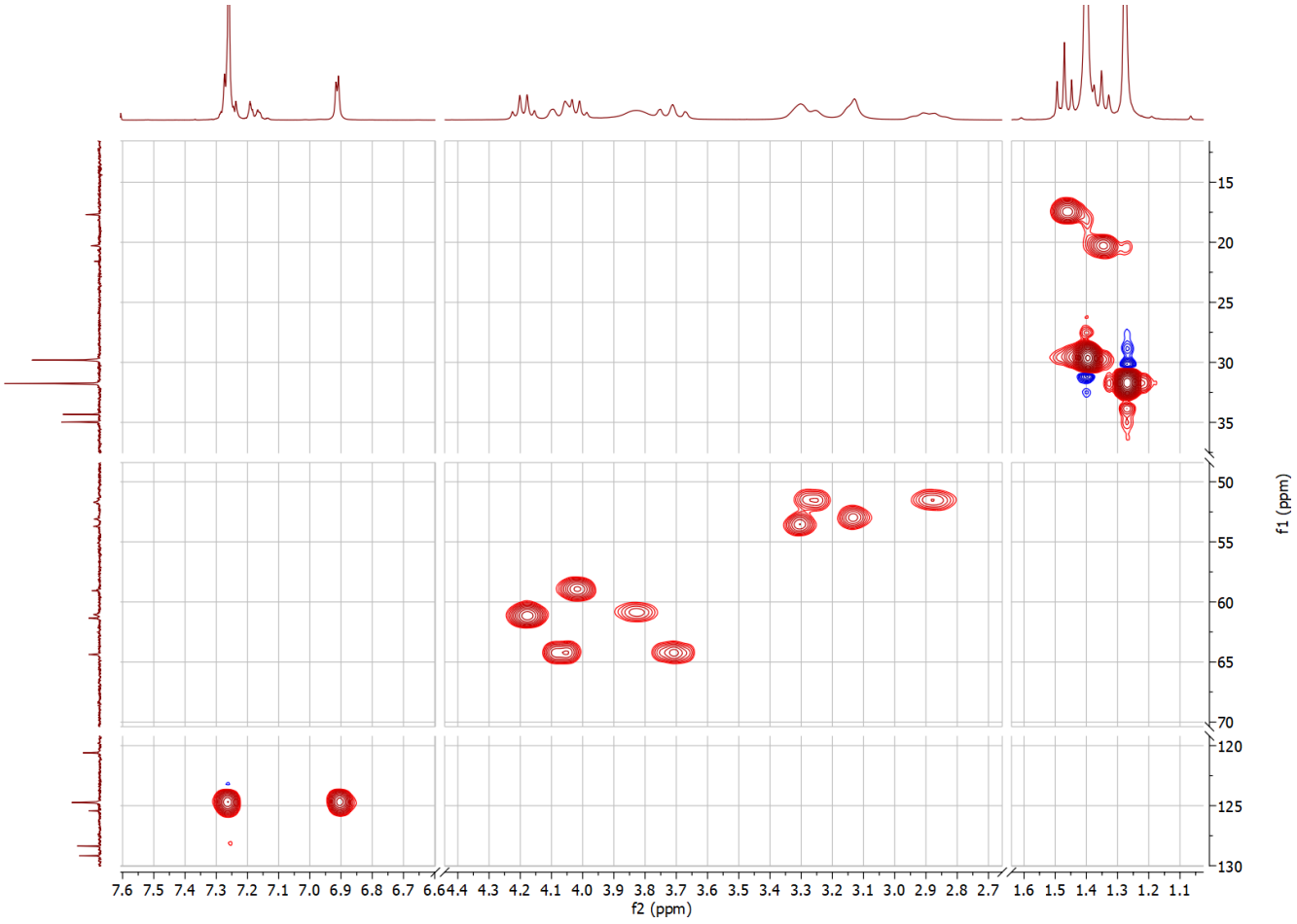

Figure A.35. HSQC spectrum of **3.5** + 2 equiv EtOH ($CDCl_3$, 298 K)

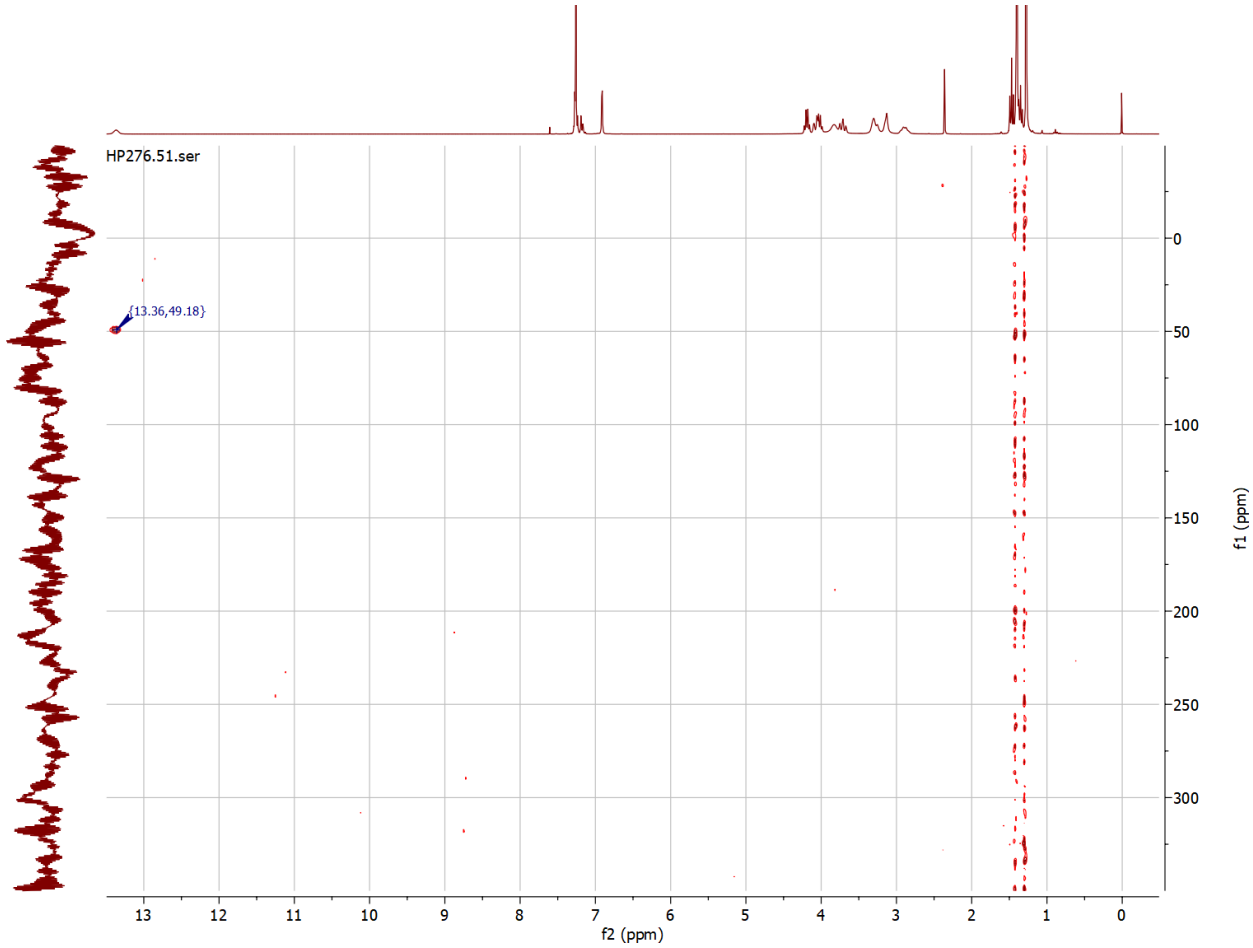

Figure A.36. $^{1}H–^{15}N$ HSQC spectrum of **3.5** + 2 equiv EtOH ($CDCl_3$, 298 K)

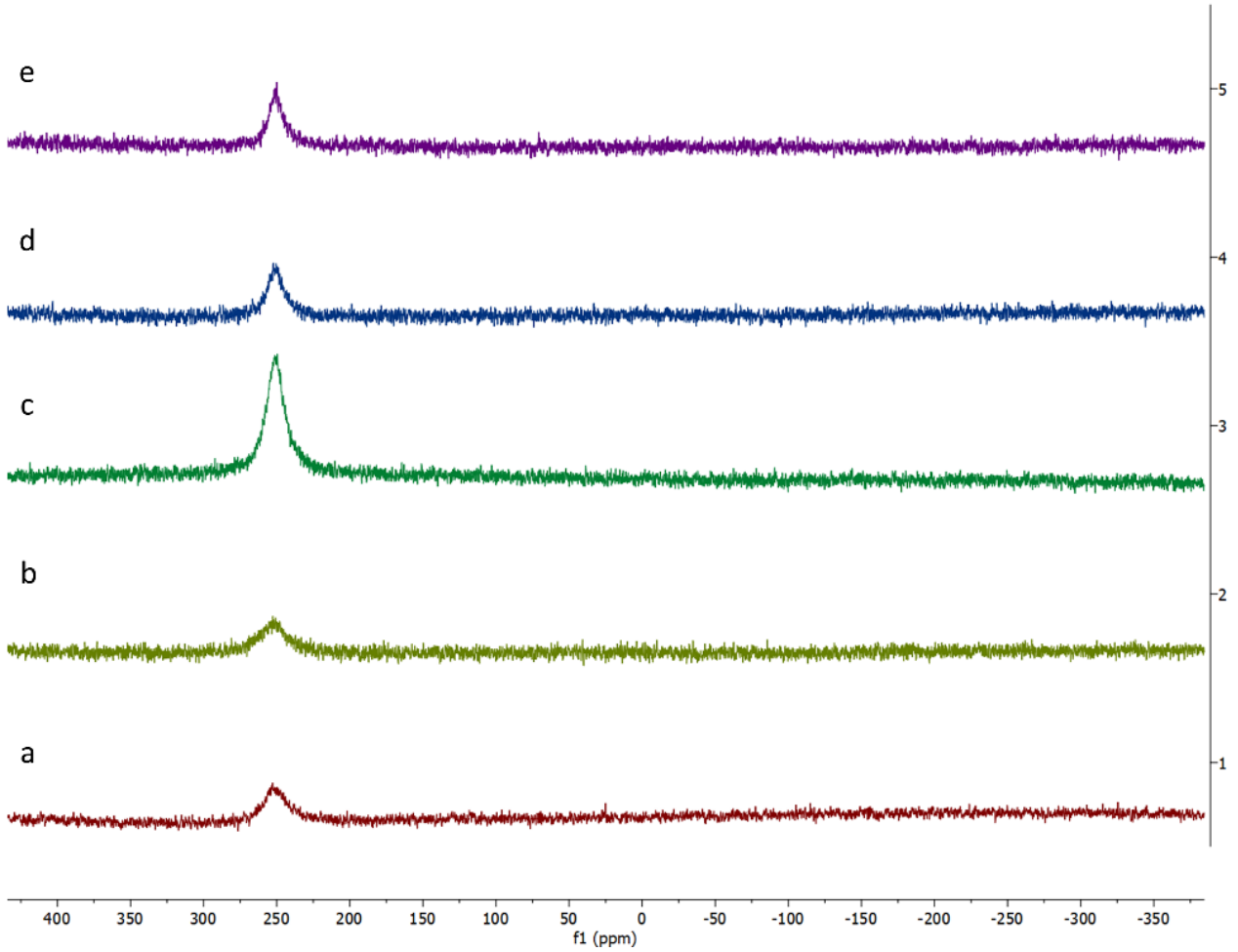

Figure A.37. ^{71}Ga NMR spectra of **3.5** ($CDCl_3$, 298 K) after addition of (a) 0 equiv, (b) 1 equiv, (c) 2 equiv, (d) 5 equiv, and (e) 10 equiv EtOH.

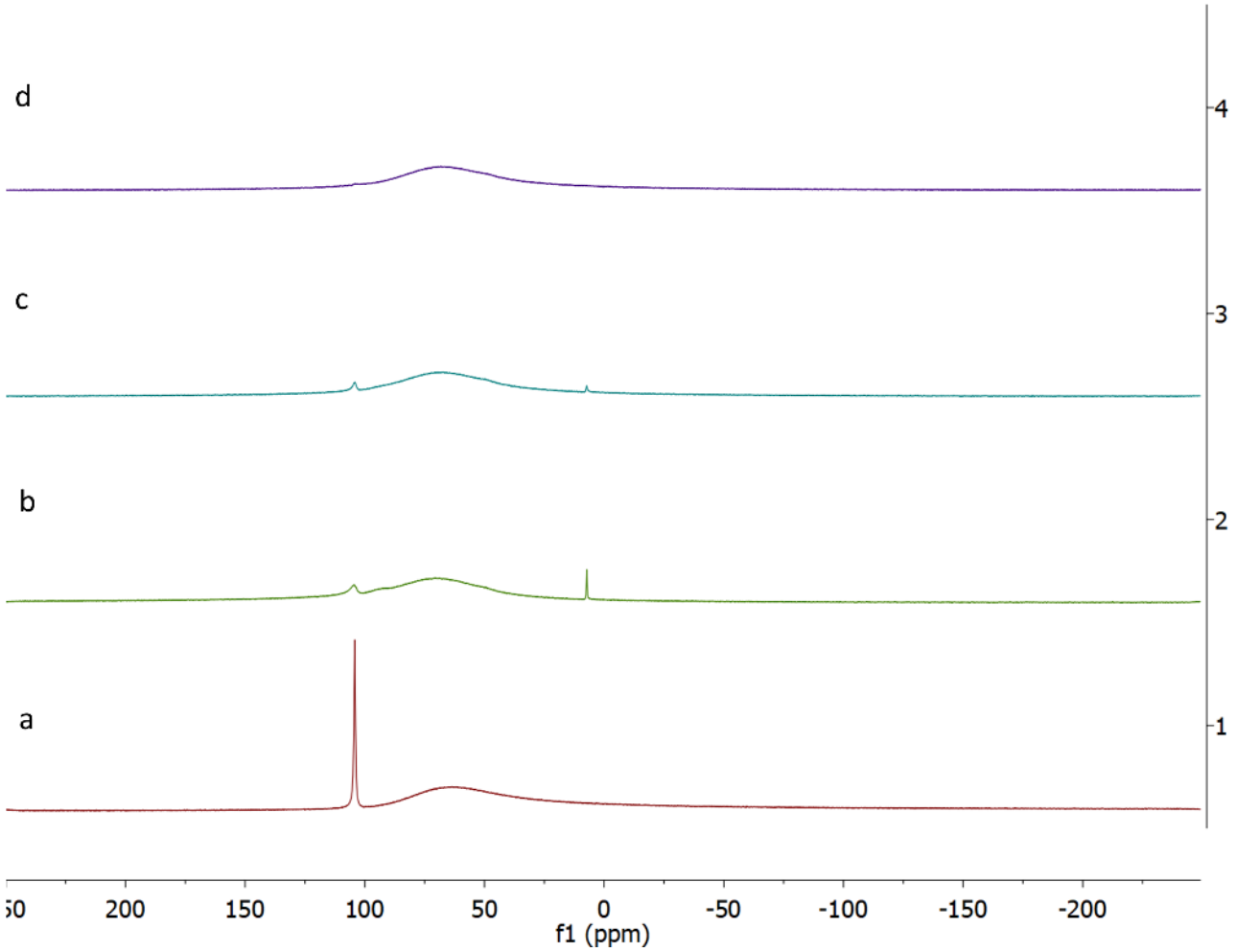

Figure A.38. ^{27}Al NMR spectra of **3.4** ($CDCl_3$, 298 K) after addition of (a) 0 equiv, (b) 1 equiv, (c) 2 equiv, and (d) 5 equiv EtOH.

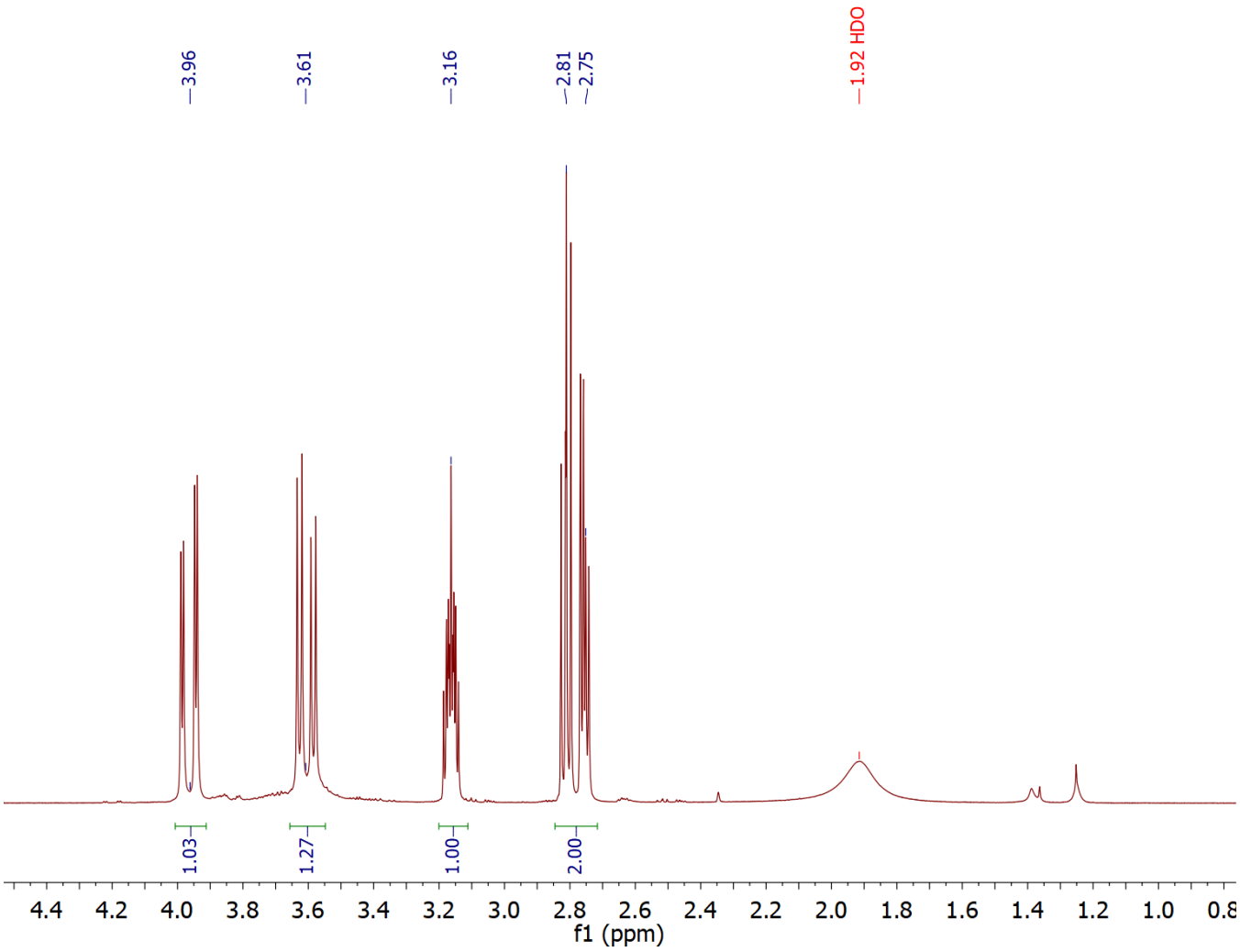

Figure A.39. ^{1}H NMR spectrum of **3.5** + 200 equiv glycidol after 3 h ($CDCl_3$, 298 K)

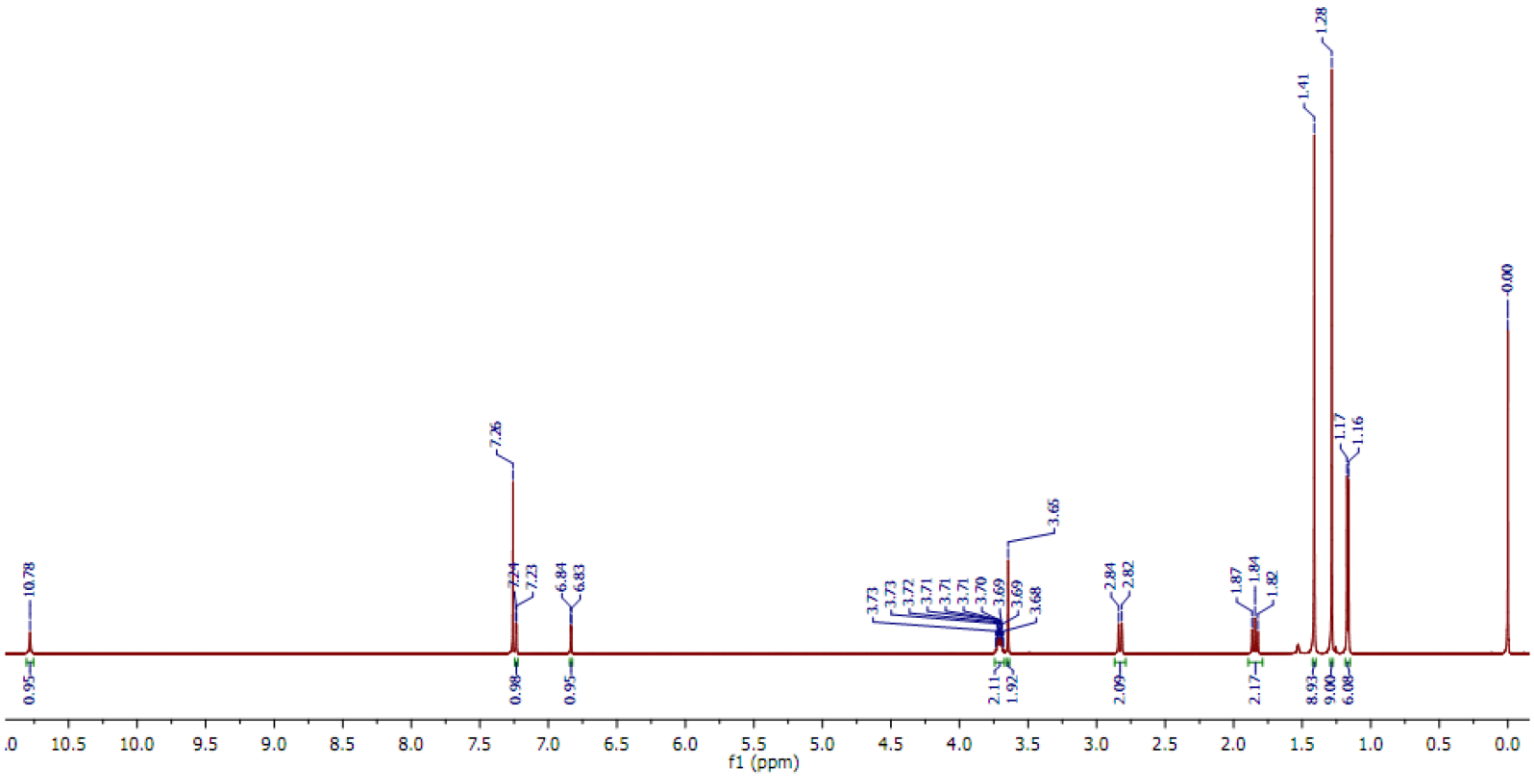

Figure A.40. ^{1}H NMR spectrum of H[**L4**] in $CDCl_3$, 298 K

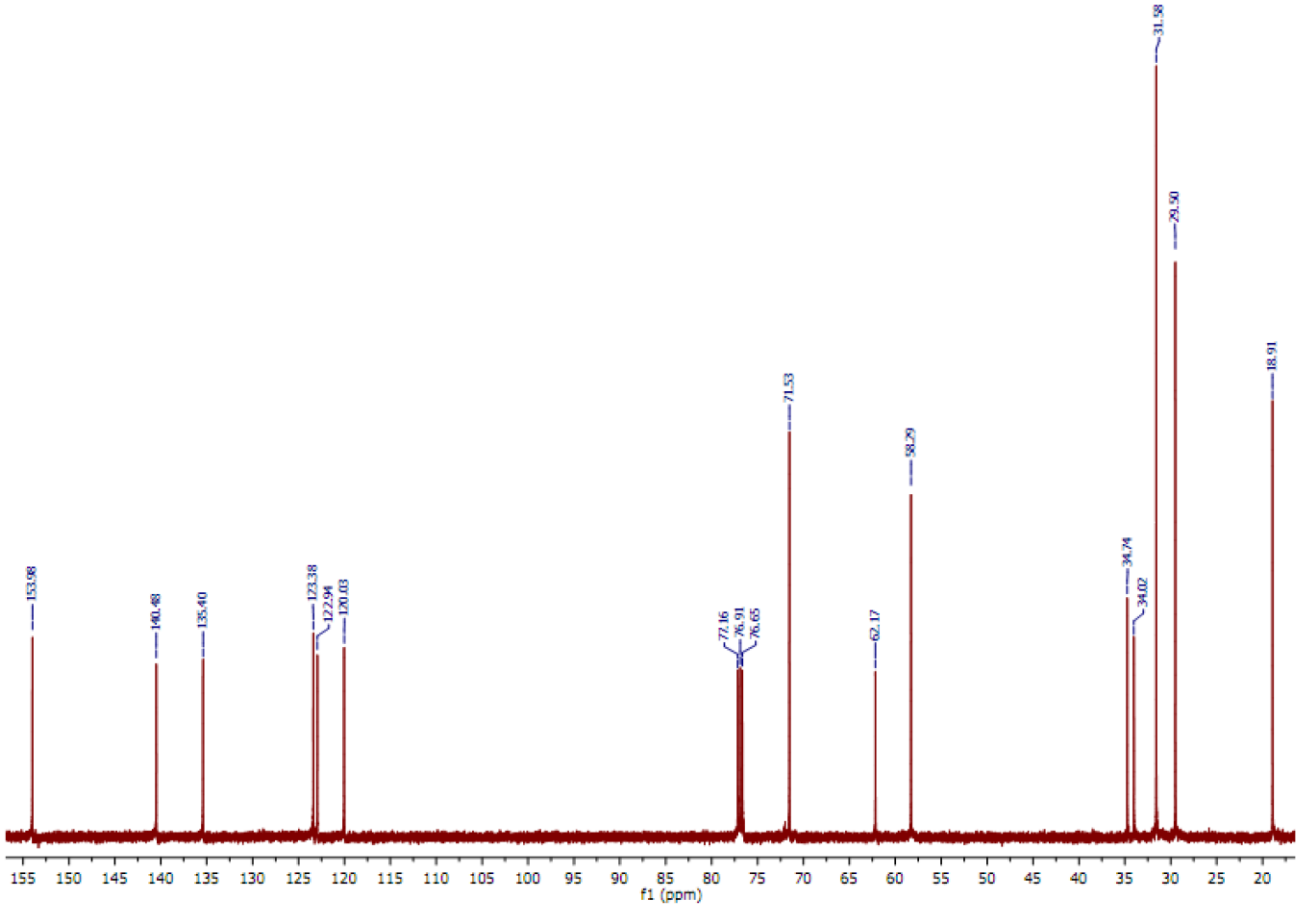

Figure A.41. $^{13}C\{^{1}H\}$ NMR spectrum of H[**L4**] in $CDCl_3$, 298 K

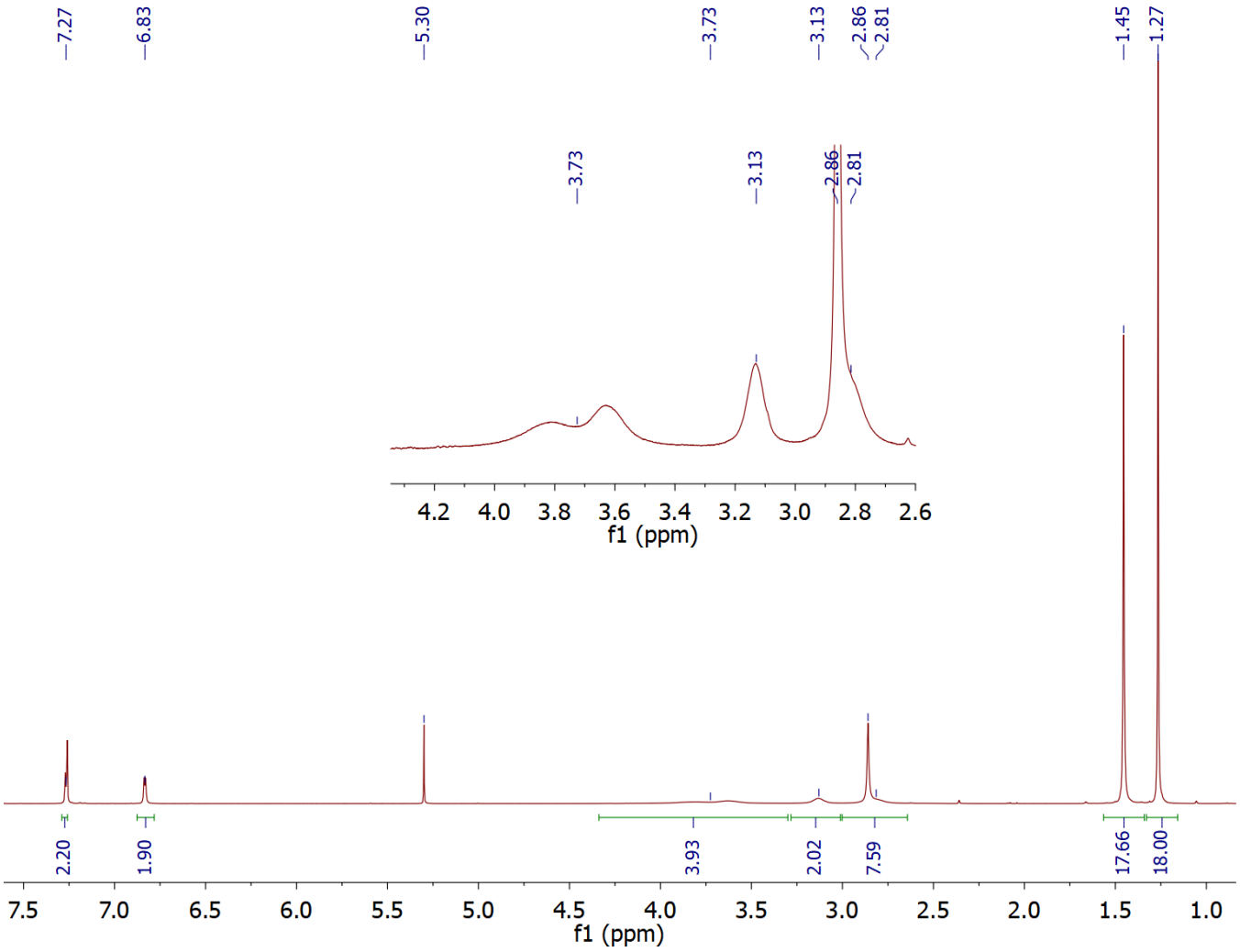

Figure A.42. ^{1}H NMR spectrum of **4.1** in $CDCl_3$, 298 K

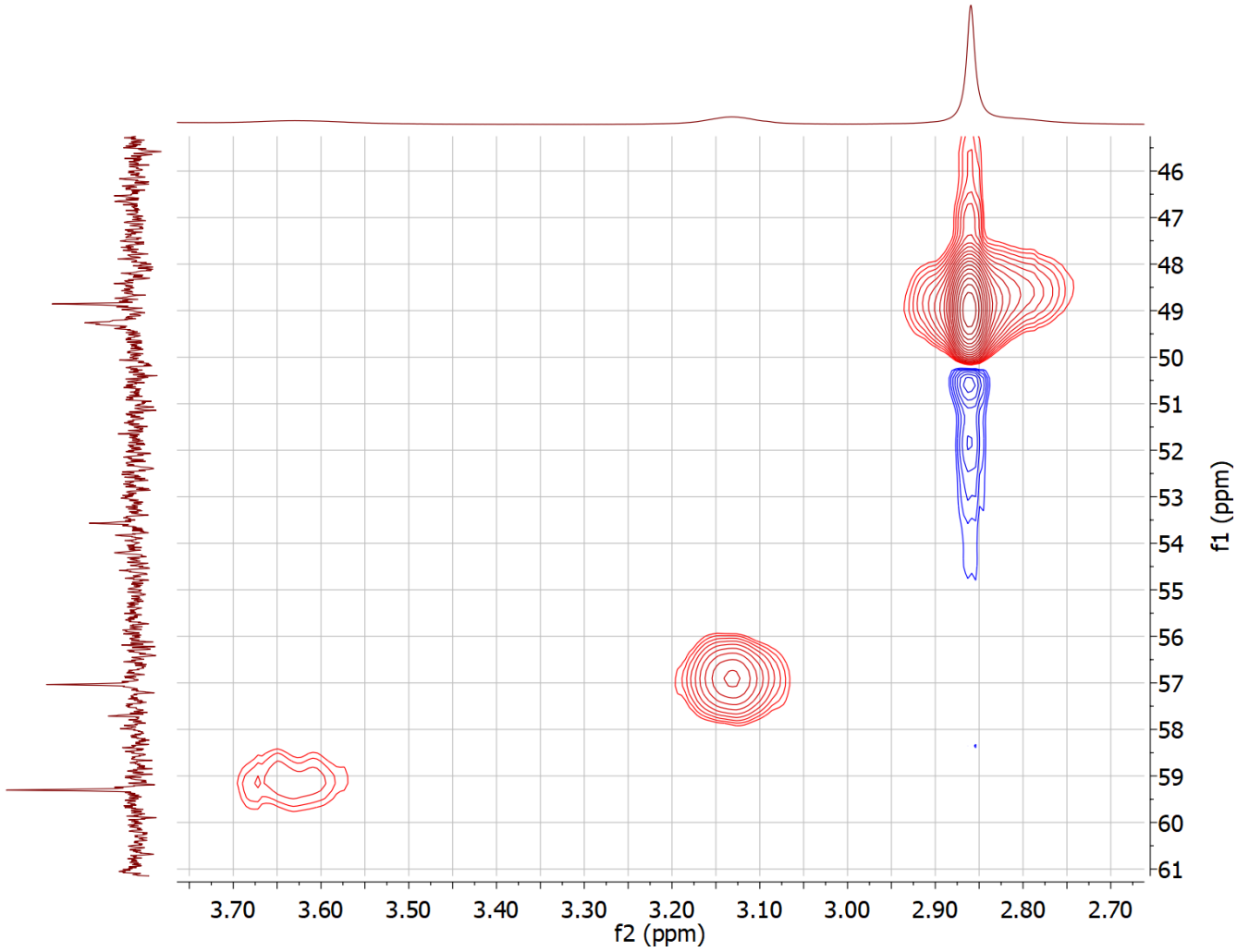

Figure A.43. HSQC spectrum of **4.1** in $CDCl_3$, 298 K

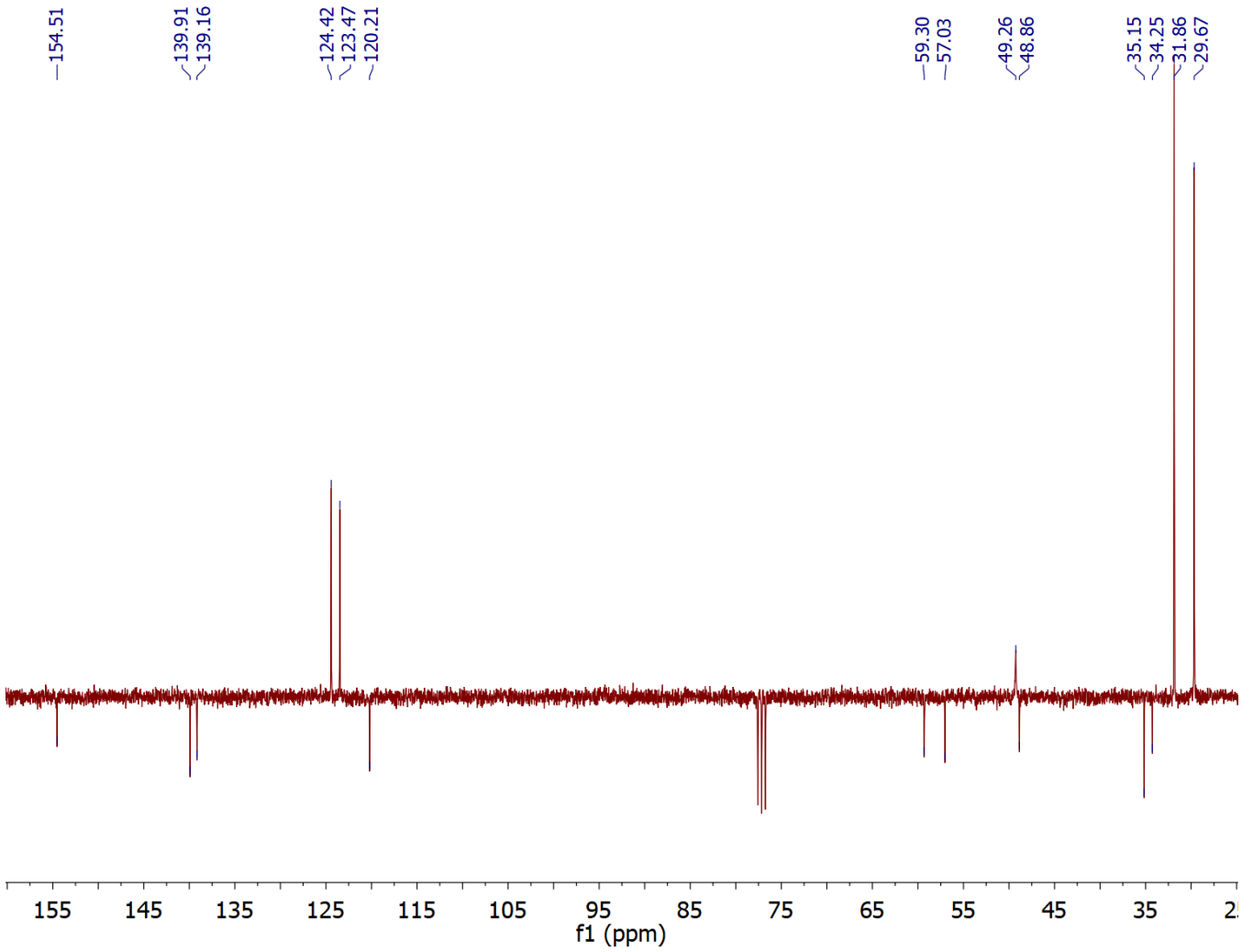

Figure A.44. ^{13}C-DEPT NMR spectrum of **4.1** in $CDCl_3$, 298 K

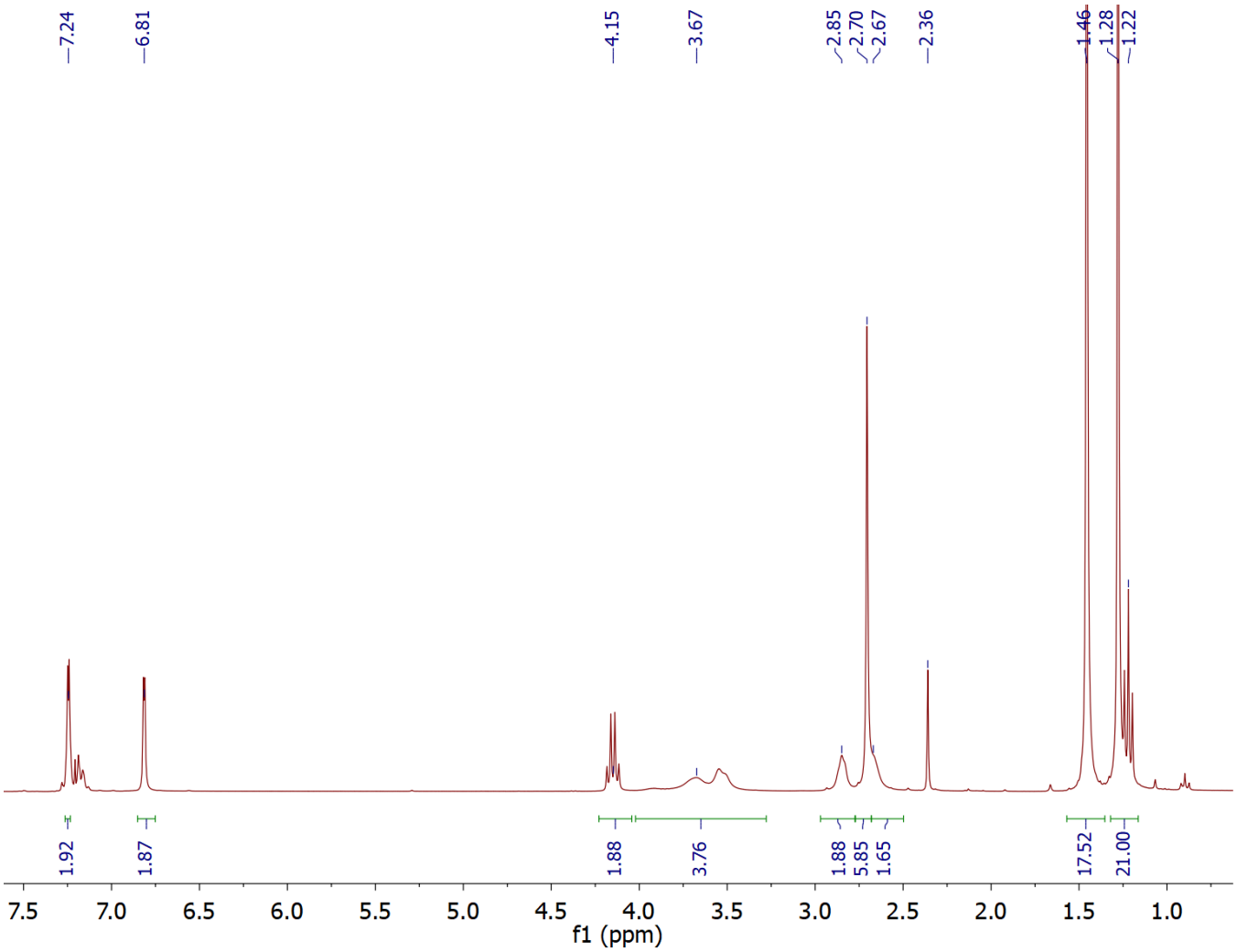

Figure A.45. ^{1}H NMR spectrum of **4.2** in $CDCl_3$, 298 K (residual toluene resonance at 2.36 ppm)

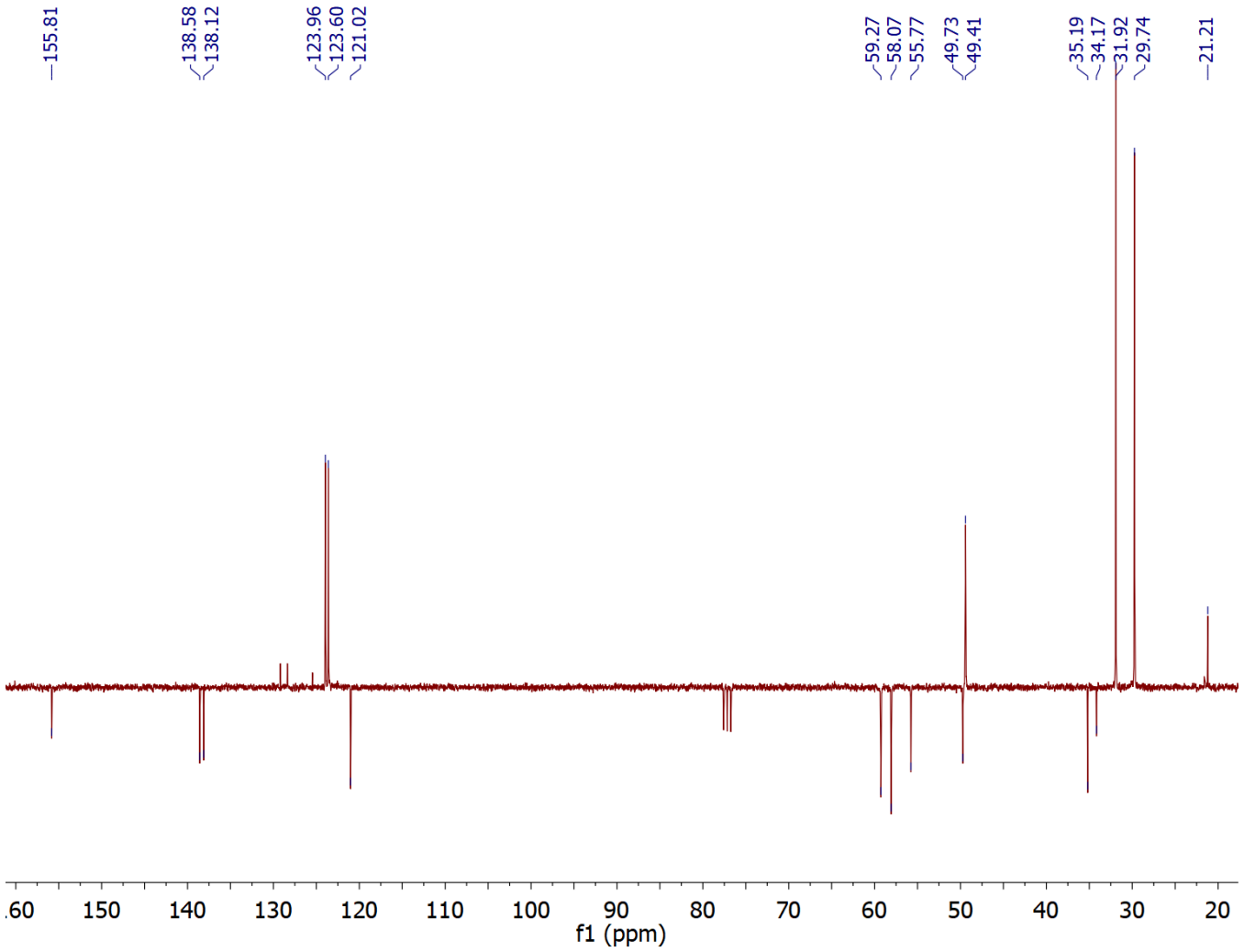

Figure A.46. ^{13}C-DEPT NMR spectrum of **4.2** in $CDCl_3$, 298 K

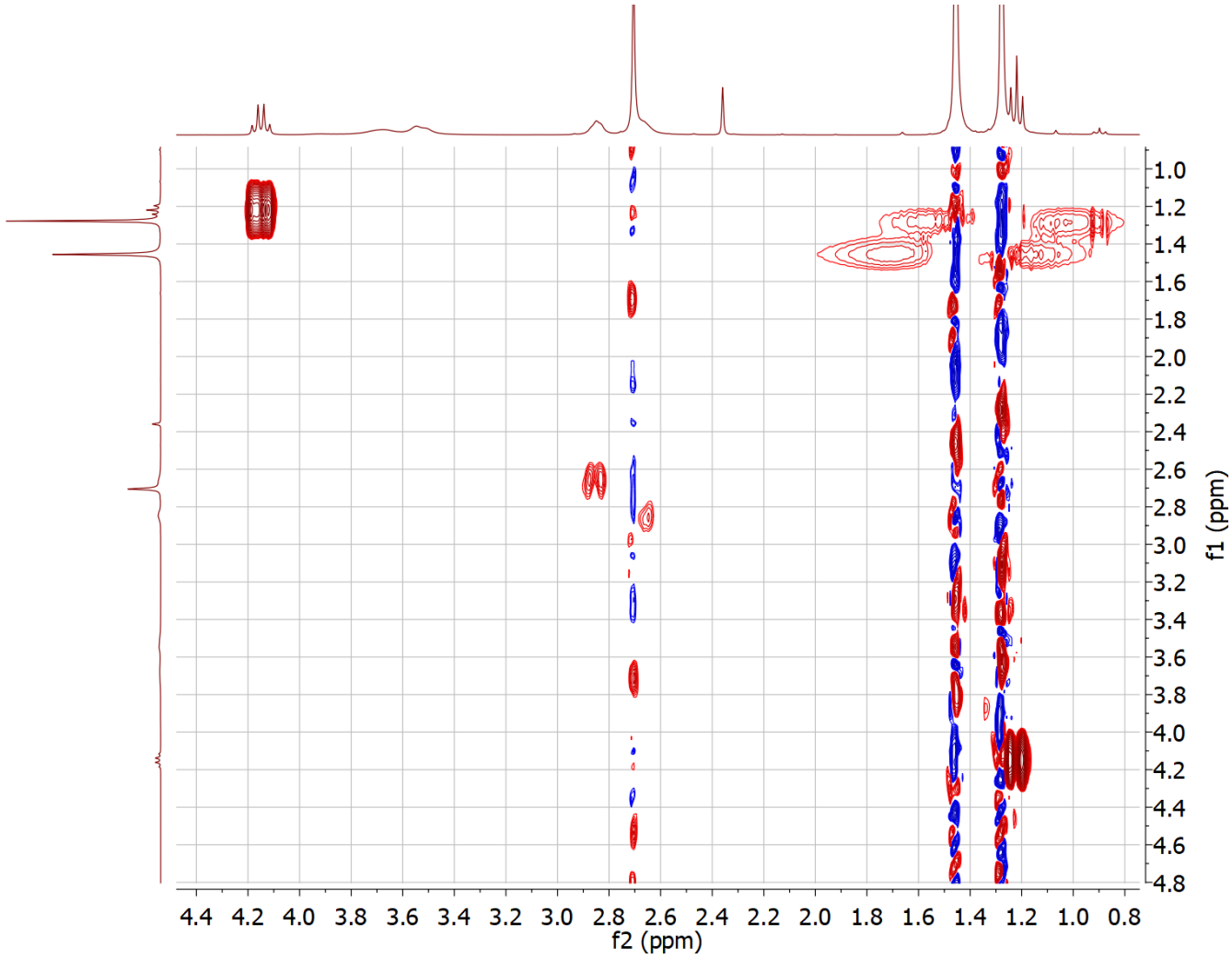

Figure A.47. COSY spectrum of **4.2** in $CDCl_3$, 298 K

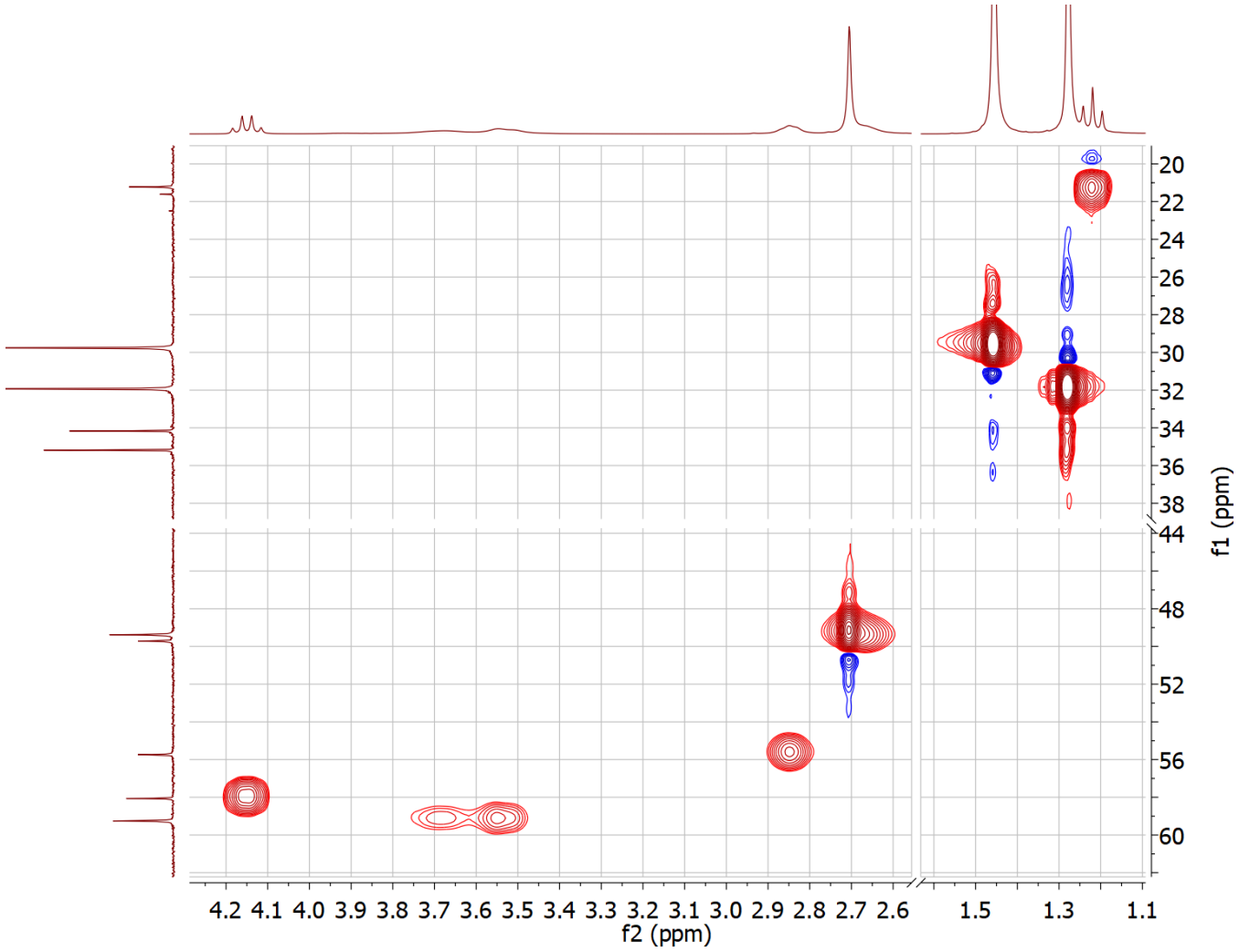

Figure A.48. HSQC spectrum of **4.2** in $CDCl_3$, 298 K

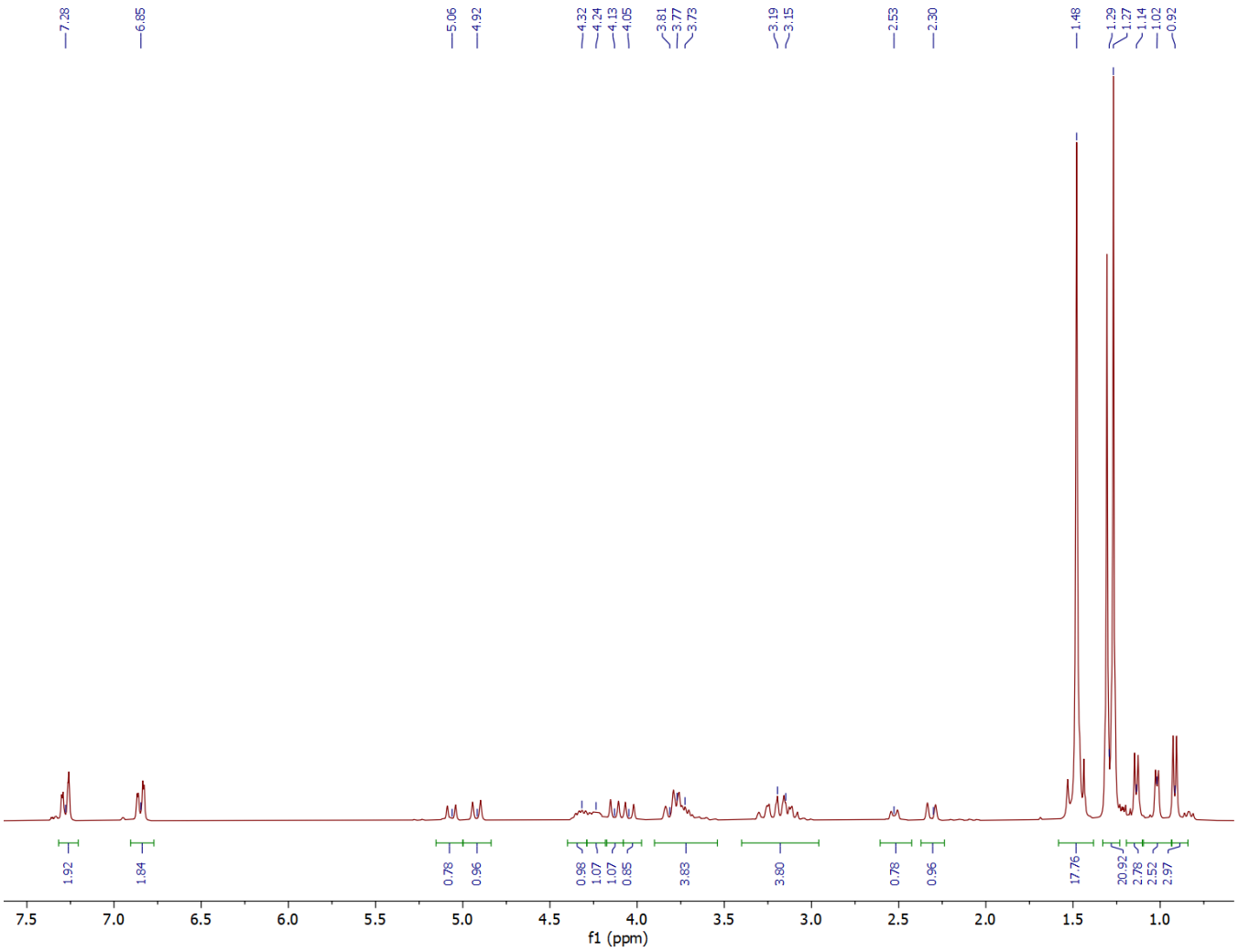

Figure A.49. ^{1}H NMR spectrum of **4.3** in $CDCl_3$, 298 K

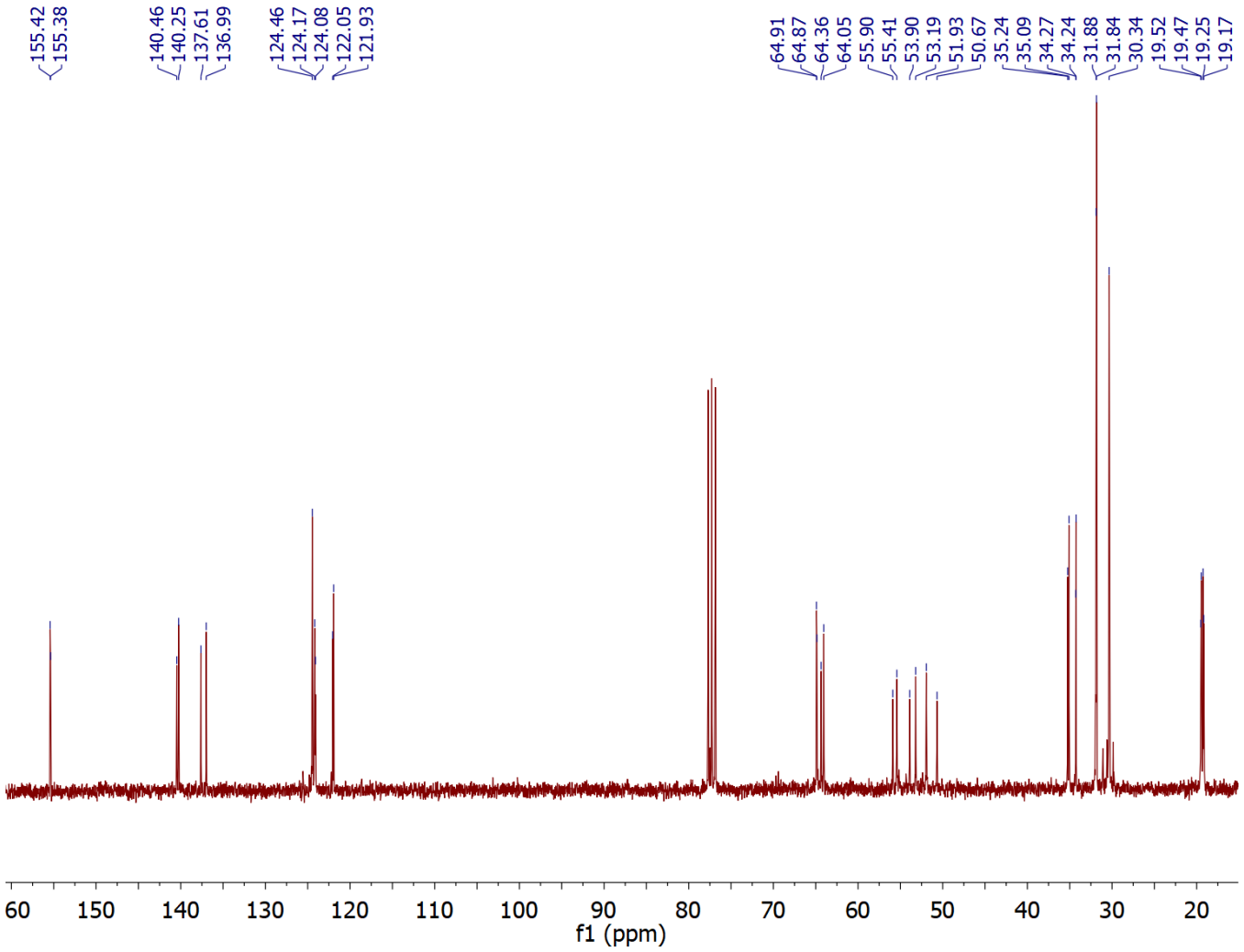

Figure A.50. $^{13}C\{^{1}H\}$ spectrum of **4.3** in $CDCl_3$, 298 K

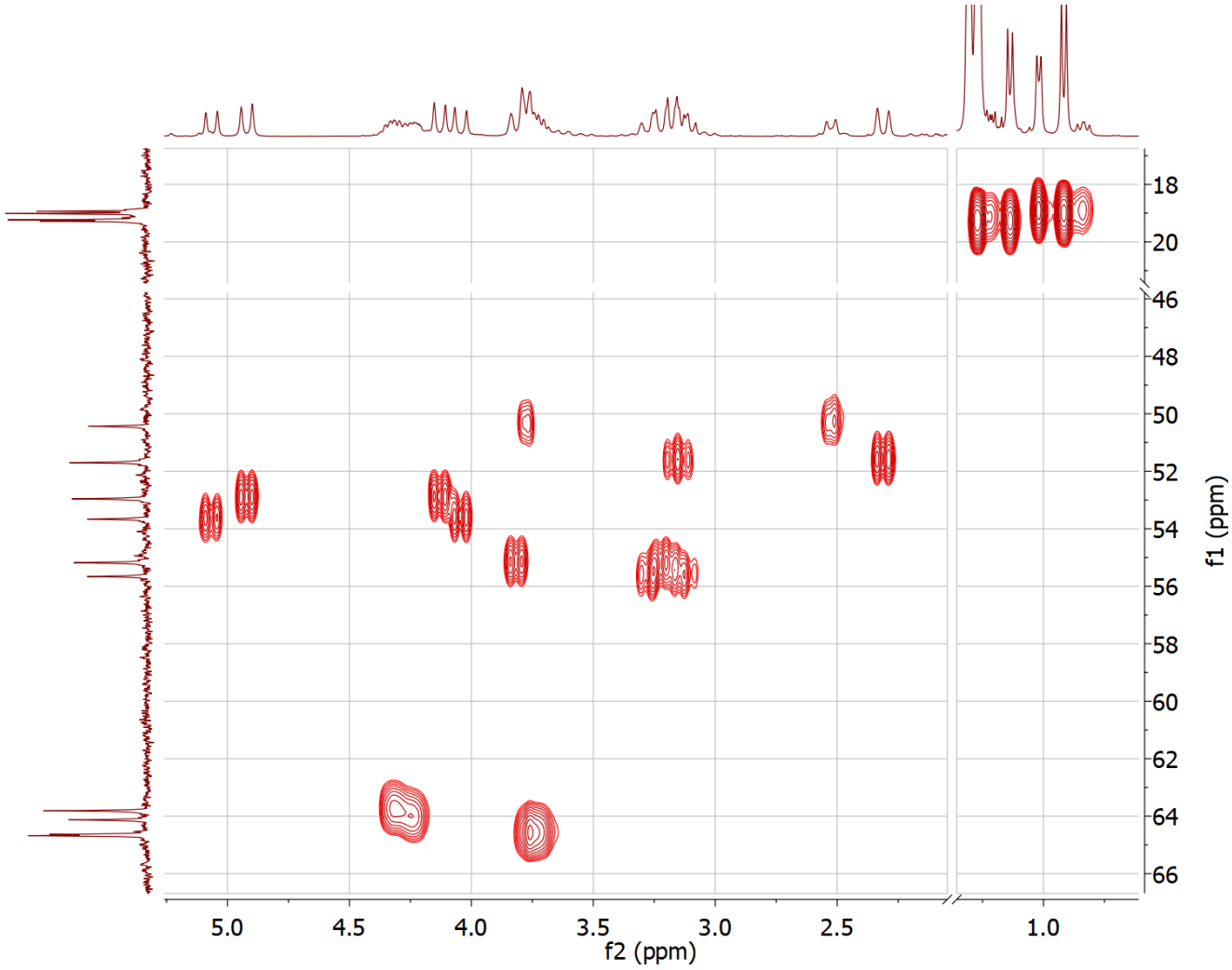

Figure A.51. HSQC spectrum of **4.3** in $CDCl_3$, 298 K

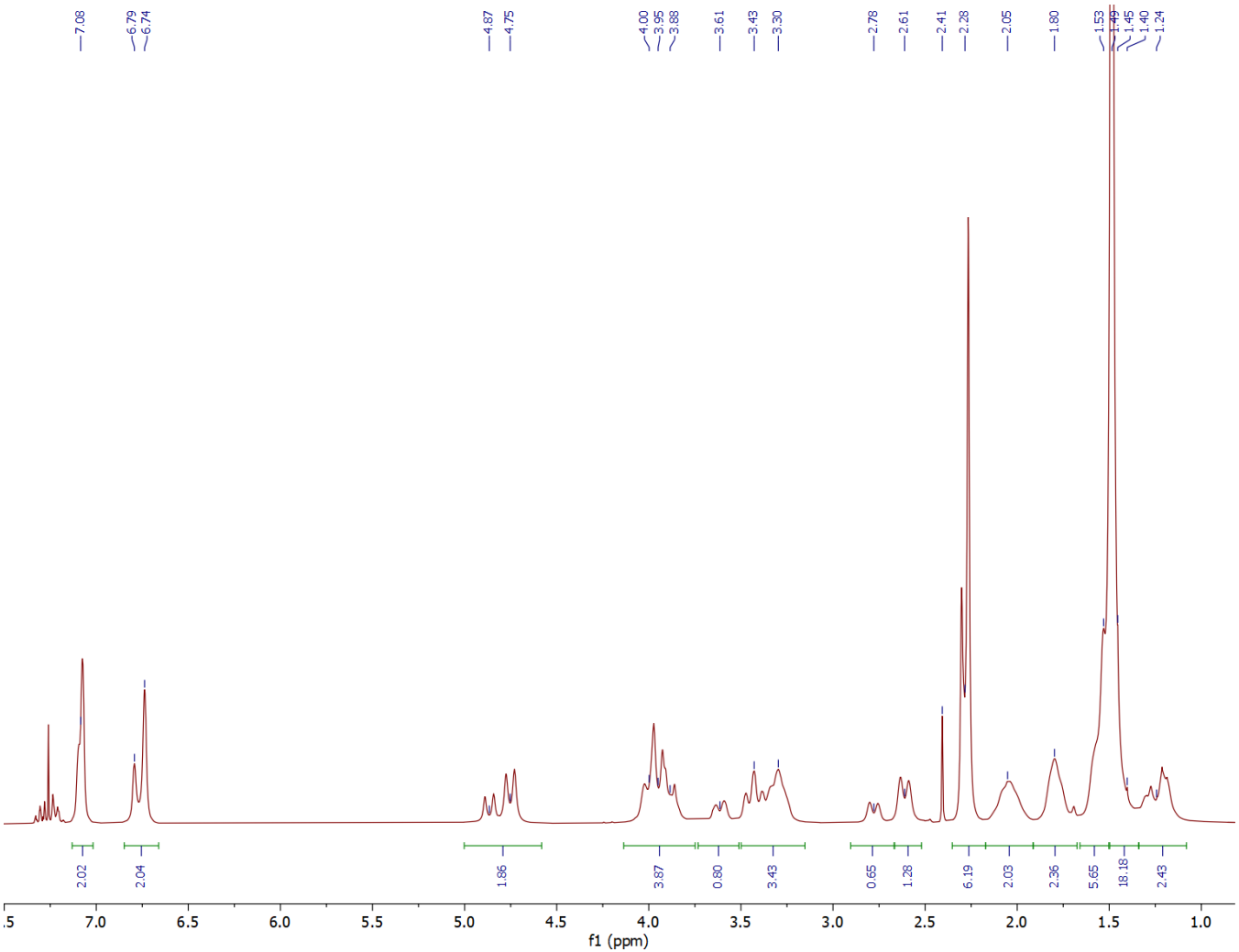

Figure A.52. ^{1}H NMR spectrum of **4.4** in $CDCl_3$, 298 K (residual toluene resonance at 2.41 ppm)

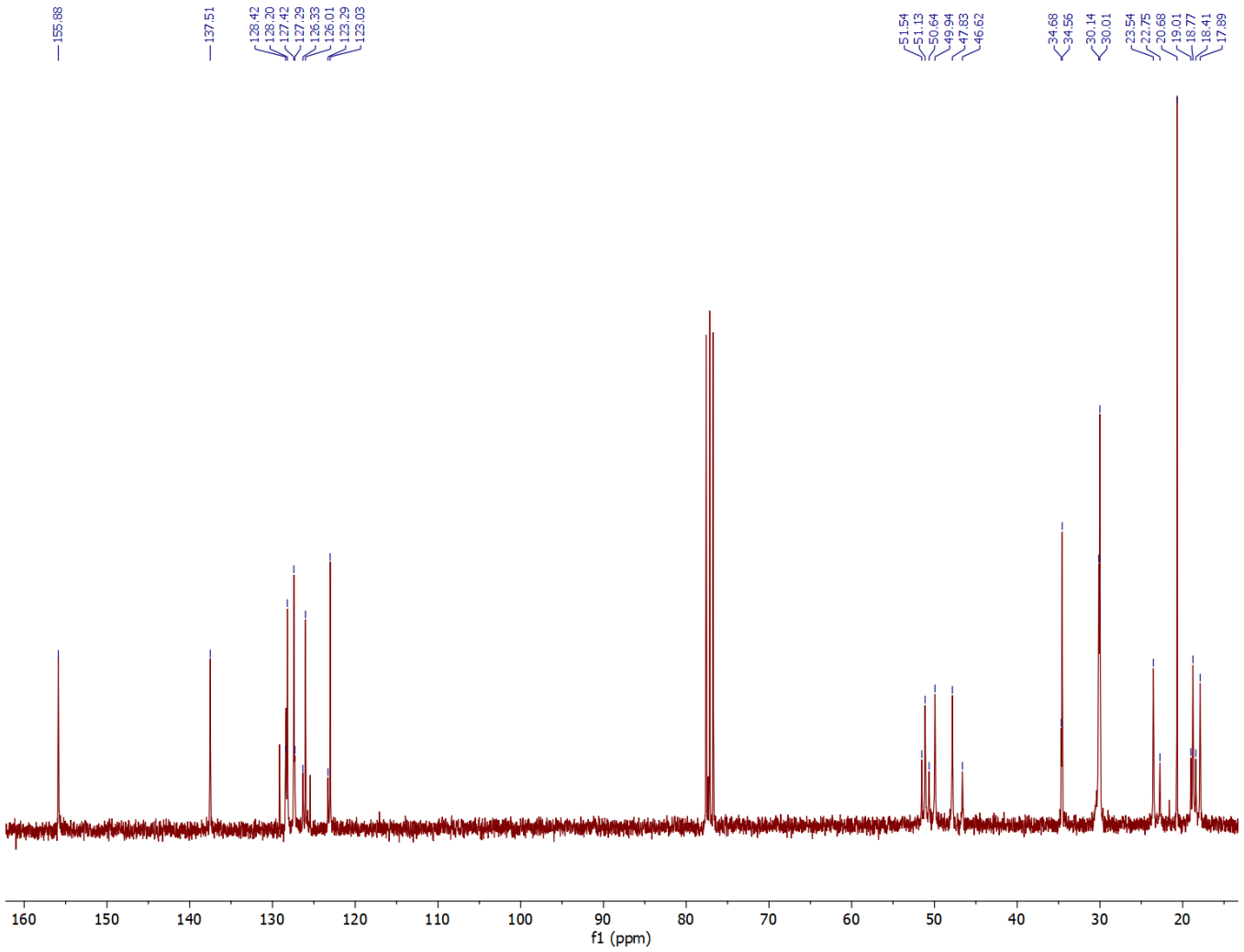

Figure A.53. $^{13}C\{^{1}H\}$ NMR spectrum of **4.4** in $CDCl_3$, 298 K

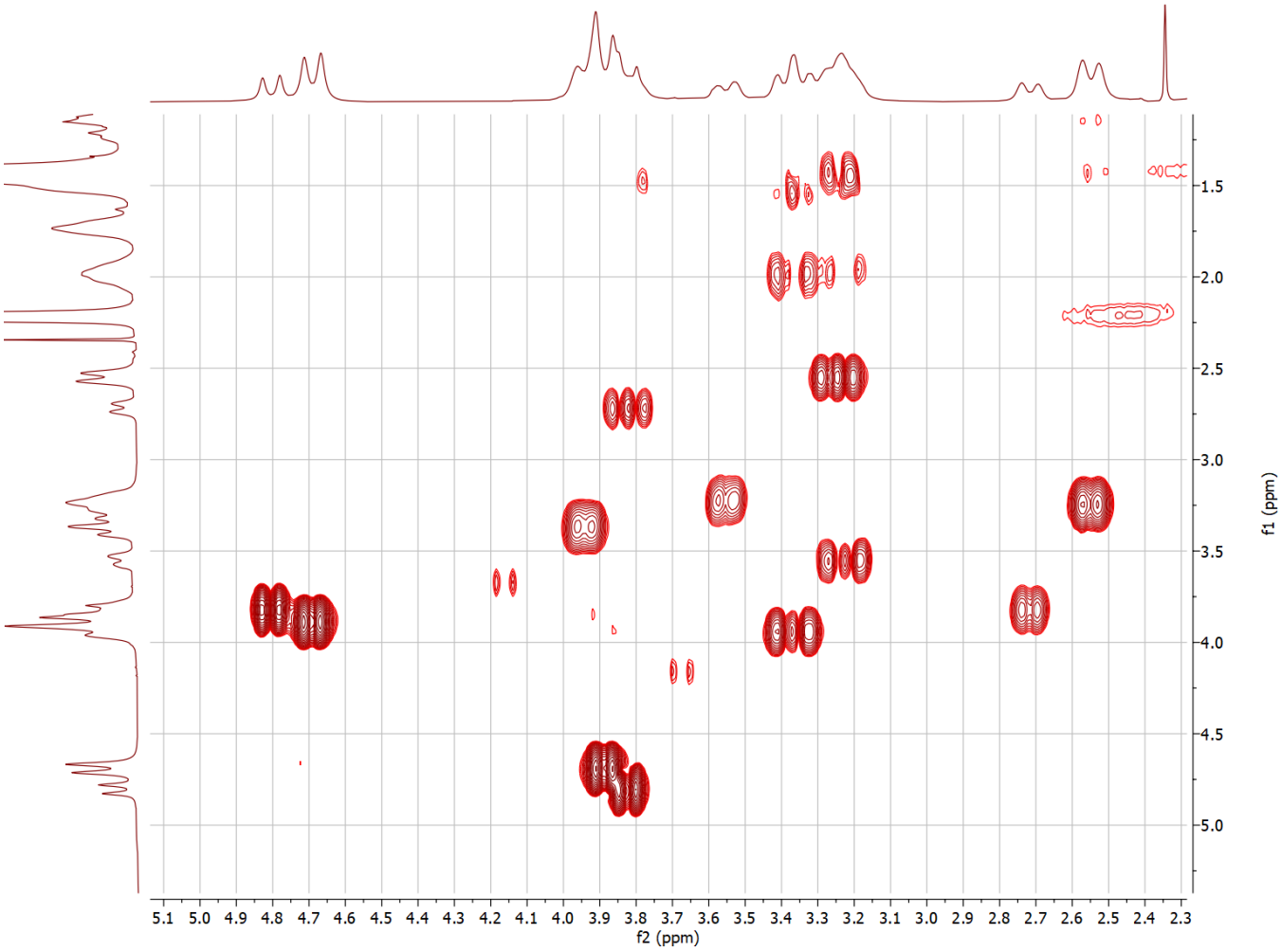

Figure A.54. COSY spectrum of **4.4** in $CDCl_3$, 298 K

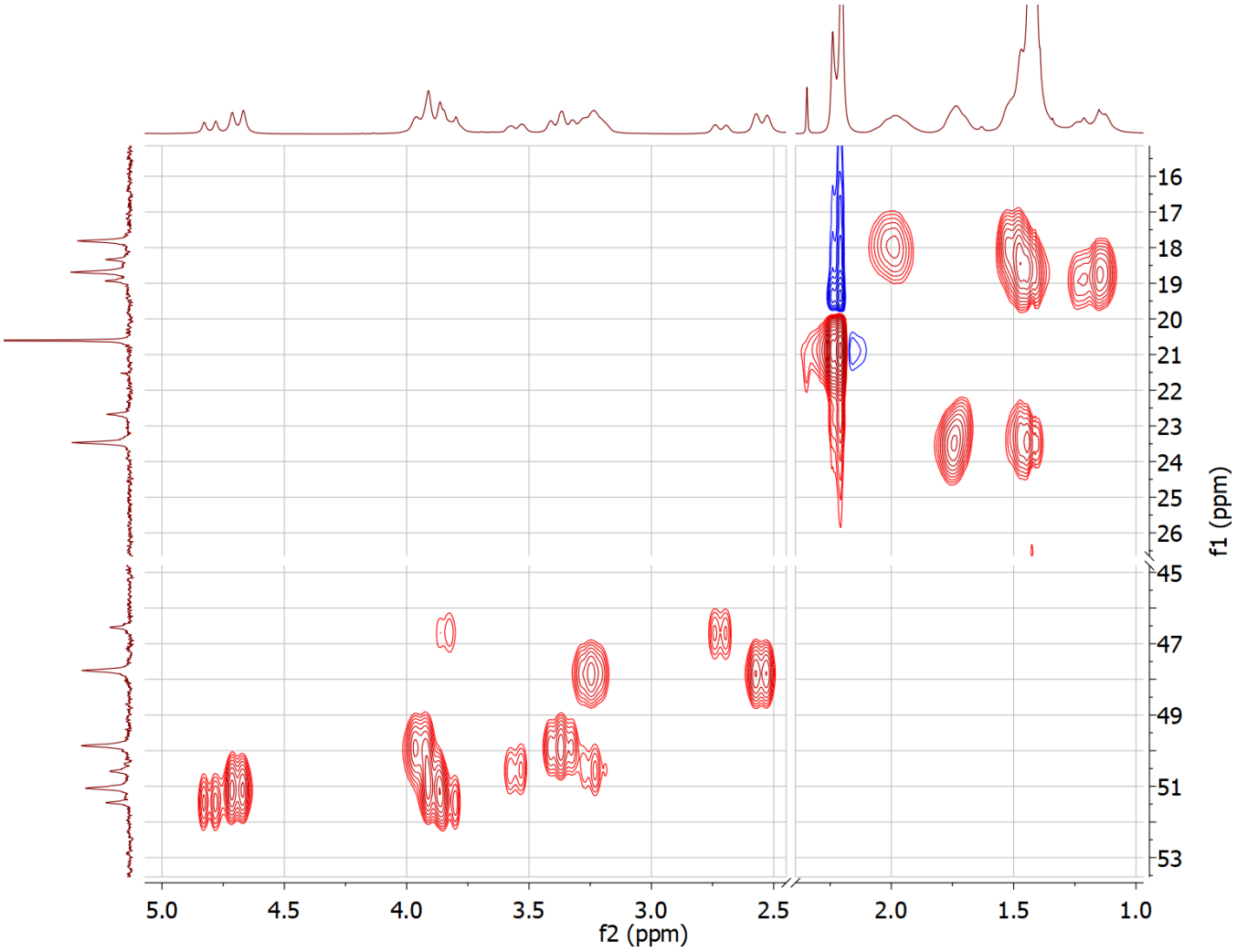

Figure A.55. HSQC spectrum of **4.4** in $CDCl_3$, 298 K

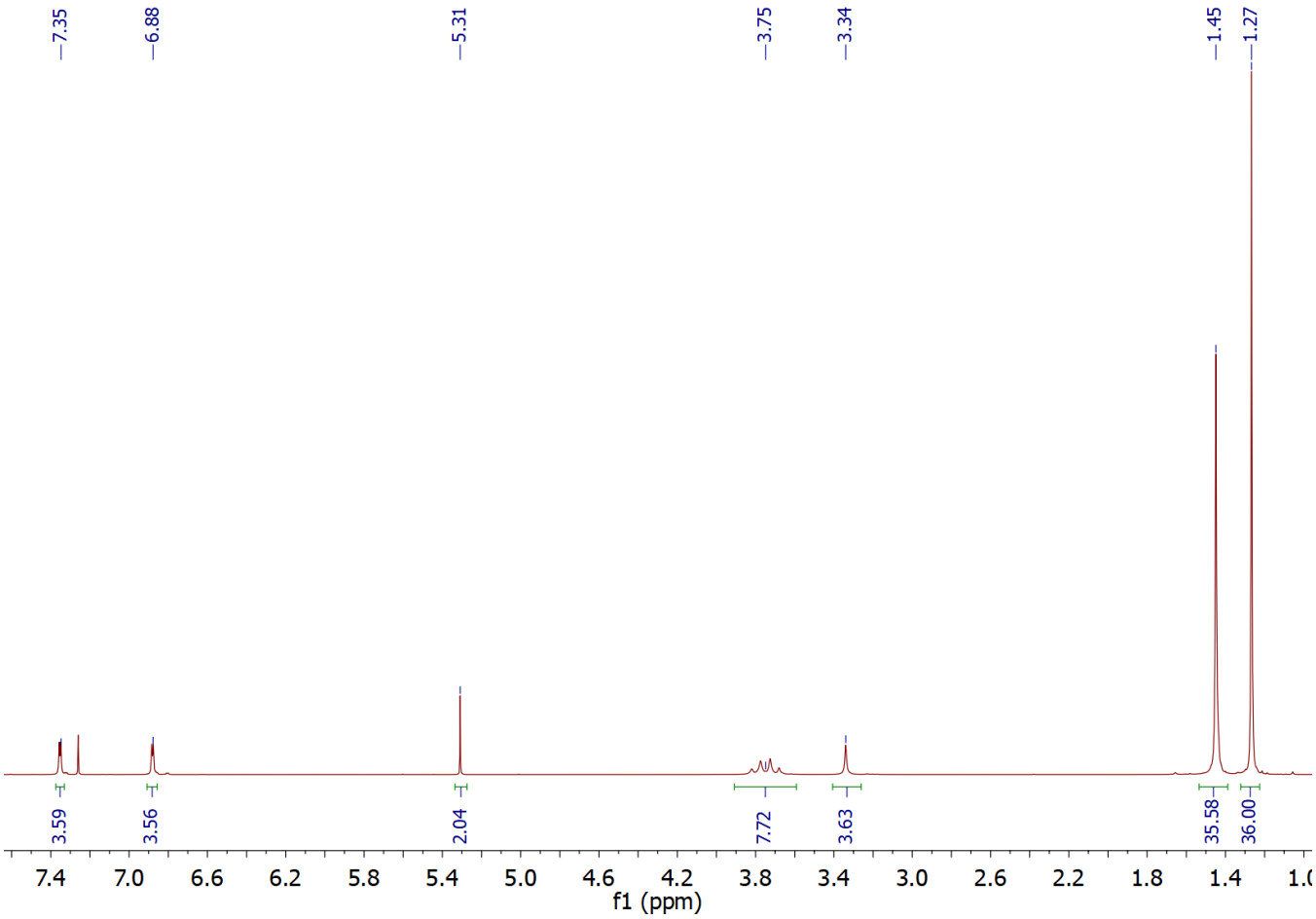

Figure A.56. ^{1}H NMR spectrum of **5.1** in $CDCl_3$, 298 K

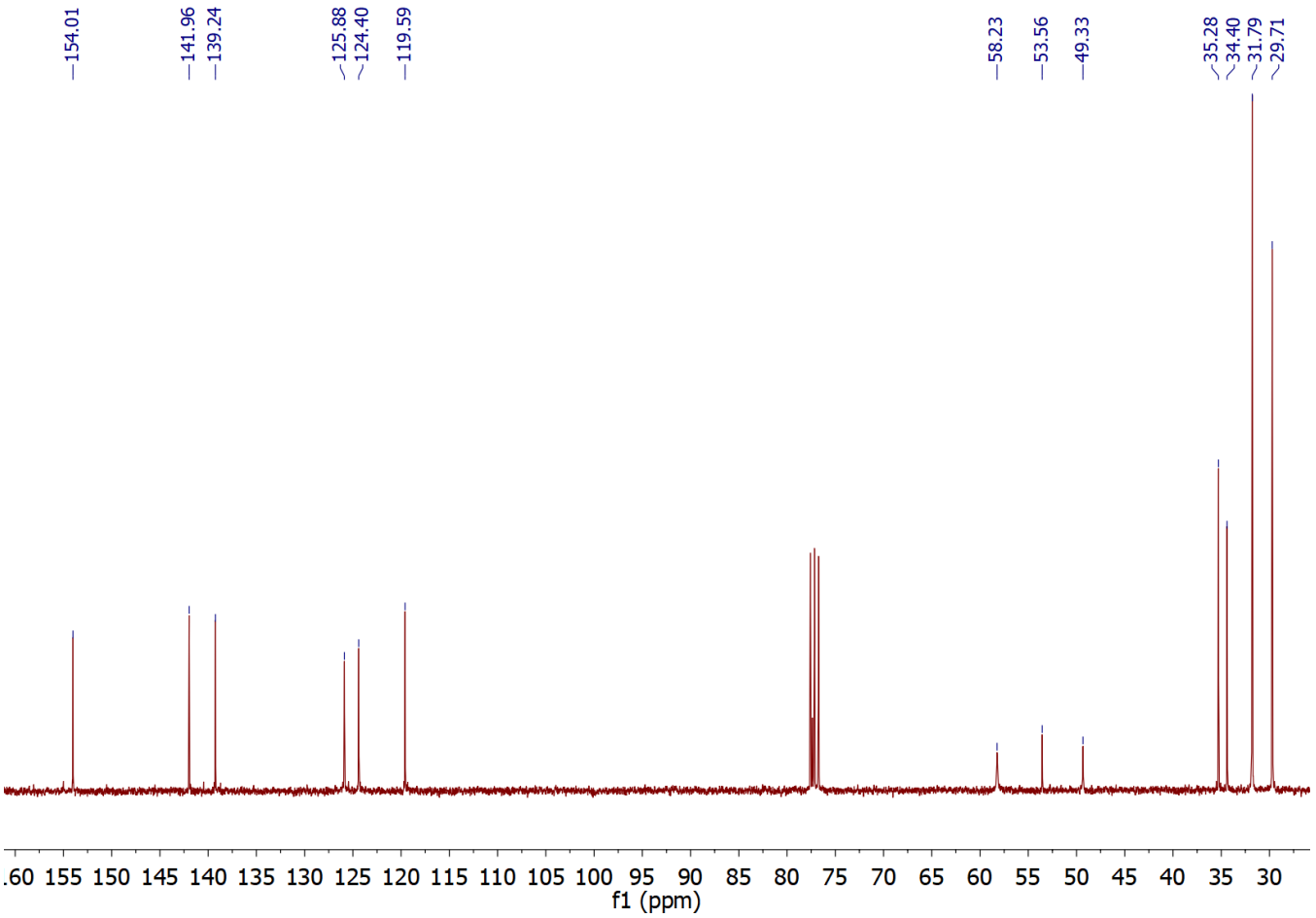

Figure A.57. $^{13}C\{^{1}H\}$ NMR spectrum of **5.1** in $CDCl_3$, 298 K

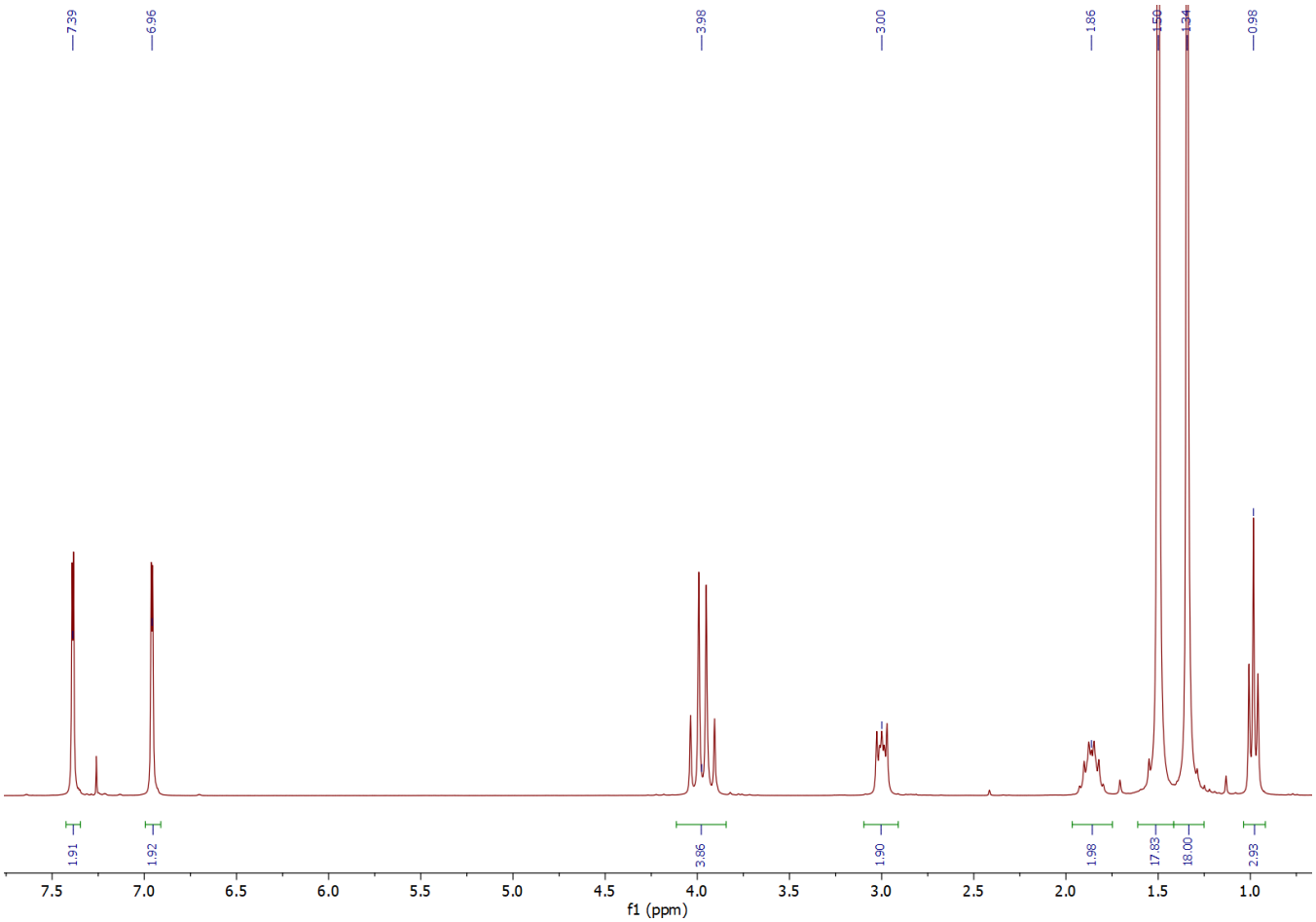

Figure A.58. ^{1}H NMR spectrum of **5.2** in $CDCl_3$, 298 K

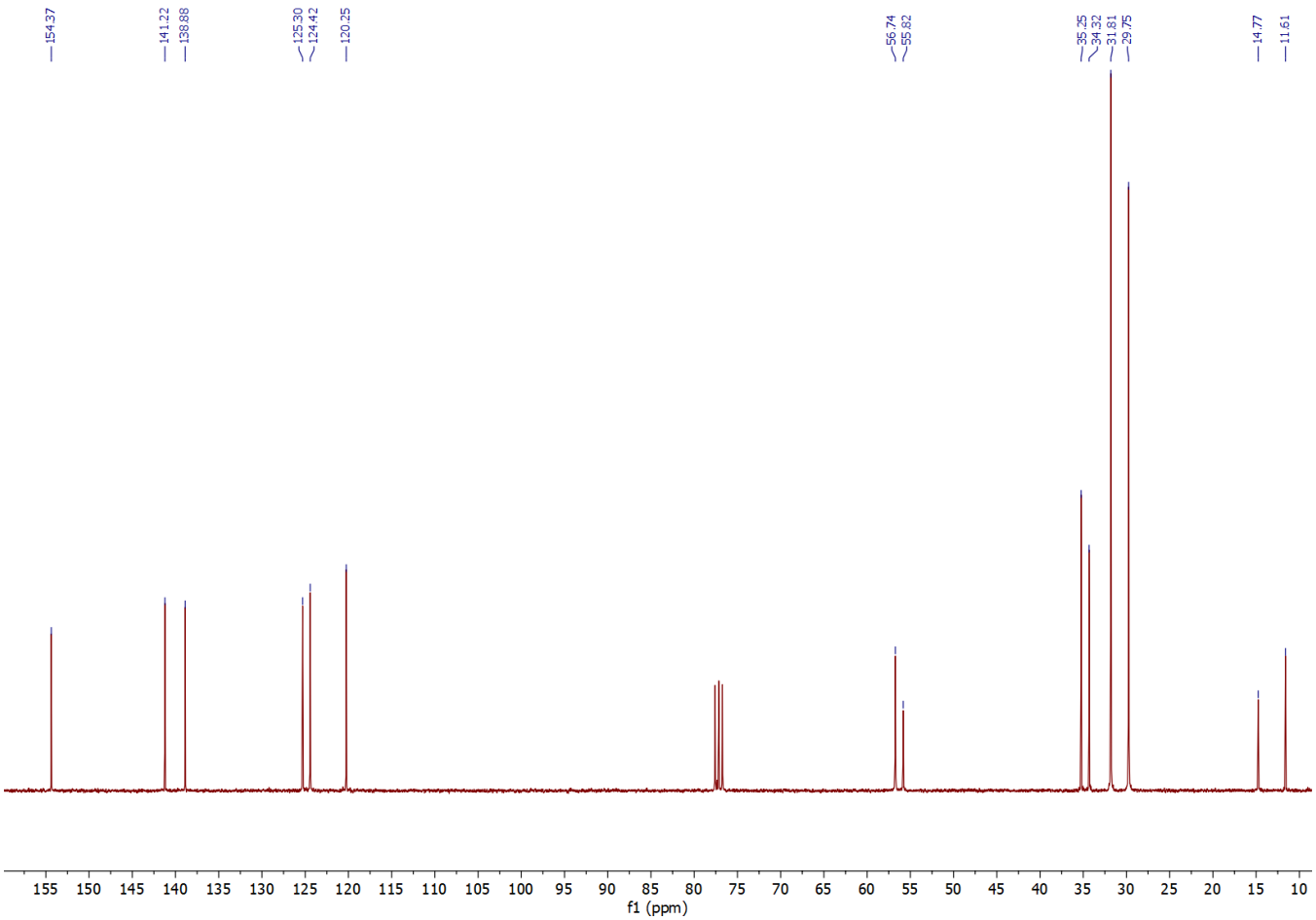

Figure A.59. $^{13}C\{^{1}H\}$ NMR spectrum of **5.2** in $CDCl_3$, 298 K

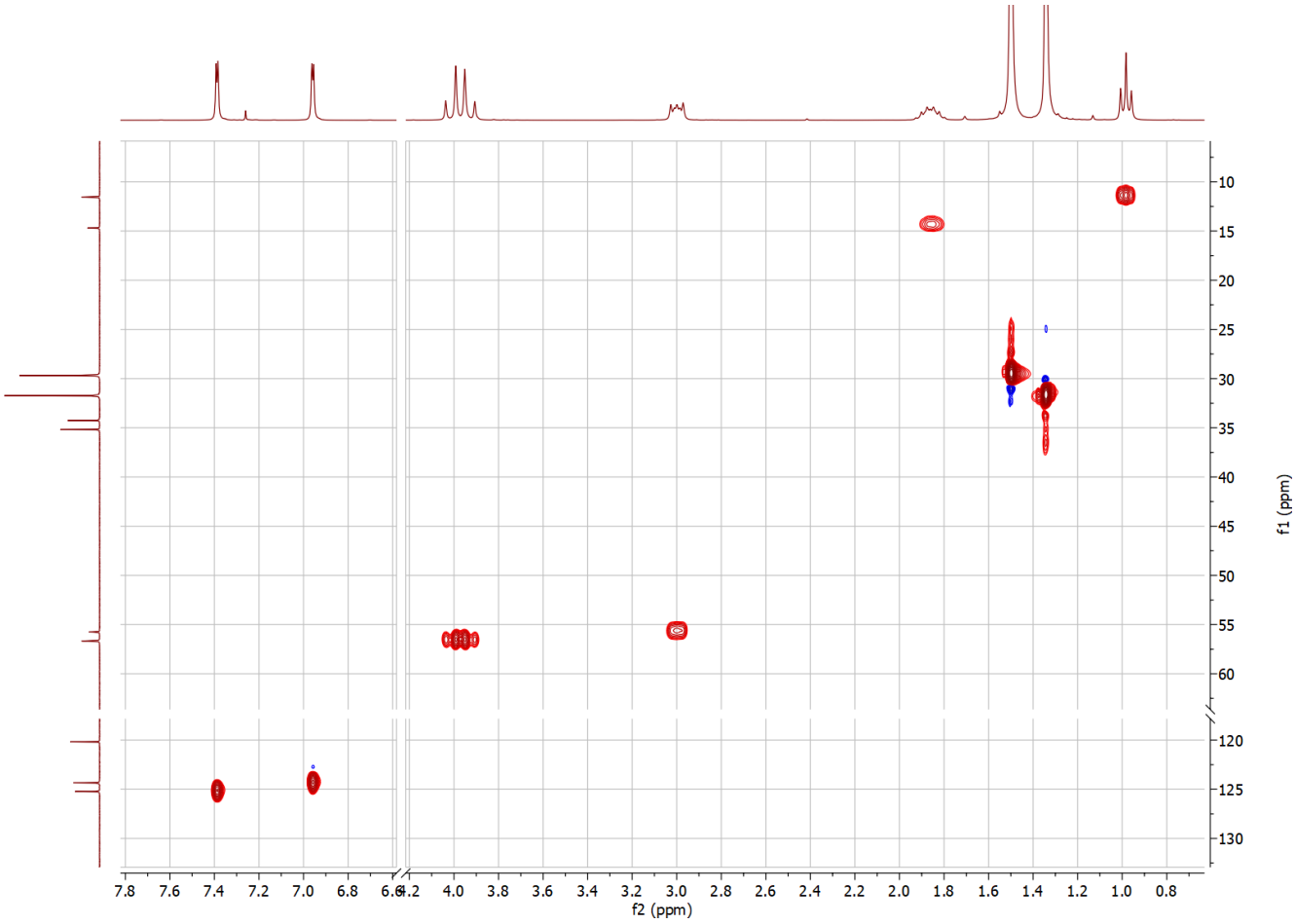

Figure A.60. HSQC spectrum of **5.2** in $CDCl_3$, 298 K

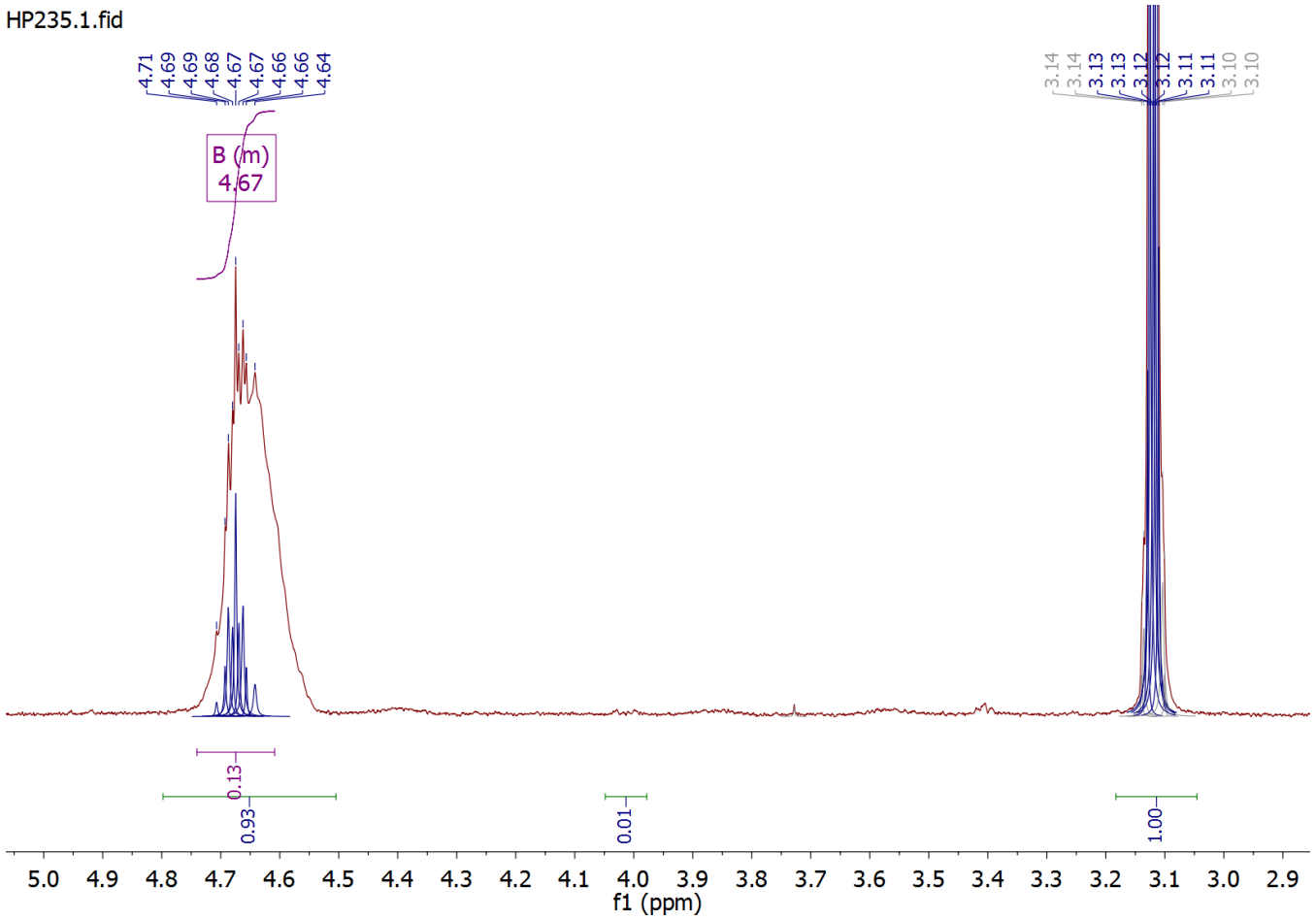

Figure A.61. Deconvoluted ^{1}H NMR spectrum of crude polymer in $CDCl_3$ (298 K) showing the relative integrations of *cis*-CHC (4.7 ppm), *trans*-CHC (4.0 ppm), and PCHC (4.6 ppm)

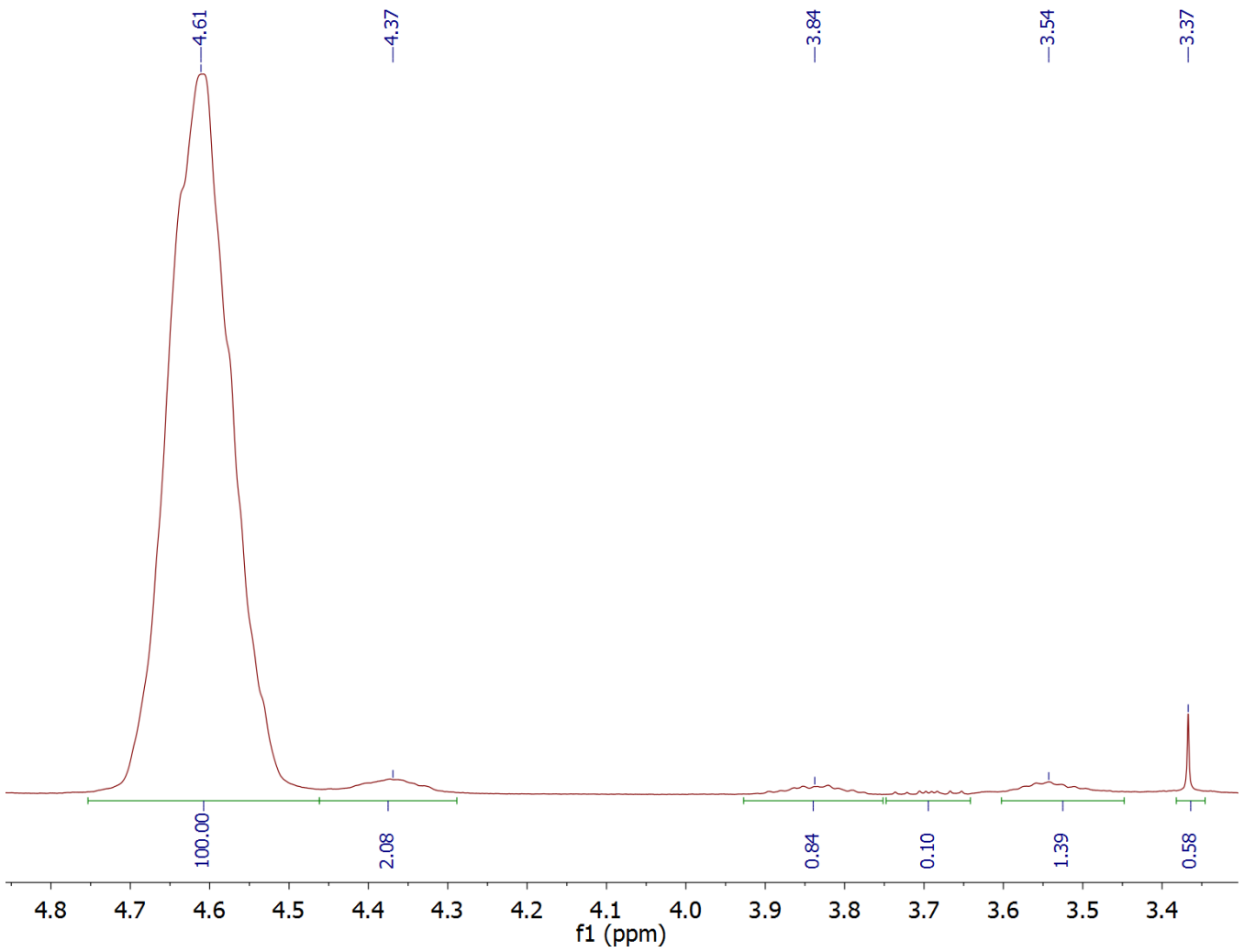

Figure A.62. ^{1}H NMR spectrum of purified PCHC in $CDCl_3$, 298 K

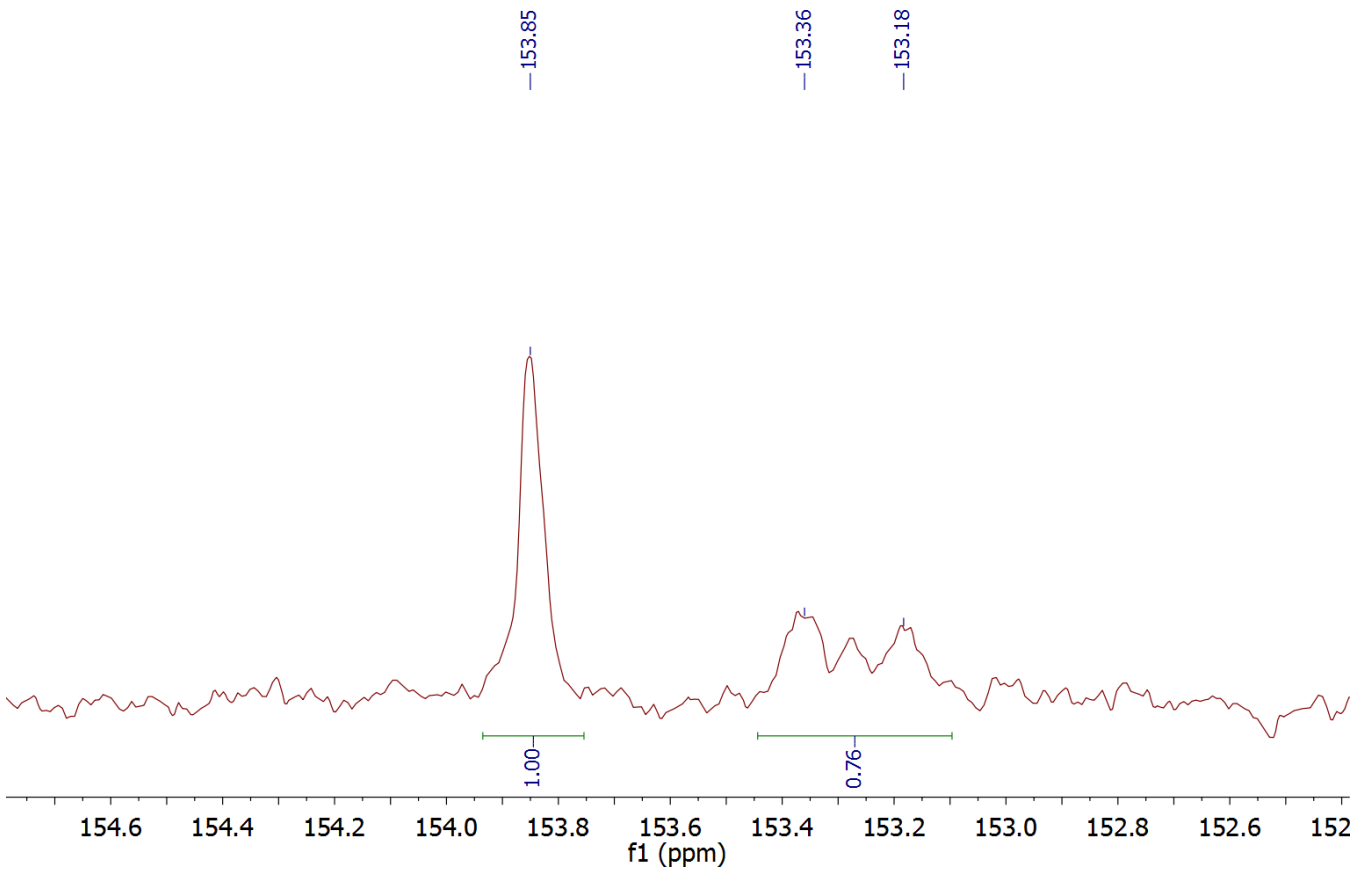

Figure A.63. $^{13}C\{^{1}H\}$ NMR spectrum of purified PCHC in $CDCl_3$ showing the presence of both syndiotactic and isotactic chains

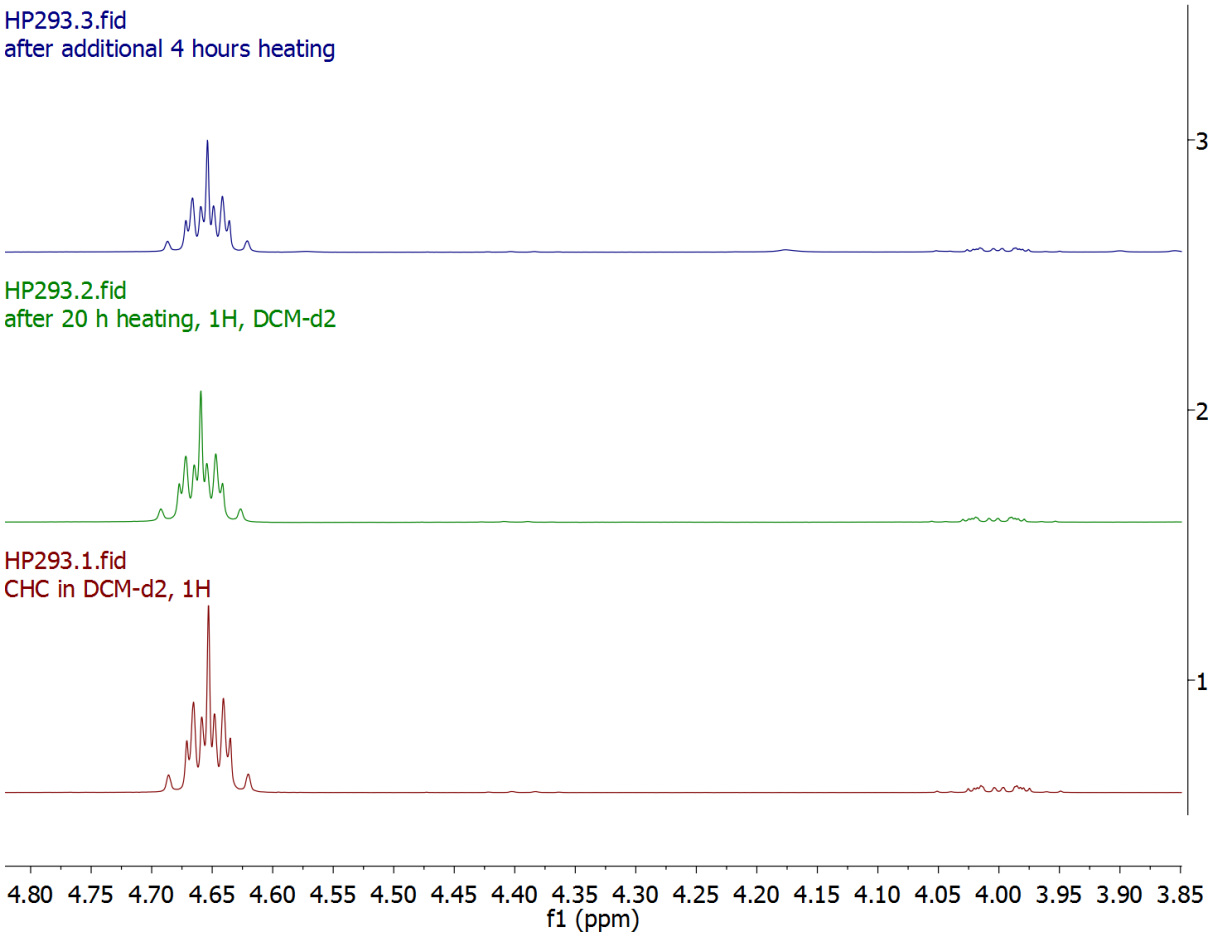

Figure A.64. ^{1}H NMR spectra of (a) CHC in CD_2Cl_2 showing the *trans* isomer as a minor side product (bottom), (b) CHC+**5.1** in CD_2Cl_2 after 20 h at 60 °C (middle), and (c) CHC+**5.1**+PPNCl in CD_2Cl_2 after 4 h at 60 °C (top). Relative integrations of the isomers did not change appreciably showing that CHC was not ring-opened by **5.1**.

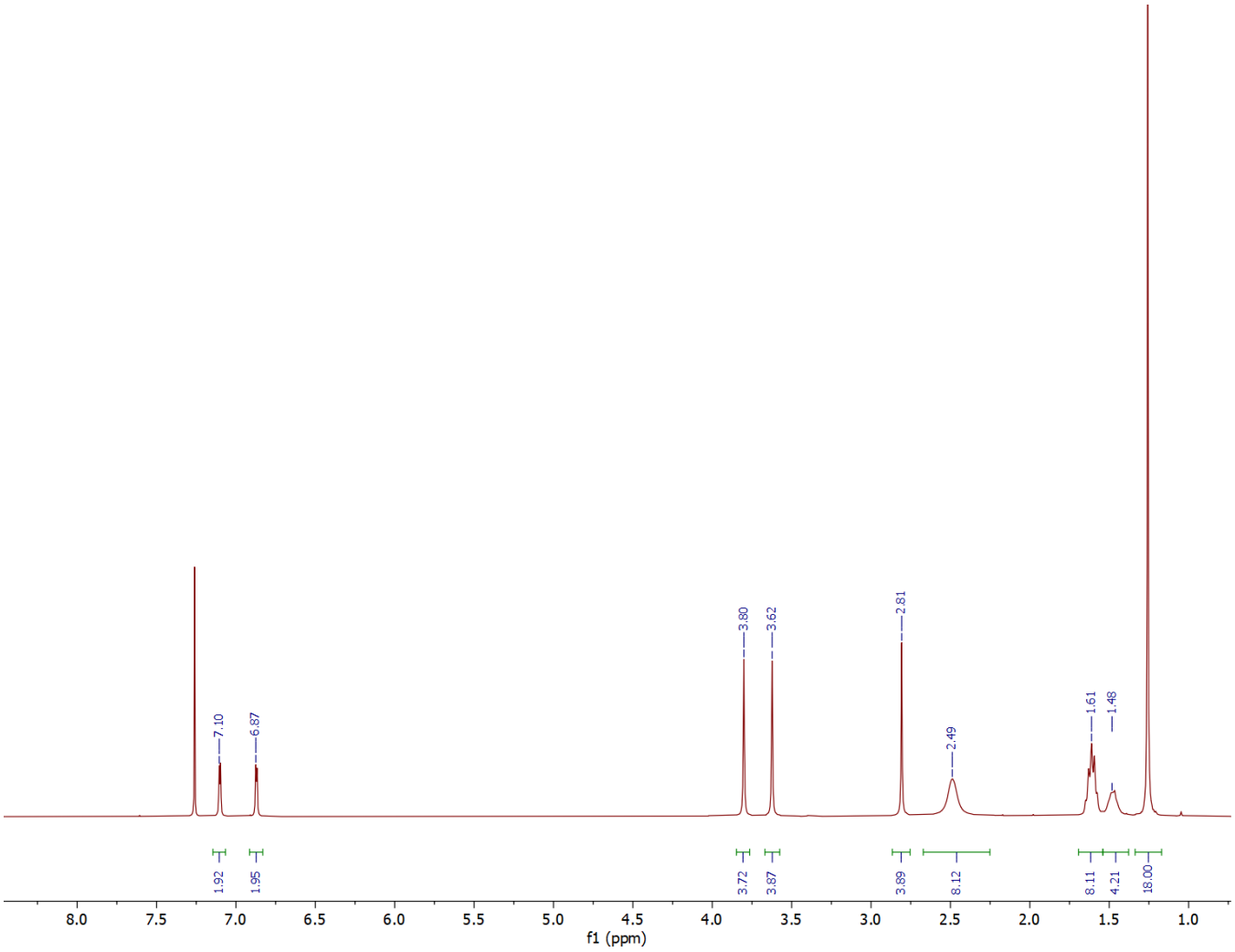

Figure A.65. ^{1}H NMR spectrum of H_2[**L8**] in $CDCl_3$, 298 K

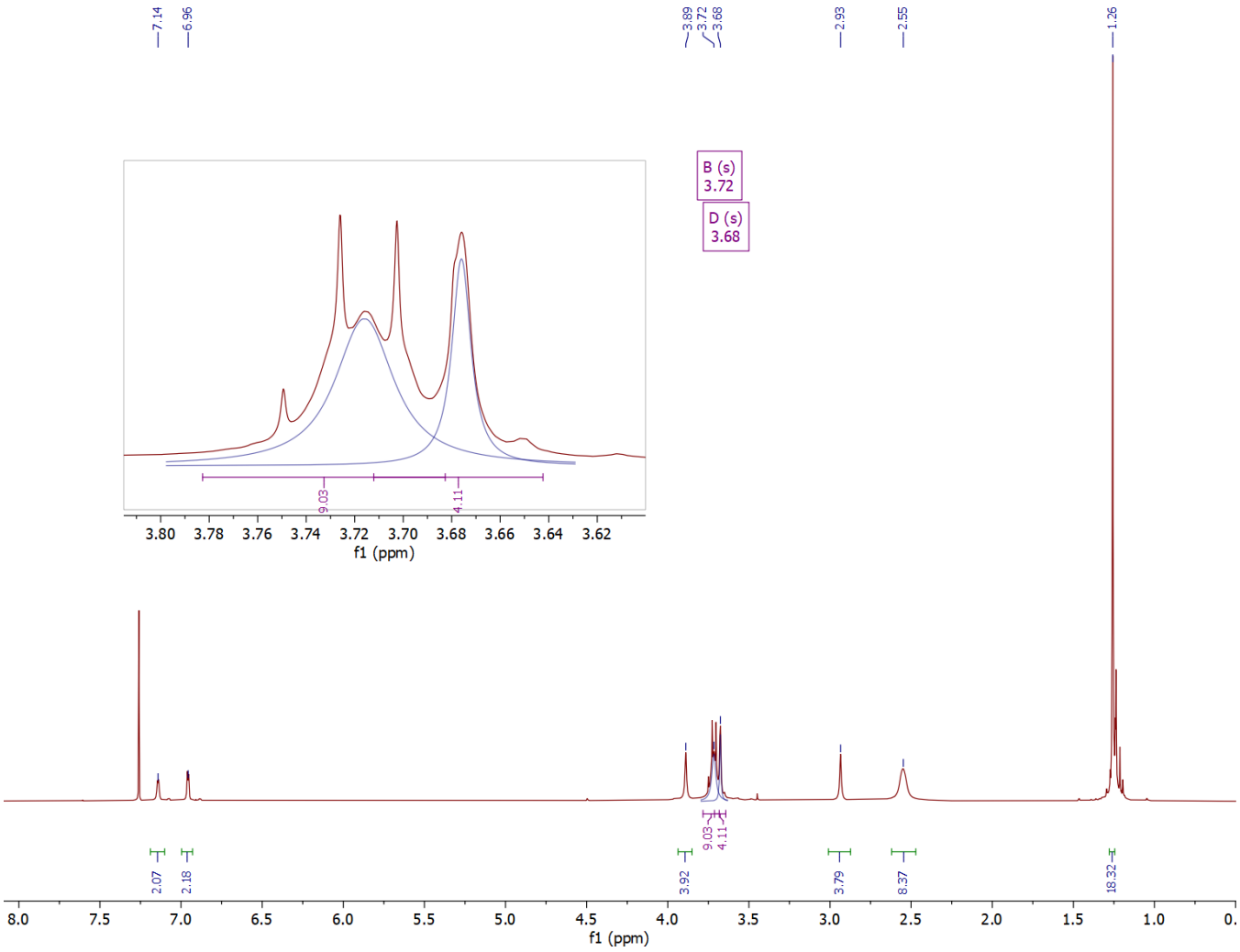

Figure A.66. ^{1}H NMR spectrum of H_2[**L9**] in $CDCl_3$, 298 K (residual EtOH resonances at 3.72 and 1.24 ppm)

Appendix B: Mass Spectrometry

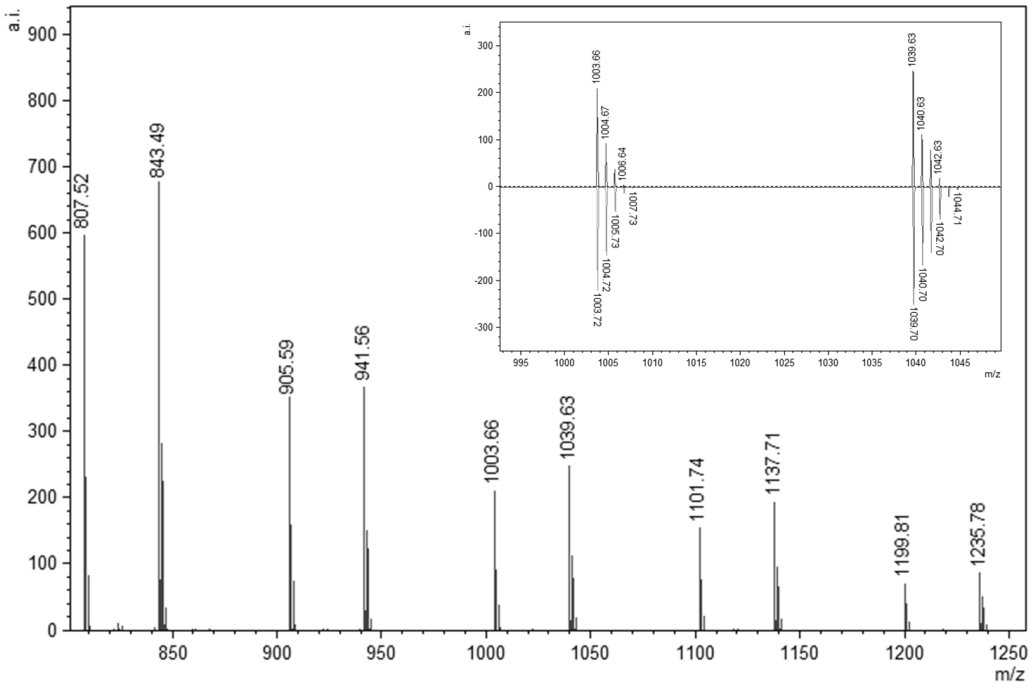

Figure B.1. MALDI-TOF mass spectrum of PCHO (Table 2.1, entry 9), inset showing isotopic match for ($\{CHO\}_{10}\cdot Na^+$) and ($Cl\{CHO\}_{10}H\cdot Na^+$)

Table B.1. ESI mass spectra (negative mode) and theoretical isotope patterns for complexes **3.4–3.7**

	Experimental	Theoretical
3.4	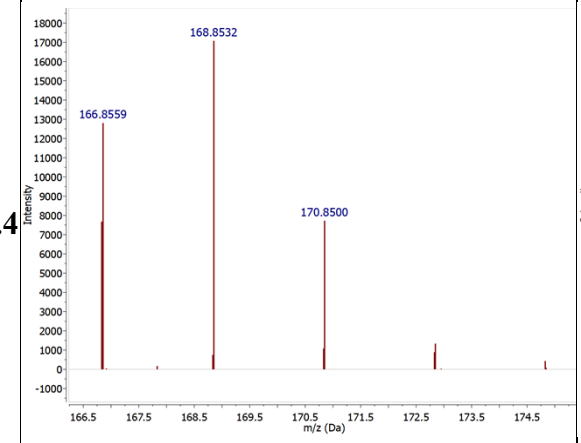	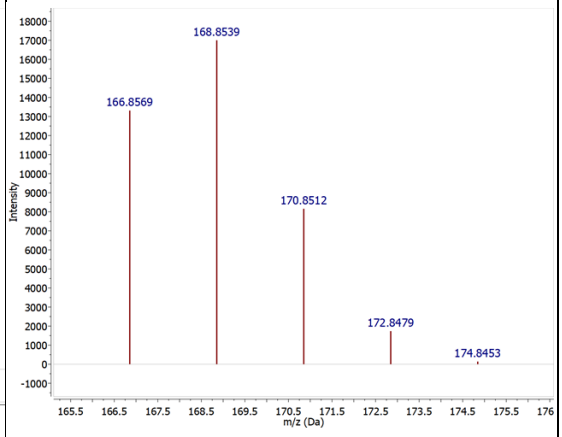
3.5	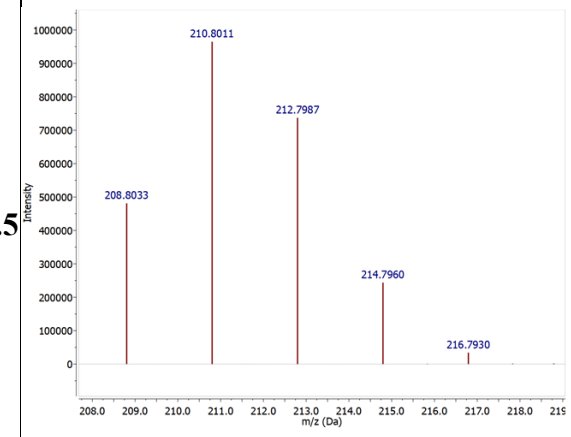	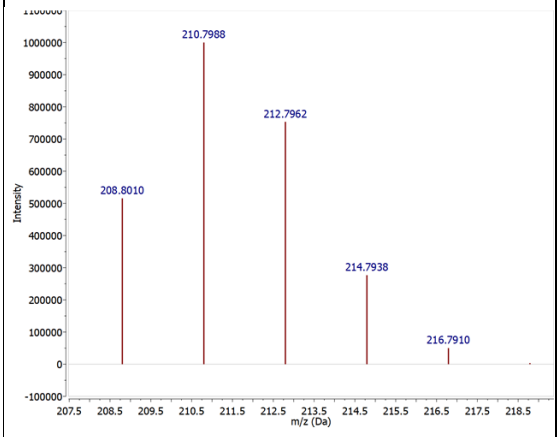

3.6	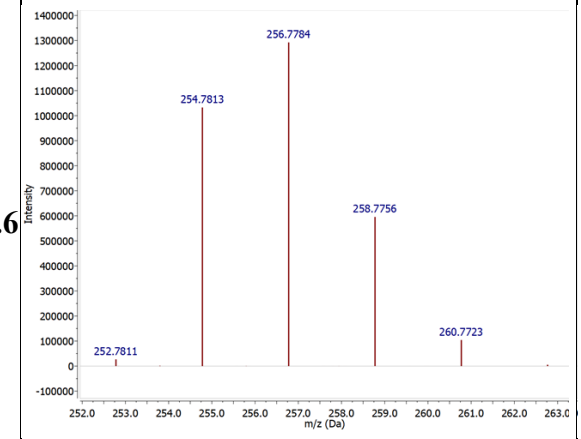 256.7784 254.7813 258.7756 260.7723 252.7811 Intensity m/z (Da)	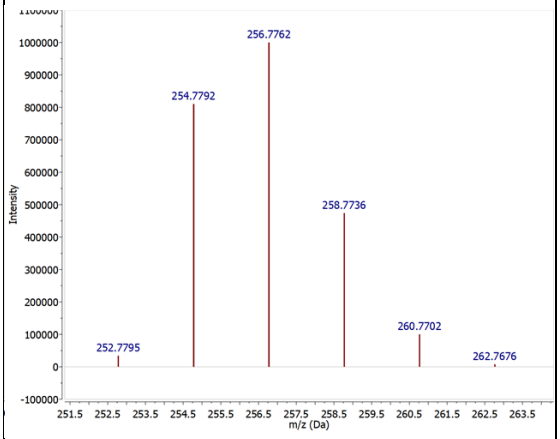 256.7762 254.7792 258.7736 260.7702 252.7795 262.7676 Intensity m/z (Da)
3.7	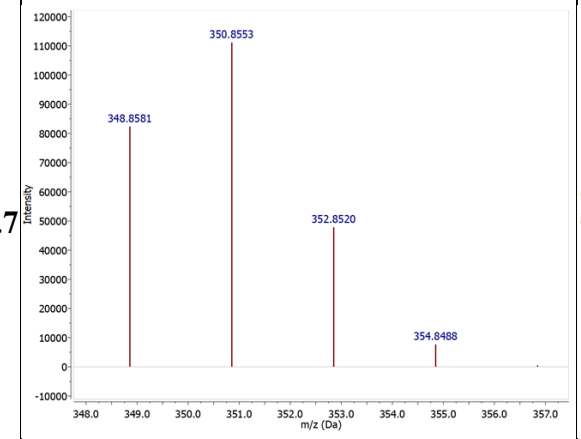 350.8553 348.8581 352.8520 354.8488 Intensity m/z (Da)	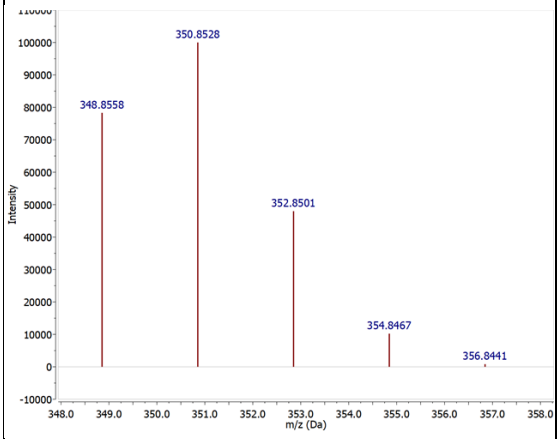 350.8528 348.8558 352.8501 354.8467 356.8441 Intensity m/z (Da)

Table B.2. ESI mass spectra (positive mode) and theoretical isotope patterns for complexes **3.1**, **3.5–3.7**

	Experimental	**Theoretical**
3.1	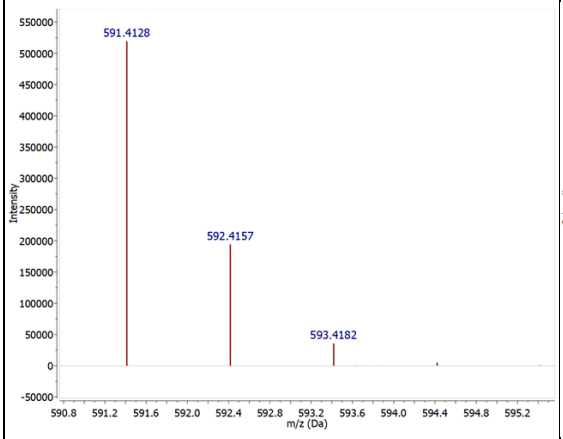	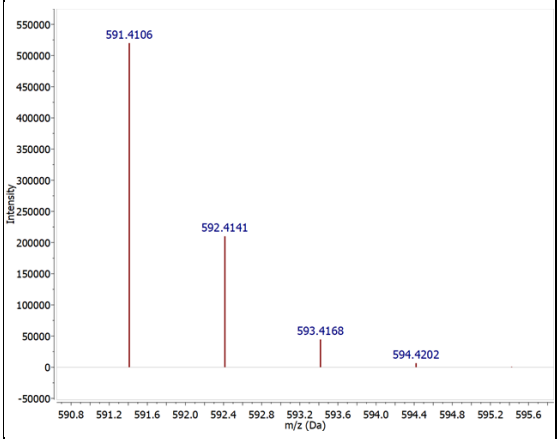
3.5	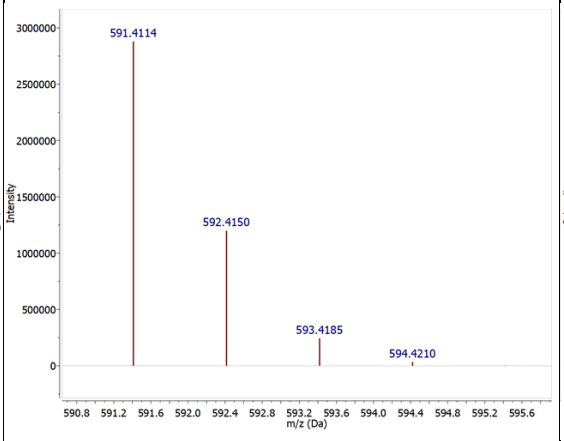	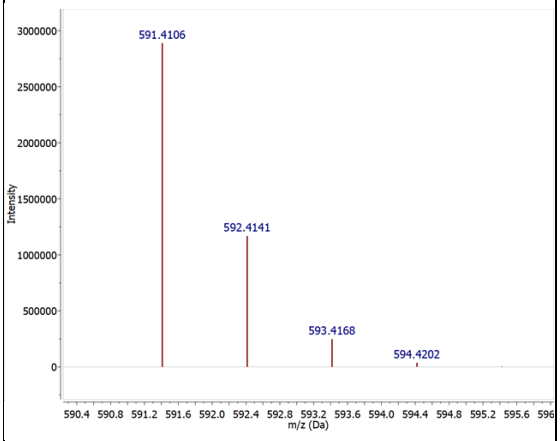

3.6	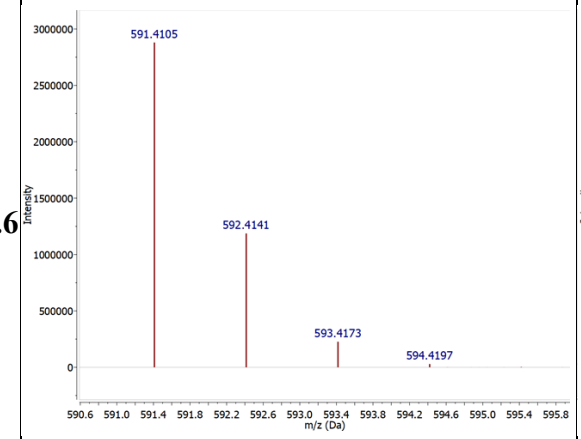 591.4105 592.4141 593.4173 594.4197 Intensity m/z (Da)	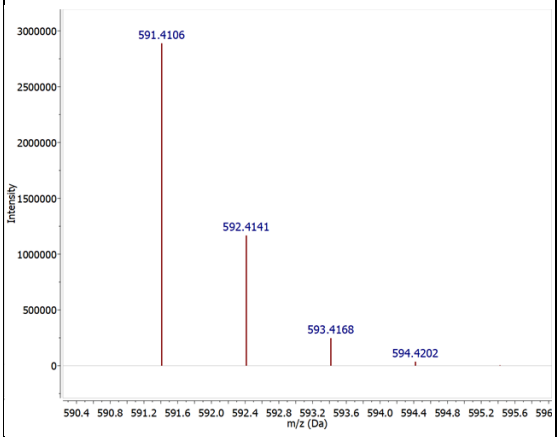 591.4106 592.4141 593.4168 594.4202 Intensity m/z (Da)
3.7	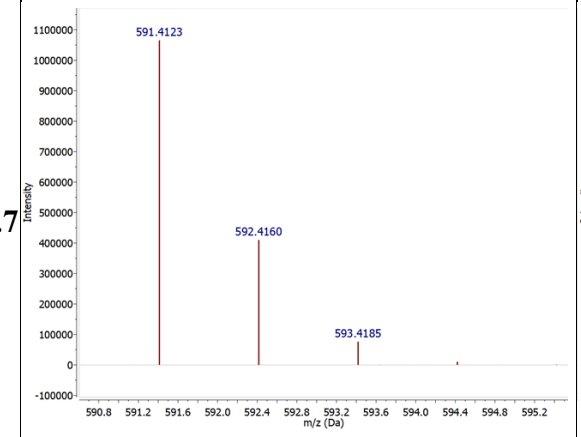 591.4123 592.4160 593.4185 Intensity m/z (Da)	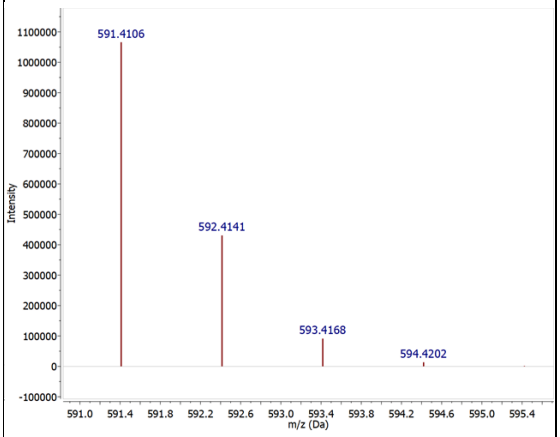 591.4106 592.4141 593.4168 594.4202 Intensity m/z (Da)

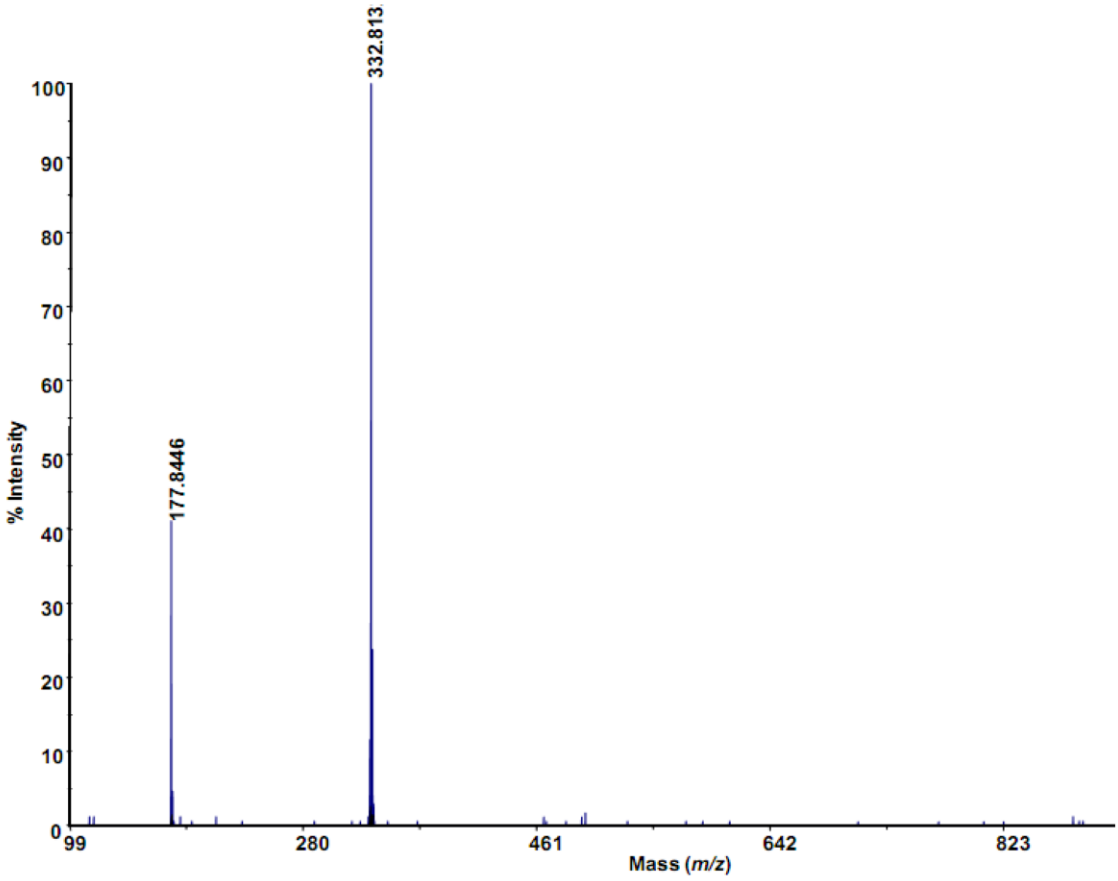

Figure B.2. MALDI-TOF mass spectrum of H[**L4**]

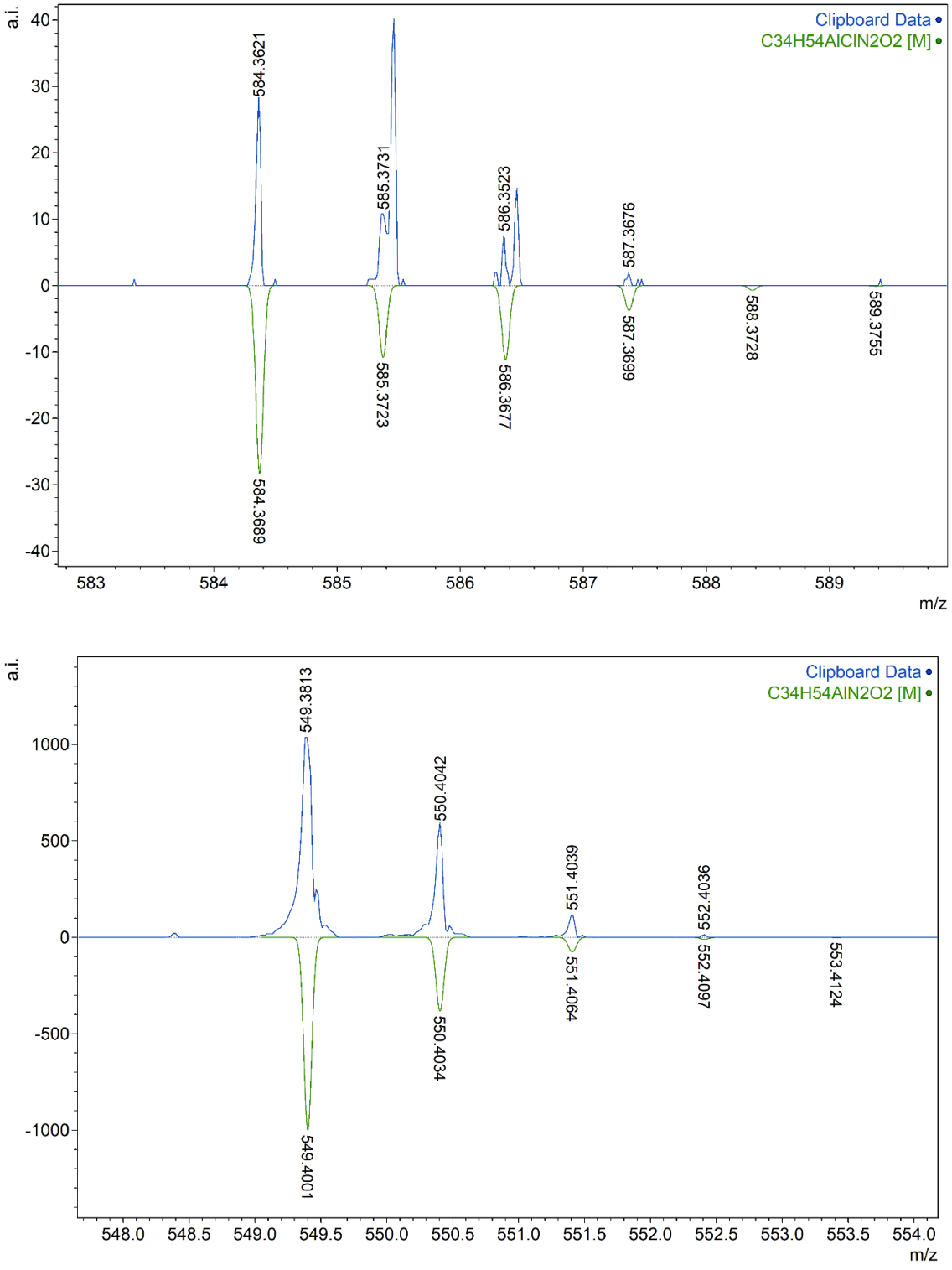

Figure B.3. MALDI-TOF MS spectra of **4.1**

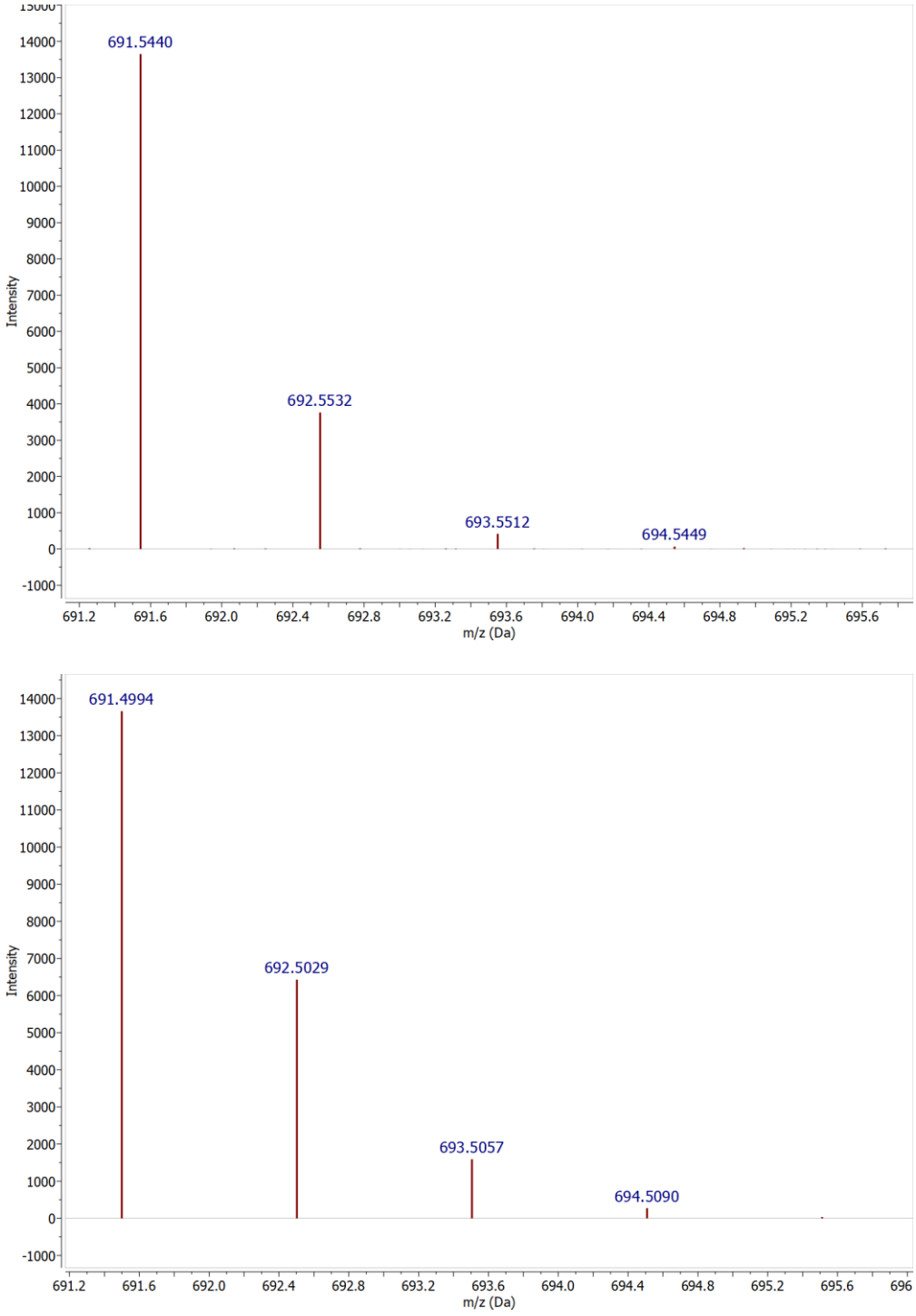

Figure B.4. MALDI-TOF mass spectra of **4.3** (experimental – top, theoretical – bottom)

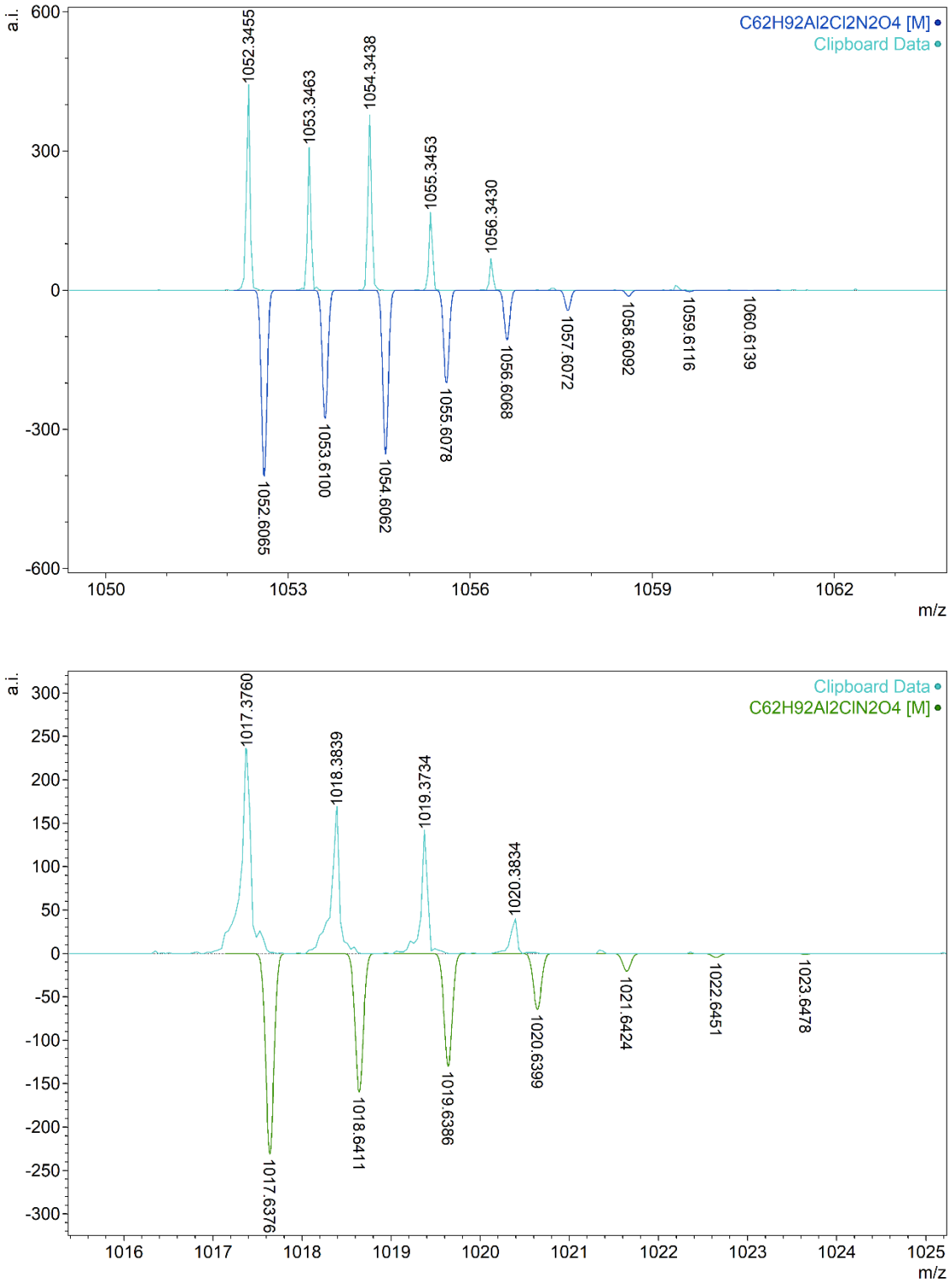

Figure B.5. MALDI-TOF mass spectra of **5.1**

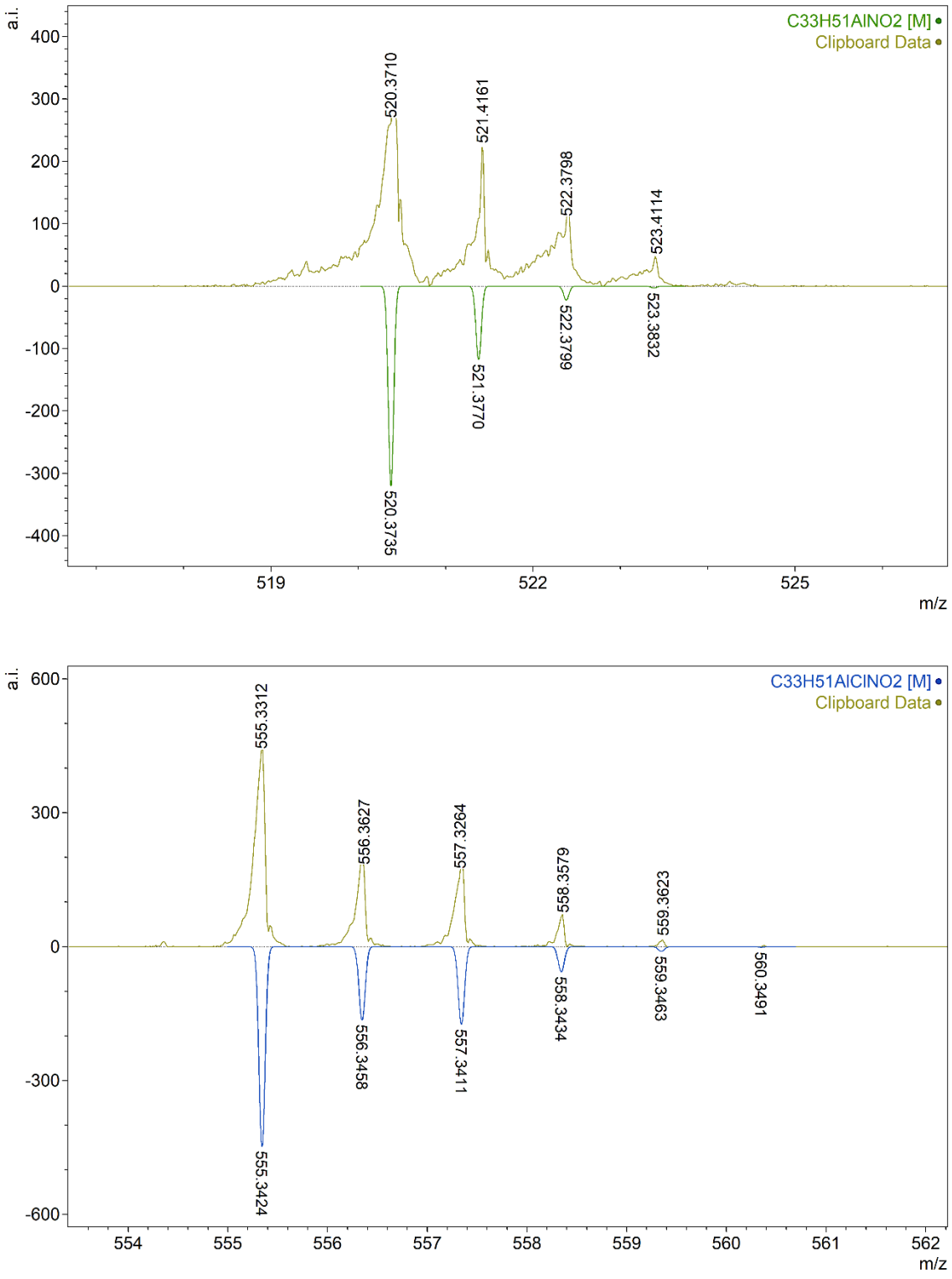

Figure B.6. MALDI-TOF mass spectra of **5.2**

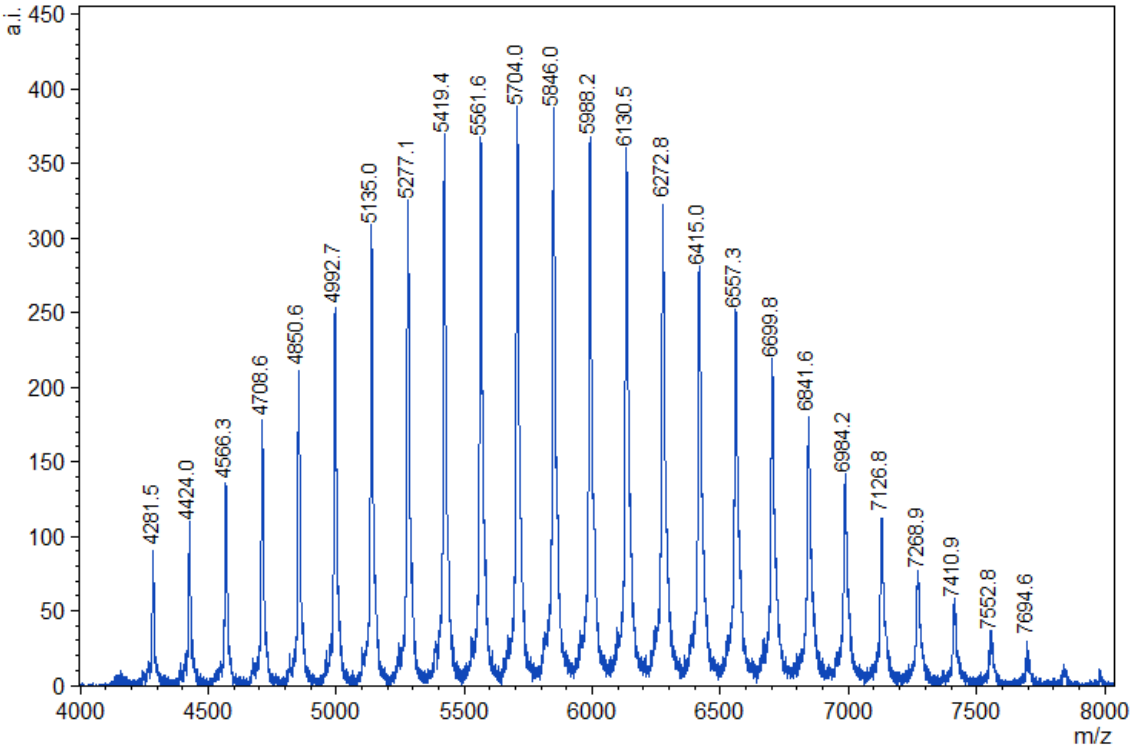

Figure B.7. Full MALDI-TOF MS spectrum of PCHC (Table 5.1, entry 2)

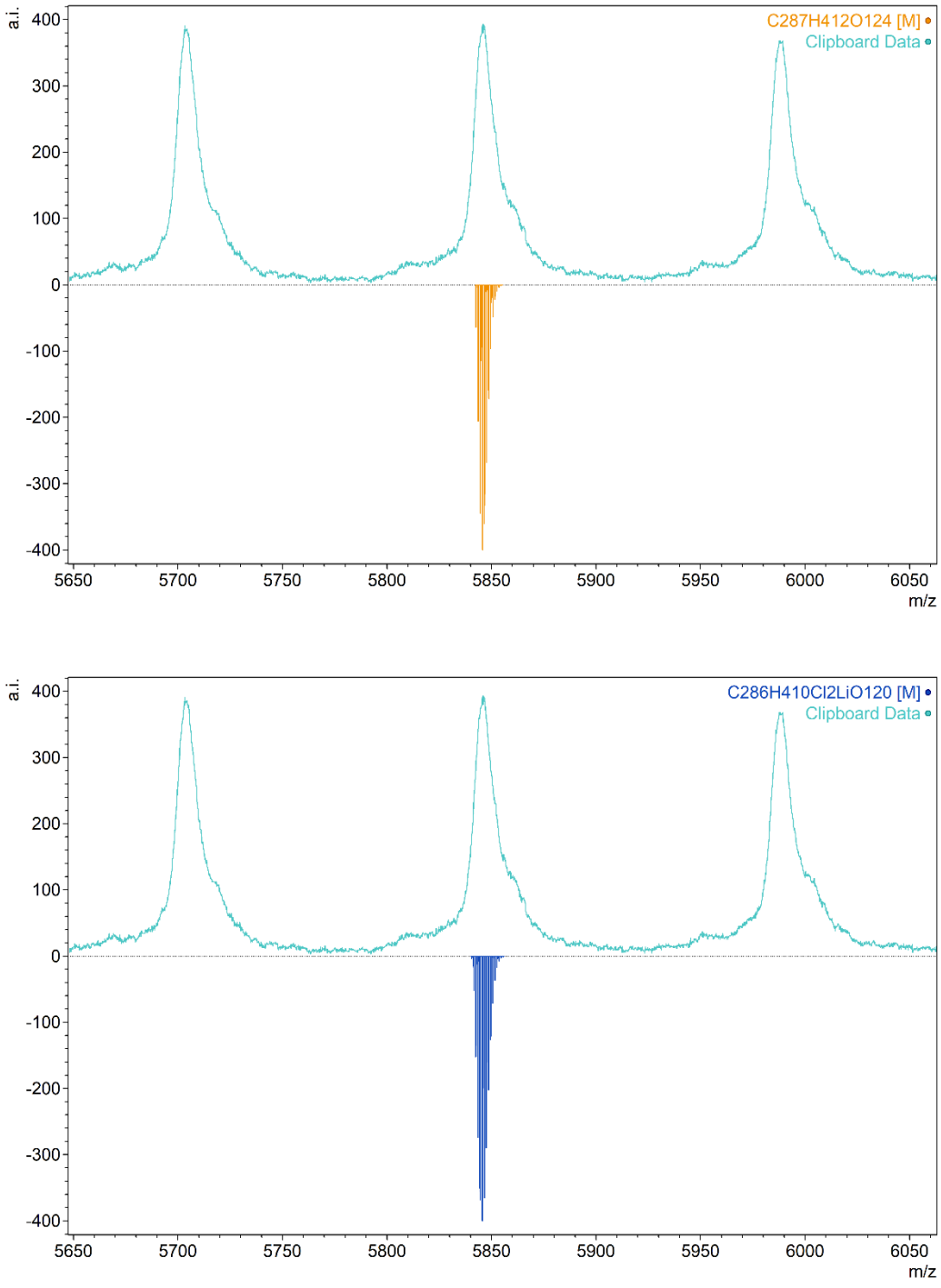

Figure B.8. Matching isotopic distributions for PCHC (Table 5.1, entry 2) showing protonated cyclic PCHC (top) and lithiated chloride-capped linear PCHC chains (bottom)

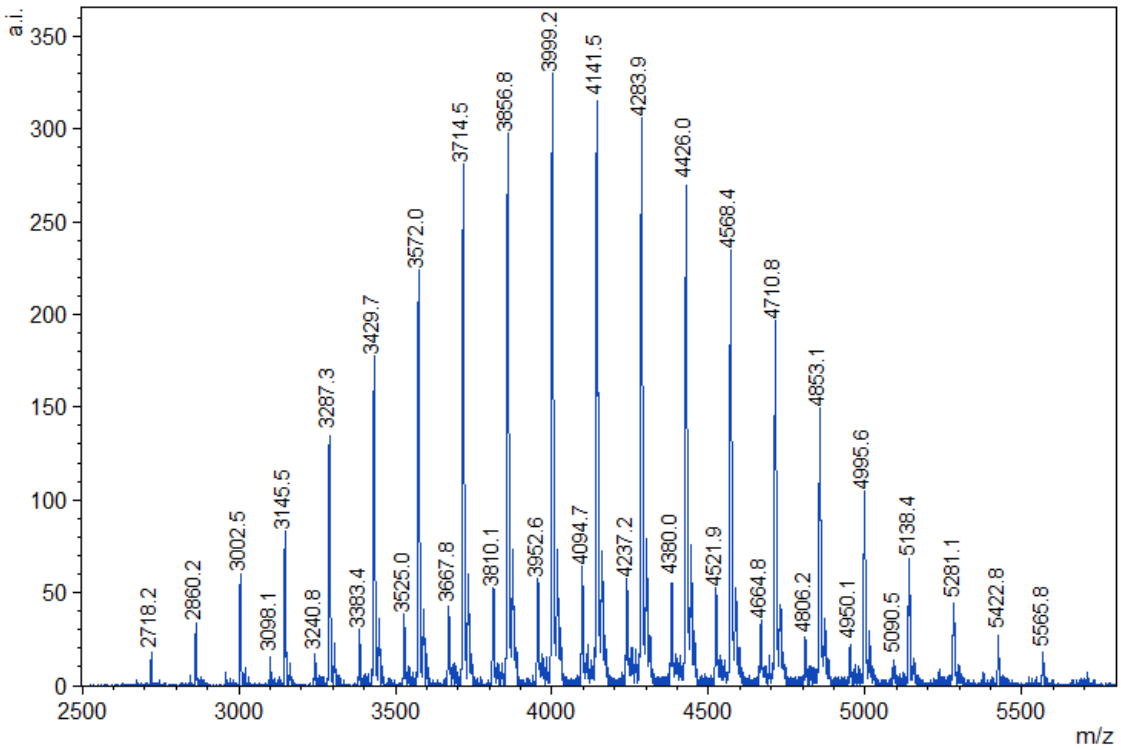

Figure B.9. Full MALDI-TOF MS spectrum of PCHC (Table 5.1, entry 4). Note: the second minor distribution residing to the right of the main peak is not labelled

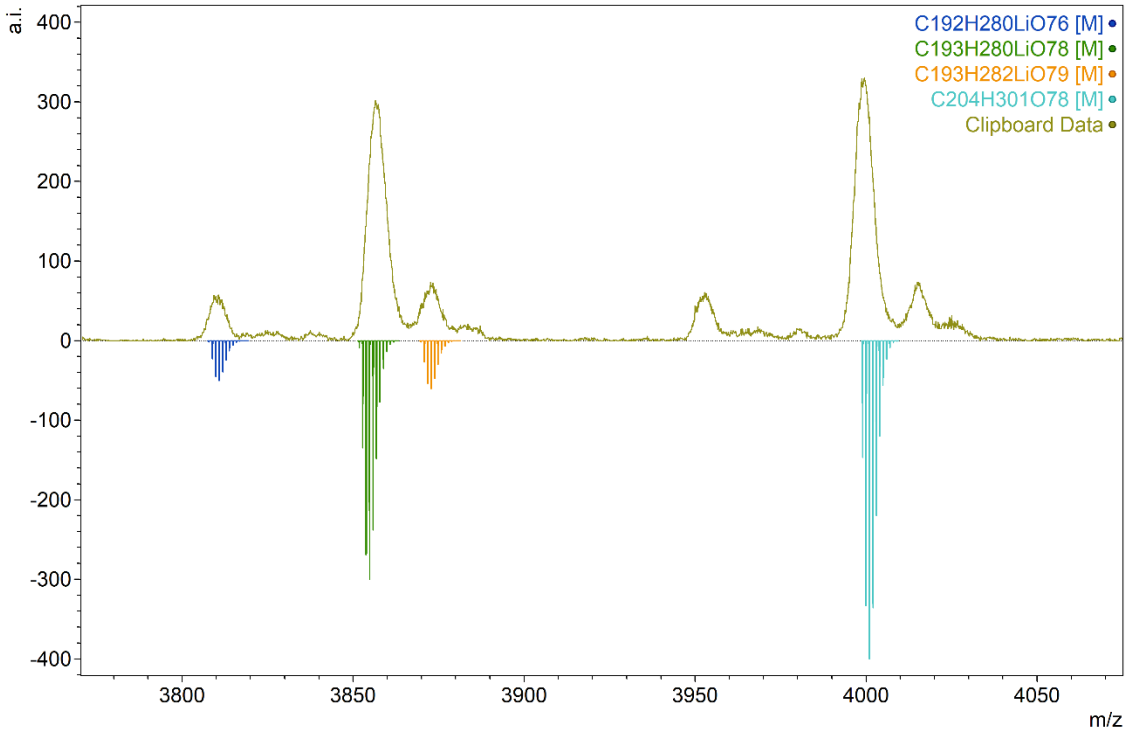

Figure B.10. Matching isotopic distributions for PCHC (Table 5.1, entry 4) showing lithiated cyclic PCHC (green and dark blue), lithiated hydroxyl-capped linear PCHC (orange), and protonated cyclic PCHC (light blue)

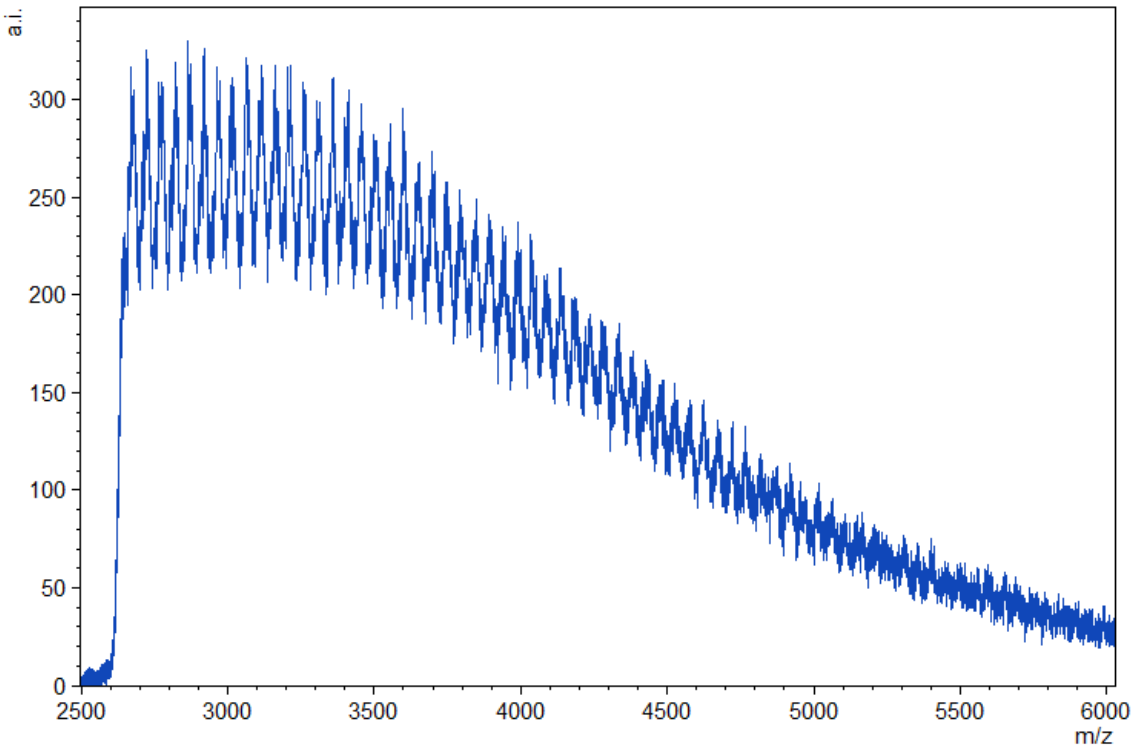

Figure B.11. Full MALDI-TOF MS spectrum of copolymer (Table 5.1, entry 3)

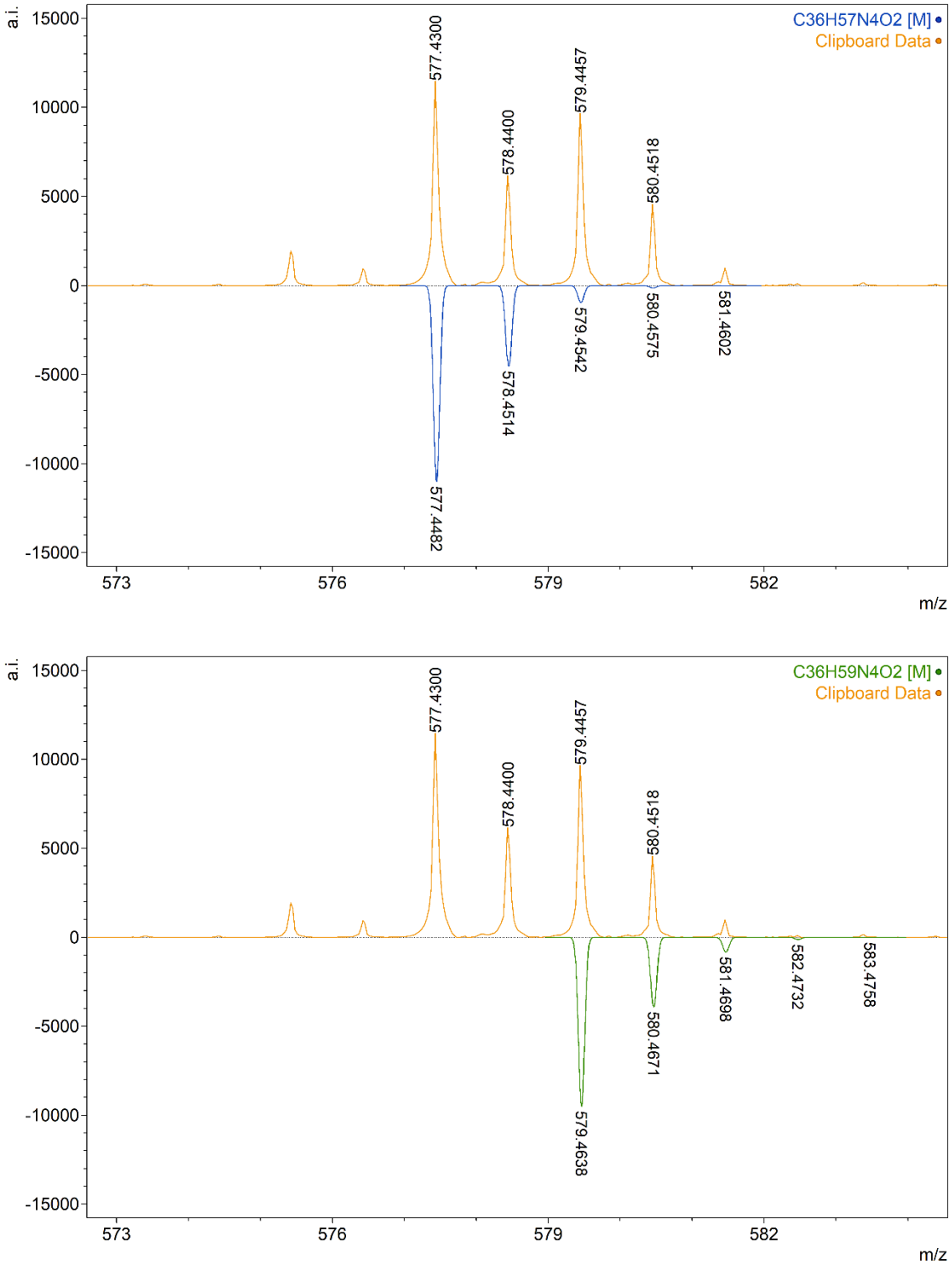

Figure B.12. MALDI-TOF mass spectra of H_2[**L8**]

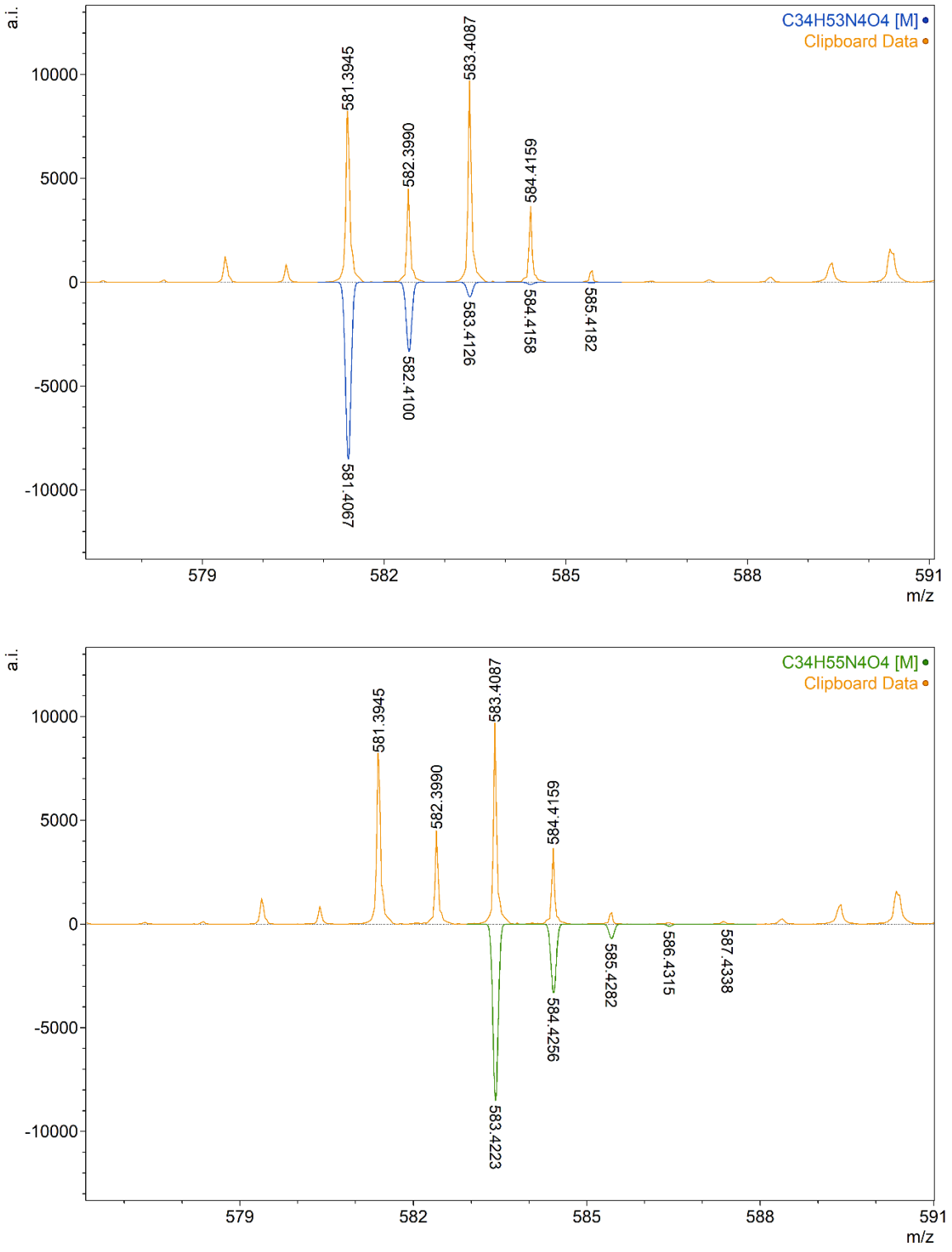

Figure B.13. MALDI-TOF mass spectra of H_2[**L9**]

Appendix C: Crystallography

Table C.1. Crystallographic and structure refinement data for complexes **3.1**, **3.2**, **3.5**, and **3.6**

Complex	**3.1**	**3.2**	**3.5**	**3.6**
Chemical formula	$C_{75}H_{116}Al_2Cl_8N_4O_6$	$C_{38}H_{61}Al_2Cl_3N_2O_3$	$C_{57}H_{80}AlCl_4GaN_2O_3$	$C_{57}H_{80}AlCl_4InN_2O_3$
Formula weight	1507.27	754.19	1079.73	1124.83
Temperature/K	100	100.15	173(2)	293(2)
Crystal system	orthorhombic	triclinic	triclinic	triclinic
Space group	Fdd2	P-1	P-1	P-1
a/Å	51.6345(14)	10.8793(6)	10.8883(3)	10.9679(3)
b/Å	28.5858(6)	14.2859(5)	16.1767(5)	16.0810(4)
c/Å	12.0220(4)	16.5954(7)	16.9669(5)	17.0324(5)
α/°	90	96.623(3)	103.973(3)	76.239(2)
β/°	90	98.586(4)	98.658(2)	81.201(2)
γ/°	90	104.093(4)	90.135(2)	89.881(2)
Volume/Å^3	17744.6(8)	2442.5(2)	2864.68(15)	2881.68(14)
Z	8	2	2	2
D_c/g cm^{-3}	1.128	1.025	1.252	1.296
Radiation type	MoKα (λ = 0.71073)	MoKα (λ = 0.71073)	MoKα (λ = 0.71073)	MoKα (λ = 0.71073)
μ(MoKα)/mm^{-1}	0.320	0.254	0.725	0.653
F(000)	6432.0	808.0	1144.0	1180.0
Reflections measured	58370	30518	37644	37818
Unique reflections	8422	8556	10884	10952
R_{int}	0.1335	0.1163	0.0590	0.0405
R_1 (all)	0.0998	0.1198	0.0858	0.0610
$wR(F^2)$ (all)	0.2072	0.2360	0.1661	0.1264
R_1 (I > 2 σ (I))[a]	0.0885	0.0865	0.0663	0.0533
$wR(F^2)$ (I > 2 σ (I))[b]	0.1965	0.2158	0.1493	0.1201
Goodness of fit on F^2	1.101	1.024	1.082	1.095
CCDC Ref.	1869236	1849724	1861938	1849725

Table C.2. Crystallographic and structure refinement data for compounds H[**L4**], **4.1**, **4.3**, and **4.4**

Compounds	H[**L4**]	**4.1**	**4.3**	**4.4**
Chemical formula	$C_{21}H_{35}NO_2$	$C_{48}H_{70}AlClN_2O_2$	$C_{42}H_{68}N_2O_2AlCl$	$C_{75}H_{111}Al_2Cl_2N_4O_4$
Formula weight	333.51	769.49	695.41	1257.53
Temperature/K	123	100	293(2)	100
Crystal system	monoclinic	monoclinic	triclinic	triclinic
Space group	$P2_1/c$	$P2_1/n$	P-1	P-1
a/Å	12.013(4)	13.1378(4)	11.4893(3)	7.7750(2)
b/Å	17.863(6)	24.9763(6)	13.7084(4)	11.1513(3)
c/Å	9.836(3)	14.4263(4)	15.1276(3)	21.4322(5)
α/°	90	90	111.101(2)	75.708(2)
β/°	101.484(5)	110.413(3)	105.252(2)	89.494(2)
γ/°	90	90	93.044(2)	74.480(2)
Volume/Å^3	2068.5(12)	4436.5(2)	2115.43(10)	1731.77(8)
Z	4	4	2	1
D_c/g cm^{-3}	1.071	1.152	1.092	1.206
Radiation type	MoKα (λ = 0.71075)	MoKα (λ = 0.71073)	MoKα (λ = 0.71073)	MoKα (λ = 0.71073)
μ (MoKα)/mm^{-1}	0.067	0.145	0.145	0.171
F(000)	736	1672.0	760.0	681.0
Reflections measured	21073	56957	27634	22667
Unique reflections	4291	8121	8009	6588
R_{int}	0.0239	0.1011	0.0425	0.0403
R_1 (all)	0.0529	0.1157	0.0604	0.0675
$wR(F^2)$ (all)	0.1276	0.1875	0.1249	0.1563
R_1 (I > 2 σ (I))[a]	0.0497	0.0981	0.0491	0.0598
$wR(F^2)$ (I > 2 σ (I))[b]	–	0.1769	0.1161	0.1499
Goodness of fit on F^2	1.112	1.181	1.058	1.086
CCDC Ref.	1912327	1936692	1936648	1936691

Table C.3. Crystallographic and structure refinement data for complexes **5.1** and **5.2**

Complex	**5.1**	**5.2**
Chemical formula	$C_{64}H_{96}Al_2Cl_6N_2O_4$	$C_{33}H_{51}AlClNO_2$
Formula weight	1224.08	556.17
Temperature/K	100	100
Crystal system	monoclinic	orthorhombic
Space group	$P2_1/c$	$P2_12_12_1$
a/Å	10.3454(3)	9.5210(2)
b/Å	11.7689(3)	12.1315(2)
c/Å	28.1885(8)	28.1492(5)
α/°	90	90
β/°	96.201(3)	90
γ/°	90	90
Volume/Å^3	3412.00(17)	3251.35(10)
Z	2	4
D_c/g cm^{-3}	1.191	1.136
Radiation type	MoKα (λ = 0.71073)	MoKα (λ = 0.71073)
μ (MoKα)/mm^{-1}	0.322	0.173
F(000)	1308.0	1208.0
Reflections measured	51353	43577
Unique reflections	8869	6176
R_{int}	0.0397	0.1053
R_1 (all)	0.0583	0.0702
$wR(F^2)$ (all)	0.1323	0.1557
R_1 (I > 2 σ (I))[a]	0.0491	0.0657
$wR(F^2)$ (I > 2 σ (I))[b]	0.1258	0.1517
Goodness of fit on F^2	1.053	1.108

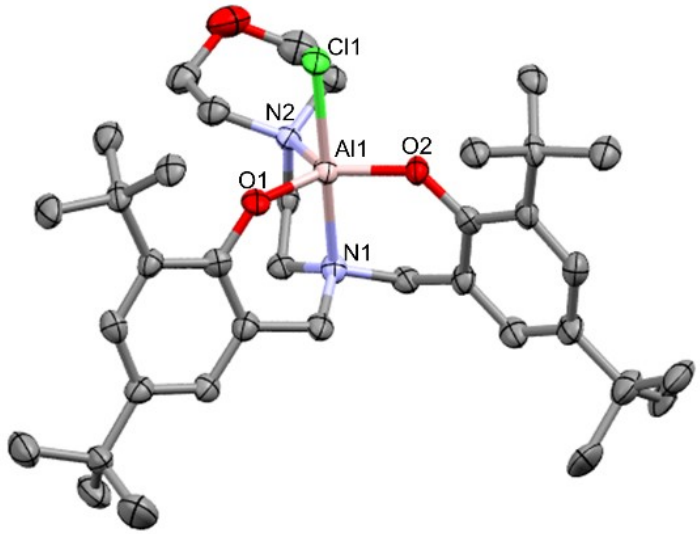

Figure C.1. Molecular structure and partial numbering of **3.1** (thermal ellipsoids drawn at 50% probability; H atoms, two co-crystallized CH_2Cl_2 molecules, and one disordered *tert*-butyl group excluded for clarity).

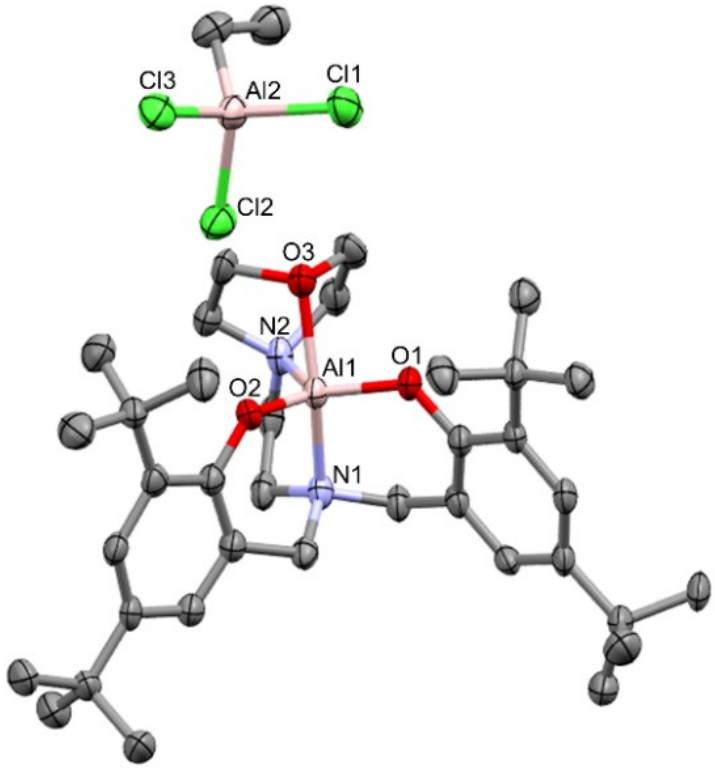

Figure C.2. Molecular structure and partial numbering of **3.2** (thermal ellipsoids drawn at 50% probability; H atoms excluded for clarity). Selected bond distances (Å) and angles (°): Al(1)–O(1), 1.729(2); Al(1)–O(2), 1.726(3); Al(1)–O(3), 2.031(3); Al(1)–N(1), 2.000(3); Al(1)–N(2), 2.008(3); O(1)–Al(1)–O(3), 90.50(11); O(1)–Al(1)–N(1), 97.11(12); O(1)–Al(1)–N(2), 116.75(13); O(2)–Al(1)–O(1), 124.15(13); O(2)–Al(1)–O(3), 95.28(12); O(2)–Al(1)–N(1), 98.40(13); O(2)–Al(1)–N(2), 117.98(13); N(1)–Al(1)–O(3), 156.83(13); N(1)–Al(1)–N(2), 84.29(13); N(2)–Al(1)–O(3), 72.77(12).

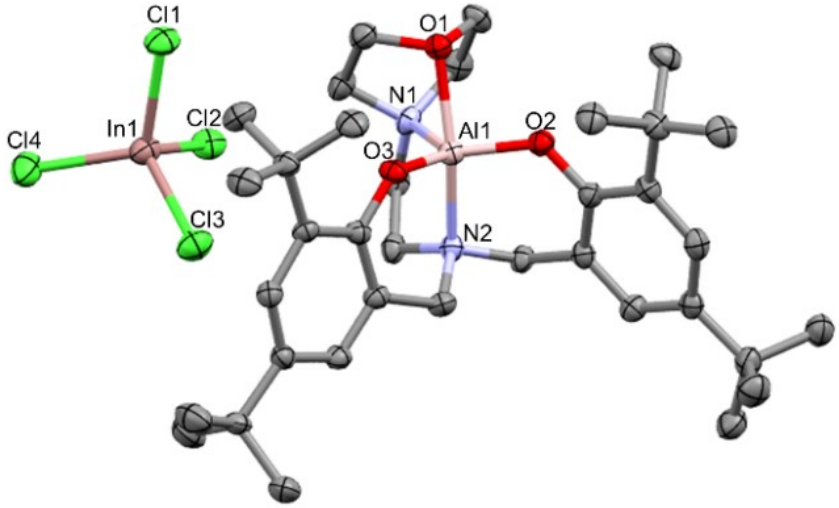

Figure C.3. Molecular structure and partial numbering of **3.6** (thermal ellipsoids drawn at 50% probability; H atoms and three co-crystallized toluene molecules excluded for clarity). Selected bond distances (Å) and angles (°): Al(1)–O(1), 2.024(2); Al(1)–O(2), 1.723(2); Al(1)–O(3), 1.719(2); Al(1)–N(1), 2.002(3); Al(1)–N(2), 1.994(3); O(2)–Al(1)–O(1), 90.26(10); O(2)–Al(1)–N(1), 117.34(11); O(2)–Al(1)–N(2), 97.96(11); O(3)–Al(1)–O(1), 94.69(10); O(3)–Al(1)–O(2), 125.14(11); O(3)–Al(1)–N(1), 116.26(11); O(3)–Al(1)–N(2), 97.54(11); N(1)–Al(1)–O(1), 72.84(10); N(2)–Al(1)–O(1), 157.49(11); N(2)–Al(1)–N(1), 84.80(11).

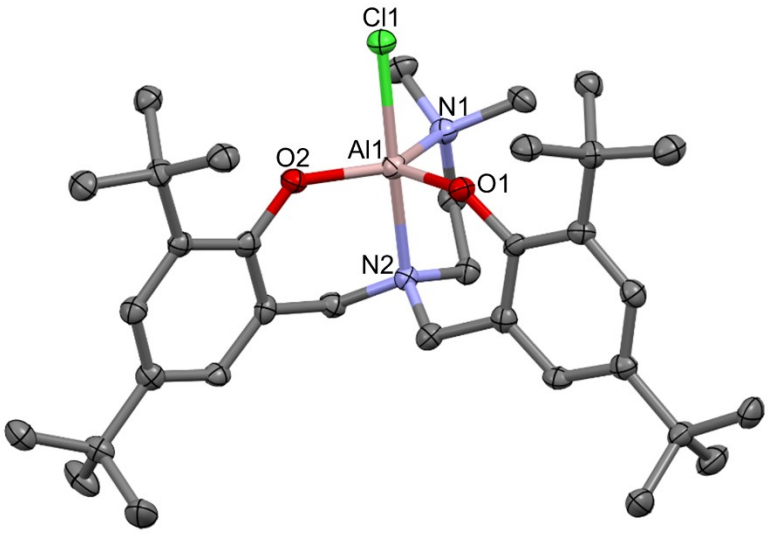

Figure C.4. Molecular structure and partial numbering of **4.1** (thermal ellipsoids drawn at 50% probability; H atoms and two co-crystallized toluene molecules excluded for clarity). Selected bond distances (Å) and angles (°): Cl(1)–Al(1), 2.2532(13); Al(1)–O(1), 1.752(3); Al(1)–O(2), 1.745(3); Al(1)–N(1), 2.069(3); Al(1)–N(2), 2.116(3); O(1)–Al(1)–Cl(1), 93.88(9); O(1)–Al(1)–N(1), 113.11(12); O(1)–Al(1)–N(2), 91.21(12); O(2)–Al(1)–Cl(1), 91.05(9); O(2)–Al(1)–O(1), 124.52(13); O(2)–Al(1)–N(1), 122.09(13); O(2)–Al(1)–N(2), 90.72(12); N(1)–Al(1)–Cl(1), 90.40(9); N(1)–Al(1)–N(2), 82.40(12); N(2)–Al(1)–Cl(1), 172.39(10).

Appendix D: Kinetic Plots

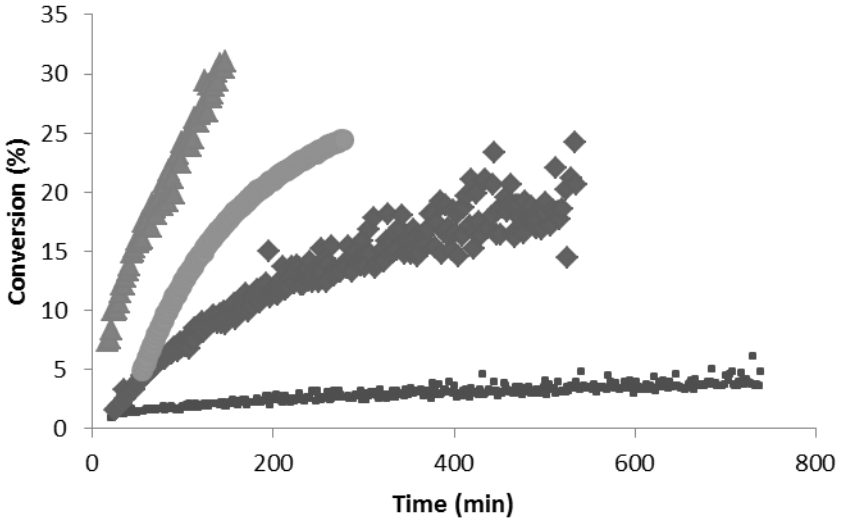

Figure D.1. Plot of CHO conversion versus time for the polymerization of CHO using **2.2** at various concentrations (0.4 mol%, 0.2 mol%, 0.1 mol%, 0.01 mol%). Data collected *via* ^{1}H NMR spectroscopy using a co-axial NMR tube containing $CDCl_3$ for lock.

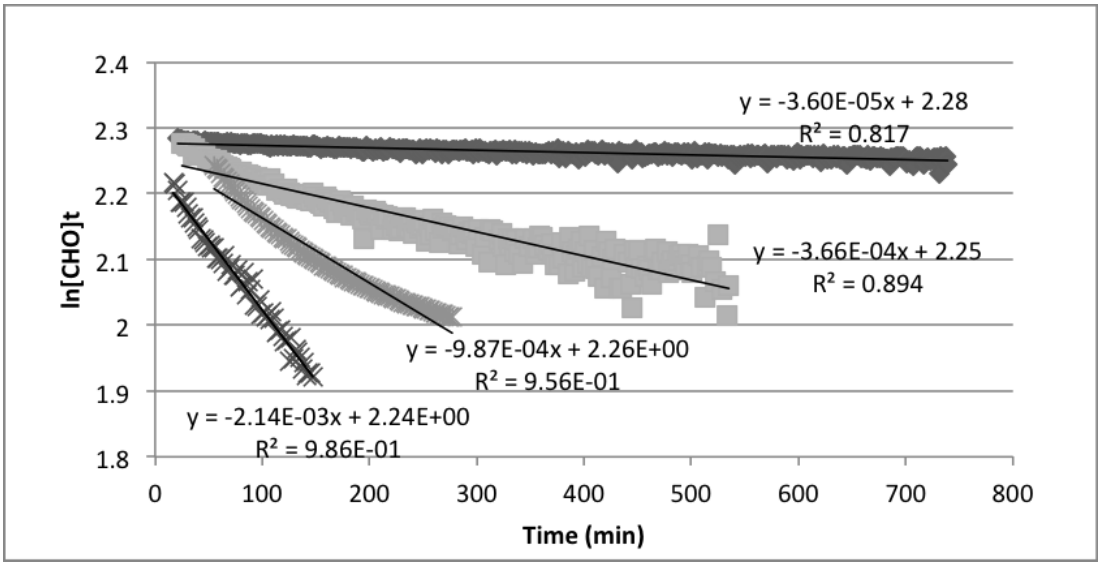

Figure D.2. Detailed plot of ln[CHO] against time at catalyst loadings 0.01, 0.1, 0.2, and 0.4 mol% using **2.2**.

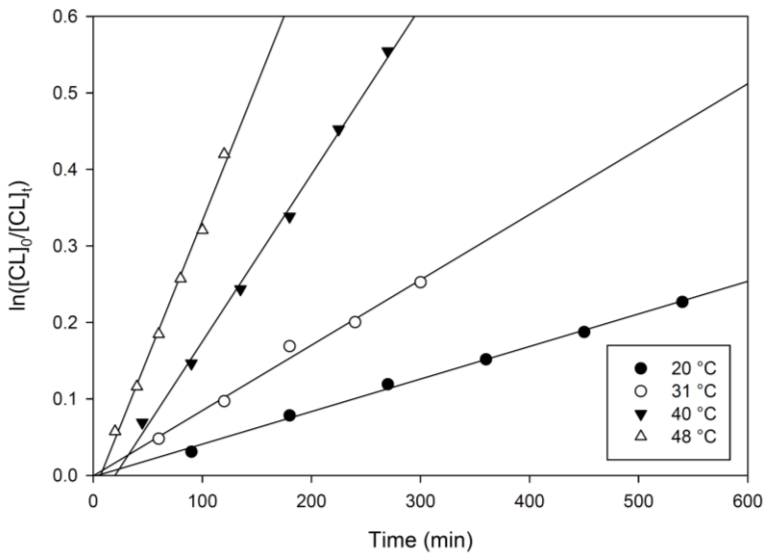

Figure D.3. Semilogarithmic plots of the monomer conversion stated as $\ln[CL]_0/[CL]_t$ versus the reaction time for the polymerization of ε-CL at different temperatures catalyzed by **3.5**/EtOH

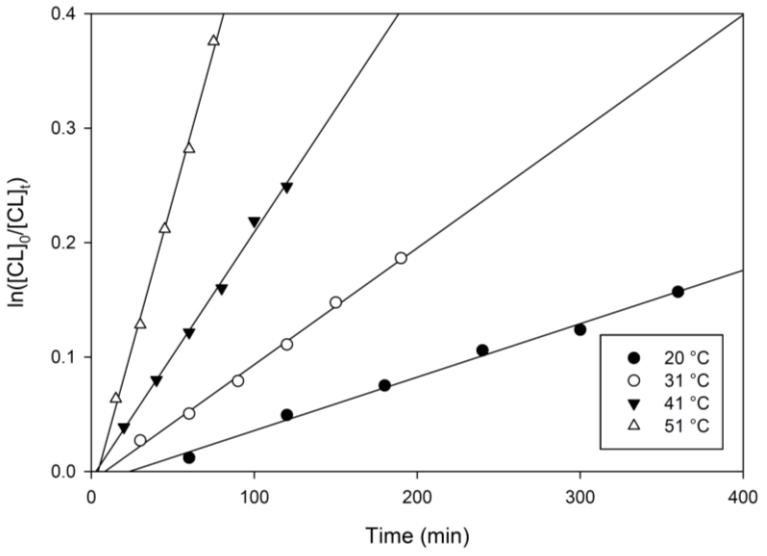

Figure D.4. Semilogarithmic plots of the monomer conversion stated as $\ln[CL]_0/[CL]_t$ versus the reaction time for the polymerization of ε-CL at different temperatures catalyzed by **3.6**/EtOH

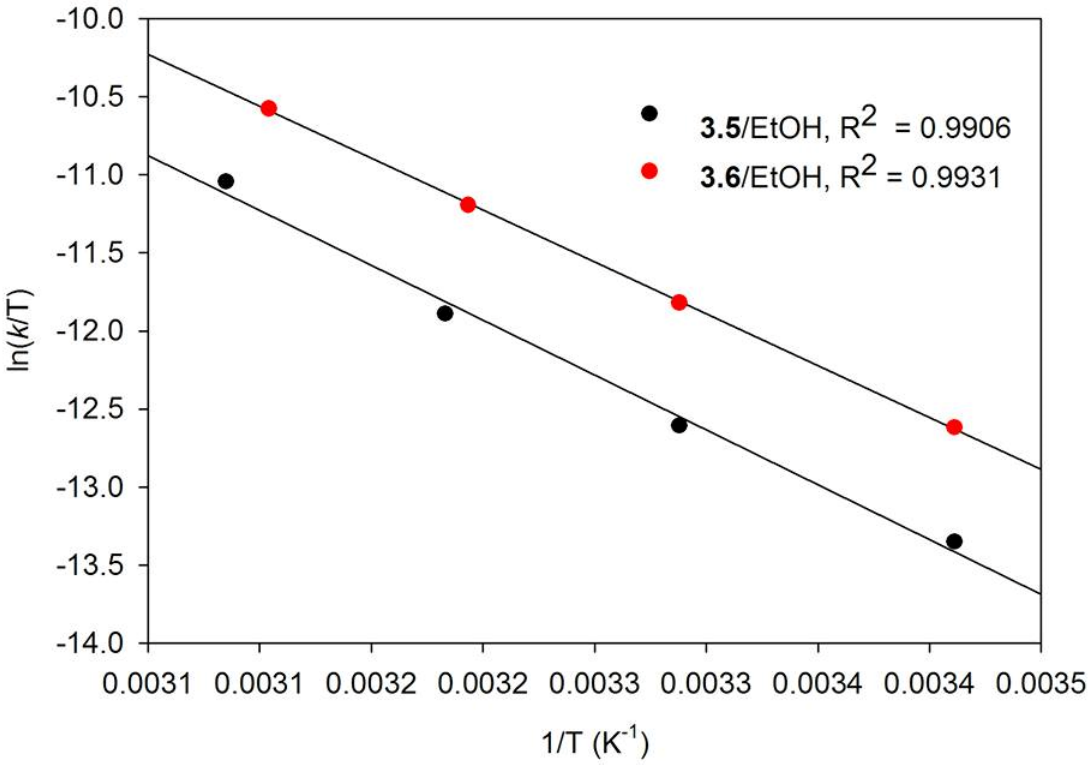

Figure D.5. Eyring plots for the polymerization of ε-CL catalyzed by (a) **3.5**/EtOH and (b) **3.6**/EtOH

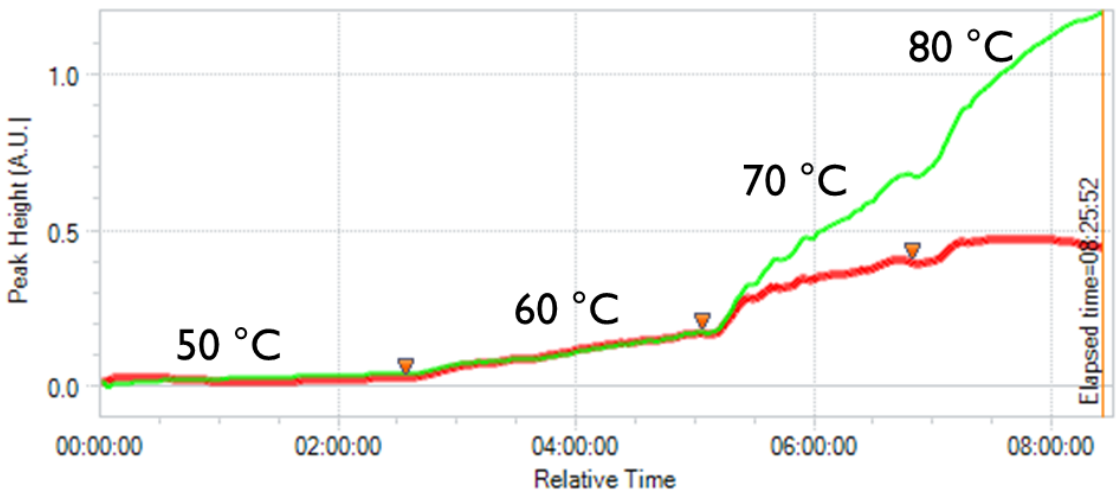

Figure D.6. IR absorptions over time of **3.1**+PPNCl+CHO (1/1/500) at 40 bar CO_2. Red (1800 cm^{-1}, CHC) and green (1750 cm^{-1}, PCHC)

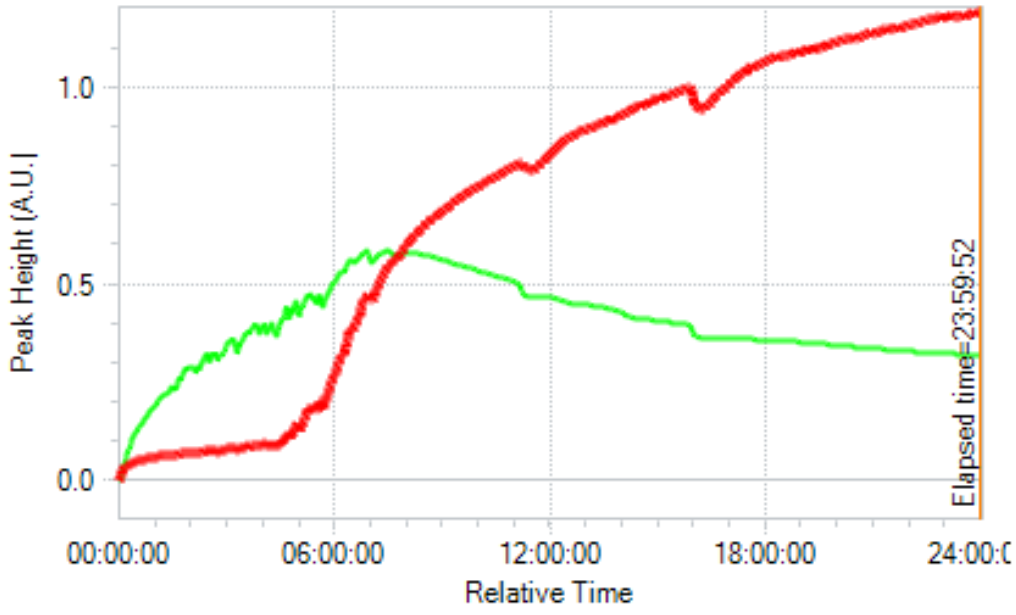

Figure D.7. Time profile of peak heights corresponding to PCHC (1749 cm^{-1}) and CHC (1810 cm^{-1}).

Appendix E: Thermomechanical data

Table E.1. PCL thermomechanical properties

System used to prepare PCL	Melting point (peak) (°C)	Melting point (onset) (°C)	Enthalpy of fusion ΔH_m (J/g)	Crystallinity $\{X_c\}$ (%)
3.5	55.1	49.5	37.1	27
3.5/EtOH	56.4	53.1	44.5	32

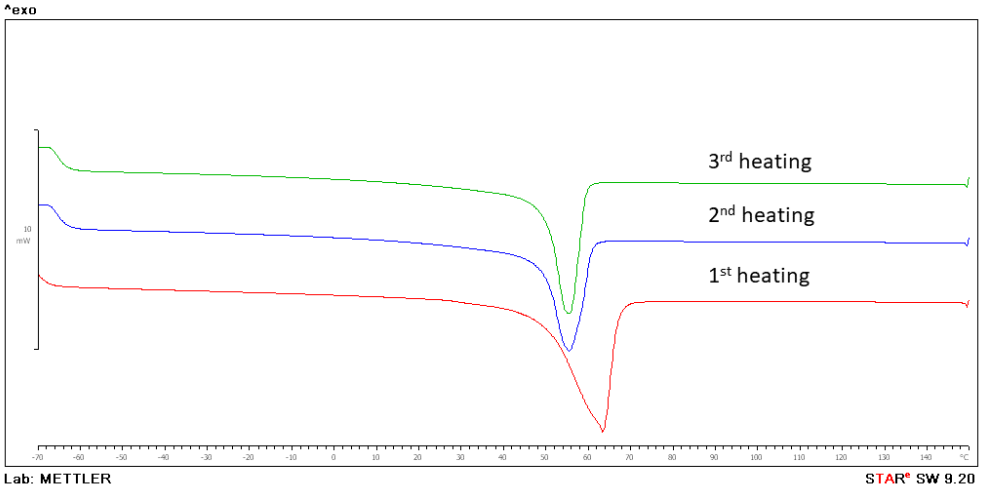

Figure E.1. DSC thermogram of PCL prepared with **3.5**

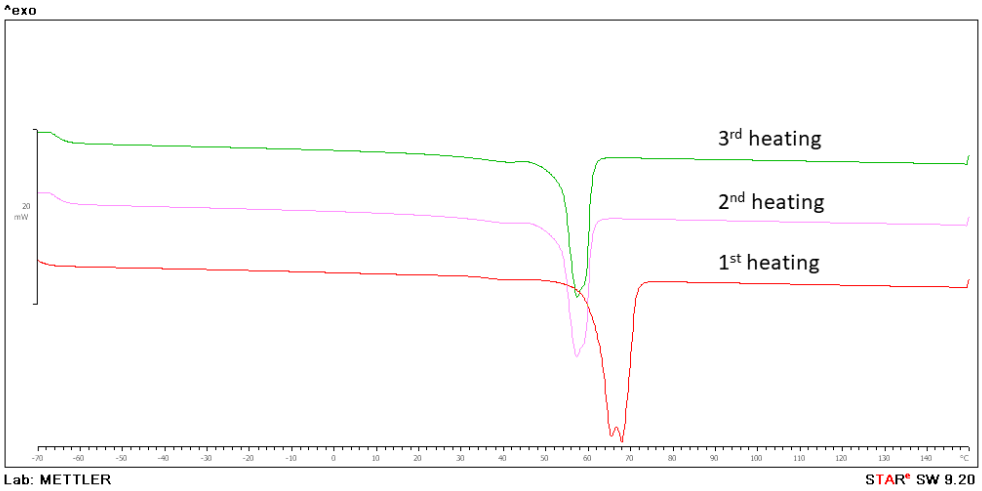

Figure E.2. DSC thermogram of PCL prepared with **3.5**/EtOH

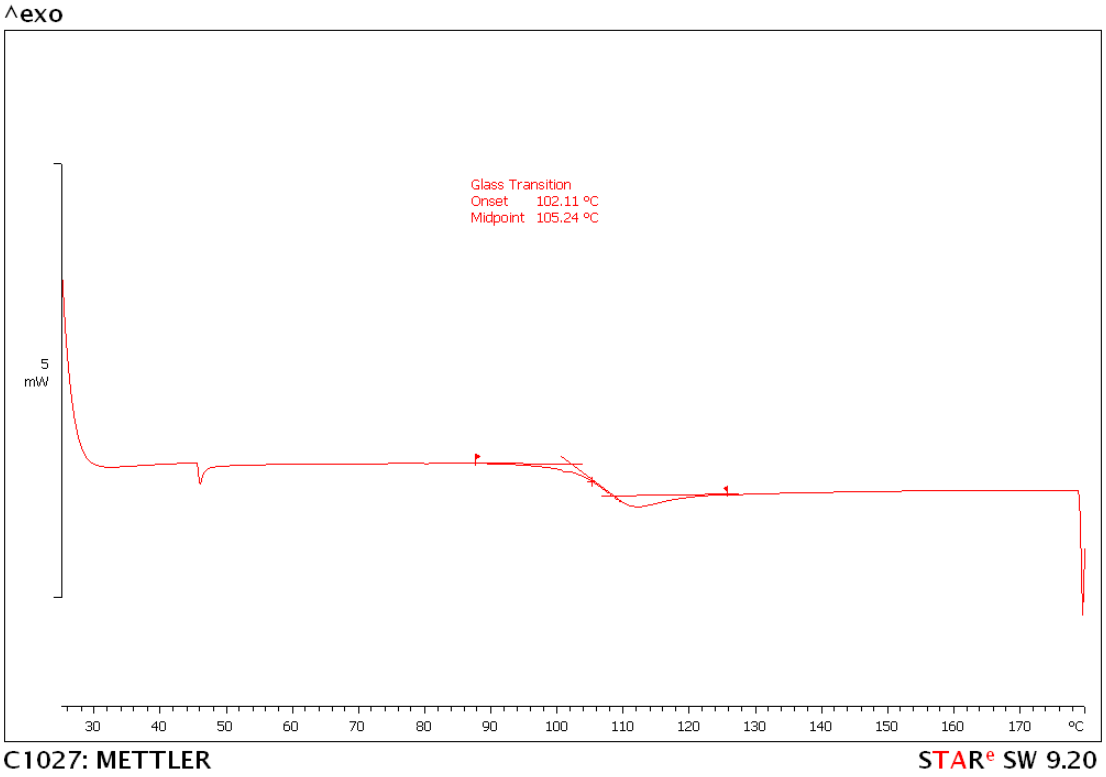

Figure E.3. DSC thermogram of PCHC (Table 5.1, entry 2)

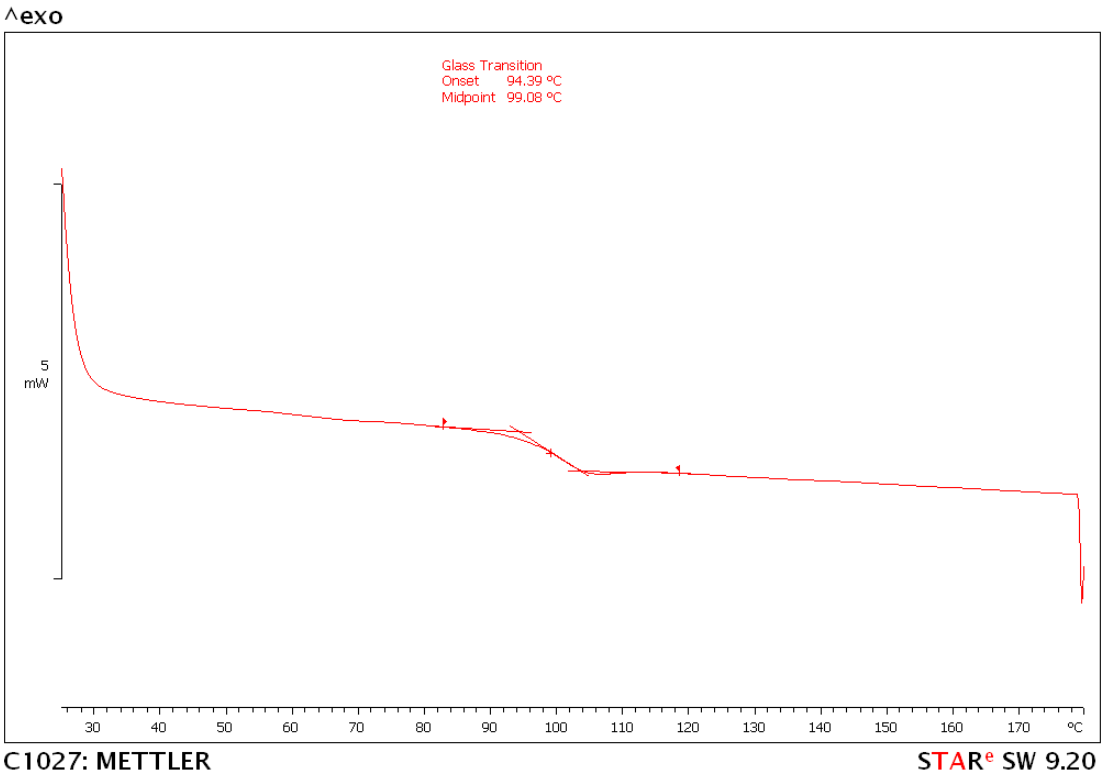

Figure E.4. DSC thermogram of PCHC (Table 5.1, entry 4)

Appendix F: Miscellaneous Data

Table F.1. Attempted ROP of other epoxides using **2.1–2.3**[a]

Entry	Epoxide[e]	Complex	t (h)
1	PO	**2.1**	24
2	PO	**2.2**	24
3	SO	**2.1**	24
4	SO	**2.2**	24
5	(−)-LO	**2.1**	24
6	ECH	**2.1**	24
7[b]	PO	**2.1**	0.33
8[c]	(−)-LO	**2.1**	1.67
9[d]	PO	**2.3**	4
10[d]	SO	**2.3**	4

[a] Reactions were performed neat at room temperature for the time indicated with 0.5 mol% complex (unless otherwise indicated). All samples showed 0% conversion according to ^{1}H NMR spectroscopy. [b] Performed in a microwave reactor at 60 °C with 2.7 mol% **2.1**. [c] Performed in a microwave reactor at 130 °C with 2.7 mol% **2.1**. [d] 0.2 mol% **2.3**. [e] SO = styrene oxide; ECH = epichlorohydrin.

Table F.2. Calculated charges of pendent nitrogen in initial pro-ligands and Al-Cl complexes

Pro-ligand	Mulliken		MSK		CM5		NBO		DDEC6	
	Initial	Al-Cl	Initial	Al-Cl	Initial	Al-Cl	Initial	Al-Cl	Initial	Al-Cl
H_2[**L2**]	−0.03	−0.97	−0.49	−0.34	−0.39	−0.32	−0.59	−0.66	−0.22	−0.22
H_2[**L3**]	−0.10	−1.11	−0.28	−0.20	−0.40	−0.32	−0.59	−0.69	−0.16	−0.15